SPRINGER BRIEFS IN MATHEMATICS

Andrea Cangiani
Zhaonan Dong
Emmanuil H. Georgoulis
Paul Houston

hp-Version Discontinuous Galerkin Methods on Polygonal and Polyhedral Meshes

Springer

SpringerBriefs in Mathematics

SpringerBriefs in Mathematics showcase expositions in all areas of mathematics and applied mathematics. Manuscripts presenting new results or a single new result in a classical field, new field, or an emerging topic, applications, or bridges between new results and already published works, are encouraged. The series is intended for mathematicians and applied mathematicians.

More information about this series at http://www.springer.com/series/10030

Andrea Cangiani • Zhaonan Dong •
Emmanuil H. Georgoulis • Paul Houston

hp-Version Discontinuous Galerkin Methods on Polygonal and Polyhedral Meshes

Springer

Andrea Cangiani
Department of Mathematics
University of Leicester
Leicester, United Kingdom

Zhaonan Dong
Department of Mathematics
University of Leicester
Leicester, United Kingdom

Emmanuil H. Georgoulis
Department of Mathematics
University of Leicester
Leicester, United Kingdom

Department of Mathematics
National Technical University of Athens
Greece

Paul Houston
School of Mathematical Sciences
University of Nottingham
Nottingham, United Kingdom

ISSN 2191-8198 ISSN 2191-8201 (electronic)
SpringerBriefs in Mathematics
ISBN 978-3-319-67671-5 ISBN 978-3-319-67673-9 (eBook)
DOI 10.1007/978-3-319-67673-9

Library of Congress Control Number: 2017946703

Mathematics Subject Classification (2010): 65M12, 65M15, 65M50, 65M60

Printed on acid-free paper

This Springer imprint is published by Springer Nature
The registered company is Springer International Publishing AG
The registered company address is: Gewerbestrasse 11, 6330 Cham, Switzerland

To

Johanna, Shuheng, Elektra, and Kelly

for their patience while writing this volume.

Contents

Chapter 1
Introduction

The purpose of this volume is to present some recent developments concerning the mathematical aspects of discontinuous Galerkin finite element methods on general computational meshes consisting of polygonal/polyhedral (henceforth, jointly referred to as polytopic) element domains. We begin by providing some historical background and motivation for this work, as well as introducing some standard notation.

1.1 Background

Finite element methods (FEMs) represent an indispensable computational tool for the accurate, efficient, and rigorous numerical approximation of continuum models arising in engineering, physics, biology, and many other disciplines. Key reasons for the astounding success of FEMs is their applicability to general classes of partial differential equations (PDEs), simple treatment of complicated computational geometries and enforcement of boundary conditions, and ease of adaptivity including both local mesh subdivision (h-refinement) and local polynomial enrichment (p-refinement). Furthermore, from a mathematical point of view, tools are available for their rigorous error analysis, both in the a priori and a posteriori settings; this latter topic is of particular practical interest for both error quantification and automatic adaptive mesh design.

However, the exploitation of classical (conforming) FEMs for the numerical approximation of hyperbolic, or 'nearly' hyperbolic problems, and other strongly non-self-adjoint PDE problems is, generally speaking, unsatisfactory in the sense that the underlying numerical scheme lacks sufficient stability. This typically manifests itself through the production of spurious or unphysical oscillatory behaviour in the computed approximation in the vicinity of strong gradients in the analytical solution, for example, near boundary and internal layers. As a remedy, over the last

A. Cangiani et al., *hp-Version Discontinuous Galerkin Methods on Polygonal and Polyhedral Meshes*, SpringerBriefs in Mathematics,
DOI 10.1007/978-3-319-67673-9_1

40 years or so, Petrov-Galerkin, or more generally, stabilized variants of the standard FEM, have been devised; perhaps the most popular approach is the streamline upwind Petrov-Galerkin (SUPG) scheme, cf. [46, 110], for example. However, stabilized schemes often involve the determination of hard-to-evaluate user-defined parameters. While this topic is beyond the scope of the current volume, we refer to [43, 44, 51, 97], and the references cited therein.

At the other end of the spectrum, finite volume methods (FVMs) have been predominantly used in industrial software packages, especially in computational fluid dynamics (CFD), due to their efficiency of implementation, particularly on parallel computer architectures, as well as their robustness. While, in principle, these methods are typically second-order accurate, in practice, their convergence order may deteriorate on irregular and/or highly stretched meshes. Thereby, for reliable numerical predictions to be made by such methods, extremely fine meshes with a large number of degrees of freedom are required; this, in turn, leads to excessively long computing times. As an alternative approach, in recent years there has been significant interest in the development of high-order discretization methods. On a given computational mesh they allow for improved predictions of critical flow phenomena, as well as force coefficients, such as, for example, the lift, drag, or moment of a body immersed in a fluid. In particular, high-order methods are capable of achieving the same level of accuracy while exploiting significantly fewer degrees of freedom compared to classical FVMs.

In this volume, we focus on an extremely powerful class of arbitrary-order numerical schemes referred to as *discontinuous Galerkin finite element methods* (DGFEMs). Loosely speaking, DGFEMs can be considered as a hybrid between classical FEMs and FVMs. Indeed, in common with FEMs, DGFEMs approximate the underlying PDE solution by employing polynomials of arbitrary degree, defined over local element domains, but without the enforcement of any continuity constraints between neighbouring elements. Instead, elements are coupled via numerical flux functions in a similar manner to the design of FVMs. In the lowest-order case, i.e., when piecewise constant functions are employed, the corresponding DGFEM is equivalent to a cell-centred FVM, without a local recovery operator. Thereby, given the construction of DGFEMs as Galerkin procedures, rigorous error analysis is available for a variety of PDE problems.

The first DGFEM was introduced by Reed and Hill [148] for the numerical solution of the neutron-transport equation. This method was later analysed by Lesaint and Raviart [135] and by Johnson and Pitkäranta [127]; see, for example, [41, 66, 68, 69, 71, 72, 93], and the volume [73]. In the context of elliptic PDEs, Nitsche [143] introduced the idea of weakly imposing inhomogeneous essential boundary conditions for (classical) FEMs. This was subsequently studied by Baker [27] who proposed the first modern DGFEM for elliptic problems, later followed by Wheeler [173], Arnold [16], Baker et al. [28], and others; cf., also, the related penalty FEM studied in [23].

Over the last 20 years tremendous progress has been made on the development of both the analytical and computational aspects of DGFEMs for the numerical approximation of a wide variety of PDEs; see, for example, the recent mono-

graphs [73, 79, 117, 151] and the review articles [18, 65]. This progress has been stimulated by a number of important factors: firstly, the combination of FVM-type stability with the exploitation of high-order polynomials within the FEM setting means that DGFEMs can treat advection-dominated diffusion problems, without excessive numerical stabilization, in an accurate and efficient manner. Furthermore, the lack of continuity between neighbouring elements, allows for extremely general meshes to be employed; in particular, DGFEMs offer higher-order discretizations with a minimal computational stencil, irrespective of the element shape. On a more technical level, the simple communication via numerical fluxes at element interfaces afforded by DGFEMs allows for the natural incorporation of so-called hanging nodes, thereby simplifying local mesh refinement (*h*-refinement). Additionally, the mode of communication at elemental interfaces is independent of the order of the method which simplifies the use of schemes with different polynomial orders p in adjacent elements. This allows for the variation of the order of polynomials over the computational domain (p-refinement), which in combination with *h*-refinement leads to so-called *hp*-version approximations. Recent advances in domain decomposition techniques have highlighted that DGFEMs naturally admit Schwarz-type preconditioners, cf. [3–7, 11, 94]; see, also, [10, 13, 15] for the design of multigrid algorithms for DGFEMs. As a final remark, the level of generality offered by DGFEMs, in terms of both the method definition via numerical fluxes and the flexibility in the mesh design, has contributed to their use in practically relevant simulations for a wide variety of applications, ranging from CFD and electromagnetics to structural mechanics and mathematical biology; indeed, DGFEMs naturally treat multi-physics problems within a unified manner, cf. [120, 159].

On the other hand, many practitioners often conclude that DGFEMs are computationally expensive, since for a given mesh and polynomial order, DGFEMs lead to an increase in the number of degrees of freedom compared to classical FEMs with comparable accuracy, though it is important to note that such statements are typically made in the context of discretizing second-order self-adjoint elliptic PDEs. This is a rather simplistic argument, since it overlooks all of the key aforementioned and other potential advantages of DGFEMs in terms of their applicability, versatility, and mesh-flexibility. Indeed, as we shall see below, within the DGFEM framework, it is possible to employ the same underlying approximating space of discontinuous piecewise polynomials, irrespective of the structure of the PDE of interest and the type of computational mesh exploited. Moreover, the flexibility offered by different choices of numerical fluxes allows for the design of DGFEMs with desirable conservation properties of important quantities, such as, for example, mass, momentum, and energy. Furthermore, in the context of implicit discretizations, the size of the resulting linear systems can be reduced in such a manner that DGFEMs may be either competitive or, in some cases, cheaper to compute than the corresponding standard (conforming) FEM. Indeed, we first mention the pioneering work of Cockburn and his collaborators on the so-called hybridizable DGFEM (HDG), see, for example, [67, 74]. In this setting, additional unknowns are introduced on the boundary of each element within the underlying

computational mesh. Thereby, through a process of static condensation, a global matrix problem involving *only* the additional unknowns needs to be solved; the remaining unknowns are then recovered by solving local elementwise problems.

Secondly, we highlight the fact that, within the DGFEM framework, elemental polynomial bases can be constructed which contain less degrees of freedom than their FEM counterparts on quadrilateral/hexahedral elements. The essential idea is to construct a basis in the physical frame, without resorting to the use of local element mappings to a given reference element. In this way, spaces of polynomials of total degree p, denoted by $\mathscr{P}_p$, may be employed, irrespective of the shape of the element; see, for example, [32–34, 54]. We also refer to [35] where this technique was first used to exactly resolve curved boundaries. Thereby, the order of convergence of the underlying method is *independent* of the element shape; we refer to [17, 19] for a detailed discussion of this issue when element mappings are employed. Indeed, as noted in our recent work [54], when the underlying mesh consists of tensor-product elements, for example, quadrilaterals in 2D and hexahedra in 3D, the use of $\mathscr{P}_p$ polynomial spaces not only renders the underlying DGFEM more efficient than the standard DGFEM using tensor-product polynomials of degree p in each coordinate direction ($\mathscr{Q}_p$), but also more efficient than the corresponding standard FEM, as the polynomial degree p increases. Going one step further, the exploitation of DGFEMs using polynomial spaces defined in the physical frame, means that DGFEMs naturally allow for the use of computational meshes consisting of general polytopic elements; indeed, this is the principle topic of this volume.

Numerical methods defined on computational meshes consisting of polytopic elements, with, potentially, many faces, have gained substantial traction in recent years for a number of important reasons. Clearly, a key underlying issue for all classes of FEMs/FVMs is the design of a suitable computational mesh upon which the underlying PDE problem will be discretized. The task of generating the mesh must address two competing issues: on the one hand, the mesh should provide a good representation of the given computational geometry with sufficient resolution for the computation of accurate numerical approximations. On the other hand, the mesh should not be so fine that computational turn-around times are too high, or in some cases even intractable, due to the high number of degrees of freedom in the resulting FEM/FVM. Traditionally, standard mesh generators generate grids consisting of triangular/quadrilateral elements in 2D and tetrahedral/hexahedral/prismatic/pyramidal elements in 3D; these will, henceforth, be collectively referred to as *standard element shapes*. In the presence of essentially lower-dimensional solution features, for example, boundary/internal layers, anisotropic meshing may be exploited. However, in regions of high curvature, the use of such highly-stretched elements may lead to element self-intersection, unless the curvature of the geometry is carefully 'propagated' into the interior of the mesh through the use of (computationally expensive) isoparametric element mappings. These issues are particularly pertinent in the context of high-order methods, since in this setting, accuracy is often achieved by exploiting coarse meshes in combination with local high-order polynomial basis functions. Thereby, flexibility, in terms of

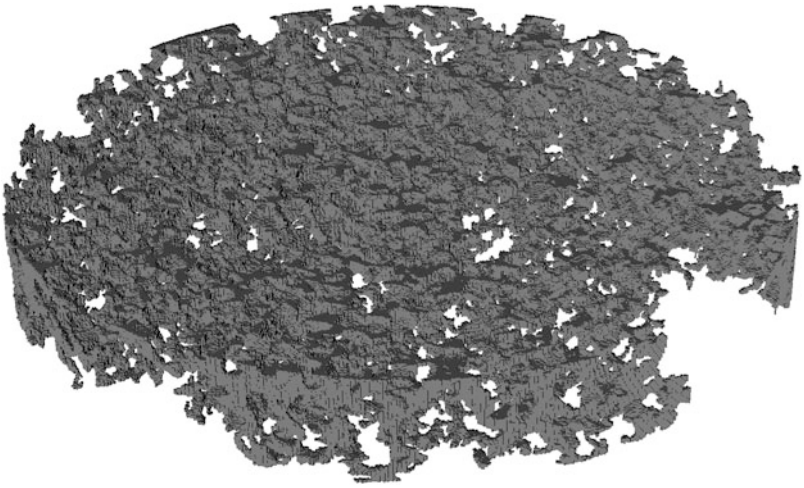

Fig. 1.1 Example of a porous scaffold used for in vitro bone tissue growth, cf. [12, 21, 22]

the shape of the elements admitted within a given coarse mesh, is crucial in this context for the efficient approximation of localized geometrical features present in the underlying geometry. Indeed, we highlight that the use of standard element shapes necessitates the exploitation of very fine computational meshes when the geometry possesses small details or microstructures. In such situations, an extremely large number of elements may be required for a given mesh generator to produce even a 'coarse' mesh which adequately describes the underlying geometry. As an example arising in biomedical applications, in Fig. 1.1 we show a finite element mesh, consisting of 3.2 million hexahedral elements, for a porous scaffold employed for in vitro bone tissue growth, cf. [12, 21, 22]. This computationally taxing mesh granularity is necessitated by the domain representation only. By dramatically increasing the flexibility in terms of the set of admissible element shapes present in the computational mesh, the resulting FEM/FVM can potentially deliver dramatic savings in computational costs. Indeed, allowing for polytopic element shapes, the number of elements can be substantially reduced without enforcing any domain approximation.

In the context of designing FEMs posed on meshes consisting of polytopic elements, a number of prominent techniques have been developed within the literature. For the discretization of PDEs in complicated geometries, Composite Finite Elements (CFEs) were originally proposed in the conforming setting by Hackbusch and Sauter [106, 107]; these techniques have been generalized to include DGFEMs in the series of articles [8, 12, 103]. We point out that CFEs are defined on general meshes consisting of polytopic elements generated as agglomerates of standard shaped elements. A closely related technique is the so-called agglomerated DGFEM [32–34]; this is very similar in spirit to the DGFEM CFE developed in [8], though the CFE methodology admits more general classes

of elemental shape functions. Another approach supporting general meshes is the recently introduced Hybrid High-Order method [80, 81, 83] which is related to the aforementioned HDG [75]. In the conforming setting, we also mention the Polygonal FEM [164] and the Extended FEM [98]; these two approaches achieve conformity by enriching/modifying the standard polynomial finite element spaces, in the spirit of the Generalized Finite Element framework of Babuška and Osborn [24]. Typically, the handling of non-standard shape functions carries an increase in computational effort. The recently proposed Virtual Element Method [2, 37, 39, 59], overcomes this difficulty, achieving the extension of conforming FEMs to polytopic elements, while maintaining the ease of implementation of these schemes; see, also, the closely related Mimetic Finite Difference method, cf. the monograph [38] and the references cited therein. We further refer to the volume [30] for a collection of review articles on the aforementioned techniques.

The ability to incorporate polytopic meshes offers a number of advantages also in the context of multilevel linear solvers, such as Schwarz-based domain decomposition preconditioners and multigrid. Indeed, a key difficulty in the implementation of the latter is the construction of a hierarchy of coarser meshes starting from a given fine one. The use of simple coarsening strategies may lead to the generation of 'holes' in the coarse meshes, and the poor approximation of fine scale geometric features; consequently, this can lead to a degradation in the performance of the resulting solver. This issue is trivially resolved when polytopic meshes are admitted, since hierarchies of coarser meshes can be constructed via agglomeration of fine-scale elements into coarser polytopes; see, for example, [9, 15, 102], and the references cited therein. Moreover, unstructured and/or hybrid meshes, consisting of mixed element shapes and nonconforming meshes containing hanging nodes, may be easily treated. DGFEMs are particularly pertinent in this context, as coarsening and refinement via element agglomeration and subdivision produce hierarchically-related approximation spaces. This is of crucial importance when projecting from one mesh to another, for example, in adaptive methods for evolution PDEs.

In conclusion, from a meshing point of view, the exploitation of general polytopic elements provides enormous flexibility. In addition to meshing complicated geometries using a minimal number of elements, polytopic elements are naturally suited to applications in complicated/moving domains, for example, in solid mechanics, fluid-structure interaction, geophysical problems including earthquake engineering and flows in fractured porous media, and mathematical biology. Indeed, general element shapes are often exploited as transitional elements in finite element meshes, for example, when fictitious domain methods, unfitted methods, or overlapping meshes are employed, cf., for example, [48–50, 125, 137]. The use of similar techniques in the context of characteristic-based/Lagrange–Galerkin methods is also relevant.

The principal aim of this volume is to provide a comprehensive mathematical introduction to the construction and analysis of DGFEMs on extremely general classes of meshes consisting of polytopic elements. Particular importance will be given to the key issue that, under mesh enrichment, shape-regular polytopes in $\mathbb{R}^d$, $d > 1$, may permit degenerate $(d-k)$-dimensional facets, $k = 1, \ldots, d-1$.

This issue does not typically arise when studying FEMs on standard shape-regular meshes consisting of simplicial/tensor-product elements. Indeed, shape-regular (cf. Definition 2 below for the precise meaning) d-dimensional polytopes with more than $d+1$ faces may admit arbitrarily small $(d-k)$-dimensional facets, $k = 1, \ldots, d-1$, relative to their diameter. This issue is intimately related to the correct choice of the (user-defined) discontinuity-penalization function present in the DGFEM discretization of second-order elliptic PDE problems. In the analysis presented below, stability and *hp*-version a priori error bounds will be established, which are sharp with respect to this type of degeneration. Additionally, under mesh refinement, the number of faces that each polytopic element possesses may not remain uniformly bounded; conditions under which this type of degeneration can be admitted will also be studied. While the following exposition is, naturally, focused on areas of interest of the authors, the concepts presented here are far-reaching; where applicable, we shall highlight potential extensions throughout this volume.

1.2 Overview and Scope

We assume that the reader is familiar with the derivation and construction of classical FEMs based on employing continuous piecewise polynomials defined over a given fixed computational mesh $\mathscr{T}_h$; for background, we refer, for example, to [42, 90, 126, 133]. The outline of this volume is as follows. The construction of DGFEMs starting from a local elementwise formulation with weakly imposed boundary conditions, together with the corresponding flux formulation for first-order hyperbolic problems, is covered in the first part of Chap. 2. On the basis of this flux formulation, the treatment of second-order PDEs is then also considered. The key theoretical tools needed to analyze DGFEMs on general polytopic meshes are outlined in Chap. 3; here, both *hp*-version inverse inequalities and approximation results are established. On the basis of these bounds, in Chap. 4 we consider the a priori error analysis of the so-called symmetric interior penalty DGFEM for the numerical approximation of pure diffusion problems, though we stress that the analysis naturally extends to include other DGFEM formulations. The analysis is extended to general second-order PDEs with nonnegative characteristic form in Chap. 5; here, we also consider the treatment of space-time DGFEMs for the numerical approximation of parabolic PDEs. The implementation aspects of DGFEMs on general polytopes are discussed in Chap. 6. Here the three main practical challenges, namely, mesh generation, construction of the elemental polynomial basis, and numerical integration, are discussed. To demonstrate the flexibility of this approach, in Chap. 7 we discuss automatic mesh refinement for DGFEMs posed on general agglomerated elements, based on exploiting dual-weighted-residual a posteriori error indicators. Finally, in Chap. 8 we summarize the work presented in this volume and outline potential future areas of research.

1.3 Preliminaries

In this section, we recall some standard notation used throughout this volume. Firstly, given two sets X and Y in $\mathbb{R}^d$, $d \geq 1$, we write $\text{dist}(X, Y)$ to denote the Hausdorff distance between X and Y, defined by

$$\text{dist}(X, Y) := \sup_{x \in X} \inf_{y \in Y} |x - y|. \tag{1.1}$$

Throughout this work, we let Ω be a bounded open subset of $\mathbb{R}^d$, $d \geq 1$, with boundary $\partial\Omega$; moreover, we write $|\Omega|$ to denote the measure of the domain Ω. For $1 \leq p \leq \infty$, we let $L^p(\Omega)$ denote the usual Lebesgue space of real-valued functions with norm $\|\cdot\|_{L^p(\Omega)}$, defined by

$$\|v\|_{L^p(\Omega)} := \left(\int_\Omega |v(\mathbf{x})|^p \, \mathrm{d}\mathbf{x} \right)^{1/p},$$

in the case $1 \leq p < \infty$, and

$$\|v\|_{L^\infty(\Omega)} := \text{ess} \sup_{\mathbf{x} \in \Omega} |v(\mathbf{x})|,$$

in the case $p = \infty$.

Given a multi-index $\alpha = (\alpha_1, \ldots, \alpha_d)$, $\alpha_i \in \mathbb{N}_0 := \mathbb{N} \cup \{0\}$, $i = 1, \ldots, d$, of length $|\alpha| := \sum_{i=1}^d \alpha_i$, we define the differential operator $D^\alpha := D_1^{\alpha_1} \ldots D_d^{\alpha_d}$ with $D_j := \partial/\partial x_j$, for $j = 1, \ldots, d$. For $m \in \mathbb{N}_0 \cup \{\infty\}$, we denote by $C^m(\Omega)$ the set of all continuous real-valued functions defined on Ω such that $D^\alpha v$ is continuous on Ω for all $|\alpha| \leq m$. In particular, when $m = 0$ we simply write $C(\Omega)$ instead of $C^0(\Omega)$. Furthermore, we write $C_0^m(\Omega)$ to denote the subspace of $C^m(\Omega)$ consisting of functions with compact support on Ω. Next, we recall the definition of a Sobolev space, cf., for example, [1]; in this context, with a slight abuse of notation, we also write $D^\alpha v$ to denote the weak derivative of a sufficiently smooth function v.

Definition 1 For $m \in \mathbb{N}_0$, we define the *Sobolev space* $W^{m,p}(\Omega)$ over an open domain $\Omega \subset \mathbb{R}^d$, by

$$W^{m,p}(\Omega) := \{u \in L^p(\Omega) : D^\alpha u \in L^p(\Omega) \text{ for } |\alpha| \leq m\}, \tag{1.2}$$

with associated norm $\|\cdot\|_{W^{m,p}(\Omega)}$ and seminorm $|\cdot|_{W^{m,p}(\Omega)}$ given by

$$\|u\|_{W^{m,p}(\Omega)} := \left(\sum_{|\alpha| \leq m} \|D^\alpha u\|_{L^p(\Omega)}^p \right)^{1/p}, \quad |u|_{W^{m,p}(\Omega)} := \left(\sum_{|\alpha| = m} \|D^\alpha u\|_{L^p(\Omega)}^p \right)^{1/p},$$

for $p \in [1, \infty)$, and

$$\|u\|_{W^{m,\infty}(\Omega)} := \max_{|\alpha| \leq m} \|D^\alpha u\|_{L^\infty(\Omega)}, \quad |u|_{W^{m,\infty}(\Omega)} := \max_{|\alpha|=m} \|D^\alpha u\|_{L^\infty(\Omega)},$$

for $p = \infty$, respectively.

Further, $W_0^{m,p}(\Omega)$ denotes the closure of $C_0^\infty(\Omega)$ in the norm of $W^{m,p}(\Omega)$. For $p = 2$, we write $H^m(\Omega)$ and $H_0^m(\Omega)$ for $W^{m,2}(\Omega)$ and $W_0^{m,2}(\Omega)$, respectively. Negative and fractional order Sobolev spaces, i.e., where the *Sobolev index* $m \in \mathbb{R}$, are also defined by (standard) duality and function-space interpolation procedures, respectively; for more details concerning these techniques, we refer to [1], for example. We also make use of Sobolev spaces on manifolds, as we are interested in the regularity properties of functions on boundaries of domains. These are defined in a standard fashion via diffeomorphisms and partition of unity arguments; for a nice exposition of this topic, we refer to [150].

Throughout this volume, we denote by $\mathscr{T}_h$ a subdivision of the domain Ω into disjoint open elements κ such that $\bar{\Omega} = \cup_{\kappa \in \mathscr{T}_h} \bar{\kappa}$. Moreover, for $\kappa \in \mathscr{T}_h$, we define $h_\kappa := \text{diam}(\kappa)$ to be the diameter of the element κ. Following [64] we introduce the concept of shape-regularity of the subdivision $\mathscr{T}_h$.

Definition 2 The subdivision $\mathscr{T}_h$ is said to be shape-regular if there exists a positive constant C_r such that:

$$\forall \kappa \in \mathscr{T}_h, \quad \frac{h_\kappa}{\rho_\kappa} \leq C_\text{r},$$

independently of the mesh parameters, where ρ_κ denotes the diameter of the largest ball contained in κ.

We stress that when $\kappa \in \mathscr{T}_h$ is a general polytope, it is possible for κ to be shape-regular *and*, simultaneously, have faces with arbitrarily small diameters compared to h_κ; such an example is given in Fig. 3.2 in Chap. 3.

On the basis of the subdivision $\mathscr{T}_h$ we define the broken Sobolev space $H^\mathbf{s}(\Omega, \mathscr{T}_h)$, up to composite order $\mathbf{s}$, in the following manner:

$$H^\mathbf{s}(\Omega, \mathscr{T}_h) := \{u \in L^2(\Omega) : u|_\kappa \in H^{s_\kappa}(\kappa) \quad \forall \kappa \in \mathscr{T}_h\}.$$

Moreover, for $v \in H^1(\Omega, \mathscr{T}_h)$, we define the broken gradient $\nabla_h v$ by $(\nabla_h v)|_\kappa = \nabla(v|_\kappa), \kappa \in \mathscr{T}_h$.

Chapter 2
Introduction to Discontinuous Galerkin Methods

We begin by providing an overview concerning the construction of DGFEMs for both first-order hyperbolic and second-order elliptic PDEs. For further details, we refer to [18, 79, 117, 151] and the references cited therein. To this end, we first introduce a general class of PDEs referred to as second-order equations with nonnegative characteristic form, cf. [121, 144]. We then develop the DGFEM discretization for both the first-order transport equation, as well as a uniformly elliptic second-order PDE problem; on the basis of these schemes, we then state the DGFEM for the general second-order PDE of mixed type.

2.1 PDEs with Nonnegative Characteristic Form

To highlight the versatility of DGFEMs, throughout this volume we primarily focus our attention on the discretization of *linear second-order PDEs with nonnegative characteristic form*. To this end, given an open bounded Lipschitz domain Ω in $\mathbb{R}^d$, $d \geq 1$, with boundary $\partial\Omega$, consider the following PDE: find u such that

$$-\nabla \cdot (a\nabla u) + \nabla \cdot (\mathbf{b}u) + cu = f \quad \text{in } \Omega. \tag{2.1}$$

Here, $a = \{a_{ij}\}_{i,j=1}^{d}$, with $a_{ij} \in L^\infty(\Omega)$ and $a_{ij} = a_{ji}$, for $i,j = 1,\ldots,d$, $\mathbf{b} = (b_1,\ldots,b_d)^\top \in \left[W^{1,\infty}(\Omega)\right]^d$, $c \in L^\infty(\Omega)$, and $f \in L^2(\Omega)$. The PDE (2.1) is

A. Cangiani et al., *hp-Version Discontinuous Galerkin Methods on Polygonal and Polyhedral Meshes*, SpringerBriefs in Mathematics,
DOI 10.1007/978-3-319-67673-9_2

referred to as an equation with nonnegative characteristic form on the set $\Omega \subset \mathbb{R}^d$ if, at each $\mathbf{x}$ in $\bar{\Omega}$,

$$\sum_{i,j=1}^{d} a_{ij}(\mathbf{x})\xi_i\xi_j \geq 0 \tag{2.2}$$

for any vector $\boldsymbol{\xi} = (\xi_1, \ldots, \xi_d)$ in $\mathbb{R}^d$.

This class of equations includes second-order elliptic and parabolic PDEs, ultra-parabolic equations, first-order hyperbolic problems, the Kolmogorov-Fokker-Planck equations of Brownian motion, cf. [31], the equations of boundary layer theory in hydrodynamics, and various other degenerate equations. Moreover, according to a well-known result of Hörmander [118], second-order hypoelliptic operators have nonnegative characteristic form at each point of the domain Ω, after possible multiplication by -1.

To supplement (2.1) with suitable boundary conditions, following [121, 144], we first subdivide the boundary $\partial\Omega$ of the computational domain Ω into appropriate subsets. To this end, let

$$\partial_0\Omega := \left\{\mathbf{x} \in \partial\Omega : \sum_{i,j=1}^{d} a_{ij}(\mathbf{x})n_i n_j > 0\right\},$$

where $\mathbf{n} = (n_1, \ldots, n_d)^\top$ denotes the unit outward normal vector to $\partial\Omega$. Loosely speaking, we may think of $\partial_0\Omega$ as being the 'elliptic' portion of the boundary $\partial\Omega$. On the 'hyperbolic' portion of the boundary $\partial\Omega\backslash\partial_0\Omega$, we define the inflow and outflow boundaries $\partial_-\Omega$ and $\partial_+\Omega$, respectively, by

$$\partial_-\Omega := \{\mathbf{x} \in \partial\Omega\backslash\partial_0\Omega : \mathbf{b}(\mathbf{x}) \cdot \mathbf{n}(\mathbf{x}) < 0\},$$
$$\partial_+\Omega := \{\mathbf{x} \in \partial\Omega\backslash\partial_0\Omega : \mathbf{b}(\mathbf{x}) \cdot \mathbf{n}(\mathbf{x}) \geq 0\}.$$

If $\partial_0\Omega$ is nonempty, we shall further divide it into two disjoint subsets $\partial\Omega_{\mathrm{D}}$ and $\partial\Omega_{\mathrm{N}}$, with $\partial\Omega_{\mathrm{D}}$ nonempty and relatively open in $\partial\Omega$. It is evident from these definitions that $\partial\Omega = \partial\Omega_{\mathrm{D}} \cup \partial\Omega_{\mathrm{N}} \cup \partial_-\Omega \cup \partial_+\Omega$. For an illustrative example of this decomposition of the boundary, we refer to Fig. 2.1.

Assuming the (physically reasonable) hypothesis that $\mathbf{b}\cdot\mathbf{n} \geq 0$ on $\partial\Omega_{\mathrm{N}}$, whenever $\partial\Omega_{\mathrm{N}}$ is nonempty, we impose the following boundary conditions:

$$u = g_{\mathrm{D}} \quad \text{on } \partial\Omega_{\mathrm{D}} \cup \partial_-\Omega, \qquad \mathbf{n} \cdot (a\nabla u) = g_{\mathrm{N}} \quad \text{on } \partial\Omega_{\mathrm{N}}. \tag{2.3}$$

For an extension of this setting, allowing also for $\mathbf{b} \cdot \mathbf{n} < 0$ on $\partial\Omega_{\mathrm{N}}$, we refer to [52]. The well-posedness of the boundary value problem (2.1), (2.3), in the case of homogeneous boundary conditions, has been studied in [121]; see also [95, 96, 144]

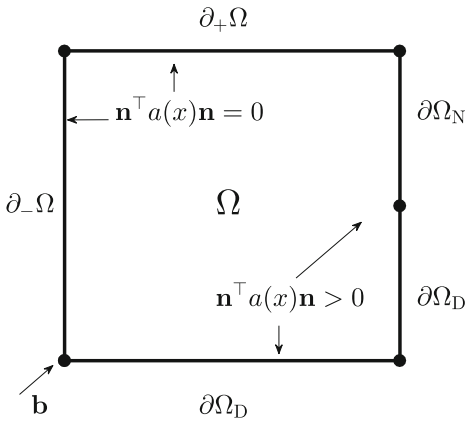

Fig. 2.1 Boundary decomposition

and the references cited therein for well-posedness results for the respective PDE in strong form.

Example 3 We provide a number of practically relevant examples which are included in the above PDE problem:

1. Select $a = I_d$, $\mathbf{b} = \mathbf{0}$, and $c = 0$, where I_d denotes the $d \times d$ identity matrix and $\mathbf{0}$ denotes the zero vector/matrix whose dimension will always be clear in the given context. With this choice we recover the Poisson equation $-\Delta u = f$ in Ω.
2. Define $a = \mathbf{0}$, $\mathbf{b} \in [W^{1,\infty}(\Omega)]^d$, and $c \in L^\infty(\Omega)$; this choice gives rise to the first-order transport equation $\nabla \cdot (\mathbf{b}u) + cu = f$, with one variable possibly signifying the time direction.
3. Let $a \in \mathbb{R}^{d\times d}$ and $\mathbf{b} \in \mathbb{R}^d$, be given by

$$a = \begin{pmatrix} 0 & \mathbf{0} \\ \mathbf{0} & I_{d-1} \end{pmatrix}, \qquad \mathbf{b} = \begin{pmatrix} 1 \\ \mathbf{0} \end{pmatrix},$$

   and $c = 0$; this selection gives rise to the heat equation with the first coordinate direction signifying the time direction.
4. For $d = 2$, let

$$a = \begin{pmatrix} 1 & 0 \\ 0 & y^r \end{pmatrix},$$

   $\mathbf{b} = \mathbf{0}$, and $c = 0$, for $r > 0$. Assuming that the computational domain Ω contains the line $y = 0$, (2.1) is the degenerate equation of Keldyš [131, 144].

5. Let $(t,x,y)^\top \in \Omega \subset \mathbb{R}^3$. For $i,j = 1,2,3$, setting $a_{ij}(t,x,y) = 1$ for $i = 2 = j$ and $a_{ij}(t,x,y) = 0$ otherwise, $\mathbf{b}(t,x,y) = (1,0,-x)^\top$, and $c = 0$, (2.1) yields the celebrated hypoelliptic equation of Kolmogorov $u_t - u_{xx} - xu_y = 0$.

In the following sections, we consider the development of DGFEMs for the discretization of different PDE operators encapsulated within (2.1).

2.2 Discretization of First-Order Hyperbolic PDEs

To highlight the key aspects concerning the construction of DGFEMs, while keeping notation to a minimum, we first consider the discretization of the first-order transport equation, i.e., $a \equiv \mathbf{0}$ and hence $\partial_0\Omega = \emptyset$: find $u \in \mathscr{G}(\mathscr{L},\Omega)$ such that

$$\mathscr{L}u := \nabla\cdot(\mathbf{b}u) + cu = f \quad \text{in } \Omega, \tag{2.4}$$

$$u = g_{\mathrm{D}} \quad \text{on } \partial_-\Omega, \tag{2.5}$$

where $\mathscr{G}(\mathscr{L},\Omega)$ denotes the graph space given by

$$\mathscr{G}(\mathscr{L},\Omega) := \{v \in L^2(\Omega) : \mathscr{L}v \in L^2(\Omega)\}.$$

Before introducing the DGFEM approximation of (2.4), (2.5), we first consider a standard continuous FEM discretization based on employing *weakly imposed* boundary conditions, cf. [126], for example. To this end, we write $\mathscr{T}_h$ to denote a shape-regular partition of the computational domain Ω, consisting of, for simplicity, non-overlapping d-dimensional open simplicial elements $\kappa \in \mathscr{T}_h$, such that $\bar{\Omega} = \cup_{\kappa\in\mathscr{T}_h}\bar{\kappa}$. Writing $p \in \mathbb{N}$ to denote the polynomial degree, we introduce the finite element space

$$V_C^p(\mathscr{T}_h) := \{u \in C(\Omega) : u|_\kappa \in \mathscr{P}_p(\kappa), \kappa \in \mathscr{T}_h\},$$

where $\mathscr{P}_p(\kappa)$ denotes the space of polynomials of total degree p on κ.

The standard continuous FEM reads: find $u_h \in V_C^p(\mathscr{T}_h)$, such that

$$\int_\Omega (\nabla\cdot(\mathbf{b}u_h) + cu_h)\, v_h \,\mathrm{d}\mathbf{x} - \int_{\partial_-\Omega} \mathbf{b}\cdot\mathbf{n}\, u_h v_h \,\mathrm{d}s = \int_\Omega f v_h \,\mathrm{d}\mathbf{x} - \int_{\partial_-\Omega} \mathbf{b}\cdot\mathbf{n}\, g_{\mathrm{D}} v_h \,\mathrm{d}s \tag{2.6}$$

for all $v_h \in V_C^p(\mathscr{T}_h)$.

It is well-known that the FEM defined by (2.6) may exhibit numerical instabilities in the form of spurious oscillations in the vicinity of sharp features present in the analytical solution, such as fronts or discontinuities. Moreover, the FEM solution, even when free of spurious oscillations, typically converges at a suboptimal

rate when compared with the approximation power of $V_C^p(\mathscr{T}_h)$. To address these concerns, (2.6) should be supplemented by appropriate numerical diffusion in order to render the underlying scheme stable; for example, by employing the so-called streamline-diffusion FEM, whereby the test function present in the volume integrals is replaced by $v_h + \delta \mathbf{b} \cdot \nabla v_h$, where δ is a positive, discretization dependent, parameter. In the h-version setting, i.e., when the polynomial degree p is kept fixed, the analysis in [128] indicates that $\delta = \mathscr{O}(h)$; the generalisation to the hp-setting outlined in [123] suggests that $\delta = \mathscr{O}(h/p)$.

The essential idea behind the DGFEM discretization of (2.4), (2.5) is to employ the scheme (2.6) elementwise, subject to a prescribed boundary condition on the inflow boundary of each element. This way we enhance the numerical stability of the approximation at the expense of introducing more degrees of freedom (for this d-simplicial mesh). To make this precise, we first need to introduce some notation. For $p \geq 0$ we define the DGFEM space

$$V^p(\mathscr{T}_h) := \{u \in L^2(\Omega) : u|_\kappa \in \mathscr{P}_p(\kappa), \kappa \in \mathscr{T}_h\}.$$

For simplicity of the exposition, here, we only consider a uniform polynomial degree distribution over the mesh $\mathscr{T}_h$; the general hp-version case will be treated below. For an element $\kappa \in \mathscr{T}_h$, we write $\partial\kappa$ to denote its boundary; then, the inflow and outflow parts of $\partial\kappa$ are defined, respectively, by

$$\partial_-\kappa := \{\mathbf{x} \in \partial\kappa, \quad \mathbf{b}(\mathbf{x}) \cdot \mathbf{n}_\kappa(\mathbf{x}) < 0\}, \quad \partial_+\kappa := \{\mathbf{x} \in \partial\kappa, \quad \mathbf{b}(\mathbf{x}) \cdot \mathbf{n}_\kappa(\mathbf{x}) \geq 0\},$$

where $\mathbf{n}_\kappa(\mathbf{x})$ denotes the unit outward normal vector to $\partial\kappa$ at $\mathbf{x} \in \partial\kappa$.

Given $\kappa \in \mathscr{T}_h$, we denote by v_κ^+, the trace of a function $v \in H^1(\Omega, \mathscr{T}_h)$ on $\partial\kappa$, relative to κ. Then, for almost every $\mathbf{x} \in \partial\kappa \backslash \partial\Omega$, there exists a unique element $\kappa' \in \mathscr{T}_h$, such that $\mathbf{x} \in \partial\kappa'$; thereby, the outer or exterior trace v_κ^- of v on $\partial\kappa \backslash \partial\Omega$, relative to κ, is defined as the inner trace $v_{\kappa'}^+$ relative to the element(s) κ', such that the intersection of $\partial\kappa'$ with $\partial\kappa \backslash \partial\Omega$ has positive $(d-1)$-dimensional measure. Below, when it is clear from the context to which element κ in the subdivision $\mathscr{T}_h$ the quantities $v_\kappa^\pm$ correspond to, we shall suppress the letter κ in the subscript and write, respectively, $v^\pm$ instead.

With this notation, motivated by (2.6), we introduce the following local FEM formulation: for each $\kappa \in \mathscr{T}_h$, find $u_h \in V^p(\mathscr{T}_h)$ such that

$$\int_\kappa (\nabla \cdot (\mathbf{b}u_h) + cu_h)\, v_h \,\mathrm{d}\mathbf{x} - \int_{\partial_-\kappa} \mathbf{b} \cdot \mathbf{n}_\kappa \, u_h^+ v_h^+ \,\mathrm{d}s = \int_\kappa f v_h \,\mathrm{d}\mathbf{x} - \int_{\partial_-\kappa} \mathbf{b} \cdot \mathbf{n}_\kappa \, \hat{g} v_h^+ \,\mathrm{d}s \quad (2.7)$$

for all $v_h \in V^p(\mathscr{T}_h)$, where

$$\hat{g}(\mathbf{x}) := \begin{cases} u_h^-(\mathbf{x}), & \mathbf{x} \in \partial_-\kappa \backslash \partial\Omega, \\ g_{\mathrm{D}}(\mathbf{x}), & \mathbf{x} \in \partial_-\kappa \cap \partial\Omega. \end{cases}$$

Summing (2.7) over $\kappa \in \mathscr{T}_h$ and employing the definition of $\hat{g}$, the DGFEM approximation to (2.4), (2.5) is given by: find $u_h \in V^p(\mathscr{T}_h)$, such that

$$\sum_{\kappa\in\mathscr{T}_h}\left\{\int_\kappa (\nabla\cdot(\mathbf{b}u_h)+cu_h)\,v_h\,\mathrm{d}\mathbf{x}-\int_{\partial_-\kappa\setminus\partial\Omega}\mathbf{b}\cdot\mathbf{n}_\kappa\,(u_h^+-u_h^-)v_h^+\,\mathrm{d}s\right.$$
$$\left.-\int_{\partial_-\kappa\cap\partial\Omega}\mathbf{b}\cdot\mathbf{n}_\kappa\,u_h^+v_h^+\,\mathrm{d}s\right\}=\sum_{\kappa\in\mathscr{T}_h}\left\{\int_\kappa f\,v_h\,\mathrm{d}\mathbf{x}-\int_{\partial_-\kappa\cap\partial\Omega}\mathbf{b}\cdot\mathbf{n}_\kappa\,g_\mathrm{D}v_h^+\,\mathrm{d}s\right\} \quad (2.8)$$

for all $v_h \in V^p(\mathscr{T}_h)$. Integrating the first term in (2.8) by parts gives rise to the following equivalent formulation: find $u_h \in V^p(\mathscr{T}_h)$, such that

$$\sum_{\kappa\in\mathscr{T}_h}\left\{\int_\kappa(-u_h\mathbf{b}\cdot\nabla v_h+cu_hv_h)\,\mathrm{d}\mathbf{x}+\int_{\partial_-\kappa\setminus\partial\Omega}\mathbf{b}\cdot\mathbf{n}_\kappa\,u_h^-v_h^+\,\mathrm{d}s\right.$$
$$\left.+\int_{\partial_+\kappa}\mathbf{b}\cdot\mathbf{n}_\kappa\,u_h^+v_h^+\,\mathrm{d}s\right\}=\sum_{\kappa\in\mathscr{T}_h}\left\{\int_\kappa f\,v_h\,\mathrm{d}\mathbf{x}-\int_{\partial_-\kappa\cap\partial\Omega}\mathbf{b}\cdot\mathbf{n}_\kappa\,g_\mathrm{D}v_h^+\,\mathrm{d}s\right\} \quad (2.9)$$

for all $v_h \in V^p(\mathscr{T}_h)$.

To motivate the potential benefits in terms of the improved stability of the DGFEM (2.9), when compared to the FEM defined by (2.6), let us consider a componentwise constant velocity field $\mathbf{b}$. In this setting, we observe that $v_h + \delta\mathbf{b}\cdot\nabla v_h \in V^p(\mathscr{T}_h)$ for all $\delta > 0$, when $v_h \in V^p(\mathscr{T}_h)$. Thereby, the additional degrees of freedom included in the DGFEM space $V^p(\mathscr{T}_h)$ ensure that the streamwise derivative of the basis functions also lie in $V^p(\mathscr{T}_h)$, which, in conjunction with the weak imposition of the elemental boundary conditions, leads to enhanced stability.

An alternative approach to derive the DGFEM (2.9), which is more generally applicable for the discretization of first-order nonlinear hyperbolic conservation laws, is to employ the concept of numerical fluxes, exploited widely within FVMs, see, for example, [115]. The idea now is to consider again a local weak formulation of (2.4), (2.5), whereby we integrate the leading order term by parts. With this in mind, multiplying (2.4) by a smooth test function v and integrating over a single element $\kappa \in \mathscr{T}_h$ gives: find $u|_\kappa$, such that $u|_{\partial_-\Omega} = g_\mathrm{D}$ and

$$\int_\kappa(-u\mathbf{b}\cdot\nabla v+cuv)\,\mathrm{d}\mathbf{x}+\int_{\partial\kappa}\mathbf{b}\cdot\mathbf{n}_\kappa\,u^+v^+\,\mathrm{d}s=\int_\kappa fv\,\mathrm{d}\mathbf{x}. \quad (2.10)$$

The DGFEM discretization of (2.10) is then based on replacing the analytical solution u by the DGFEM approximation u_h and the test function v by v_h, where both u_h and v_h belong to $V^p(\mathscr{T}_h)$. Additionally, since u_h is discontinuous between neighbouring elements, we must replace the flux $\mathbf{b}\cdot\mathbf{n}_\kappa\,u^+$ by a numerical flux function $\mathscr{H}(u_h^+, u_h^-, \mathbf{n}_\kappa)$, which depends on both the inner- and outer-trace of u_h

on $\partial\kappa$, $\kappa \in \mathscr{T}_h$, and the unit outward normal vector $\mathbf{n}_\kappa$ to $\partial\kappa$. Summing over the elements κ in the mesh $\mathscr{T}_h$ yields the DGFEM: find $u_h \in V^p(\mathscr{T}_h)$, such that

$$\sum_{\kappa\in\mathscr{T}_h}\left\{\int_\kappa(-u_h\mathbf{b}\cdot\nabla v_h + cu_h v_h)\,\mathrm{d}\mathbf{x} + \int_{\partial\kappa}\mathscr{H}(u_h^+, u_h^-, \mathbf{n}_\kappa)v_h^+\,\mathrm{d}s\right\} = \sum_{\kappa\in\mathscr{T}_h}\int_\kappa f v_h\,\mathrm{d}\mathbf{x} \quad (2.11)$$

for all $v_h \in V^p(\mathscr{T}_h)$.

We emphasize that the choice of the numerical flux function is *independent* of the finite element space employed. Indeed, the two key properties that the numerical flux function $\mathscr{H}(\cdot,\cdot,\cdot)$ should satisfy are:

1. *Consistency:* for each $\kappa \in \mathscr{T}_h$ we require that $\mathscr{H}(v, v, \mathbf{n}_\kappa)|_{\partial\kappa} = (\mathbf{b}v)\cdot\mathbf{n}_\kappa$.
2. *Conservation:* given any two neighbouring elements κ and κ' from the finite element mesh $\mathscr{T}_h$, at each point $\mathbf{x} \in \partial\kappa \cap \partial\kappa' \neq \emptyset$, noting that $\mathbf{n}_{\kappa'} = -\mathbf{n}_\kappa$, we have that $\mathscr{H}(v, w, \mathbf{n}_\kappa) = -\mathscr{H}(w, v, -\mathbf{n}_\kappa)$.

In the current setting, the most natural choice is the classical upwind numerical flux, given by

$$\mathscr{H}(u_h^+, u_h^-, \mathbf{n}_\kappa)|_{\partial\kappa} := \begin{cases} \mathbf{b}\cdot\mathbf{n}_\kappa \lim_{s\to 0+} u_h(\mathbf{x} - s\mathbf{b}) & \mathbf{x} \in \partial\kappa\backslash\partial_-\Omega, \\ \mathbf{b}\cdot\mathbf{n}_\kappa\, g_{\mathrm{D}}(\mathbf{x}) & \mathbf{x} \in \partial\kappa \cap \partial_-\Omega, \end{cases} \quad (2.12)$$

for $\kappa \in \mathscr{T}_h$; indeed, upon substituting (2.12) into (2.11), we immediately recover the DGFEM scheme given in (2.9). For further details on the construction of appropriate numerical flux functions for nonlinear first-order hyperbolic conservation laws, we refer to, for example, [132, 167] and in the context of DGFEMs to [65].

Remark 4 Assuming that $\mathbf{b}$ does not vanish within Ω, it is possible to number the elements in the computational mesh $\mathscr{T}_h$ in an appropriate 'upwind' fashion. In this way, the resulting DGFEM matrix stemming from (2.11), cf. also (2.8), is block upper triangular and, thereby, may be efficiently solved by blockwise backward substitution. Moreover, this technique can easily be implemented without the need to construct the global DGFEM matrix, cf. [135]. We note that this idea has recently been exploited in [108] to design efficient *hp*-version DGFEMs for the numerical approximation of the neutron transport equation, cf., also, the seminal work by Reed and Hill [148].

2.3 Discretization of Second-Order Elliptic PDEs

We now consider the DGFEM discretization of a simple self-adjoint second-order elliptic PDE; its construction is based on the following key steps.

1. Rewrite the underlying PDE as a first-order system of equations and derive an elemental weak formulation.

2. Introduce appropriate numerical flux functions in a similar fashion to that undertaken in the previous section; this gives rise to the so-called *flux formulation*.
3. Eliminate the auxiliary variables introduced in step 1. to yield the underlying *primal formulation*.

To demonstrate each of these steps in a clear fashion, here we consider, as model elliptic problem, the Poisson equation ($a = I_d$, $\mathbf{b} = \mathbf{0}$, and $c = 0$), subject to a Dirichlet boundary condition ($\partial\Omega_{\mathrm{D}} = \partial\Omega$ and $\partial\Omega_{\mathrm{N}} = \emptyset$), given by: find $u \in H^1(\Omega)$ such that

$$-\Delta u = f \quad \text{in } \Omega, \tag{2.13}$$

$$u = g_{\mathrm{D}} \quad \text{on } \partial\Omega. \tag{2.14}$$

Step 1. We rewrite (2.13) as the first-order system: find u and $\mathbf{s}$ such that

$$\mathbf{s} - \nabla u = 0, \qquad -\nabla \cdot \mathbf{s} = f, \tag{2.15}$$

subject to the boundary condition (2.14). Upon multiplication by test functions $\boldsymbol{\tau}$ and v, respectively, integration by parts gives the following elementwise formulation: for each $\kappa \in \mathscr{T}_h$, find u and $\mathbf{s}$ such that $u|_{\partial\Omega} = g_{\mathrm{D}}$ and

$$\int_\kappa \mathbf{s} \cdot \boldsymbol{\tau} \,\mathrm{d}\mathbf{x} + \int_\kappa u \nabla \cdot \boldsymbol{\tau} \,\mathrm{d}\mathbf{x} - \int_{\partial\kappa} u \boldsymbol{\tau} \cdot \mathbf{n}_\kappa \,\mathrm{d}s = 0,$$

$$\int_\kappa \mathbf{s} \cdot \nabla v \,\mathrm{d}\mathbf{x} - \int_{\partial\kappa} \mathbf{s} \cdot \mathbf{n}_\kappa v \,\mathrm{d}s = \int_\kappa f v \,\mathrm{d}\mathbf{x}.$$

Step 2. To derive the *flux formulation* of the DGFEM approximation to (2.13), (2.14), we introduce the numerical flux functions $\hat{u} = \hat{u}(u_h)$ and $\hat{\mathbf{s}} = \hat{\mathbf{s}}(u_h, \nabla_h u_h)$ which represent approximations to u and $\mathbf{s}$, respectively, on the boundary of each element κ in the computational mesh $\mathscr{T}_h$. Thereby, replacing $(u, \mathbf{s})$ by $(u_h, \mathbf{s}_h) \in V^p(\mathscr{T}_h) \times \boldsymbol{\Sigma}^p(\mathscr{T}_h)$, $\boldsymbol{\Sigma}^p(\mathscr{T}_h) = [V^p(\mathscr{T}_h)]^d$, and $(v, \boldsymbol{\tau})$ by $(v_h, \boldsymbol{\tau}_h) \in V^p(\mathscr{T}_h) \times \boldsymbol{\Sigma}^p(\mathscr{T}_h)$, and summing over $\kappa \in \mathscr{T}_h$ gives rise to the DGFEM: find $(u_h, \mathbf{s}_h) \in V^p(\mathscr{T}_h) \times \boldsymbol{\Sigma}^p(\mathscr{T}_h)$ such that

$$\sum_{\kappa\in\mathscr{T}_h} \int_\kappa \mathbf{s}_h \cdot \boldsymbol{\tau}_h \,\mathrm{d}\mathbf{x} + \sum_{\kappa\in\mathscr{T}_h} \int_\kappa u_h \nabla \cdot \boldsymbol{\tau}_h \,\mathrm{d}\mathbf{x} - \sum_{\kappa\in\mathscr{T}_h} \int_{\partial\kappa} \hat{u} \boldsymbol{\tau}_h^+ \cdot \mathbf{n}_\kappa \,\mathrm{d}s = 0, \tag{2.16}$$

$$\sum_{\kappa\in\mathscr{T}_h} \int_\kappa \mathbf{s}_h \cdot \nabla v_h \,\mathrm{d}\mathbf{x} - \sum_{\kappa\in\mathscr{T}_h} \int_{\partial\kappa} \hat{\mathbf{s}} \cdot \mathbf{n}_\kappa v_h^+ \,\mathrm{d}s = \sum_{\kappa\in\mathscr{T}_h} \int_\kappa f v_h \,\mathrm{d}\mathbf{x} \tag{2.17}$$

for all $(v_h, \boldsymbol{\tau}_h) \in V^p(\mathscr{T}_h) \times \boldsymbol{\Sigma}^p(\mathscr{T}_h)$.

Step 3. The flux formulation given in (2.16), (2.17) involves the additional (auxiliary) unknowns $\mathbf{s}_h$; these may be eliminated in the following manner. Setting $\boldsymbol{\tau}_h|_\kappa = \nabla(v_h|_\kappa)$, $\kappa \in \mathscr{T}_h$, in (2.16) and integrating by parts gives

$$\sum_{\kappa\in\mathscr{T}_h}\int_\kappa \mathbf{s}_h\cdot\nabla v_h\,\mathrm{d}\mathbf{x} - \sum_{\kappa\in\mathscr{T}_h}\int_\kappa \nabla u_h\cdot\nabla v_h\,\mathrm{d}\mathbf{x} + \sum_{\kappa\in\mathscr{T}_h}\int_{\partial\kappa}(u_h^+ - \hat{u})\nabla v_h^+\cdot\mathbf{n}_\kappa\,\mathrm{d}s = 0. \quad (2.18)$$

Inserting (2.18) into (2.17) gives rise to the primal DGFEM formulation: find $u_h \in V^p(\mathscr{T}_h)$ such that

$$\sum_{\kappa\in\mathscr{T}_h}\int_\kappa \nabla u_h\cdot\nabla v_h\,\mathrm{d}\mathbf{x} - \sum_{\kappa\in\mathscr{T}_h}\int_{\partial\kappa}(u_h^+ - \hat{u})\nabla v_h^+\cdot\mathbf{n}_\kappa\,\mathrm{d}s - \sum_{\kappa\in\mathscr{T}_h}\int_{\partial\kappa}\hat{\mathbf{s}}\cdot\mathbf{n}_\kappa v_h^+\,\mathrm{d}s = \sum_{\kappa\in\mathscr{T}_h}\int_\kappa f v_h\,\mathrm{d}\mathbf{x} \quad (2.19)$$

for all $v_h \in V^p(\mathscr{T}_h)$.

Before we consider the choice of the numerical flux functions $\hat{u}$ and $\hat{\mathbf{s}}$, we first rewrite (2.19) in terms of integrals arising on each face in the underlying mesh $\mathscr{T}_h$. To this end, we denote by $\mathscr{F}_h$ the set of open $(d-1)$-dimensional element faces associated with $\mathscr{T}_h$. Further, we write $\mathscr{F}_h = \mathscr{F}_h^{\mathscr{I}} \cup \mathscr{F}_h^{\mathscr{B}}$, where $\mathscr{F}_h^{\mathscr{I}}$ denotes the set of interior element faces, i.e., $F \subset \Omega$ for $F \in \mathscr{F}_h^{\mathscr{I}}$, and $\mathscr{F}_h^{\mathscr{B}}$ is the set of boundary element faces, i.e., $F \subset \partial\Omega$ for $F \in \mathscr{F}_h^{\mathscr{B}}$. The boundary $\partial\kappa$ of an element κ and the sets $\partial\kappa \setminus \partial\Omega$ and $\partial\kappa \cap \partial\Omega$ will be identified in a natural way with the corresponding subsets of $\mathscr{F}_h$.

Next, we introduce some trace operators. Let κ_i and κ_j be two adjacent elements of $\mathscr{T}_h$ and let $\mathbf{x}$ be an arbitrary point on the interior face $F \in \mathscr{F}_h^{\mathscr{I}}$ given by $F = \partial\kappa_i \cap \partial\kappa_j$. We write $\mathbf{n}_{\kappa_i}$ and $\mathbf{n}_{\kappa_j}$ to denote the outward unit normal vectors on F, relative to $\partial\kappa_i$ and $\partial\kappa_j$, respectively. Furthermore, let v and $\mathbf{q}$ be scalar- and vector-valued functions, which are smooth inside both elements κ_i and κ_j. Using the above notation, we write $(v_{\kappa_i}^+, \mathbf{q}_{\kappa_i}^+)$ and $(v_{\kappa_j}^+, \mathbf{q}_{\kappa_j}^+)$ to denote the traces of $(v, \mathbf{q})$ on F taken from within the interior of κ_i and κ_j, respectively. The averages of v and $\mathbf{q}$ at $\mathbf{x} \in F \in \mathscr{F}_h^{\mathscr{I}}$ are given by

$$\{\!\{v\}\!\} := \frac{1}{2}(v_{\kappa_i}^+ + v_{\kappa_j}^+), \quad \{\!\{\mathbf{q}\}\!\} := \frac{1}{2}(\mathbf{q}_{\kappa_i}^+ + \mathbf{q}_{\kappa_j}^+),$$

respectively. Similarly, the jumps of v and $\mathbf{q}$ at $\mathbf{x} \in F \in \mathscr{F}_h^{\mathscr{I}}$ are defined by

$$[\![v]\!] := v_{\kappa_i}^+\,\mathbf{n}_{\kappa_i} + v_{\kappa_j}^+\,\mathbf{n}_{\kappa_j}, \quad [\![\mathbf{q}]\!] := \mathbf{q}_{\kappa_i}^+\cdot\mathbf{n}_{\kappa_i} + \mathbf{q}_{\kappa_j}^+\cdot\mathbf{n}_{\kappa_j},$$

respectively. On a boundary face $F \in \mathscr{F}_h^{\mathscr{B}}$, such that $F \subset \partial\kappa_i$, $\kappa_i \in \mathscr{T}_h$, we set

$$\{\!\{v\}\!\} := v_{\kappa_i}^+, \quad \{\!\{\mathbf{q}\}\!\} := \mathbf{q}_{\kappa_i}^+, \quad [\![v]\!] := v_{\kappa_i}^+\mathbf{n}_{\kappa_i} \quad [\![\mathbf{q}]\!] := \mathbf{q}_{\kappa_i}^+\cdot\mathbf{n}_{\kappa_i},$$

with $\mathbf{n}_{\kappa_i} \equiv \mathbf{n}$ denoting the unit outward normal vector on the boundary $\partial\Omega$. As in the previous section, given that it will always be clear from the context to which element κ in the subdivision $\mathscr{T}_h$ the quantities $v_\kappa^\pm$, and so on, correspond to, for the sake of notational simplicity we shall suppress the letter κ in the subscript and write, respectively, $v^\pm$ instead. Throughout this volume, we use the shorthand notation for integrals over any set of faces $\mathscr{F}_h^s \subseteq \mathscr{F}_h$:

$$\int_{\mathscr{F}_h^s} \mathrm{d}s := \sum_{F \in \mathscr{F}_h^s} \int_F \mathrm{d}s.$$

With this notation, we note the following elementary identity holds:

$$\sum_{\kappa \in \mathscr{T}_h} \int_{\partial\kappa} \mathbf{q}^+ \cdot \mathbf{n}_\kappa \, v^+ \, \mathrm{d}s = \int_{\mathscr{F}_h} \{\!\{\mathbf{q}\}\!\} \cdot [\![v]\!] \, \mathrm{d}s + \int_{\mathscr{F}_h^{\mathscr{I}}} [\![\mathbf{q}]\!] \{\!\{v\}\!\} \, \mathrm{d}s, \tag{2.20}$$

cf. [18, 114]. Exploiting (2.20), the primal formulation of the DGFEM (2.19) may be rewritten in the following equivalent manner: find $u_h \in V^p(\mathscr{T}_h)$ such that

$$\begin{aligned} \int_\Omega \nabla_h u_h \cdot \nabla_h v_h \, \mathrm{d}\mathbf{x} + \int_{\mathscr{F}_h} ([\![\hat{u} - u_h]\!] \cdot \{\!\{\nabla_h v_h\}\!\} - \{\!\{\hat{\mathbf{s}}\}\!\} \cdot [\![v_h]\!]) \, \mathrm{d}s \\ + \int_{\mathscr{F}_h^{\mathscr{I}}} (\{\!\{\hat{u} - u_h\}\!\} [\![\nabla_h v_h]\!] - [\![\hat{\mathbf{s}}]\!] \{\!\{v_h\}\!\}) \, \mathrm{d}s = \int_\Omega f v_h \, \mathrm{d}\mathbf{x} \end{aligned} \tag{2.21}$$

for all $v_h \in V^p(\mathscr{T}_h)$, where $\nabla_h v_h$ denotes the broken gradient, cf. Sect. 1.3.

The choice of the numerical flux functions $\hat{u}$ and $\hat{\mathbf{s}}$ arising in the DGFEM (2.21) has been studied extensively within the literature: different choices of numerical flux functions lead to DGFEMs with quite different consistency, stability, and convergence properties; for a review, we refer to [18]. In the interest of simplicity of presentation, here we consider one popular family of schemes, referred to as *interior penalty (IP) methods*. We stress, however, that the theoretical developments presented below are applicable to many other DGFEMs. For IP methods, we select

$$\hat{u} = \hat{u}(u_h) = \begin{cases} \{\!\{u_h\}\!\} + \frac{1+\theta}{2} \mathbf{n}_F \cdot [\![u_h]\!] & \text{on } F \in \mathscr{F}_h^{\mathscr{I}}, \\ (1+\theta) u_h - \theta g_{\mathrm{D}} & \text{on } F \in \mathscr{F}_h^{\mathscr{B}}, \end{cases}$$

$$\hat{\mathbf{s}} = \hat{\mathbf{s}}(u_h, \nabla_h u_h) = \begin{cases} \{\!\{\nabla_h u_h\}\!\} - \sigma [\![u_h]\!] & \text{on } F \in \mathscr{F}_h^{\mathscr{I}}, \\ \nabla u_h - \sigma (u_h - g_{\mathrm{D}}) \mathbf{n} & \text{on } F \in \mathscr{F}_h^{\mathscr{B}}, \end{cases}$$

where $\theta \in [-1, 1]$ and for $F \in \mathscr{F}_h^{\mathscr{I}}$, $F \subset \partial\kappa_i \cap \partial\kappa_j$, $\mathbf{n}_F = \mathbf{n}_{\kappa_i}$. Moreover, $\sigma : \mathscr{F}_h \mapsto \mathbb{R}$ is referred to as the *discontinuity-penalization* function; the precise definition of σ depends on the local mesh size and local polynomial degree. In the current setting, i.e., assuming that the underlying simplicial mesh $\mathscr{T}_h$ is shape-regular and that the polynomial degree p is constant over $\mathscr{T}_h$, the analysis undertaken in [124], for example, indicates that $\sigma = \mathscr{O}(p^2/h)$. The precise definition for general

polytopic meshes and variable elemental polynomial degrees is a key question in this work and will be discussed in detail in Chap. 4, cf. Definition 26 and Lemma 35, and Chap. 5, cf. Lemma 37.

Given the above definition of $\hat{u}$ and $\hat{\mathbf{s}}$, we deduce the following family of DGFEMs: find $u_h \in V^p(\mathscr{T}_h)$, such that

$$\int_\Omega \nabla_h u_h \cdot \nabla_h v_h \,\mathrm{d}\mathbf{x} + \int_{\mathscr{F}_h} (-\{\!\{\nabla_h u_h\}\!\} \cdot [\![v_h]\!] + \theta \{\!\{\nabla_h v_h\}\!\} \cdot [\![u_h]\!]) \,\mathrm{d}s$$
$$+ \int_{\mathscr{F}_h} \sigma [\![u_h]\!] \cdot [\![v_h]\!] \,\mathrm{d}s = \int_\Omega f v_h \,\mathrm{d}\mathbf{x} + \int_{\mathscr{F}_h^{\mathscr{B}}} g_\mathrm{D}(\theta \nabla_h v_h \cdot \mathbf{n} + \sigma v_h) \,\mathrm{d}s \tag{2.22}$$

for all $v_h \in V^p(\mathscr{T}_h)$. Selecting the parameter $\theta = 1$ gives rise to the so-called Nonsymmetric Interior Penalty (NIP) DGFEM, cf. [152], $\theta = 0$ is the Incomplete Interior Penalty (IIP) DGFEM, cf. [77], while setting $\theta = -1$ yields the Symmetric Interior Penalty (SIP) scheme, cf. [85].

2.4 DGFEMs for PDEs with Nonnegative Characteristic Form

Finally, on the basis of the schemes (2.8), cf., also, (2.11), and (2.22), in this section we state the DGFEM discretization of general second-order PDEs with nonnegative characteristic form (2.1), (2.3). To this end, we begin by assuming, for simplicity, that $a \in V^q(\mathscr{T}_h)$, $q \geq 0$; this assumption will be removed in Chap. 5. Furthermore, we assume that the computational mesh $\mathscr{T}_h$ respects the decomposition of $\partial\Omega$ in the sense that the set of boundary faces $\mathscr{F}_h^{\mathscr{B}}$ of $\mathscr{T}_h$ can be subdivided as $\mathscr{F}_h^{\mathscr{B}} = \mathscr{F}_h^{\mathrm{D}} \cup \mathscr{F}_h^{\mathrm{N}} \cup \mathscr{F}_h^{-} \cup \mathscr{F}_h^{+}$, such that each $F \in \mathscr{F}_h^{s}$, $s \in \{\mathrm{D}, \mathrm{N}, -, +\}$, belongs to the interior of $\partial\Omega_\mathrm{D}$, $\partial\Omega_\mathrm{N}$, $\partial_-\Omega$, and $\partial_+\Omega$, respectively.

Thereby, the DGFEM discretization of (2.1), (2.3) is given by: find $u_h \in V^p(\mathscr{T}_h)$ such that

$$\int_\Omega \big(a\nabla_h u_h \cdot \nabla_h v_h + \nabla_h \cdot (\mathbf{b} u_h) v_h + c u_h v_h\big) \,\mathrm{d}\mathbf{x}$$
$$+ \int_{\mathscr{F}_h^{\mathscr{I}} \cup \mathscr{F}_h^{\mathrm{D}}} \big(- \{\!\{a\nabla_h u_h\}\!\} \cdot [\![v_h]\!] + \theta \{\!\{a\nabla_h v_h\}\!\} \cdot [\![u_h]\!] + \sigma [\![u_h]\!] \cdot [\![v_h]\!]\big) \,\mathrm{d}s$$
$$- \sum_{\kappa \in \mathscr{T}_h} \int_{\partial_-\kappa \setminus \partial\Omega} \mathbf{b} \cdot \mathbf{n}_\kappa \, (u_h^+ - u_h^-) v_h^+ \,\mathrm{d}s - \sum_{\kappa \in \mathscr{T}_h} \int_{\partial_-\kappa \cap (\partial\Omega_\mathrm{D} \cup \partial_-\Omega)} \mathbf{b} \cdot \mathbf{n} \, u_h^+ v_h^+ \,\mathrm{d}s$$
$$= \int_\Omega f \, v_h \,\mathrm{d}\mathbf{x} + \int_{\partial\Omega_\mathrm{D}} g_\mathrm{D}(\theta \nabla_h v_h \cdot \mathbf{n} + \sigma v_h) \,\mathrm{d}s + \int_{\partial\Omega_\mathrm{N}} g_\mathrm{N} v_h \,\mathrm{d}s$$
$$- \sum_{\kappa \in \mathscr{T}_h} \int_{\partial_-\kappa \cap (\partial\Omega_\mathrm{D} \cup \partial_-\Omega)} \mathbf{b} \cdot \mathbf{n} \, g_\mathrm{D} v_h^+ \,\mathrm{d}s \tag{2.23}$$

for all $v_h \in V^p(\mathscr{T}_h)$. This method was originally proposed and analysed in [124], assuming that $a \in V^q(\mathscr{T}_h)$; this condition is satisfied for all cases but the fourth in Example 3. To remove this assumption, in Chap. 5, we exploit the variant of the above DGFEM, first presented in [100].

Remark 5 We remark that when the diffusion tensor a has high contrast over the computational domain Ω, then diffusivity-dependent weighted averages may be employed within the definition of the DGFEM scheme (2.23); cf. [82, 91] for the treatment of standard element shapes in this setting. For simplicity of presentation, we do not consider this case within this work.

Chapter 3
Inverse Estimates and Polynomial Approximation on Polytopic Meshes

In this chapter we develop the key mathematical tools needed to study the stability and convergence properties of *hp*-version DGFEMs on polytopic meshes. These results will be exploited below with the ultimate goal of tackling general second-order PDEs with nonnegative characteristic form. While results of this type are readily available within the literature for standard element types, such as simplicial and tensor-product elements, cf. [25, 26, 62, 142, 156], we shall concentrate on the extension of these bounds to general meshes consisting of polytopic elements. A key issue in this setting is that general shape-regular polytopic meshes may, under mesh refinement, possess elements with $(d-k)$-dimensional facets, $k = 1, 2, \ldots, d-1$, which degenerate as the mesh size tends to zero. Thereby, care must be taken to ensure that the resulting inverse estimates and polynomial approximation results are sensitive to this type of degeneracy. The key approach adopted here is to exploit known results for standard elements, both within an L^2- and L^∞-setting, and to take the minimum of the resulting bounds, cf. [54, 55]. In this way, bounds which are optimal in both the *h*-version and *p*-version setting may be deduced, which directly account for $(d-k)$-dimensional facet degeneration, $k = 1, 2, \ldots, d-1$.

In Sect. 3.1, we begin by introducing the classes of meshes which may be admitted within the analysis presented below. Under these assumptions, in Sects. 3.2 and 3.3 we derive *hp*-version inverse and approximation results, respectively.

3.1 Polytopic Meshes

We define a very general class of computational meshes consisting of polytopic elements, together with some underlying technical assumptions. The notation introduced here will be employed throughout this volume.

Let $\mathcal{T}_h$ be a subdivision of the computational domain $\Omega \subset \mathbb{R}^d$, $d \in \mathbb{N}$, into disjoint open polytopic elements κ constructed in such a manner that the union of

A. Cangiani et al., *hp-Version Discontinuous Galerkin Methods on Polygonal and Polyhedral Meshes*, SpringerBriefs in Mathematics,
DOI 10.1007/978-3-319-67673-9_3

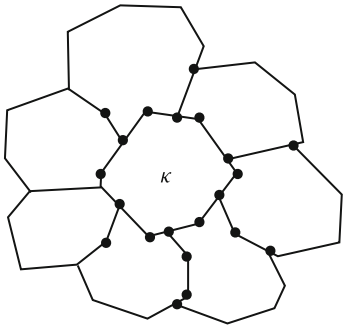

Fig. 3.1 Polygonal element κ, $\kappa \in \mathcal{T}_h$, and its face-wise neighbours; hanging nodes are highlighted with a *filled circle*

the closures of the elements $\kappa \in \mathcal{T}_h$ forms a covering of the closure of Ω, i.e., $\bar{\Omega} = \cup_{\kappa \in \mathcal{T}_h} \bar{\kappa}$. Furthermore, we denote by h_κ, the diameter of $\kappa \in \mathcal{T}_h$, i.e., $h_\kappa := \text{diam}(\kappa)$. From a mesh adaptation point of view DGFEMs are advantageous in the sense that they can naturally handle meshes which contain irregular/hanging nodes. With this in mind, we allow $\mathcal{T}_h$ to consist of general elements which may possess several hanging nodes on their $(d-k)$-dimensional facets, $k = 1, 2, \ldots, d-1$, cf. Fig. 3.1.

The stability and approximation theorems developed in this chapter rely on respective results for standard element shapes; in fact, here we shall rely on *hp*-version bounds for simplices. For this reason, we introduce the notion of both element interfaces and element faces; the latter being assumed to be simplices in $\mathbb{R}^{d-1}$. To this end, and to facilitate the presence of hanging nodes, we define the *interfaces* of the computational mesh $\mathcal{T}_h$ to be the intersection of the $(d-1)$-dimensional facets of neighbouring elements. In the two-dimensional setting (i.e., $d = 2$), the interfaces of $\mathcal{T}_h$ are simply piecewise linear line segments, i.e., they consist of a set of $(d-1)$-dimensional simplices. However, in general for $d = 3$, (or indeed $d \geq 3$) the interfaces of $\mathcal{T}_h$ consist of general polygonal surfaces in $\mathbb{R}^3$ (or polyhedral surfaces in $\mathbb{R}^d$, $d > 3$, respectively). Thereby, we assume that each planar section of each interface of an element $\kappa \in \mathcal{T}_h$ may be subdivided into a set of co-planar triangles ($(d-1)$-dimensional simplices, respectively). We refer to these $(d-1)$-dimensional simplices, whose union form the interfaces of $\mathcal{T}_h$, as the *faces* of the computational mesh $\mathcal{T}_h$, and denote by $\mathcal{F}_h$ the set of all such faces. We remark that, throughout the remainder of this volume, these will play the role of the element faces appearing in the definition of the DGFEM.

With this notation, we assume that the sub-tessellation of element interfaces into $(d-1)$-dimensional simplices is given. We point out that this assumption is not very restrictive; indeed, if the underlying mesh $\mathcal{T}_h$ stems from an agglomeration of a given fine simplicial mesh $\mathcal{T}_h^{\text{fine}}$, cf. Sect. 6.1, then the set of faces may be directly determined from the faces present in $\mathcal{T}_h^{\text{fine}}$ which form part of the interface of an agglomerated element $\kappa \in \mathcal{T}_h$. For general polytopic meshes, the faces must be computed by a local simplicial mesh subdivision algorithm on each interface, cf. [137], for example.

In the following sections, we outline the key assumptions required to be satisfied by the computational mesh $\mathscr{T}_h$ in order to derive suitable inverse inequalities and approximation results for general polytopic elements.

3.2 Inverse Estimates

Inverse estimates are widely used in the error analysis of numerical methods employed for the discretization of both PDEs and integral equations. For a simplicial or tensor-product element T, let $(X(T), \|\cdot\|_{X(T)})$ and $(Y(T), \|\cdot\|_{Y(T)})$ be two function spaces such that $\mathscr{P}_p(T) \subset X(T) \subset Y(T)$. Classical inverse estimates are bounds of the form

$$\|v\|_{X(T)} \leq C(C_{\mathrm{r}}, p) h_T^{-s} \|v\|_{Y(T)}$$

for all $v \in \mathscr{P}_p(T)$, for some $s \geq 0$, with the constant $C(C_{\mathrm{r}}, p)$ depending at most on the shape-regularity constant C_{r} (cf. Definition 2) and the polynomial degree p. Evidently, as $p \to \infty$, we expect $C(C_{\mathrm{r}}, p) \to \infty$ also. Indeed, explicit knowledge of the dependence of the constant $C(C_{\mathrm{r}}, p)$ on the polynomial degree p is available for many pairs of spaces $X(T)$ and $Y(T)$ within the literature; we refer, for example, to [40, 60, 156, 172] and the references cited therein. In the following lemma we recall the key inverse inequalities which will be exploited throughout this section.

Lemma 6 *Given a simplex T in $\mathbb{R}^d$, $d = 2, 3$, we write $F \subset \partial T$ to denote one of its faces. Then, for $v \in \mathscr{P}_p(T)$, the following inverse inequalities hold*

$$\|v\|_{L^2(F)}^2 \leq C_{\mathrm{inv},1} p^2 \frac{|F|}{|T|} \|v\|_{L^2(T)}^2, \tag{3.1}$$

$$\|v\|_{L^\infty(T)}^2 \leq C_{\mathrm{inv},2} \frac{p^{2d}}{|T|} \|v\|_{L^2(T)}^2, \tag{3.2}$$

$$\|\nabla v\|_{L^2(T)}^2 \leq C_{\mathrm{inv},3} \frac{p^4}{h_T^2} \|v\|_{L^2(T)}^2, \tag{3.3}$$

with $C_{\mathrm{inv},i}$, $i = 1, 2, 3$, positive constants, which are independent of v, p, and h_T. In particular, $C_{\mathrm{inv},3}$ depends on the shape-regularity of T, cf. Definition 2.

Proof The detailed proof of (3.1) can be found in [172], and is based on solving the eigenvalue problem for polynomial functions. We point out that the precise bound is given by:

$$\|v\|_{L^2(F)}^2 \leq \frac{(p+1)(p+d)}{d} \frac{|F|}{|T|} \|v\|_{L^2(T)}^2. \tag{3.4}$$

The proofs of (3.2) and (3.3) are given in [156].

We shall now consider the generalization of (3.1) and (3.3) to general meshes consisting of polytopic elements. We remark that (3.1) is required to establish the stability of the DGFEM approximation of second-order elliptic PDEs, cf. Lemmas 27, 35, and 37 below, while (3.3) will be utilized to determine an inf-sup condition in the presence of first-order transport terms, cf. Theorem 42 below. In order to extend (3.1) to general polytopic elements κ, $\kappa \in \mathscr{T}_h$, we first introduce the following family of (overlapping) simplices associated with each face $F \subset \partial\kappa$. Note that this is precisely the reason why we require that each face F is a $(d-1)$-dimensional simplex.

Definition 7 For each element κ in the computational mesh $\mathscr{T}_h$, we define the family $\mathscr{F}_\flat^\kappa$ of all possible d-dimensional simplices contained in κ and having at least one face in common with κ. Moreover, we write $\kappa_\flat^F$ to denote a simplex belonging to $\mathscr{F}_\flat^\kappa$ which shares with $\kappa \in \mathscr{T}_h$ the specific face $F \subset \partial\kappa$.

With the above definition, we may now employ (3.1) directly to deduce the corresponding inverse estimate on a general polytopic element. To this end, given $\kappa \in \mathscr{T}_h$, and the face $F \in \mathscr{F}_h$, such that $F \subset \partial\kappa$, consider $\kappa_\flat^F \in \mathscr{F}_\flat^\kappa$ given in Definition 7. Then, for $v \in \mathscr{P}_p(\kappa)$, applying (3.1) on $\kappa_\flat^F$, we immediately deduce that

$$\|v\|^2_{L^2(F)} \leq C_{\mathrm{inv},1} p^2 \frac{|F|}{|\kappa_\flat^F|} \|v\|^2_{L^2(\kappa_\flat^F)} \leq C_{\mathrm{inv},1} p^2 \frac{|F|}{|\kappa_\flat^F|} \|v\|^2_{L^2(\kappa)}, \tag{3.5}$$

where $C_{\mathrm{inv},1}$ is a positive constant, independent of v, $|F|$, $|\kappa_\flat^F|$, and p. Clearly, the choice of $\kappa_\flat^F$ is not unique; thereby, we may select $\kappa_\flat^F$ to have the largest possible measure $|\kappa_\flat^F|$. Hence, on the basis of (3.5), the following inverse inequality holds:

$$\|v\|^2_{L^2(F)} \leq C_{\mathrm{inv},1} p^2 \frac{|F|}{\sup_{\kappa_\flat^F \subset \kappa} |\kappa_\flat^F|} \|v\|^2_{L^2(\kappa)}. \tag{3.6}$$

For a fixed element size h_κ, the inverse inequality (3.6) is sharp with respect to the polynomial degree p, cf. [172]. However, for fixed polynomial order p, (3.6) lacks sharpness with respect to $(d-k)$-dimensional facet degeneration, $k = 1, \ldots, d-1$; or more precisely, it is not sensitive to the magnitude of the face measure relative to the measure of the polytopic element κ. To illustrate this in a clear manner, we consider the two-dimensional example presented in [54].

Example 8 In order to demonstrate the lack of sharpness of the inverse inequality (3.6) with respect to one of its lower-dimensional facets degenerating, we consider the quadrilateral domain κ given by

$$\kappa := \{(x,y) \in \mathbb{R}^2 : x > 0, y > 0, x+y < 1\} \cup \{(x,y) \in \mathbb{R}^2 : x > 0, y \leq 0, x-y < \epsilon\},$$

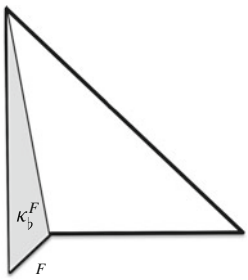

Fig. 3.2 Illustration of the quadrilateral in Example 8

for some $\epsilon > 0$, cf. Fig. 3.2. Given $v \in \mathscr{P}_p(\kappa)$, let $F := \{(x, y) \in \mathbb{R}^2 : x - y = \epsilon\}$, then exploiting (3.6) gives

$$\|v\|^2_{L^2(F)} \leq C_{\text{inv},1} \frac{\sqrt{2}p^2\epsilon}{|\kappa_\flat^F|} \|v\|^2_{L^2(\kappa)}, \tag{3.7}$$

where

$$\kappa_\flat^\kappa := \{(x, y) \in \mathbb{R}^2 : x > 0,\ x + \epsilon y < \epsilon,\ x - y < \epsilon\}.$$

Noting that $|\kappa_\flat^F| = \epsilon(1 + \epsilon)/2$, inequality (3.7) becomes

$$\|v\|^2_{L^2(F)} \leq C_{\text{inv},1} \frac{2\sqrt{2}p^2}{1 + \epsilon} \|v\|^2_{L^2(\kappa)}.$$

Hence, if we let $\epsilon \to 0$, the left-hand side $\|v\|^2_{L^2(F)} \to 0$, whereas the right-hand side $\frac{2\sqrt{2}p^2}{1+\epsilon}\|v\|^2_{L^2(\kappa)} \to 2\sqrt{2}p^2\|v\|^2_{L^2(\kappa)} \neq 0$ in general.

The above example clearly indicates that the inverse inequality (3.6) may not be sharp with respect to element facets of degenerating measure. In the context of employing such a bound to deduce the stability of the DGFEM approximation of a given second-order elliptic PDE, cf. Sects. 4.2.1, 4.3.1, and 5.2 below, this will typically lead to an excessively large penalization term within the underlying scheme; this in turn may result in ill conditioning of the resulting system of equations.

To address this issue, we proceed by deriving an alternative inverse inequality under suitable mesh assumptions. We begin by observing that, since $F \subset \partial\kappa_\flat^F$, we have

$$\|v\|^2_{L^2(F)} \leq |F| \|v\|^2_{L^\infty(\kappa_\flat^F)}. \tag{3.8}$$

In order to bound the right-hand side of (3.8), we need to introduce some additional requirements on the elements $\kappa \in \mathscr{T}_h$. These are based on the following result which represents the generalization of Lemma 3.7 in [99].

Lemma 9 *Let K be a shape-regular simplex in $\mathbb{R}^d$, $d = 2, 3$. Then, for each $v \in \mathscr{P}_p(K)$, there exists a simplex $\hat{\kappa} \subset K$, having the same shape as K and faces parallel to the faces of K, with $\operatorname{dist}(\partial\hat{\kappa}, \partial K) > C_{as} \operatorname{diam}(K)/p^2$, where C_{as} is a positive constant, independent of v, K, and p, such that*

$$\|v\|_{L^2(\hat{\kappa})} \geq \frac{1}{2}\|v\|_{L^2(K)}.$$

Here, we recall that $\operatorname{dist}(\partial\hat{\kappa}, \partial K)$ *denotes the Haussdorff distance between $\partial\hat{\kappa}$ and ∂K, cf.* (1.1)*.*

Proof For simplicity, here we present the proof for the case when K is a triangle, i.e., $d = 2$; the generalisation to tetrahedral elements in $\mathbb{R}^3$ follows in an analogous fashion, cf. the proof of Lemma 3.7 in [99] for further details.

We first consider the case when K is the reference triangle with vertices $(0, 0), (1, 0)$, and $(0, 1)$. Thereby, we may introduce the splitting of K into four disjoint subdomains as follows, cf. Fig. 3.3: we first let $\hat{\kappa}$ be the triangle having the same shape as K, with faces parallel to K, such that $\operatorname{dist}(\partial\hat{\kappa}, \partial K) = \delta$. Then, we split $K\backslash\hat{\kappa}$ into the three disjoint parts $\{\hat{\kappa}_i\}_{i=1}^3$ depicted in Fig. 3.3. For $\hat{\kappa}_1$, we have

$$\begin{aligned}
\|v\|^2_{L^2(\hat{\kappa}_1)} &= \int_0^{\delta}\int_0^{1/2} v^2(x,y)\,\mathrm{d}x\,\mathrm{d}y + \int_{\delta}^{1/2}\int_0^{\delta} v^2(x,y)\,\mathrm{d}x\,\mathrm{d}y \\
&\leq \int_0^{1/2} \delta\|v(x,\cdot)\|^2_{L^\infty(0,\delta)}\,\mathrm{d}x + \int_{\delta}^{1/2} \delta\|v(\cdot,y)\|^2_{L^\infty(0,\delta)}\,\mathrm{d}y \\
&\leq \int_0^{1/2} \delta\|v(x,\cdot)\|^2_{L^\infty(0,1/2)}\,\mathrm{d}x + \int_0^{1/2} \delta\|v(\cdot,y)\|^2_{L^\infty(0,1/2)}\,\mathrm{d}y \\
&\leq 4\delta C_{\mathrm{inv},2} p^2 \|v\|^2_{L^2(A_1)}, \qquad (3.9)
\end{aligned}$$

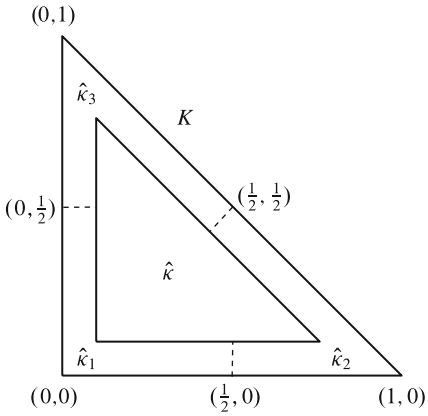

Fig. 3.3 Splitting triangle K into $\hat{\kappa}$ and $\{\hat{\kappa}_i\}_{i=1}^3$

where $A_1 = (0, 1/2)^2$; in the last inequality we have used the one-dimensional analogue of the inverse inequality (3.2).

For $\hat{\kappa}_2$, we make the linear change of variables $(x, y) \to (\tilde{x}, \tilde{y})$, where $\tilde{x} = x + y$ and $\tilde{y} = y$. Then, we have

$$\begin{aligned}
\|v\|^2_{L^2(\hat{\kappa}_2)} &= \int_0^{\delta} \int_{1/2}^{1} v^2(\tilde{x} - \tilde{y}, \tilde{y})\, \mathrm{d}\tilde{x}\, \mathrm{d}\tilde{y} + \int_{\delta}^{1/2} \int_{1-\delta}^{1} v^2(\tilde{x} - \tilde{y}, \tilde{y})\, \mathrm{d}\tilde{x}\, \mathrm{d}\tilde{y} \\
&\leq \int_{1/2}^{1} \delta \|v(\tilde{x} - \cdot, \cdot)\|^2_{L^\infty(0,\delta)}\, \mathrm{d}\tilde{x} + \int_{\delta}^{1/2} \delta \|v(\cdot - \tilde{y}, \tilde{y})\|^2_{L^\infty(1-\delta,1)}\, \mathrm{d}\tilde{y} \\
&\leq \int_{1/2}^{1} \delta \|v(\tilde{x} - \cdot, \cdot)\|^2_{L^\infty(0,1/2)}\, \mathrm{d}\tilde{x} + \int_{0}^{1/2} \delta \|v(\cdot - \tilde{y}, \tilde{y})\|^2_{L^\infty(1/2,1)}\, \mathrm{d}\tilde{y} \\
&\leq 4\delta C_{\mathrm{inv},2} p^2 \|v\|^2_{L^2(A_2)}, \qquad (3.10)
\end{aligned}$$

where A_2 denotes the parallelogram with vertices $(1/2, 0), (1, 0), (1/2, 1/2), (0, 1/2)$.

For $\hat{\kappa}_3$, we make the change of variables $(x, y) \to (\tilde{x}, \tilde{y})$, where $\tilde{x} = x$ and $\tilde{y} = x + y$. Then, in an analogous fashion to the case of $\hat{\kappa}_2$, we obtain

$$\|v\|^2_{L^2(\hat{\kappa}_3)} \leq 4\delta C_{\mathrm{inv},2} p^2 \|v\|^2_{L^2(A_3)}, \qquad (3.11)$$

where A_3 denotes the parallelogram with vertices $(1/2, 0), (1/2, 1/2), (0, 1), (0, 1/2)$. Combining (3.9)–(3.11), we note that

$$\|v\|^2_{L^2(K\setminus\hat{\kappa})} \leq 12\delta C_{\mathrm{inv},2} p^2 \|v\|^2_{L^2(K)}.$$

Selecting $\delta = (16 C_{\mathrm{inv},2} p^2)^{-1}$, gives $\|v\|^2_{L^2(K\setminus\hat{\kappa})} \leq 3/4 \|v\|^2_{L^2(K)}$; thereby, we deduce that

$$\|v\|^2_{L^2(\hat{\kappa})} = \|v\|^2_{L^2(K)} - \|v\|^2_{L^2(K\setminus\hat{\kappa})} \geq \|v\|^2_{L^2(K)} - \frac{3}{4}\|v\|^2_{L^2(K)} = \frac{1}{4}\|v\|^2_{L^2(K)}.$$

For general triangles K in $\mathbb{R}^2$, by employing standard scaling arguments, it is easy to observe that the above inequality holds for all $\hat{\kappa} \subset K$ such that $\mathrm{dist}(\partial\hat{\kappa}, \partial K) \leq C\,\mathrm{diam}(K)/p^2$, where C is a positive constant which only depends on the shape-regularity of K. Thereby, it follows that there exists another constant $C_{as} > 0$ such that, for any K, we can find a simplex $\hat{\kappa}$ contained in K, with $\mathrm{dist}(\partial\hat{\kappa}, \partial K) > C_{as}\,\mathrm{diam}(K)/p^2$, such that $\|v\|_{L^2(\hat{\kappa})} \geq 1/2 \|v\|_{L^2(K)}$, as required.

Motivated by the result of Lemma 9, we introduce the following definition.

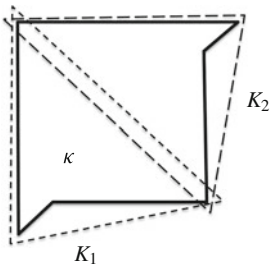

Fig. 3.4 Illustration of a covering of a polygon, cf. Definition 10: this polygon is p-coverable for p sufficiently small, but not for all p

Definition 10 An element $\kappa \in \mathscr{T}_h$ is said to be *p-coverable* with respect to $p \in \mathbb{N}$, if there exists a set of m_κ overlapping shape-regular simplices K_i, $i = 1, \ldots, m_\kappa$, $m_\kappa \in \mathbb{N}$, such that

$$\operatorname{dist}(\kappa, \partial K_i) < C_{as} \frac{\operatorname{diam}(K_i)}{p^2}, \qquad \text{and} \qquad |K_i| \geq c_{as}|\kappa| \tag{3.12}$$

for all $i = 1, \ldots, m_\kappa$, where C_{as} and c_{as} are positive constants, independent of κ and $\mathscr{T}_h$.

Following [54], in Fig. 3.4 we present a polygonal element κ in $\mathbb{R}^2$ which may be covered by two triangles K_1 and K_2, i.e., $m_\kappa = 2$. We observe that Definition 10 admits very general polytopic elements $\kappa \in \mathscr{T}_h$ which may contain $(d-k)$-dimensional facets, $k = 1, \ldots, d-1$, whose measure is arbitrarily small, relative to the measure of κ itself. Returning to Example 8, we note that the quadrilateral element κ depicted in Fig. 3.2 is p-coverable when $\epsilon < C_{as}/p^2$ for some constant $C_{as} > 0$.

Equipped with (3.6), (3.8), Lemma 9, and Definition 10, we are now in a position to present the following *hp*-version inverse inequality for general polytopic elements which directly accounts for elemental facet degeneration.

Lemma 11 *Let $\kappa \in \mathscr{T}_h$, $F \subset \partial\kappa$ denote one of its faces. Then, for each $v \in \mathscr{P}_p(\kappa)$, the following inverse inequality holds*

$$\|v\|^2_{L^2(F)} \leq C_{\mathrm{INV}}(p, \kappa, F) p^2 \frac{|F|}{|\kappa|} \|v\|^2_{L^2(\kappa)}, \tag{3.13}$$

where

$$C_{\mathrm{INV}}(p, \kappa, F) := \begin{cases} C_{\mathrm{inv},4} \min\left\{ \dfrac{|\kappa|}{\sup_{\kappa_\flat^F \subset \kappa} |\kappa_\flat^F|}, p^{2(d-1)} \right\}, & \text{if } \kappa \text{ is } p\text{-coverable}, \\ C_{\mathrm{inv},1} \dfrac{|\kappa|}{\sup_{\kappa_\flat^F \subset \kappa} |\kappa_\flat^F|}, & \text{otherwise}, \end{cases} \tag{3.14}$$

and with $\kappa_\flat^F \in \mathscr{F}_\flat^\kappa$ as in Definition 7. Furthermore, $C_{\mathrm{inv},1}$ and $C_{\mathrm{inv},4}$ are positive constants which are independent of $|\kappa|/\sup_{\kappa_\flat^F \subset \kappa} |\kappa_\flat^F|$, $|F|$, p, and v.

Proof If κ is not p-coverable, then the above inverse inequality follows immediately from the bound (3.6). Thereby, we now consider the case when κ is p-coverable. In this case, we proceed by further bounding (3.8); hence we require a bound for $\|v\|_{L^\infty(\kappa_\flat^F)}$ for all $\kappa_\flat^F \in \mathscr{F}_\flat^\kappa$. Recalling Definition 10, the element κ may be covered by shape-regular simplices K_i, $i = 1, \ldots, m_\kappa$. Hence, given $\kappa_\flat^F \in \mathscr{F}_\flat^\kappa$, $F \subset \partial\kappa$, cf. Definition 7, we note that

$$\kappa_\flat^F \subset \kappa \subset \cup_{i=1}^{m_\kappa} K_i,$$

with $|K_i| \geq c_{as}|\kappa|$, $i = 1, \ldots, m_\kappa$.

Employing the inverse estimate (3.2) on each K_i, $i = 1, \ldots, m_\kappa$, together with Definition 10, we deduce that

$$\begin{aligned}\|v\|^2_{L^\infty(\kappa_\flat^F)} &\leq \max_{i=1,\ldots,m_\kappa} \|v\|^2_{L^\infty(K_i)} \\ &\leq C_{\mathrm{inv},2} p^{2d} \max_{i=1,\ldots,m_\kappa} \frac{\|v\|^2_{L^2(K_i)}}{|K_i|} \\ &\leq \frac{C_{\mathrm{inv},2}}{c_{as}} \frac{p^{2d}}{|\kappa|} \max_{i=1,\ldots,m_\kappa} \|v\|^2_{L^2(K_i)}. \end{aligned} \tag{3.15}$$

We now define $\hat{\kappa}_i \subset K_i$ to denote the simplex relative to K_i defined in Lemma 9; hence, exploiting Lemma 9 and Definition 10, and noting that, by construction, $\hat{\kappa}_i \subset \kappa \cap K_i \subset K_i$ and, trivially, $K_i \cap \kappa \subset \kappa$, for each $i = 1, \ldots, m_\kappa$, we deduce that

$$\frac{1}{4}\|v\|^2_{L^2(K_i)} \leq \|v\|^2_{L^2(\hat{\kappa}_i)} \leq \|v\|^2_{L^2(K_i \cap \kappa)} \leq \|v\|^2_{L^2(\kappa)}. \tag{3.16}$$

Combining (3.15) and (3.16), we arrive at the inequality

$$\|v\|^2_{L^\infty(\kappa_\flat^F)} \leq \frac{4\, C_{\mathrm{inv},2}}{c_{as}} \frac{p^{2d}}{|\kappa|} \|v\|^2_{L^2(\kappa)}. \tag{3.17}$$

Inserting (3.17) into (3.8) gives

$$\|v\|^2_{L^2(F)} \leq \frac{4\, C_{\mathrm{inv},2}}{c_{as}} \frac{|F|}{|\kappa|} p^{2d} \|v\|^2_{L^2(\kappa)}. \tag{3.18}$$

Taking the minimum between (3.6) and (3.18), we deduce the desired result, with a positive constant $C_{\mathrm{inv},4} = \max\{C_{\mathrm{inv},1}, 4\, C_{\mathrm{inv},2}/c_{as}\}$. □

Remark 12 For a fixed mesh size, the inverse inequality stated in (3.13) is sharp with respect to the polynomial degree p; indeed, for a p-coverable element κ, $\kappa \in \mathscr{T}_h$, as $p \to \infty$ the minimum in (3.14) will be equal to $|\kappa| / \sup_{\kappa_\flat^F \subset \kappa} |\kappa_\flat^F|$. Moreover, (3.13) is sensitive with respect to $(d-k)$-dimensional facet degeneration,

$k = 1, \ldots, d-1$. Indeed, recalling Example 8, we observe that the left- and right-hand sides of (3.13) degenerate at the same rate as $\epsilon \to 0$, for fixed p.

We conclude this section by presenting a further inverse inequality which provides a bound on the $H^1(\kappa)$-norm of a polynomial function v, $\kappa \in \mathscr{T}_h$, with respect to the $L^2(\kappa)$-norm of v, thereby, extending the estimate (3.3) stated for simplices to general polytopes; this result will be required to deduce the inf-sup estimate derived in Theorem 42. As expected, it is now necessary to assume shape-regularity of the polytopic mesh $\mathscr{T}_h$.

Assumption 13 *The subdivision $\mathscr{T}_h$ is shape-regular, cf. Definition 2, i.e., there exists a positive constant C_{r}, independent of the mesh parameters, such that*

$$\forall \kappa \in \mathscr{T}_h, \quad \frac{h_\kappa}{\rho_\kappa} \leq C_{\mathrm{r}}.$$

Lemma 14 *Given that Assumption 13 is satisfied, then, for any $\kappa \in \mathscr{T}_h$ which is p-coverable and $v \in \mathscr{P}_p(\kappa)$, the following inverse inequality holds*

$$\|\nabla v\|^2_{L^2(\kappa)} \leq C_{\mathrm{inv},5} \frac{p^4}{h_\kappa^2} \|v\|^2_{L^2(\kappa)}, \tag{3.19}$$

where $C_{\mathrm{inv},5}$ is a positive constant, which is independent of v, h_κ, and p, but depends on the shape-regularity constant of the covering of κ.

Proof From Definition 10 there exists a covering of κ by shape-regular simplices K_i, $i = 1, \ldots, m_\kappa$, such that $|K_i| \geq c_{as}|\kappa|$, $i = 1, \ldots, m_\kappa$. Thereby, we note that the following inequalities hold for $i = 1, \ldots, m_\kappa$:

$$h_{K_i}^d \geq |K_i| \geq c_{as}|\kappa| \geq c_{as}\rho_\kappa^d \geq \frac{c_{as}}{C_{\mathrm{r}}^d} h_\kappa^d,$$

from which we deduce

$$h_{K_i} \geq \frac{c_{as}^{1/d}}{C_{\mathrm{r}}} h_\kappa,$$

for $i = 1, \ldots, m_\kappa$. Employing (3.3) and Definition 10 gives

$$\begin{aligned} \|\nabla v\|^2_{L^2(\kappa)} \leq \sum_{i=1}^{m_\kappa} \|\nabla v\|^2_{L^2(K_i)} &\leq C_{\mathrm{inv},3} \sum_{i=1}^{m_\kappa} \frac{p^4}{h_{K_i}^2} \|v\|^2_{L^2(K_i)} \\ &\leq \frac{C_{\mathrm{inv},3} C_{\mathrm{r}}^2}{c_{as}^{2/d}} \frac{p^4}{h_\kappa^2} \sum_{i=1}^{m_\kappa} \|v\|^2_{L^2(K_i)}. \end{aligned} \tag{3.20}$$

Recalling (3.16) in the proof of Lemma 11, inequality (3.20) yields

$$\|\nabla v\|^2_{L^2(\kappa)} \leq \frac{4\, C_{\mathrm{inv},3} C_{\mathrm{r}}^2 m_\kappa}{c_{as}^{2/d}} \frac{p^4}{h_\kappa^2} \|v\|^2_{L^2(\kappa)},$$

as required. Thereby, the statement of the lemma holds with

$$C_{\mathrm{inv},5} = 4\, C_{\mathrm{inv},3} C_{\mathrm{r}}^2 m_\kappa / c_{as}^{2/d}.$$

Remark 15 We note that polytopic elements which admit a uniformly-bounded shape-regular simplicial sub-partition, i.e., regular polytopes which do not contain degenerating $(d-k)$-dimensional facets, $k = 1, 2, \ldots, d-1$, are trivially p-coverable for any p. In this special case, the inverse estimate given in Lemma 14 can be directly derived, without the need to employ Lemma 9, cf. [57, 80]. More precisely, consider the subset of polytopic elements $\kappa \in \mathscr{T}_h$ admitting a sub-partition into at most n_κ, $n_\kappa \in \mathbb{N}$, shape-regular simplices $\mathfrak{s}_i$, $i = 1, 2, \ldots, n_\kappa$, such that $|\mathfrak{s}_i| \geq c_{\mathfrak{s}} |\kappa|$, $i = 1, \ldots, n_\kappa$, where $c_{\mathfrak{s}}$ is a positive constant, independent of κ and $\mathscr{T}_h$. For any such κ, following the steps in the proof of Lemma 14 but exploiting, this time, the sub-partition, yields

$$\|\nabla v\|^2_{L^2(\kappa)} = \sum_{i=1}^{n_\kappa} \|\nabla v\|^2_{L^2(\mathfrak{s}_i)} \leq \frac{C_{\mathrm{inv},3} C_{\mathrm{r}}^2}{c_{\mathfrak{s}}^{2/d}} \frac{p^4}{h_\kappa^2} \|v\|^2_{L^2(\kappa)}; \tag{3.21}$$

here, we have used the inequality $h_{\mathfrak{s}_i} \geq (c_{\mathfrak{s}}^{1/d}/C_{\mathrm{r}})\, h_\kappa$, for $i = 1, \ldots, n_\kappa$, where $h_{\mathfrak{s}_i} := \mathrm{diam}(\mathfrak{s}_i)$, $i = 1, \ldots, n_\kappa$. Hence, (3.19) holds with $C_{\mathrm{inv},5} = C_{\mathrm{inv},3} C_{\mathrm{r}}^2 / c_{\mathfrak{s}}^{2/d}$.

Remark 16 Assumption 13, which imposes a shape-regularity condition on the mesh $\mathscr{T}_h$, is *only* needed for the proof of Lemma 14. This result extends the classical inverse estimate, bounding the H^1-seminorm of a polynomial function with its L^2-norm on a simplex (3.3), to polytopic elements. Such inverse estimates depend on the shape-regularity of the elements, even in the case of simplicial elements, cf. [169]. Assumption 13 and Lemma 14 are only used for proving the inf-sup stability result derived in Chap. 5, cf. Theorem 42.

3.3 *hp*-Approximation Bounds

For the approximation theory on polytopic domains presented below, we require the existence of a suitable covering of the mesh by an overlapping set of simplices in $\mathbb{R}^d$.

Definition 17 We define the *covering* $\mathscr{T}_h^\sharp = \{\mathscr{K}\}$ related to the computational mesh $\mathscr{T}_h$ as a set of open shape-regular d-simplices $\mathscr{K}$, such that, for each $\kappa \in \mathscr{T}_h$,

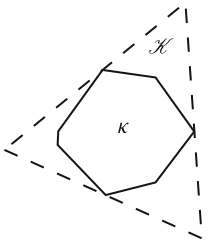

Fig. 3.5 Polygonal element κ, $\kappa \in \mathscr{T}_h$, in $\mathbb{R}^2$ and the corresponding simplex $\mathscr{K} \in \mathscr{T}_h^\sharp$, $\kappa \subset \mathscr{K}$

there exists a $\mathscr{K} \in \mathscr{T}_h^\sharp$, such that $\kappa \subset \mathscr{K}$. Given $\mathscr{T}_h^\sharp$, we denote by $\Omega_\sharp$ the *covering domain* given by $\bar{\Omega}_\sharp := \cup_{\mathscr{K} \in \mathscr{T}_h^\sharp} \bar{\mathscr{K}}$.

In Fig. 3.5 we show a single polygonal element κ, $\kappa \in \mathscr{T}_h$, in $\mathbb{R}^2$ and the corresponding simplex $\mathscr{K} \in \mathscr{T}_h^\sharp$, such that $\kappa \subset \mathscr{K}$. With the definition of the simplicial covering $\mathscr{T}_h^\sharp$ associated with the computational mesh $\mathscr{T}_h$ given in Definition 17, we make the following key assumption regarding the amount of allowable overlap between elements in $\mathscr{T}_h$ and the simplices present in $\mathscr{T}_h^\sharp$.

Assumption 18 *We assume that there exists a covering $\mathscr{T}_h^\sharp$ of $\mathscr{T}_h$ and a positive constant $\mathscr{O}_\Omega$, independent of the mesh parameters, such that*

$$\max_{\kappa \in \mathscr{T}_h} card\Big\{\kappa' \in \mathscr{T}_h : \kappa' \cap \mathscr{K} \neq \emptyset,\ \mathscr{K} \in \mathscr{T}_h^\sharp \ \text{such that}\ \kappa \subset \mathscr{K}\Big\} \leq \mathscr{O}_\Omega,$$

and

$$h_{\mathscr{K}} := \operatorname{diam}(\mathscr{K}) \leq C_{\text{diam}} h_\kappa,$$

for each pair $\kappa \in \mathscr{T}_h$, $\mathscr{K} \in \mathscr{T}_h^\sharp$, with $\kappa \subset \mathscr{K}$, for a constant $C_{\text{diam}} > 0$, uniformly with respect to the mesh size.

Remark 19 Assumption 18 requires shape-regularity of the mesh covering $\mathscr{T}_h^\sharp$, but *not* shape-regularity of the computational mesh $\mathscr{T}_h$ itself. We refer to Fig. 3.6 for an example of how the two shape-regularity concepts may differ substantially.

To derive appropriate *hp*-version approximation estimates on general polytopic elements κ, $\kappa \in \mathscr{T}_h$, we observe that standard results, for example, from [25, 26, 156] are applicable by noting that each κ is a subset of a d-simplex belonging to the covering $\mathscr{T}_h^\sharp$ and that the local finite element spaces will consist of polynomials *without* the use of element mappings to a reference/canonical element. With this in mind, we recall the following standard *hp*-approximation results on d-simplices.

Lemma 20 ([25, 26]) *Let T be a simplex in $\mathbb{R}^d$, $d = 2, 3$, with diameter h_T. Suppose further that $v|_T \in H^l(T)$, for some $l \geq 0$. Then, for $p \in \mathbb{N}$, there exists $\Pi_p v \in \mathscr{P}_p(T)$, such that*

$$\|v - \Pi_p v\|_{H^q(T)} \leq C_{\text{I},1} \frac{h_T^{s-q}}{p^{l-q}} \|v\|_{H^l(T)}, \quad l \geq 0, \tag{3.22}$$

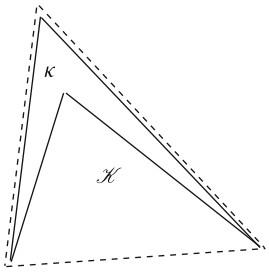

Fig. 3.6 Polygonal element κ, $\kappa \in \mathcal{T}_h$, in $\mathbb{R}^2$ and the corresponding simplex $\mathcal{K} \in \mathcal{T}_h^\sharp$, $\kappa \subset \mathcal{K}$; the covering simplex $\mathcal{K}$ has fixed shape-regularity constant, while κ's shape-regularity constant can become arbitrarily large by moving the two upper vertices closer together

for $0 \le q \le l$, *and*

$$\|v - \Pi_p v\|_{L^\infty(T)} \le C_{\mathrm{I},2} \frac{h_T^{s-d/2}}{p^{l-d/2}} \|v\|_{H^l(T)}, \quad l > d/2. \tag{3.23}$$

Here, $s = \min\{p+1, l\}$ *and* $C_{\mathrm{I},1}$ *and* $C_{\mathrm{I},2}$ *are positive constants which depend on the shape-regularity of* T, *but are independent of* v, h_T, *and* p.

In order to extend Lemma 20 to the case of general polytopic elements, we first note that functions defined on Ω can be extended to the covering domain $\Omega_\sharp$ using the following classical extension operator.

Theorem 21 ([162]) *Let* Ω *be a domain with a Lipschitz boundary. Then there exists a linear extension operator* $\mathfrak{E} : H^s(\Omega) \mapsto H^s(\mathbb{R}^d)$, $s \in \mathbb{N}_0$, *such that* $\mathfrak{E}v|_\Omega = v$ *and*

$$\|\mathfrak{E}v\|_{H^s(\mathbb{R}^d)} \le C_{\mathfrak{E}} \|v\|_{H^s(\Omega)},$$

where $C_{\mathfrak{E}}$ *is a positive constant depending only on* s *and* Ω.

The assumptions stated in Theorem 21 on the domain Ω may be weakened. Indeed, [162] only requires that Ω is a domain with a minimally smooth boundary; the extension to domains which are simply connected, but may contain microscales, is treated in [154].

We also recall the following multiplicative trace inequality.

Lemma 22 *Given a simplex* T *in* $\mathbb{R}^d$, $d = 2, 3$, *we write* $F \subset \partial T$ *to denote one of its faces. Then, given* $v \in H^1(T)$, *the following inequality holds:*

$$\|v\|_{L^2(F)}^2 \le C_t \frac{|F|}{|T|} \left(\|v\|_{L^2(T)}^2 + h_T \|v\|_{L^2(T)} \|\nabla v\|_{L^2(T)} \right), \tag{3.24}$$

where C_t *is a positive constant which depends on* d, *but is independent of* v, h_T, $|T|$, $|F|$, *and the shape-regularity of* T.

Proof See, for example, Lemma 1.49 in [79], or [61, 139], yielding (3.24) with $C_t := \max(1, 2/d)$; clearly, for $d = 2, 3$, we have that $C_t = 1$.

Given the projection operator Π_p defined in Lemma 20 and the extension operator $\mathfrak{E}$ given in Theorem 21, we now proceed to define a suitable projection operator on a general polytopic element κ, $\kappa \in \mathcal{T}_h$. To this end, for $v \in L^2(\Omega)$, we define $\tilde{\Pi}_p v \in \mathcal{P}_p(\kappa)$ as follows: for each $\kappa \in \mathcal{T}_h$, given the associated element $\mathscr{K} \in \mathcal{T}_h^\sharp$, such that $\kappa \subset \mathscr{K}$, cf. Definition 17, we write

$$\tilde{\Pi}_p v := \Pi_p(\mathfrak{E}v|_{\mathscr{K}})|_\kappa, \tag{3.25}$$

where $\Pi_p : L^2(\mathscr{K}) \to \mathcal{P}_p(\mathscr{K})$ is defined in Lemma 20. With this definition, we now state the following *hp*-version approximation bounds.

Lemma 23 *Let $\kappa \in \mathcal{T}_h$, $F \subset \partial\kappa$ denote one of its faces, and $\mathscr{K} \in \mathcal{T}_h^\sharp$ be the corresponding simplex, such that $\kappa \subset \mathscr{K}$, cf. Definition 17. Suppose that $v \in L^2(\Omega)$ is such that $\mathfrak{E}v|_{\mathscr{K}} \in H^{l_\kappa}(\mathscr{K})$, for some $l_\kappa \geq 0$. Then, given Assumption 18 is satisfied, the following bounds hold*

$$\|v - \tilde{\Pi}_p v\|_{H^q(\kappa)} \leq C_{\mathrm{I},3} \frac{h_\kappa^{s_\kappa - q}}{p^{l_\kappa - q}} \|\mathfrak{E}v\|_{H^{l_\kappa}(\mathscr{K})}, \quad l_\kappa \geq 0, \tag{3.26}$$

for $0 \leq q \leq l_\kappa$, and

$$\|v - \tilde{\Pi}_p v\|_{L^2(F)} \leq C_{\mathrm{I},4} |F|^{1/2} \frac{h_\kappa^{s_\kappa - d/2}}{p^{l_\kappa - 1/2}} C_m(p, \kappa, F)^{1/2} \|\mathfrak{E}v\|_{H^{l_\kappa}(\mathscr{K})}, \; l_\kappa > d/2, \tag{3.27}$$

where

$$C_m(p, \kappa, F) = \min\left\{ \frac{h_\kappa^d}{\sup_{\kappa_\flat^F \subset \kappa} |\kappa_\flat^F|}, p^{d-1} \right\},$$

$s_\kappa = \min\{p + 1, l_\kappa\}$ and $C_{\mathrm{I},3}$ and $C_{\mathrm{I},4}$ are positive constants, which depend on the shape-regularity of $\mathscr{K}$, but are independent of v, h_κ, and p.

Proof To prove (3.26), we note that

$$\|v - \tilde{\Pi}_p v\|_{H^q(\kappa)} = \|\mathfrak{E}v - \Pi_p(\mathfrak{E}v)\|_{H^q(\kappa)} \leq \|\mathfrak{E}v - \Pi_p(\mathfrak{E}v)\|_{H^q(\mathscr{K})}.$$

Thereby, upon application of (3.22) and noting that Assumption 18 holds, the desired bound follows immediately with $C_{\mathrm{I},3} = C_{\mathrm{I},1} C_{\mathrm{diam}}^{s_\kappa - q}$.

To prove (3.27), we let $\kappa_\flat^F \in \mathscr{F}_\flat^\kappa$, cf. Definition 7; then, applying the multiplicative trace inequality (3.24), together with (3.26), and noting that $\kappa_\flat^F \subset \kappa$, we obtain

$$\begin{aligned}\|v-\tilde{\Pi}_p v\|_{L^2(F)}^2 &\le C_{\mathrm{t}}\frac{|F|}{|\kappa_\flat^F|}\Big(\|v-\tilde{\Pi}_p v\|_{L^2(\kappa_\flat^F)}^2\\ &\qquad + h_{\kappa_\flat^F}\|v-\tilde{\Pi}_p v\|_{L^2(\kappa_\flat^F)}\|\nabla(v-\tilde{\Pi}_p v)\|_{L^2(\kappa_\flat^F)}\Big)\\ &\le C_{\mathrm{t}}\,C_{\mathrm{I},1}^2\,C_{\mathrm{diam}}^{2s_\kappa-1}\frac{|F|}{|\kappa_\flat^F|}\left(C_{\mathrm{diam}}\frac{h_\kappa}{p}+h_{\kappa_\flat^F}\right)\frac{h_\kappa^{2s_\kappa-1}}{p^{2l_\kappa-1}}\|\mathfrak{E}v\|_{H^{l_\kappa}(\mathscr{K})}^2. \quad (3.28)\end{aligned}$$

Given that $h_{\kappa_\flat^F} \le h_\kappa$ and $\kappa_\flat^F$ is arbitrary, from (3.28) we conclude that

$$\|v-\tilde{\Pi}v\|_{L^2(F)}^2 \le C_{\mathrm{t}}\,C_{\mathrm{I},1}^2\,C_{\mathrm{diam}}^{2s_\kappa-1}(C_{\mathrm{diam}}+1)\frac{|F|}{\sup_{\kappa_\flat^F\subset\kappa}|\kappa_\flat^F|}\frac{h_\kappa^{2s_\kappa}}{p^{2l_\kappa-1}}\|\mathfrak{E}v\|_{H^{l_\kappa}(\mathscr{K})}^2. \quad (3.29)$$

On the other hand, proceeding as in the proof of Lemma 11, we observe that

$$\|v-\tilde{\Pi}_p v\|_{L^2(F)}^2 \le |F|\|v-\tilde{\Pi}_p v\|_{L^\infty(F)}^2.$$

Hence, employing the definition of the projection operator $\tilde{\Pi}_p$, together with (3.23) and Assumption 18, we deduce that

$$\|v-\tilde{\Pi}_p v\|_{L^2(F)}^2 \le C_{\mathrm{I},2}^2\,C_{\mathrm{diam}}^{2s_\kappa-d}\,|F|\frac{h_\kappa^{2s_\kappa-d}}{p^{2l_\kappa-d}}\|\mathfrak{E}v\|_{H^{l_\kappa}(\mathscr{K})}^2, \quad (3.30)$$

for $l_\kappa > d/2$. Thereby, taking the minimum of the two bounds (3.29) and (3.30), the approximation result stated in (3.27) holds with

$$C_{\mathrm{I},4} = \max(C_{\mathrm{I},1}\,C_{\mathrm{diam}}^{s_\kappa-1/2}\sqrt{C_{\mathrm{t}}(C_{\mathrm{diam}}+1)},\,C_{\mathrm{I},2}C_{\mathrm{diam}}^{s_\kappa-d/2}).$$

Remark 24 We note that (3.29) is valid for $l_\kappa \ge 1$; for simplicity of presentation, we have omitted this level of generality in the statement of Lemma 23, since it is of no consequence to the proceeding work.

On the basis of the technical results developed above, in the following chapters we study the DGFEM discretization for a range of linear PDEs.

Chapter 4
DGFEMs for Pure Diffusion Problems

In this chapter we study the stability and *hp*-version a priori error analysis of the DGFEM discretization of a pure diffusion problem; referring back to (2.1), (2.3), this corresponds to the case when a is positive definite, $\mathbf{b} \equiv \mathbf{0}$, and $c \equiv 0$. In particular, we develop the underlying theory for two different sets of shape assumptions, which the polytopic elements forming the computational mesh $\mathscr{T}_h$ must satisfy. In the first instance, we assume that the number of faces each element κ, $\kappa \in \mathscr{T}_h$, possesses remains uniformly bounded under mesh refinement, but without the restriction of shape-regularity in the classical sense, cf. Assumption 25 below; see, also, [54]. We will then pursue the analysis in the case when this assumption is violated, i.e., when polytopic elements are permitted to have an arbitrary number of faces under mesh refinement; however, in this setting, a generalized shape-regularity assumption must be satisfied, cf. Assumption 30 below. This latter condition was first considered in [56]. The outline of this chapter is as follows. Upon recalling the diffusion model problem, we introduce the corresponding DGFEM in Sect. 4.1; the latter is based on the general scheme outlined in Sect. 2.4. For simplicity of presentation, here we focus on the symmetric version of the interior penalty DGFEM, though we stress that the analysis presented here naturally generalizes to both the IIP- and NIP-DGFEMs, as well as other DGFEMs proposed within the literature. Then, in Sects. 4.2 and 4.3 we pursue the error analysis under the two different mesh assumptions, respectively. Moreover, for the analysis of the second case, when elements with an arbitrary number of faces are permitted, we also prove the necessary trace inverse estimate, along with a polynomial approximation result. Finally, in Sect. 4.4 we discuss the relationship between these different mesh assumptions and conclude on the generality of polytopic meshes covered by our analysis.

A. Cangiani et al., *hp-Version Discontinuous Galerkin Methods on Polygonal and Polyhedral Meshes*, SpringerBriefs in Mathematics,
DOI 10.1007/978-3-319-67673-9_4

4.1 Model Problem and Discretization

Given an open bounded Lipschitz domain Ω in $\mathbb{R}^d$, $d \in \mathbb{N}$, with boundary $\partial\Omega$, we consider the following PDE boundary-value problem: find u such that

$$-\nabla \cdot (a\nabla u) = f \quad \text{in } \Omega, \tag{4.1}$$

$$u = g_{\mathrm{D}} \quad \text{on } \partial\Omega_{\mathrm{D}}, \tag{4.2}$$

$$\mathbf{n} \cdot (a\nabla u) = g_{\mathrm{N}} \quad \text{on } \partial\Omega_{\mathrm{N}}. \tag{4.3}$$

Here, $f \in L^2(\Omega)$, $a = \{a_{ij}\}_{i,j=1}^d$, with $a_{ij} \in L^\infty(\Omega)$ and $a_{ij} = a_{ji}$, for $i, j = 1, \ldots, d$, and, at each $\mathbf{x}$ in $\bar{\Omega}$,

$$\sum_{i,j=1}^{d} a_{ij}(\mathbf{x})\xi_i\xi_j \geq \theta|\boldsymbol{\xi}|^2 > 0, \tag{4.4}$$

where θ is a positive constant, for any vector $\boldsymbol{\xi} = (\xi_1, \ldots, \xi_d)$ in $\mathbb{R}^d$. Here, the boundary of the computational domain Ω is subdivided into the two disjoint subsets $\partial\Omega_{\mathrm{D}}$ and $\partial\Omega_{\mathrm{N}}$ whose union is $\partial\Omega$, with $\partial\Omega_{\mathrm{D}}$ nonempty and relatively open in $\partial\Omega$. The well-posedness of the boundary value problem (4.1)–(4.3), under the uniform ellipticity condition (4.4) can be deduced, based on employing the Lax-Milgram Theorem; see, for example, [42, 64].

As in Chap. 3, we write $\mathscr{T}_h$ to denote a subdivision of the computational domain $\Omega \subset \mathbb{R}^d$, $d > 1$, into disjoint open polytopic elements κ constructed such that $\bar{\Omega} = \cup_{\kappa\in\mathscr{T}_h}\bar{\kappa}$. Recalling that $\mathscr{F}_h$ denotes the set of open $(d-1)$-dimensional simplicial element faces associated with the computational mesh $\mathscr{T}_h$, employing the notation introduced in Chap. 2, we write $\mathscr{F}_h = \mathscr{F}_h^{\mathscr{I}} \cup \mathscr{F}_h^{\mathscr{B}}$, where $\mathscr{F}_h^{\mathscr{I}}$ denotes the set of interior element faces, and $\mathscr{F}_h^{\mathscr{B}}$ is the set of boundary element faces. For simplicity, we assume that $\mathscr{T}_h$ respects the decomposition of $\partial\Omega$ in the sense that each $F \in \mathscr{F}_h^{\mathscr{B}}$ belongs to the interior of exactly one of $\partial\Omega_{\mathrm{D}}$ or $\partial\Omega_{\mathrm{N}}$. Hence, we write $\mathscr{F}_h^D, \mathscr{F}_h^N \subset \mathscr{F}_h^{\mathscr{B}}$ to denote the subsets of boundary faces belonging to $\partial\Omega_{\mathrm{D}}, \partial\Omega_{\mathrm{N}}$, respectively.

To facilitate *hp*-adaptivity, to each element $\kappa \in \mathscr{T}_h$, we associate a local polynomial degree $p_\kappa \geq 1$, and collect the p_κ, $\kappa \in \mathscr{T}_h$, in the vector $\mathbf{p} := (p_\kappa : \kappa \in \mathscr{T}_h)$. With this notation, we define the finite element space $V^{\mathbf{p}}(\mathscr{T}_h)$ with respect to $\mathscr{T}_h$ and $\mathbf{p}$ by

$$V^{\mathbf{p}}(\mathscr{T}_h) := \{u \in L^2(\Omega) : u|_\kappa \in \mathscr{P}_{p_\kappa}(\kappa), \kappa \in \mathscr{T}_h\},$$

where, we recall that $\mathscr{P}_p(\kappa)$ denotes the space of polynomials of total degree p on κ. By construction, the local elemental polynomial spaces employed within the definition of $V^{\mathbf{p}}(\mathscr{T}_h)$ are defined in the physical space, without the need to map from a given reference or canonical frame, as is typically the case for classical FEMs; we refer to Chap. 6 concerning implementation aspects of the elementwise polynomial basis.

Following the derivation presented in Sect. 2.3, we recall the (SIP) DGFEM bilinear form

$$B_{\mathrm{d}}(w_h, v_h) := \sum_{\kappa \in \mathscr{T}_h} \int_\kappa a \nabla w_h \cdot \nabla v_h \, \mathrm{d}\mathbf{x} - \int_{\mathscr{F}_h^{\mathscr{I}} \cup \mathscr{F}_h^D} (\{\!\{a \nabla w_h\}\!\} \cdot [\![v_h]\!] + \{\!\{a \nabla v_h\}\!\} \cdot [\![w_h]\!] - \sigma [\![w_h]\!] \cdot [\![v_h]\!]) \, \mathrm{d}s,$$

and linear functional

$$\ell(v_h) := \sum_{\kappa \in \mathscr{T}_h} \int_\kappa f v_h \, \mathrm{d}\mathbf{x} - \int_{\mathscr{F}_h^D} g_{\mathrm{D}} (a \nabla v_h \cdot \mathbf{n} - \sigma v_h) \, \mathrm{d}s + \int_{\mathscr{F}_h^N} g_{\mathrm{N}} v_h \, \mathrm{d}s,$$

for $w_h, v_h \in V^{\mathbf{p}}(\mathscr{T}_h)$. Thereby, the corresponding DGFEM is given by: find $u_h \in V^{\mathbf{p}}(\mathscr{T}_h)$ such that

$$B_{\mathrm{d}}(u_h, v_h) = \ell(v_h) \tag{4.5}$$

for all $v_h \in V^{\mathbf{p}}(\mathscr{T}_h)$.

The well-posedness and stability properties of the above method depend on the choice of the discontinuity-penalization function σ. These are analyzed in the next two sections based on employing different assumptions on the elements present in the computational mesh $\mathscr{T}_h$. Clearly, we expect that the choice of σ will be sensitive to the size of each face F, $F \in \mathscr{F}_h$, relative to the size of the element(s) which form F. In order to focus on the treatment of general polytopic subdivisions, throughout this chapter, we make the simplifying assumption that the entries of a are constant on each element κ, $\kappa \in \mathscr{T}_h$, i.e.,

$$a \in [V^{\mathbf{0}}(\mathscr{T}_h)]^{d \times d}_{\mathrm{sym}}. \tag{4.6}$$

We note that the proceeding results follow immediately, with only very minor changes, in the case when $a \in [V^{\mathbf{q}}(\mathscr{T}_h)]^{d \times d}_{\mathrm{sym}}$, where $\mathbf{q} := (q_\kappa : \kappa \in \mathscr{T}_h)$, such that $q_\kappa \in \mathbb{N}_0$ for all $\kappa \in \mathscr{T}_h$. The extension of the analysis to general positive (semi-)definite diffusion tensors will be treated later on in Chap. 5 when we consider the DGFEM discretization of general second-order PDEs with nonnegative characteristic form.

4.2 Error Analysis I: Bounded Number of Element Faces

We study the stability and a priori error analysis of the DGFEM (4.5) under the following assumption, which guarantees that the number of faces each element possesses remains bounded under mesh refinement.

Assumption 25 (Limited Number of Faces) *For each element $\kappa \in \mathscr{T}_h$, we define*

$$C_\kappa := card\Big\{F \in \mathscr{F}_h : F \subset \partial\kappa\Big\}.$$

We assume there exists a positive constant C_F, independent of the mesh parameters, such that

$$\max_{\kappa \in \mathscr{T}_h} C_\kappa \leq C_F.$$

We stress that *no* shape-regularity condition is required to be satisfied by $\mathscr{T}_h$ for the analysis in this section to hold.

4.2.1 Well-Posedness of the DGFEM

Firstly, we write $\sqrt{a} \in [V^{\mathbf{0}}(\mathscr{T}_h)]^{d\times d}_{\text{sym}}$ to denote the unique (positive definite) square-root of the symmetric matrix a and $\bar{a}_\kappa := |\sqrt{a}|^2_2|_\kappa$, $\kappa \in \mathscr{T}_h$, where $|\cdot|_2$ denotes the matrix norm subordinate to the l_2-vector norm on $\mathbb{R}^d$, cf. [124]. With this notation, we define the discontinuity-penalization function $\sigma : \mathscr{F}_h \to \mathbb{R}$ in the following manner.

Definition 26 Assuming that (4.6) holds, the discontinuity-penalization function $\sigma : \mathscr{F}_h \to \mathbb{R}$ arising in (4.5) is given by

$$\sigma(\mathbf{x}) := \begin{cases} C_\sigma \max\limits_{\kappa \in \{\kappa^+,\kappa^-\}} \Big\{C_{\text{INV}}(p_\kappa,\kappa,F)\,\dfrac{\bar{a}_\kappa p_\kappa^2|F|}{|\kappa|}\Big\}, & \mathbf{x} \in F \in \mathscr{F}_h^{\mathscr{I}},\ F \subset \partial\kappa^+ \cap \partial\kappa^-, \\ C_\sigma C_{\text{INV}}(p_\kappa,\kappa,F)\,\dfrac{\bar{a}_\kappa p_\kappa^2|F|}{|\kappa|}, & \mathbf{x} \in F \in \mathscr{F}_h^{D},\ F \subset \partial\kappa. \end{cases} \tag{4.7}$$

Here, C_{INV} is the constant arising in the inverse inequality derived in Lemma 11, cf. (3.14), and C_σ is a positive constant independent of p_κ, $|F|$, and $|\kappa|$.

In accordance with the mesh terminology introduced in Sect. 3.1, we note that the value of the discontinuity-penalization function σ on a given elemental interface is independently determined on each constituent $(d-1)$-dimensional simplicial mesh face which forms the given interface. In this way, σ is independent of any local mesh size or polynomial degree quasi-uniformity assumption, as well as any local regularity condition on the location of hanging nodes on the boundary of each element κ, $\kappa \in \mathscr{T}_h$. In particular, for standard simplicial and tensor product meshes, which contain hanging nodes, the independent piecewise constant definition of the discontinuity-penalization function allows for the treatment of *irregular* hanging nodes, i.e., nodes which are arbitrarily positioned on the element interface, in a simple manner. This is in contrast to the usual error analysis of DGFEMs on meshes

consisting of standard element shapes, whereby irregular hanging nodes are not permitted, since the discontinuity-penalization function definition typically relies on the face, and the corresponding interface which it belongs to, to be of comparable size to that of the element, cf. [124].

The first issue encountered when analyzing the DGFEM (4.5) is that this formulation is not well-defined for functions in $H^1(\Omega)$. Indeed, square-integrable functions, i.e., those that belong to $L^2(\Omega)$, do not have a well-defined trace on $\mathscr{F}_h$ and hence the terms $\{\!\{\nabla v\}\!\}$ are not well-defined for $v \in H^1(\Omega)$. Hence, unless we assume that the analytical solution of (4.1) possesses additional regularity, we cannot directly exploit Galerkin orthogonality. At first sight, this may not appear to be a pertinent issue in the context of a priori error bounds, whereby local solution regularity is routinely assumed to be sufficiently high. However, the presence of $\{\!\{\nabla v\}\!\}|_F$, for a face F, in the bilinear form, results in terms of the form $\{\!\{\nabla(u-\Pi u)\}\!\}|_F$, where $\Pi u \in V^{\mathbf{p}}(\mathscr{T}_h)$ is some approximation of u; this must then be estimated optimally to establish an (optimal) a priori error bound. Unfortunately, as the proof of Lemma 23 shows, to derive *hp*-approximation estimates for the $H^1(F)$-seminorm on polytopic meshes in the spirit of (3.30), we would additionally need an *hp*-approximation estimate on simplicial elements in the $W^{1,\infty}$-norm, (cf. (3.23)) which is neither available nor practical for it would increase further the solution regularity requirements artificially.

To overcome this issue, we introduce suitable extensions of the bilinear form $B_{\mathrm{d}}(\cdot,\cdot)$ and linear functional $\ell(\cdot)$. To this end, we write $\boldsymbol{\Pi}_{L^2} : [L^2(\Omega)]^d \to [V^{\mathbf{p}}(\mathscr{T}_h)]^d$ to denote the orthogonal L^2-projection onto the finite element space $[V^{\mathbf{p}}(\mathscr{T}_h)]^d$. Thereby, following [100, 147], we define the bilinear form

$$\tilde{B}_{\mathrm{d}}(w,v) := \sum_{\kappa\in\mathscr{T}_h}\int_\kappa a\nabla w\cdot\nabla v\,\mathrm{d}\mathbf{x} \tag{4.8}$$

$$-\int_{\mathscr{F}_h^{\mathscr{I}}\cup\mathscr{F}_h^D}(\{\!\{a\boldsymbol{\Pi}_{L^2}(\nabla w)\}\!\}\cdot[\![v]\!]+\{\!\{a\boldsymbol{\Pi}_{L^2}(\nabla v)\}\!\}\cdot[\![w]\!]-\sigma[\![w]\!]\cdot[\![v]\!]\,\mathrm{d}s), \tag{4.9}$$

and linear functional

$$\tilde{\ell}(v) := \sum_{\kappa\in\mathscr{T}_h}\int_\kappa fv\,\mathrm{d}\mathbf{x}-\int_{\mathscr{F}_h^D} g_{\mathrm{D}}(a\boldsymbol{\Pi}_{L^2}(\nabla v)\cdot\mathbf{n}-\sigma v)\,\mathrm{d}s+\int_{\mathscr{F}_h^N} g_{\mathrm{N}}v\,\mathrm{d}s$$

for all $v, w \in \mathscr{V} := H^1(\Omega) + V^{\mathbf{p}}(\mathscr{T}_h)$. Then the DGFEM formulation (4.5) may be rewritten in the following equivalent manner: find $u_h \in V^{\mathbf{p}}(\mathscr{T}_h)$ such that

$$\tilde{B}_{\mathrm{d}}(u_h, v_h) = \tilde{\ell}(v_h) \tag{4.10}$$

for all $v_h \in V^{\mathbf{p}}(\mathscr{T}_h)$.

Of course, for all $w, v \in V^{\mathbf{p}}(\mathscr{T}_h)$, we have $\tilde{B}_{\mathrm{d}}(w, v) = B_{\mathrm{d}}(w, v)$ and $\tilde{\ell}(v) = \ell(v)$, i.e., (4.10) and (4.5) give rise to the same DGFEM. However, the bilinear form $\tilde{B}_{\mathrm{d}}(\cdot, \cdot)$ is inconsistent due to the discrete nature of the projection operator $\boldsymbol{\Pi}_{L^2}$; thereby, Galerkin orthogonality no longer holds. Nevertheless, this formulation enables us to pursue the analysis without requiring $W^{1,\infty}$-norm approximation estimates, as we shall see below. Moreover, we are able to deduce both the coercivity and continuity of the (extended) bilinear form $\tilde{B}_{\mathrm{d}}(\cdot, \cdot)$ on $\mathscr{V} \times \mathscr{V}$.

We introduce the associated DGFEM energy norm given by

$$|||v|||_{\mathrm{DG}}^2 := \sum_{\kappa \in \mathscr{T}_h} \|\sqrt{a}\nabla v\|_{L^2(\kappa)}^2 + \int_{\mathscr{F}_h^{\mathscr{I}} \cup \mathscr{F}_h^D} \sigma |[\![v]\!]|^2 \, \mathrm{d}s. \tag{4.11}$$

Here, and in the following, we shall often make use of the arithmetic-geometric mean inequality, written in the following form:

$$ab \leq a^2\epsilon + \frac{b^2}{4\epsilon}, \tag{4.12}$$

which holds for any $a, b \in \mathbb{R}$ and $\epsilon > 0$.

Lemma 27 *Given that Assumption 25 holds, with σ defined as in Definition 26, where C_σ is a sufficiently large positive constant, the bilinear form $\tilde{B}_{\mathrm{d}}(\cdot, \cdot)$ is coercive and continuous over $\mathscr{V} \times \mathscr{V}$, i.e.,*

$$\tilde{B}_{\mathrm{d}}(v, v) \geq C_{\mathrm{coer}} |||v|||_{\mathrm{DG}}^2 \quad \textit{for all} \quad v \in \mathscr{V}, \tag{4.13}$$

and

$$\tilde{B}_{\mathrm{d}}(w, v) \leq C_{\mathrm{cont}} |||w|||_{\mathrm{DG}} \, |||v|||_{\mathrm{DG}} \quad \textit{for all} \quad w, v \in \mathscr{V}, \tag{4.14}$$

respectively, where C_{coer} and C_{cont} are positive constants, independent of the local mesh sizes h_κ and local polynomial degree orders p_κ, $\kappa \in \mathscr{T}_h$.

Proof The proof is based on employing standard arguments, cf. [79], for example; in particular, the analysis exploits the inverse inequality stated in Lemma 11 for general polytopic elements. Firstly, to prove (4.13), we note that, for any $v \in \mathscr{V}$, we have the following identity

$$\tilde{B}_{\mathrm{d}}(v, v) = |||v|||_{\mathrm{DG}}^2 - 2 \int_{\mathscr{F}_h^{\mathscr{I}} \cup \mathscr{F}_h^D} \{\!\{ a \boldsymbol{\Pi}_{L^2}(\nabla v) \}\!\} \cdot [\![v]\!] \, \mathrm{d}s. \tag{4.15}$$

We now proceed by bounding the second term on the right-hand side of (4.15). To this end, given $F \in \mathscr{F}_h^{\mathscr{I}}$, such that $F \subset \partial\kappa^+ \cap \partial\kappa^-$, $\kappa^\pm \in \mathscr{T}_h$, upon application of the Cauchy–Schwarz inequality and the arithmetic-geometric mean inequality, we

deduce that

$$\begin{aligned}\int_F \{\!\{a\boldsymbol{\Pi}_{L^2}(\nabla v)\}\!\} \cdot [\![v]\!]\,\mathrm{d}s &\leq \frac{1}{2}\left(\|\frac{1}{\sqrt{\sigma}}a\boldsymbol{\Pi}_{L^2}(\nabla v^+)\|_{L^2(F)}+\|\frac{1}{\sqrt{\sigma}}a\boldsymbol{\Pi}_{L^2}(\nabla v^-)\|_{L^2(F)}\right)\\ &\quad\times\|\sqrt{\sigma}[\![v]\!]\|_{L^2(F)}\\ &\leq \epsilon\left(\|\frac{1}{\sqrt{\sigma}}a\boldsymbol{\Pi}_{L^2}(\nabla v^+)\|^2_{L^2(F)}+\|\frac{1}{\sqrt{\sigma}}a\boldsymbol{\Pi}_{L^2}(\nabla v^-)\|^2_{L^2(F)}\right)\\ &\quad+\frac{1}{8\epsilon}\|\sqrt{\sigma}[\![v]\!]\|^2_{L^2(F)}.\end{aligned}$$

Employing the inverse inequality stated in Lemma 11, the definition of the discontinuity-penalization function σ, the assumption on the diffusion tensor, cf. (4.6), and the stability of the L^2-projector $\boldsymbol{\Pi}_{L^2}$ in the L^2-norm, namely that $\|\boldsymbol{\Pi}_{L^2}\mathbf{v}\|_{L^2(\kappa)} \leq \|\mathbf{v}\|_{L^2(\kappa)}$, for $\mathbf{v} \in [\mathscr{V}]^d$, $\kappa \in \mathscr{T}_h$, gives

$$\begin{aligned}&\int_F \{\!\{a\boldsymbol{\Pi}_{L^2}(\nabla v)\}\!\} \cdot [\![v]\!]\,\mathrm{d}s\\ &\leq \epsilon\left(C_{\mathrm{INV}}(p_{\kappa^+},\kappa^+,F)\frac{\bar{a}_{\kappa^+}p^2_{\kappa^+}|F|}{|\kappa^+|}\|\frac{1}{\sqrt{\sigma}}\sqrt{a}\boldsymbol{\Pi}_{L^2}(\nabla v)\|^2_{L^2(\kappa^+)}\right.\\ &\quad\left.+\,C_{\mathrm{INV}}(p_{\kappa^-},\kappa^-,F)\frac{\bar{a}_{\kappa^-}p^2_{\kappa^-}|F|}{|\kappa^-|}\|\frac{1}{\sqrt{\sigma}}\sqrt{a}\boldsymbol{\Pi}_{L^2}(\nabla v)\|^2_{L^2(\kappa^-)}\right)+\frac{1}{8\epsilon}\|\sqrt{\sigma}[\![v]\!]\|^2_{L^2(F)}\\ &\leq \frac{\epsilon}{C_\sigma}\left(\|\sqrt{a}\nabla v\|^2_{L^2(\kappa^+)}+\|\sqrt{a}\nabla v\|^2_{L^2(\kappa^-)}\right)+\frac{1}{8\epsilon}\|\sqrt{\sigma}[\![v]\!]\|^2_{L^2(F)}.\end{aligned}\tag{4.16}$$

Similarly, for $F \in \mathscr{F}_h^D$, where $F \subset \partial\kappa$, $\kappa \in \mathscr{T}_h$, we get

$$\int_F \{\!\{a\boldsymbol{\Pi}_{L^2}(\nabla v)\}\!\} \cdot [\![v]\!]\,\mathrm{d}s \leq \frac{\epsilon}{C_\sigma}\|\sqrt{a}\nabla v\|^2_{L^2(\kappa)}+\frac{1}{4\epsilon}\|\sqrt{\sigma}[\![v]\!]\|^2_{L^2(F)}.\tag{4.17}$$

Inserting (4.16) and (4.17) into (4.15), we deduce that

$$\tilde{B}_{\mathrm{d}}(v,v) \geq \left(1-\frac{2C_F}{C_\sigma}\epsilon\right)\sum_{\kappa\in\mathscr{T}_h}\|\sqrt{a}\nabla v\|^2_{L^2(\kappa)}+\left(1-\frac{1}{2\epsilon}\right)\sum_{F\in\mathscr{F}_h^{\mathscr{I}}\cup\mathscr{F}_h^D}\|\sqrt{\sigma}[\![v]\!]\|^2_{L^2(F)},$$

since the number of elemental faces is uniformly bounded by Assumption 25. Hence the bilinear form $\tilde{B}_{\mathrm{d}}(\cdot,\cdot)$ is coercive over $\mathscr{V}\times\mathscr{V}$ if $C_\sigma > 2C_F\epsilon$ for some $\epsilon > 1/2$.

The proof of continuity of $\tilde{B}_{\mathrm{d}}(\cdot,\cdot)$ follows immediately, based on employing the Cauchy-Schwarz inequality, together with analogous arguments to establish upper bounds on the face terms, cf. (4.16) and (4.17) above.

The above analysis extends well-known results derived for meshes consisting of standard element shapes to the case when general polytopes are admitted. We

stress that the proof is based on exploiting the new inverse inequality derived in Lemma 11, in order to provide a suitable upper bound on the face terms arising in the DGFEM (4.5), cf., also, (4.10), assuming that Assumption 25 holds. This approach has the crucial advantage of permitting very general polytopic meshes in the sense that shape-regularity of the underlying mesh $\mathscr{T}_h$ is not directly required.

4.2.2 A Priori Error Analysis

We now embark on the error analysis of the *hp*-version DGFEM (4.5), cf., also, (4.10). To this end, we quote the following abstract error bound, which is an instance of Strang's Second Lemma [64, 163], whereby the error is controlled by the sum of a quasi-optimal approximation term and a residual term.

Lemma 28 *Let $u \in H^1(\Omega)$ be the weak solution of (4.3) and $u_h \in V^{\mathbf{p}}(\mathscr{T}_h)$ the DGFEM solution defined by (4.5). Under the hypotheses of Lemma 27, the following abstract error bound holds*

$$|||u-u_h|||_{\mathrm{DG}} \leq \left(1+\frac{C_{\mathrm{cont}}}{C_{\mathrm{coer}}}\right) \inf_{v_h \in V^{\mathbf{p}}(\mathscr{T}_h)} |||u-v_h|||_{\mathrm{DG}} + \frac{1}{C_{\mathrm{coer}}} \sup_{w_h \in V^{\mathbf{p}}(\mathscr{T}_h)\setminus\{0\}} \frac{|\tilde{B}_{\mathrm{d}}(u,w_h)-\tilde{\ell}(w_h)|}{|||w_h|||_{\mathrm{DG}}}. \tag{4.18}$$

Proof Employing the triangle inequality gives

$$|||u-u_h|||_{\mathrm{DG}} \leq |||u-v_h|||_{\mathrm{DG}} + |||v_h-u_h|||_{\mathrm{DG}} \tag{4.19}$$

for all $v_h \in V^{\mathbf{p}}(\mathscr{T}_h)$. Thereby, we simply need to bound $|||v_h-u_h|||_{\mathrm{DG}}$; to this end, we exploit the coercivity and continuity of $\tilde{B}_{\mathrm{d}}(\cdot,\cdot)$ on $\mathscr{V}\times\mathscr{V}$, cf. Lemma 27, to obtain

$$\begin{aligned}
|||v_h-u_h|||_{\mathrm{DG}}^2 &\leq \frac{1}{C_{\mathrm{coer}}}\tilde{B}_{\mathrm{d}}(v_h-u_h,v_h-u_h)\\
&= \frac{1}{C_{\mathrm{coer}}}(\tilde{B}_{\mathrm{d}}(v_h-u,v_h-u_h)+\tilde{B}_{\mathrm{d}}(u-u_h,v_h-u_h))\\
&\leq \frac{C_{\mathrm{cont}}}{C_{\mathrm{coer}}}|||u-v_h|||_{\mathrm{DG}}|||v_h-u_h|||_{\mathrm{DG}}\\
&\quad + \frac{1}{C_{\mathrm{coer}}}(\tilde{B}_{\mathrm{d}}(u,v_h-u_h)-\tilde{\ell}(v_h-u_h)).
\end{aligned}$$

Thereby, dividing both sides by $|||v_h-u_h|||_{\mathrm{DG}}$, and noting that $v_h \in V^{\mathbf{p}}(\mathscr{T}_h)$ is arbitrary, upon substitution into (4.19), we deduce the statement of the lemma.

The abstract error bound of Lemma 28 may now be employed to establish an *hp*-version a priori error bound for the DGFEM (4.5), based on exploiting the approximation results stated in Lemma 23. To this end, we assume that, given the polytopic mesh $\mathscr{T}_h$, there exists a shape-regular covering $\mathscr{T}_h^\sharp = \{\mathscr{K}\}$, cf. Definition 17, which satisfies Assumption 18. Furthermore, we assume that $u|_\kappa \in H^{l_\kappa}(\kappa)$, for some $l_\kappa > 1 + d/2$, for each $\kappa \in \mathscr{T}_h$, so that, by Theorem 21, $\mathfrak{E}u|_{\mathscr{K}} \in H^{l_\kappa}(\mathscr{K})$, where $\mathscr{K} \in \mathscr{T}_h^\sharp$, with $\kappa \subset \mathscr{K}$. Thereby, defining $\tilde{\Pi}_{\mathbf{p}}$ by $\tilde{\Pi}_{\mathbf{p}}|_\kappa := \tilde{\Pi}_{p_\kappa}$, for $\kappa \in \mathscr{T}_h$, upon application of Lemma 23, together with Assumption 25, we deduce that

$$\begin{aligned}
&\inf_{v_h \in V^{\mathbf{p}}(\mathscr{T}_h)} |||u - v_h|||_{\mathrm{DG}}^2 \le |||u - \tilde{\Pi}_{\mathbf{p}} u|||_{\mathrm{DG}}^2 \\
&\le \sum_{\kappa \in \mathscr{T}_h} \left(\|\sqrt{a}\nabla(u - \tilde{\Pi}_{p_\kappa} u)\|_{L^2(\kappa)}^2 + 2 \sum_{F \subset \partial\kappa \setminus \partial\Omega_{\mathrm{N}}} \sigma \|(u - \tilde{\Pi}_{p_\kappa} u)|_\kappa\|_{L^2(F)}^2 \right) \\
&\le C \sum_{\kappa \in \mathscr{T}_h} \frac{h_\kappa^{2(s_\kappa - 1)}}{p_\kappa^{2(l_\kappa - 1)}} \left(\bar{a}_\kappa + \frac{h_\kappa^{-d+2}}{p_\kappa} \sum_{F \subset \partial\kappa \setminus \partial\Omega_{\mathrm{N}}} C_m(p_\kappa, \kappa, F)\sigma|F| \right) \|\mathfrak{E}u\|_{H^{l_\kappa}(\mathscr{K})}^2,
\end{aligned} \tag{4.20}$$

with $s_\kappa = \min\{p_\kappa + 1, l_\kappa\}$ and C a positive constant, which depends on the shape-regularity of the covering $\mathscr{T}_h^\sharp$, but is independent of the discretization parameters; also, from Lemma 23, we recall that

$$C_m(p, \kappa, F) = \min\left\{ \frac{h_\kappa^d}{\sup_{\kappa_\flat^F \subset \kappa} |\kappa_\flat^F|}, \frac{1}{p^{1-d}} \right\}.$$

We now proceed to bound the residual term arising in (4.18). To this end, we first note that applying integration by parts elementwise, together with the identity (2.20), and noting that u is the analytical solution of (4.1), we get

$$\begin{aligned}
\left| \tilde{B}_{\mathrm{d}}(u, w_h) - \tilde{\ell}(u, w_h) \right| &= \left| \int_{\mathscr{F}_h^{\mathscr{I}} \cup \mathscr{F}_h^D} \{\!\{ a(\nabla u - \boldsymbol{\Pi}_{L^2}(\nabla u)) \}\!\} \cdot [\![w_h]\!] \, \mathrm{d}s \right| \\
&\le \left(\int_{\mathscr{F}_h^{\mathscr{I}} \cup \mathscr{F}_h^D} \sigma^{-1} |\{\!\{ a(\nabla u - \boldsymbol{\Pi}_{L^2}(\nabla u)) \}\!\}|^2 \, \mathrm{d}s \right)^{1/2} |||w_h|||_{\mathrm{DG}}.
\end{aligned}$$

We write $\tilde{\boldsymbol{\Pi}}_{\boldsymbol{p}}$ to denote the vector-valued *hp*-projection operator obtained by applying the operator $\tilde{\Pi}_{\boldsymbol{p}}$ componentwise. Thereby, adding and subtracting $\tilde{\boldsymbol{\Pi}}_{\boldsymbol{p}}(\nabla u)$,

gives

$$\begin{aligned}
&\int_{\mathscr{F}_h^{\mathscr{I}}\cup\mathscr{F}_h^D} \sigma^{-1}|\{\!\{a(\nabla u-\boldsymbol{\Pi}_{L^2}(\nabla u))\}\!\}|^2\,\mathrm{d}s\\
&\quad\le \int_{\mathscr{F}_h^{\mathscr{I}}\cup\mathscr{F}_h^D} 2\sigma^{-1}(|\{\!\{a(\nabla u-\tilde{\boldsymbol{\Pi}}_{\boldsymbol{p}}(\nabla u))\}\!\}|^2+|\{\!\{a(\boldsymbol{\Pi}_{L^2}(\tilde{\boldsymbol{\Pi}}_{\boldsymbol{p}}(\nabla u)-\nabla u))\}\!\}|^2)\,\mathrm{d}s\\
&\quad\equiv \mathrm{I}+\mathrm{II}.
\end{aligned}$$

Using, as above, the approximation estimate (3.27) yields

$$\mathrm{I}\le C\sum_{\kappa\in\mathscr{T}_h}\bar{a}_\kappa^2\frac{h_\kappa^{2(s_\kappa-1)}}{p_\kappa^{2(l_\kappa-1)}}\frac{h_\kappa^{-d}}{p_\kappa^{-1}}\left(\sum_{F\subset\partial\kappa\setminus\partial\Omega_{\mathrm{N}}}C_m(p_\kappa,\kappa,F)\sigma^{-1}|F|\right)\|\mathfrak{E}u\|^2_{H^{l_\kappa}(\mathscr{K})}.$$

Similarly, employing the inverse inequality (3.13), the L^2-stability of the projector $\boldsymbol{\Pi}_{L^2}$, and the approximation estimate (3.26), gives

$$\mathrm{II}\le C\sum_{\kappa\in\mathscr{T}_h}\bar{a}_\kappa^2\frac{h_\kappa^{2(s_\kappa-1)}}{p_\kappa^{2(l_\kappa-1)}}\frac{|\kappa|^{-1}}{p_\kappa^{-2}}\left(\sum_{F\subset\partial\kappa\setminus\partial\Omega_{\mathrm{N}}}C_{\mathrm{INV}}(p_\kappa,\kappa,F)\sigma^{-1}|F|\right)\|\mathfrak{E}u\|^2_{H^{l_\kappa}(\mathscr{K})}.$$

Combining the above bounds, we deduce:

$$\begin{aligned}
&\sup_{w_h\in V^{\boldsymbol{p}}(\mathscr{T}_h)\setminus\{0\}}\frac{|\tilde{B}_{\mathrm{d}}(u,w_h)-\tilde{\ell}(u,w_h)|}{|||w_h|||_{\mathrm{DG}}}\\
&\quad\le\big(\mathrm{I}+\mathrm{II}\big)^{1/2}\\
&\quad\le C\Bigg(\sum_{\kappa\in\mathscr{T}_h}\bar{a}_\kappa^2\frac{h_\kappa^{2(s_\kappa-1)}}{p_\kappa^{2(l_\kappa-1)}}\\
&\qquad\times\left(\sum_{F\subset\partial\kappa\setminus\partial\Omega_{\mathrm{N}}}\Big(C_m(p_\kappa,\kappa,F)\frac{h_\kappa^{-d}}{p_\kappa^{-1}}+C_{\mathrm{INV}}(p_\kappa,\kappa,F)\frac{|\kappa|^{-1}}{p_\kappa^{-2}}\Big)\sigma^{-1}|F|\right)\\
&\qquad\times\|\mathfrak{E}u\|^2_{H^{l_\kappa}(\mathscr{K})}\Bigg)^{1/2}.
\end{aligned}\tag{4.21}$$

On the basis of the bounds (4.20) and (4.21), we state the following *hp*-version a priori error bound for the DGFEM (4.5).

Theorem 29 *Let $\mathscr{T}_h=\{\kappa\}$ be a subdivision of $\Omega\subset\mathbb{R}^d$, $d=2,3$, consisting of general polytopic elements satisfying Assumptions 18 and 25, with $\mathscr{T}_h^\sharp=\{\mathscr{K}\}$ an*

associated covering of $\mathscr{T}_h$ consisting of shape-regular d-simplices, cf. Definition 17. Let $u_h \in V^{\mathbf{p}}(\mathscr{T}_h)$, with $p_\kappa \geq 1$ for all $\kappa \in \mathscr{T}_h$, be the corresponding DGFEM solution defined by (4.5), where the discontinuity-penalization function σ is given by (4.7). If the analytical solution $u \in H^1(\Omega)$ to (4.1)–(4.3) satisfies $u|_\kappa \in H^{l_\kappa}(\kappa)$, $l_\kappa > 1+d/2$, for each $\kappa \in \mathscr{T}_h$, such that $\mathfrak{E}u|_{\mathscr{K}} \in H^{l_\kappa}(\mathscr{K})$, where $\mathscr{K} \in \mathscr{T}_h^\sharp$ with $\kappa \subset \mathscr{K}$, then

$$|||u-u_h|||_{\mathrm{DG}}^2 \leq C \sum_{\kappa \in \mathscr{T}_h} \frac{h_\kappa^{2(s_\kappa-1)}}{p_\kappa^{2(l_\kappa-1)}} \left(\bar{a}_\kappa + \mathscr{G}_\kappa(F, C_{\mathrm{INV}}, C_m, p_\kappa)\right) \|\mathfrak{E}u\|_{H^{l_\kappa}(\mathscr{K})}^2,$$

with $s_\kappa = \min\{p_\kappa + 1, l_\kappa\}$,

$$\begin{aligned}\mathscr{G}_\kappa(F, C_{\mathrm{INV}}, C_m, p_\kappa) := {} & \bar{a}_\kappa^2 p_\kappa h_\kappa^{-d} \sum_{F \subset \partial\kappa \setminus \partial\Omega_{\mathrm{N}}} C_m(p_\kappa, \kappa, F)\sigma^{-1}|F| \\ & + \bar{a}_\kappa^2 p_\kappa^2 |\kappa|^{-1} \sum_{F \subset \partial\kappa \setminus \partial\Omega_{\mathrm{N}}} C_{\mathrm{INV}}(p_\kappa, \kappa, F)\sigma^{-1}|F| \\ & + h_\kappa^{-d+2} p_\kappa^{-1} \sum_{F \subset \partial\kappa \setminus \partial\Omega_{\mathrm{N}}} C_m(p_\kappa, \kappa, F)\sigma|F|,\end{aligned}$$

where C is a positive constant, which depends on the shape-regularity of $\mathscr{T}_h^\sharp$, but is independent of the discretization parameters.

The above result generalizes well-known a priori bounds for DGFEMs defined on standard element shapes, cf. [124, 152], in two key ways. Firstly, meshes comprising of polytopic elements are admitted; secondly, elemental faces are allowed to degenerate. For $d = 3$, this also implies that positive measure interfaces may have degenerating (one-dimensional) edges. Thereby, this freedom is relevant to standard (simplicial/hexahedral) meshes with hanging nodes in the sense that no condition is required on the location of hanging nodes on the element boundaries. If, on the other hand, the diameter of the faces of each element $\kappa \in \mathscr{T}_h$ is of comparable size to the diameter of the corresponding element, for uniform orders $p_\kappa = p \geq 1$, $h = \max_{\kappa \in \mathscr{T}_h} h_\kappa$, $s_\kappa = s$, $s = \min\{p+1, l\}$, $l > 1 + d/2$, then the bound of Theorem 29 reduces to

$$|||u-u_h|||_{\mathrm{DG}} \leq C \frac{h^{s-1}}{p^{l-3/2}} \|u\|_{H^l(\Omega)},$$

cf. [54]. This coincides with the analogous result derived in [124] for standard meshes consisting of simplices or tensor-product elements. It is easy to check that the above a priori error bound is optimal in h and suboptimal in p by half an order, as expected, cf. [101].

4.3 Error Analysis II: Shape-Regular Polytopic Meshes

In this section, we pursue the error analysis on meshes which may potentially violate Assumption 25 in the sense that the number of faces that the elements possess may not be uniformly bounded under mesh refinement. We note that this may arise when sequences of coarser meshes are generated via element agglomeration of a given fine mesh $\mathscr{T}_h^{\text{fine}}$, cf. Sect. 6.1 and [15]. To this end, recalling Definition 7, we introduce the following assumption on the mesh $\mathscr{T}_h$.

Assumption 30 (Arbitrary Number of Faces) *For any $\kappa \in \mathscr{T}_h$, there exists a set of non-overlapping d-dimensional simplices $\{\kappa_\flat^F\}_{F\subset\partial\kappa} \subset \mathscr{F}_\flat^\kappa$ contained in κ, such that for all $F \subset \partial\kappa$, the following condition holds*

$$h_\kappa \leq C_s \frac{d|\kappa_\flat^F|}{|F|}, \tag{4.22}$$

where C_s is a positive constant, which is independent of the discretization parameters, the number of faces that the element possesses, and the measure of F.

In Fig. 4.1 we present two potential polygons in $\mathbb{R}^2$ which satisfy the above mesh regularity assumption. We note that Assumption 30 does not place any restriction on either the number of faces that an element κ, $\kappa \in \mathscr{T}_h$, may possess, or the relative measure of its faces compared to the measure of the element itself. Indeed, shape-irregular simplices $\kappa_\flat^F$, with base $|F|$ of small size compared to the corresponding height, defined by $d|\kappa_\flat^F|/|F|$, are admitted. However, the height must be of comparable size to h_κ, cf. the polygon depicted in Fig. 4.1a. Furthermore, we note that the union of the simplices $\kappa_\flat^F$ does not need to cover the whole element κ, as in general it is sufficient to assume that

$$\bigcup_{F\subset\partial\kappa} \bar{\kappa}_\flat^F \subseteq \bar{\kappa}; \tag{4.23}$$

cf. the polygon given in Fig. 4.1b.

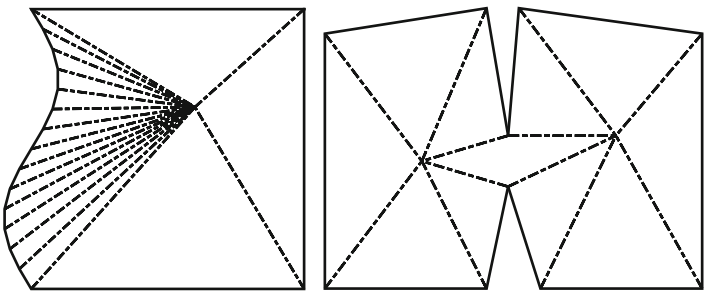

Fig. 4.1 (**a**) Polygon with many tiny faces; (**b**) Star-shaped polygon

Remark 31 We note that meshes consisting of elements which are (unions of) uniformly star-shaped polytopes satisfy Assumption 30. Moreover, it is clear that Assumption 30 is the natural generalization of the classical shape-regularity assumption, usually stated for simplicial and tensor product meshes, cf. [64] and Definition 2, to polytopic elements; in this setting, $\rho_\kappa := \min_{F\subset\partial\kappa} d|\kappa_\flat^F|/|F|$ denotes the radius of the largest inscribed ball.

Given Assumption 30 holds, we now develop an inverse estimate and polynomial approximation result on the boundary of each element κ in the computational mesh $\mathscr{T}_h$. To this end, we have the following two results, respectively.

Lemma 32 *Let $\kappa \in \mathscr{T}_h$; then assuming Assumption 30 is satisfied, for each $v \in \mathscr{P}_p(\kappa)$, the following inverse inequality holds*

$$\|v\|^2_{L^2(\partial\kappa)} \leq C_s C_{\mathrm{inv},1} d \frac{p^2}{h_\kappa} \|v\|^2_{L^2(\kappa)}. \tag{4.24}$$

Here, C_s is defined in (4.22), and is independent of v, $|\kappa|/\sup_{\kappa_\flat^F\subset\kappa}|\kappa_\flat^F|$, $|F|$, and p, cf. Assumption 30; moreover, $C_{\mathrm{inv},1}$ is given in Lemma 6, and is independent of v, p, and h_κ.

Proof The proof is based on applying Lemma 6 over each simplex $\kappa_\flat^F$ contained within κ, together with (4.22) and (4.23); thereby, we get

$$\begin{aligned}
\|v\|^2_{L^2(\partial\kappa)} &\leq \sum_{F\subset\partial\kappa} C_{\mathrm{inv},1} p^2 \frac{|F|}{|\kappa_\flat^F|} \|v\|^2_{L^2(\kappa_\flat^F)} \\
&\leq \sum_{F\subset\partial\kappa} C_s C_{\mathrm{inv},1} d \frac{p^2}{h_\kappa} \|v\|^2_{L^2(\kappa_\flat^F)} \\
&\leq C_s C_{\mathrm{inv},1} d \frac{p^2}{h_\kappa} \|v\|^2_{L^2(\kappa)},
\end{aligned}$$

with $\kappa_\flat^F \in \mathscr{F}_\flat^\kappa$ as in Definition 7.

Lemma 33 *Let $\kappa \in \mathscr{T}_h$ and $\mathscr{K} \in \mathscr{T}_h^\sharp$ the corresponding simplex such that $\kappa \subset \mathscr{K}$, cf. Definition 17. Suppose that $v \in H^1(\Omega)$ is such that $\mathfrak{E}v|_{\mathscr{K}} \in H^{l_\kappa}(\mathscr{K})$, for some $l_\kappa > 1/2$. Then, given that Assumption 30 is satisfied, the following bound holds*

$$\|v - \tilde{\Pi}_p v\|_{L^2(\partial\kappa)} \leq C_{\mathrm{I},5} \frac{h_\kappa^{s_\kappa - 1/2}}{p^{l_\kappa - 1/2}} \|\mathscr{E}v\|_{H^{l_\kappa}(\mathscr{K})}, \tag{4.25}$$

where $s_\kappa = \min\{p+1, l_\kappa\}$ and $C_{\mathrm{I},5}$ is a positive constant which depends on C_s from (4.22) and the shape-regularity of $\mathscr{K}$, but is independent of v, h_κ, p, and the number of faces per element.

Proof Exploiting Assumption 30, and in particular (4.22) and (4.23), together with the multiplicative trace inequality stated in Lemma 22, the arithmetic-geometric mean inequality, cf. (4.12) with $\epsilon = p/h_\kappa$, and the approximation result (3.26) given in Lemma 23, we deduce that

$$\begin{aligned}
\|v-\tilde{\Pi}_p v\|^2_{L^2(\partial\kappa)} &\leq \sum_{F\subset\partial\kappa} C_{\mathrm{t}}|F|\left(\frac{1}{|\kappa_\flat^F|}\|v-\tilde{\Pi}_p v\|^2_{L^2(\kappa_\flat^F)}\right.\\
&\qquad\left.+\frac{h_{\kappa_\flat^F}}{|\kappa_\flat^F|}\|v-\tilde{\Pi}_p v\|_{L^2(\kappa_\flat^F)}\|\nabla(v-\tilde{\Pi}_p v)\|_{L^2(\kappa_\flat^F)}\right)\\
&\leq C_{\mathrm{t}}\,C_s\,d\sum_{F\subset\partial\kappa}\left(\frac{1}{h_\kappa}\|v-\tilde{\Pi}_p v\|^2_{L^2(\kappa_\flat^F)}\right.\\
&\qquad\left.+\|v-\tilde{\Pi}_p v\|_{L^2(\kappa_\flat^F)}\|\nabla(v-\tilde{\Pi}_p v)\|_{L^2(\kappa_\flat^F)}\right)\\
&\leq C_{\mathrm{t}}\,C_s\,d\sum_{F\subset\partial\kappa}\left(\frac{p+1}{h_\kappa}\|v-\tilde{\Pi}_p v\|^2_{L^2(\kappa_\flat^F)}+\frac{h_k}{4p}\|\nabla(v-\tilde{\Pi}_p v)\|^2_{L^2(\kappa_\flat^F)}\right)\\
&\leq C_{\mathrm{t}}\,C_s\,d\left(\frac{p+1}{h_\kappa}\|v-\tilde{\Pi}_p v\|^2_{L^2(\kappa)}+\frac{h_k}{4p}\|\nabla(v-\tilde{\Pi}_p v)\|^2_{L^2(\kappa)}\right)\\
&\leq \frac{9}{4}\,C_{\mathrm{t}}\,C_s\,d\,C^2_{\mathrm{I},3}\frac{h_\kappa^{2s_\kappa-1}}{p^{2l_\kappa-1}}\|\mathscr{E}v\|^2_{H^{l_\kappa}(\mathscr{K})}.
\end{aligned}$$

The statement of the lemma now follows immediately with $C_{\mathrm{I},5}=3C_{\mathrm{I},3}\sqrt{C_{\mathrm{t}}\,C_s\,d}/2$.

Remark 34 Crucially, the constants arising in the inverse inequality and approximation result derived in Lemmas 32 and 33, respectively, are independent of the number of faces that a given element possesses. Here, the proofs are based on applying inverse inequalities and approximation estimates, respectively, on each individual face F in such a manner to get a bound relative to each (anisotropic) simplex $\kappa_\flat^F$ related to the corresponding face F, $F\subset\partial\kappa$, rather than with respect to the element κ itself. Thereby, the resulting individual contributions may be summed to deduce the required inequality on κ. This process can be taken to the limit, in the sense of allowing $|F|$ to tend to zero; in this manner, elements with curved faces can be treated. We refer to [58, 153] for some recent results on the respective inverse and approximation estimates for general curved elements constructed in this spirit.

4.3.1 Stability and A Priori Error Analysis

In this section we develop the stability and a priori error analysis of the DGFEM (4.5) assuming now that Assumption 30 holds. To this end, we first deduce the following coercivity and continuity bounds for the bilinear form $\tilde{B}_{\mathrm{d}}(\cdot,\cdot)$ over $\mathscr{V}\times\mathscr{V}$.

Lemma 35 *Given that Assumption 30 holds, we define the discontinuity-penalization function* $\sigma : \mathscr{F}_h \to \mathbb{R}$ *by*

$$\sigma(\mathbf{x}) := \begin{cases} C_\sigma \max\limits_{\kappa \in \{\kappa^+, \kappa^-\}} \left\{ C_{\text{inv},1} \dfrac{\bar{a}_\kappa p_\kappa^2}{h_\kappa} \right\}, & \mathbf{x} \in F \in \mathscr{F}_h^{\mathscr{I}},\ F = \partial\kappa^+ \cap \partial\kappa^-, \\ C_\sigma C_{\text{inv},1} \dfrac{\bar{a}_\kappa p_\kappa^2}{h_\kappa}, & \mathbf{x} \in F \in \mathscr{F}_h^D,\ F \subset \partial\kappa, \end{cases} \tag{4.26}$$

where C_σ *is a sufficiently large positive constant, which is independent of the number of faces per element. Then, the bilinear form* $\tilde{B}_{\text{d}}(\cdot,\cdot)$ *is coercive and continuous over* $\mathscr{V} \times \mathscr{V}$*, i.e.,*

$$\tilde{B}_{\text{d}}(v, v) \geq C_{\text{coer}} |||v|||_{\text{DG}}^2 \quad \textit{for all} \quad v \in \mathscr{V}, \tag{4.27}$$

and

$$\tilde{B}_{\text{d}}(w, v) \leq C_{\text{cont}} |||w|||_{\text{DG}} \, |||v|||_{\text{DG}} \quad \textit{for all} \quad w, v \in \mathscr{V}, \tag{4.28}$$

respectively, where C_{coer} *and* C_{cont} *are positive constants independent of the discretization parameters and the number of faces per element.*

Proof Recalling the second term on the right-hand side of (4.15) in the proof of Lemma 27, upon application of the arithmetic-geometric mean inequality (4.12), the proof of Lemma 32, and the L^2-stability of $\boldsymbol{\Pi}_{L^2}$, we deduce that

$$\begin{aligned} &\int_{\mathscr{F}_h^{\mathscr{I}} \cup \mathscr{F}_h^D} \{\!\{ a \boldsymbol{\Pi}_{L^2}(\nabla v) \}\!\} \cdot [\![v]\!] \, \mathrm{d}s \\ &\leq \epsilon \sum_{\kappa \in \mathscr{T}_h} \sum_{F \subset \partial\kappa} \bar{a}_\kappa \| \frac{1}{\sqrt{\sigma}} \sqrt{a} \boldsymbol{\Pi}_{L^2}(\nabla v) \|_{L^2(F)}^2 + \frac{1}{4\epsilon} \sum_{F \in \mathscr{F}_h^{\mathscr{I}} \cup \mathscr{F}_h^D} \| \sqrt{\sigma} [\![v]\!] \|_{L^2(F)}^2 \\ &\leq \epsilon \sum_{\kappa \in \mathscr{T}_h} \sum_{F \subset \partial\kappa} \sigma^{-1} \bar{a}_\kappa C_{\text{inv},1} p_\kappa^2 \frac{|F|}{|\kappa_\flat^F|} \| \sqrt{a} \boldsymbol{\Pi}_{L^2}(\nabla v) \|_{L^2(\kappa_\flat^F)}^2 + \frac{1}{4\epsilon} \sum_{F \in \mathscr{F}_h^{\mathscr{I}} \cup \mathscr{F}_h^D} \| \sqrt{\sigma} [\![v]\!] \|_{L^2(F)}^2 \\ &\leq \frac{\epsilon C_s d}{C_\sigma} \sum_{\kappa \in \mathscr{T}_h} \| \sqrt{a} \nabla v \|_{L^2(\kappa)}^2 + \frac{1}{4\epsilon} \sum_{F \in \mathscr{F}_h^{\mathscr{I}} \cup \mathscr{F}_h^D} \| \sqrt{\sigma} [\![v]\!] \|_{L^2(F)}^2. \end{aligned} \tag{4.29}$$

Inserting (4.29) into (4.15) we get

$$\tilde{B}_{\text{d}}(v, v) \geq \left(1 - \frac{2\epsilon C_s d}{C_\sigma} \right) \sum_{\kappa \in \mathscr{T}_h} \| \sqrt{a} \nabla v \|_{L^2(\kappa)}^2 + \left(1 - \frac{1}{2\epsilon} \right) \sum_{F \in \mathscr{F}_h^{\mathscr{I}} \cup \mathscr{F}_h^D} \| \sqrt{\sigma} [\![v]\!] \|_{L^2(F)}^2.$$

Hence, the bilinear form $\tilde{B}_{\mathrm{d}}(\cdot,\cdot)$ is coercive over $\mathcal{V}\times\mathcal{V}$ if $C_\sigma > 2C_s\epsilon d$ for some $\epsilon > 1/2$. Note that C_σ depends on C_s, but is independent of the number of faces per element. The continuity of $\tilde{B}_{\mathrm{d}}(\cdot,\cdot)$ follows analogously.

Finally, we derive an *hp*-version a priori error bound for the DGFEM (4.5), assuming that Assumption 30 holds. For brevity, we focus on the terms defined on the faces of the elements in the computational mesh, since they must be treated in a different manner to the analysis presented in Sect. 4.2. Thereby, employing (4.25) in Lemma 33, we deduce that

$$\begin{aligned}\int_{\mathcal{F}_h^{\mathcal{I}}\cup\mathcal{F}_h^{D}}\sigma[\![v-\tilde{\Pi}_p v]\!]^2\,\mathrm{d}s &\le 2\sum_{\kappa\in\mathcal{T}_h}\sum_{F\subset\partial\kappa\setminus\partial\Omega_{\mathrm{N}}}\sigma|_F\|v-\tilde{\Pi}_p v\|^2_{L^2(F)}\\ &\le 2\sum_{\kappa\in\mathcal{T}_h}\Big(\max_{F\subset\partial\kappa\setminus\partial\Omega_{\mathrm{N}}}\sigma|_F\Big)\|v-\tilde{\Pi}_p v\|^2_{L^2(\partial\kappa)}\\ &\le C\sum_{\kappa\in\mathcal{T}_h}\Big(\max_{F\subset\partial\kappa\setminus\partial\Omega_{\mathrm{N}}}\sigma|_F\Big)\frac{h_\kappa^{2s_\kappa-1}}{p^{2l_\kappa-1}}\|\mathfrak{E}v\|^2_{H^{l_\kappa}(\mathscr{K})},\end{aligned}\tag{4.30}$$

where C is a positive constant, which is independent of the number of faces per element. Bounds on the remaining terms defined on $\mathcal{F}_h^{\mathcal{I}}\cup\mathcal{F}_h^{D}$ can be derived in a completely analogous fashion; for brevity the details are omitted. Hence, we arrive at the following a priori estimate.

Theorem 36 *Let $\mathcal{T}_h=\{\kappa\}$ be a subdivision of $\Omega\subset\mathbb{R}^d$, $d=2,3$, consisting of general polytopic elements satisfying Assumptions 18 and 30, with $\mathcal{T}_h^\sharp=\{\mathscr{K}\}$ an associated covering of $\mathcal{T}_h$ consisting of shape-regular d-simplices, cf. Definition 17. Let $u_h\in V^{\mathbf{p}}(\mathcal{T}_h)$, with $p_\kappa\ge 1$ for all $\kappa\in\mathcal{T}_h$, be the corresponding DGFEM solution defined by (4.5), where the discontinuity-penalization function is given by (4.26). If the analytical solution $u\in H^1(\Omega)$ to (4.1)–(4.3) satisfies $u|_\kappa\in H^{l_\kappa}(\kappa)$, $l_\kappa>3/2$, for each $\kappa\in\mathcal{T}_h$, such that $\mathfrak{E}u|_{\mathscr{K}}\in H^{l_\kappa}(\mathscr{K})$, where $\mathscr{K}\in\mathcal{T}_h^\sharp$ with $\kappa\subset\mathscr{K}$, then*

$$|||u-u_h|||^2_{\mathrm{DG}}\le C\sum_{\kappa\in\mathcal{T}_h}\frac{h_\kappa^{2(s_\kappa-1)}}{p_\kappa^{2(l_\kappa-1)}}\left(\bar{a}_\kappa+\mathscr{G}_\kappa(h_\kappa,p_\kappa)\right)\|\mathfrak{E}u\|^2_{H^{l_\kappa}(\mathscr{K})},$$

where, $s_\kappa=\min\{p_\kappa+1,l_\kappa\}$,

$$\begin{aligned}\mathscr{G}_\kappa(h_\kappa,p_\kappa):=\bar{a}_\kappa^2p_\kappa h_\kappa^{-1}\max_{F\subset\partial\kappa\setminus\partial\Omega_{\mathrm{N}}}\sigma|_F^{-1}+\bar{a}_\kappa^2p_\kappa^2h_\kappa^{-1}\max_{F\subset\partial\kappa\setminus\partial\Omega_{\mathrm{N}}}\sigma|_F^{-1}\\ +p_\kappa^{-1}h_\kappa\max_{F\subset\partial\kappa\setminus\partial\Omega_{\mathrm{N}}}\sigma|_F,\end{aligned}$$

and C is a positive constant, independent of the discretization parameters and the number of faces per element.

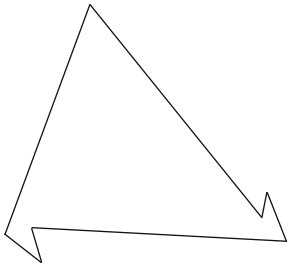

Fig. 4.2 As the small faces degenerate further, this element will not satisfy Assumption 30 but it is p-coverable and, of course, has a fixed number of faces

4.4 Mesh Assumptions for General Polytopic Elements

We conclude this chapter by discussing the relationship (or lack thereof) between the different mesh assumptions presented so far, each allowing for a proof of stability and convergence of the underlying DGFEM (4.5). On the one hand, Assumption 25 restricts the number of faces that each element in the mesh may possess; this assumption is necessary when applying the inverse estimate presented in Lemma 11 in a facewise fashion to establish stability of the DGFEM, cf. Lemma 27. On the other hand, Assumption 30, which removes this restriction on the number of element faces, is sufficient to deduce the inverse estimate stated in Lemma 32. Although one may be tempted at first sight to conclude that the latter setting includes the former, this is *not* necessarily the case. To substantiate this, consider the polygonal element depicted in Fig. 4.2; this cannot satisfy Assumption 30, with increasing degeneration of the small faces, yet it is p-coverable as these small faces degenerate for increasing p. Also the quadrilateral of Fig. 3.6 does not satisfy Assumption 30 as it fails the shape-regularity condition.

The above example shows that the two settings are applicable to different element shapes and, together, can allow for an extremely general class of admissible element shapes for which the above theory is valid. Furthermore, the two approaches may easily be combined within the same mesh allowing for mesh configurations and elements of unprecedented generality to be used to define provably convergent DGFEMs.

Chapter 5
DGFEMs for Second-Order PDEs of Mixed-Type

We now return to the discretization of the general PDE problem stated in (2.1), (2.3). In particular, we study the stability and convergence properties of a variant of the DGFEM defined in Sect. 2.4 by exploiting the scheme introduced in [100] which allows for the treatment of general diffusivity tensors, i.e., condition (4.6) is no longer required to be satisfied. While this class of second-order PDEs with nonnegative characteristic form naturally includes parabolic equations, we also pursue the analysis for this class of PDEs in a separate manner following the article [56]. The general analysis of DGFEMs for PDEs with nonnegative characteristic form is pursued under Assumption 25, i.e., assuming that the number of faces each element possesses remains bounded under mesh refinement. For the special subclass of parabolic problems discussed in Sect. 5.3 below, we adopt Assumption 30, which permits an arbitrary number of faces per element, thereby highlighting that both assumptions lead to rigorous a priori error estimates for DGFEMs applied to parabolic problems.

The outline of this chapter is as follows. In Sect. 5.1 we recall the PDE problem to be studied and introduce the corresponding DGFEM. The stability and a priori error analysis of this scheme is undertaken in Sect. 5.2. Finally, in Sect. 5.3 we develop the error analysis of the DGFEM discretization of a second-order parabolic problem.

5.1 Model Problem and Discretization

We begin by briefly recalling the general second-order PDE with nonnegative characteristic introduced in Sect. 2.1. To this end, given an open bounded Lipschitz domain Ω in $\mathbb{R}^d$, $d \geq 1$, with boundary $\partial\Omega$, we consider the PDE: find u such that

$$-\nabla \cdot (a\nabla u) + \nabla \cdot (\mathbf{b}u) + cu = f \quad \text{in } \Omega, \tag{5.1}$$

A. Cangiani et al., *hp-Version Discontinuous Galerkin Methods on Polygonal and Polyhedral Meshes*, SpringerBriefs in Mathematics,
DOI 10.1007/978-3-319-67673-9_5

$$u = g_{\mathrm{D}} \quad \text{on } \partial\Omega_{\mathrm{D}} \cup \partial_{-}\Omega, \tag{5.2}$$

$$\mathbf{n} \cdot (a\nabla u) = g_{\mathrm{N}} \quad \text{on } \partial\Omega_{\mathrm{N}}; \tag{5.3}$$

here, $f \in L^2(\Omega)$, $a = \{a_{ij}\}_{i,j=1}^{d}$, with $a_{ij} \in L^{\infty}(\Omega)$, $a_{ij} = a_{ji}$, for $i,j = 1,\ldots,d$, such that, at each $\mathbf{x}$ in $\bar{\Omega}$, we have

$$\sum_{i,j=1}^{d} a_{ij}(\mathbf{x})\xi_i\xi_j \geq 0 \tag{5.4}$$

for any vector $\boldsymbol{\xi} = (\xi_1,\ldots,\xi_d)^{\top} \in \mathbb{R}^d$, $\mathbf{b} = (b_1,\ldots,b_d)^{\top} \in \left[W^{1,\infty}(\Omega)\right]^d$, and $c \in L^{\infty}(\Omega)$. Let $\mathbf{n}$ denote the unit outward normal vector to $\partial\Omega$. We recall that $\partial_0\Omega = \partial\Omega_{\mathrm{D}} \cup \partial\Omega_{\mathrm{N}}$ and $\partial\Omega\backslash\partial_0\Omega = \partial_{-}\Omega \cup \partial_{+}\Omega$ denote the 'elliptic' and 'hyperbolic' portions of the boundary $\partial\Omega$ of the computational domain Ω, cf. Sect. 2.1 for further details.

For the proceeding analysis, we adopt the standard hypothesis: there exists a constant vector $\boldsymbol{\zeta} \in \mathbb{R}^d$ such that

$$c(\mathbf{x}) + \frac{1}{2}\,\nabla \cdot \mathbf{b}(\mathbf{x}) + \mathbf{b}(\mathbf{x}) \cdot \boldsymbol{\zeta} \geq \gamma_0 \ \text{ a.e. } \mathbf{x} \in \Omega, \tag{5.5}$$

where γ_0 is a positive constant. For simplicity of presentation, following [124] we assume throughout that (5.5) may be satisfied with $\boldsymbol{\zeta} \equiv \mathbf{0}$; we then define the positive function c_0 by

$$c_0(\mathbf{x}) := \left(c(\mathbf{x}) + \frac{1}{2}\,\nabla \cdot \mathbf{b}(\mathbf{x})\right)^{1/2} \quad \text{a.e. } \mathbf{x} \in \Omega. \tag{5.6}$$

Proceeding as in Chap. 3, we write $\mathscr{T}_h$ to denote the computational mesh associated with the domain $\Omega \subset \mathbb{R}^d$, $d > 1$, consisting of disjoint open polytopic elements κ constructed such that $\bar{\Omega} = \cup_{\kappa\in\mathscr{T}_h}\bar{\kappa}$. As before, $\mathscr{F}_h$ denotes the set of open $(d-1)$-dimensional element faces associated with $\mathscr{T}_h$, and we write $\mathscr{F}_h = \mathscr{F}_h^{\mathscr{I}} \cup \mathscr{F}_h^{\mathscr{B}}$, where $\mathscr{F}_h^{\mathscr{I}}$ denotes the set of element faces $F \in \mathscr{F}_h$ that are contained in Ω, and $\mathscr{F}_h^{\mathscr{B}}$ is the set of boundary element faces. We decompose $\mathscr{F}_h^{\mathscr{B}} = \mathscr{F}_h^{-} \cup \mathscr{F}_h^{+} \cup \mathscr{F}_h^{D} \cup \mathscr{F}_h^{N}$, where $\mathscr{F}_h^{-}, \mathscr{F}_h^{+}, \mathscr{F}_h^{D}, \mathscr{F}_h^{N} \subset \mathscr{F}_h^{\mathscr{B}}$ denote the subsets of boundary faces belonging to $\partial_{-}\Omega$, $\partial_{+}\Omega$, $\partial\Omega_{\mathrm{D}}$, and $\partial\Omega_{\mathrm{N}}$, respectively. Implicit in this definition is the assumption that $\mathscr{T}_h$ respects the decomposition of $\partial\Omega$, in the sense that each $F \in \mathscr{F}_h^{\mathscr{B}}$ belongs to the interior of exactly one of $\partial_{-}\Omega$, $\partial_{+}\Omega$, $\partial\Omega_{\mathrm{D}}$, and $\partial\Omega_{\mathrm{N}}$. The underlying finite element space is again defined by

$$V^{\mathbf{p}}(\mathscr{T}_h) := \{u \in L^2(\Omega) : u|_{\kappa} \in \mathscr{P}_{p_\kappa}(\kappa), \kappa \in \mathscr{T}_h\},$$

where the local polynomial spaces are defined in the physical frame, without the need to map from a given reference element. In addition to the jump operator $[\![\cdot]\!]$ defined in Sect. 2.3, for $\kappa \in \mathscr{T}_h$, we introduce the *upwind jump* of the scalar-valued function v across a face $F \subset \partial_- \kappa \backslash \partial\Omega$ defined by

$$\lfloor v \rfloor := v_\kappa^+ - v_\kappa^-.$$

As before, since it will always be clear to which element κ, $\kappa \in \mathscr{T}_h$, the quantities $v_\kappa^\pm$ correspond to, we suppress the subscript κ.

Throughout this chapter, we treat the case of a general diffusion tensor a, i.e., we no longer require that the condition (4.6) holds, or indeed that $a \in [V^{\mathbf{q}}(\mathscr{T}_h)]^{d\times d}_{\mathrm{sym}}$, for some composite polynomial degree vector $\mathbf{q}$, cf. Sect. 4.1. To this end, we exploit a variant of the DGFEM introduced in Sect. 2.4, based on the work undertaken in [100] for purely elliptic problems. Thereby, following [100], we introduce the bilinear form

$$B(w, v) := B_{\mathrm{ar}}(w, v) + \hat{B}_{\mathrm{d}}(w, v), \tag{5.7}$$

where $B_{\mathrm{ar}}(\cdot,\cdot)$ represents the DGFEM discretization of the advection and reaction terms defined by

$$\begin{aligned} B_{\mathrm{ar}}(w, v) := &\sum_{\kappa\in\mathscr{T}_h} \int_\kappa \Big(\nabla\cdot(\mathbf{b}w) + cw\Big)v \,\mathrm{d}\mathbf{x} - \sum_{\kappa\in\mathscr{T}_h} \int_{\partial_-\kappa\backslash\partial\Omega} (\mathbf{b}\cdot\mathbf{n})\lfloor w\rfloor v^+ \,\mathrm{d}s \\ &- \sum_{\kappa\in\mathscr{T}_h} \int_{\partial_-\kappa\cap(\partial\Omega_{\mathrm{D}}\cup\partial_-\Omega)} (\mathbf{b}\cdot\mathbf{n})w^+v^+ \,\mathrm{d}s, \end{aligned}$$

and $\hat{B}_{\mathrm{d}}(\cdot,\cdot)$ is the (modified) DGFEM discretization of the diffusion operator given by

$$\begin{aligned} \hat{B}_{\mathrm{d}}(w, v) := &\sum_{\kappa\in\mathscr{T}_h} \int_\kappa a\nabla w\cdot\nabla v \,\mathrm{d}\mathbf{x} + \int_{\mathscr{F}_h^{\mathscr{I}}\cup\mathscr{F}_h^D} \sigma[\![w]\!]\cdot[\![v]\!] \,\mathrm{d}s \\ &- \int_{\mathscr{F}_h^{\mathscr{I}}\cup\mathscr{F}_h^D} \Big(\{\!\{\sqrt{a}\boldsymbol{\Pi}_{L^2}(\sqrt{a}\nabla w)\}\!\}\cdot[\![v]\!] + \{\!\{\sqrt{a}\boldsymbol{\Pi}_{L^2}(\sqrt{a}\nabla v)\}\!\}\cdot[\![w]\!]\Big) \,\mathrm{d}s; \end{aligned}$$

here, $\boldsymbol{\Pi}_{L^2} : [L^2(\Omega)]^d \to [V^{\mathbf{p}}(\mathscr{T}_h)]^d$ denotes the orthogonal L^2-projection onto the finite element space $[V^{\mathbf{p}}(\mathscr{T}_h)]^d$, cf. Chap. 4.

Thereby, the DGFEM approximation of problem (5.1)–(5.3) is given by: find $u_h \in V^{\mathbf{p}}(\mathscr{T}_h)$ such that

$$B(u_h, v_h) = \hat{\ell}(v_h) \quad \forall v_h \in V^{\mathbf{p}}(\mathscr{T}_h), \tag{5.8}$$

where

$$\hat{\ell}(v) := \sum_{\kappa\in\mathscr{T}_h}\int_\kappa fv\,\mathrm{d}\mathbf{x} - \sum_{\kappa\in\mathscr{T}_h}\int_{\partial_-\kappa\cap(\partial\Omega_\mathrm{D}\cup\partial_-\Omega)}(\mathbf{b}\cdot\mathbf{n})g_\mathrm{D}v^+\,\mathrm{d}s$$
$$-\int_{\partial\Omega_\mathrm{D}} g_\mathrm{D}\Big(\sqrt{a}\boldsymbol{\Pi}_{L^2}(\sqrt{a}\nabla v)\cdot\mathbf{n}-\sigma v\Big)\,\mathrm{d}s + \int_{\partial\Omega_\mathrm{N}} g_\mathrm{N}v\,\mathrm{d}s.$$

Referring to the definition of $B_\mathrm{d}(\cdot,\cdot)$ given in Sect. 4.1, we observe that, in general, $\hat{B}_\mathrm{d}(w,v) \neq B_\mathrm{d}(w,v)$, for $w, v \in V^{\mathbf{p}}(\mathscr{T}_h)$; clearly, we only have equality when the diffusion tensor satisfies $\sqrt{a}\nabla v \in [V^{\mathbf{p}}(\mathscr{T}_h)]^d$ for $v \in V^{\mathbf{p}}(\mathscr{T}_h)$. Indeed, the key advantage of the above DGFEM is that it allows for the proceeding stability and a priori error analysis to be undertaken in the most general setting. Finally, $\sigma : \mathscr{F}_h^{\mathscr{I}} \cup \mathscr{F}_h^D \to \mathbb{R}$ denotes the discontinuity-penalization function, which will be precisely defined below, based on a variant of Definition 26.

5.2 Stability and A Priori Error Analysis

We now consider the stability and *hp*-version convergence analysis of the DGFEM (5.8); as already noted above, the results presented in this section assume Assumption 25 holds. To this end, we introduce the DGFEM energy norm defined by

$$|||v|||_\mathrm{DG}^2 := |||v|||_\mathrm{ar}^2 + |||v|||_\mathrm{d}^2, \tag{5.9}$$

where

$$|||v|||_\mathrm{ar}^2 := \sum_{\kappa\in\mathscr{T}_h}\Big(\|c_0v\|_{L^2(\kappa)}^2 + \frac{1}{2}\|v^+\|_{\partial_-\kappa\cap(\partial\Omega_\mathrm{D}\cup\partial_-\Omega)}^2$$
$$+\frac{1}{2}\|v^+-v^-\|_{\partial_-\kappa\setminus\partial\Omega}^2 + \frac{1}{2}\|v^+\|_{\partial_+\kappa\cap\partial\Omega}^2\Big), \tag{5.10}$$

with c_0 defined as in (5.6), and

$$|||v|||_\mathrm{d}^2 := \sum_{\kappa\in\mathscr{T}_h}\|\sqrt{a}\nabla v\|_{L^2(\kappa)}^2 + \int_{\mathscr{F}_h^{\mathscr{I}}\cup\mathscr{F}_h^D}\sigma|[\![v]\!]|^2\,\mathrm{d}s; \tag{5.11}$$

here, we use the notation $\|\cdot\|_\tau$, $\tau \subset \partial\kappa$, to denote the (semi)norm associated with the (semi)inner product $(v,w)_\tau := \int_\tau |\mathbf{b}\cdot\mathbf{n}|vw\,\mathrm{d}s$. Note that when $\mathbf{b} \equiv \mathbf{0}$ and $c \equiv 0$,

upon formally setting $c_0 = 0$, the DGFEM norm defined in (5.9) is equivalent to the corresponding norm employed in Chap. 4 for the study of the pure diffusion problem, cf. (4.11).

We define $\mathscr{V} := V + V^{\mathbf{p}}(\mathscr{T}_h)$, where $V \subset L^2(\Omega)$ is a suitable solution space for the PDE problem (5.1)–(5.3); for instance, when $a \equiv \mathbf{0}$, a natural choice is the graph space $V := \mathscr{G}(\mathscr{L}, \Omega)$, whereas when a is strictly positive definite, we can take $V := H^1(\Omega)$. After a lengthy yet elementary calculation, we deduce the identity

$$B_{\mathrm{ar}}(v, v) = |||v|||_{\mathrm{ar}}^2 \tag{5.12}$$

for all $v \in \mathscr{V}$; we refer to [124] for details. The coercivity and continuity of $\hat{B}_{\mathrm{d}}(\cdot,\cdot)$ on $\mathscr{V} \times \mathscr{V}$, with respect to the norm $|||\cdot|||_{\mathrm{d}}$, is presented in the next lemma.

Lemma 37 *Given that Assumption 25 holds, we define the discontinuity-penalization function $\sigma : \mathscr{F}_h^{\mathscr{I}} \cup \mathscr{F}_h^D \to \mathbb{R}$ by*

$$\sigma(\mathbf{x}) := \begin{cases} C_\sigma \max\limits_{\kappa \in \{\kappa^+, \kappa^-\}} \left\{ C_{\mathrm{INV}}(p_\kappa, \kappa, F)\, \dfrac{A_F|_\kappa p_\kappa^2 |F|}{|\kappa|} \right\}, & \mathbf{x} \in F \in \mathscr{F}_h^{\mathscr{I}},\ F \subset \partial\kappa^+ \cap \partial\kappa^-, \\ C_\sigma\, A_F\, C_{\mathrm{INV}}(p_\kappa, \kappa, F)\, \dfrac{p_\kappa^2 |F|}{|\kappa|}, & \mathbf{x} \in F \in \mathscr{F}_h^D,\ F \subset \partial\kappa, \end{cases} \tag{5.13}$$

where $A_F := \|\sqrt{a}\mathbf{n}\|^2_{L^\infty(F)}$, for every face $F \subset \partial\kappa$, $F \in \mathscr{F}_h^{\mathscr{I}} \cup \mathscr{F}_h^D$, and C_σ is a sufficiently large positive constant. Then, the bilinear form $\hat{B}_{\mathrm{d}}(\cdot,\cdot)$ is coercive and continuous over $\mathscr{V} \times \mathscr{V}$, that is

$$\hat{B}_{\mathrm{d}}(v, v) \geq C_{\mathrm{coer}} |||v|||_{\mathrm{d}}^2 \quad \textit{for all} \quad v \in \mathscr{V}, \tag{5.14}$$

and

$$\hat{B}_{\mathrm{d}}(w, v) \leq C_{\mathrm{cont}} |||w|||_{\mathrm{d}}\, |||v|||_{\mathrm{d}} \quad \textit{for all} \quad w, v \in \mathscr{V}, \tag{5.15}$$

respectively, where C_{coer} and C_{cont} are positive constants, independent of the discretization parameters.

Proof The proof follows in an analogous fashion to the proof of Lemma 27, cf., also, the proof of Lemma 35. For $v \in \mathscr{V}$, we note that

$$\tilde{B}_{\mathrm{d}}(v, v) = |||v|||_{\mathrm{d}}^2 - 2 \int_{\mathscr{F}_h^{\mathscr{I}} \cup \mathscr{F}_h^D} \{\!\{ \sqrt{a}\boldsymbol{\Pi}_{L^2}(\sqrt{a}\nabla v) \}\!\} \cdot [\![v]\!]\, \mathrm{d}s. \tag{5.16}$$

Given $F \in \mathscr{F}_h^{\mathscr{I}}$ such that $F \subset \partial\kappa^+ \cap \partial\kappa^-$, $\kappa^\pm \in \mathscr{T}_h$, and noting that $\sqrt{a}$ is symmetric, we deduce that

$$
\begin{aligned}
&2\int_F \{\!\{\sqrt{a}\boldsymbol{\Pi}_{L^2}(\sqrt{a}\nabla v)\}\!\} \cdot [\![v]\!]\,\mathrm{d}s \\
&\quad = \int_F \left(\boldsymbol{\Pi}_{L^2}(\sqrt{a}\nabla v)|_{\kappa^+} \cdot \sqrt{a}|_{\kappa^+}[\![v]\!] + \boldsymbol{\Pi}_{L^2}(\sqrt{a}\nabla v)|_{\kappa^-} \cdot \sqrt{a}|_{\kappa^-}[\![v]\!]\right) \mathrm{d}s \\
&\quad \leq \epsilon \sum_{\kappa\in\{\kappa^+,\kappa^-\}} \|\sqrt{A_F/\sigma}\,\boldsymbol{\Pi}_{L^2}(\sqrt{a}\nabla v)\|^2_{L^2(F\subset\partial\kappa)} + \frac{1}{4\epsilon}\|\sqrt{\sigma}[\![v]\!]\|^2_{L^2(F)}. \qquad (5.17)
\end{aligned}
$$

For simplicity of presentation, both here and throughout the rest of this section, we note that when $\sigma \equiv 0$ on a given face, then the corresponding term arising in the summation over element faces $\mathscr{F}_h$ does not arise; thereby, ensuring that $1/\sigma$ is always well-defined.

Employing the inverse inequality stated in Lemma 11, the definition of σ given in (5.13), and the stability of the L^2-projection $\boldsymbol{\Pi}_{L^2}$, gives

$$
\begin{aligned}
\|\sqrt{A_F/\sigma}\,\boldsymbol{\Pi}_{L^2}(\sqrt{a}\nabla v)\|^2_{L^2(F\subset\partial\kappa)} &\leq C_{\mathrm{INV}}(p_\kappa,\kappa,F)\frac{A_F p_\kappa^2|F|}{\sigma|F|\kappa|}\|\boldsymbol{\Pi}_{L^2}(\sqrt{a}\nabla v)\|^2_{L^2(\kappa)} \\
&\leq C_\sigma^{-1}\|\sqrt{a}\nabla v\|^2_{L^2(\kappa)},
\end{aligned}
$$

for $\kappa \in \{\kappa^+,\kappa^-\}$. An analogous bound also holds for $F \in \mathscr{F}_h^D$; thereby, we deduce that

$$
\tilde{B}_{\mathrm{d}}(v,v) \geq \left(1 - \frac{2C_F}{C_\sigma}\epsilon\right)\sum_{\kappa\in\mathscr{T}_h}\|\sqrt{a}\nabla v\|^2_{L^2(\kappa)} + \left(1-\frac{1}{2\epsilon}\right)\sum_{F\in\mathscr{F}_h^{\mathscr{I}}\cup\mathscr{F}_h^D}\|\sqrt{\sigma}[\![v]\!]\|^2_{L^2(F)}.
$$

Given that C_F is uniformly bounded, cf. Assumption 25, coercivity follows by selecting $C_\sigma > 2C_F\epsilon$ for some $\epsilon > 1/2$, cf. Lemma 27. Additionally, continuity may be deduced in a similar fashion.

Remark 38 The above proof highlights the benefit of defining the flux face terms arising in $\hat{B}_{\mathrm{d}}(\cdot,\cdot)$ in this non-standard manner. In particular, the discontinuity-penalization function σ depends only on the *normal* component $\mathbf{n}^\top a\mathbf{n}$ of the diffusion tensor a on the face F; in contrast, we note that when σ is given according to Definition 26, cf., also, Lemma 35, it depends on a within a larger subdomain of Ω, namely, over the element(s) which share the common face F. Indeed, upon observing the identity $|\sqrt{a}\mathbf{n}|^2 = (\sqrt{a}\mathbf{n})^\top(\sqrt{a}\mathbf{n}) = \mathbf{n}^\top a\mathbf{n}$, we have $A_F = \|\mathbf{n}^\top a\mathbf{n}\|_{L^\infty(F)}$, which allows for sharp face-wise control of the magnitude of the discontinuity-penalization function in regions of degeneracy of a. This choice is particularly useful for the discretization of PDEs such as the fourth equation in Example 3, where a does not satisfy condition (4.6), and moreover a is degenerate across $y = 0$. We refer to [100] for further discussion regarding this subtle issue.

5.2.1 Inf-Sup Stability

In order to bound the terms arising from the discretization of the underlying first-order PDE operator, cf. the definition of $B_{\mathrm{ar}}(\cdot,\cdot)$ above, the error analysis presented in [124] relies on exploiting optimal *hp*-approximation results for the trace of the local L^2-projection operator on a given face of an element κ in the finite element mesh $\mathscr{T}_h$, where $\mathscr{T}_h$ was assumed to consist of shape-regular, affine tensor-product elements; for analogous results on simplices, we refer to [62, 138]. However, due to the lack of corresponding *hp*-approximation results for the local L^2-projection operator on polytopic elements, it is not possible to directly generalize the analysis from [124] to the present *polytopic* context. To address this issue, we pursue an alternative approach based on establishing an inf-sup condition for the bilinear form $B(\cdot,\cdot)$ defined in (5.7), with respect to the following streamline-diffusion DGFEM norm:

$$|||v|||_{\mathrm{s}} := \left(|||v|||_{\mathrm{DG}}^2 + \sum_{\kappa\in\mathscr{T}_h} \lambda_\kappa \|\mathbf{b}\cdot\nabla v\|_{L^2(\kappa)}^2 \right)^{1/2}, \tag{5.18}$$

where

$$\lambda_\kappa := \min\left\{ \frac{1}{\|\mathbf{b}\|_{L^\infty(\kappa)}}, \frac{1}{\tilde{\sigma}_\kappa} \right\} \frac{h_\kappa^\perp}{p_\kappa^2} \quad \forall \kappa \in \mathscr{T}_h, \tag{5.19}$$

for $p_\kappa \geq 1$, and $\tilde{\sigma}_\kappa$ is given by

$$\tilde{\sigma}_\kappa := C_\sigma \max_{F\subset\partial\kappa} \left\{ \max_{\substack{\tilde{\kappa}\in\{\kappa,\kappa'\}\\ F\subset\partial\kappa\cap\partial\kappa'}} \left\{ C_{\mathrm{inv},4} \frac{\bar{a}_{\tilde{\kappa}} p_{\tilde{\kappa}}^2}{h_{\tilde{\kappa}}^\perp} d \right\} \right\} \quad \forall \kappa \subset \mathscr{T}_h,\ d = 2,3, \tag{5.20}$$

where $C_{\mathrm{inv},4}$ is given in Lemma 11, and $\bar{a}_\kappa := \||\sqrt{a}|_2^2\|_{L^\infty(\kappa)}$, $\kappa \in \mathscr{T}_h$; note that this definition of $\bar{a}_\kappa$ is a generalization of the notation introduced in Chap. 4. The constant $\tilde{\sigma}_\kappa$ may be zero locally where $\bar{a}_\kappa = 0$; in this case it is understood that λ_κ takes the value of the first term in the minimum in (5.19). Furthermore, the mesh parameter $h_\kappa^\perp$ is defined as follows:

$$h_\kappa^\perp := \min_{F\subset\partial\kappa} \frac{\sup_{\kappa_\flat^F\subset\kappa} |\kappa_\flat^F|}{|F|} d \qquad \forall \kappa \in \mathscr{T}_h,\ d = 2,3, \tag{5.21}$$

with $\kappa_\flat^F$ as in Definition 7. Additionally, we note that the following relation holds:

$$h_\kappa^\perp \leq h_\kappa. \tag{5.22}$$

Remark 39 The coefficient λ_κ is an indicator function for each element $\kappa \in \mathscr{T}_h$, measuring the length scale of competition between advection and diffusion over κ.

More precisely, if the underlying PDE is advection-dominated over the subdomain κ, then λ_κ is equal to the first term in the minimum; on the other hand, in the diffusion-dominated regime, λ_κ will be equal to the second term. Through this choice of λ_κ, the resulting inf-sup stability condition shown below holds for both regimes.

Remark 40 With a slight loss of generality, the case $p_\kappa = 0$, which is relevant in the hyperbolic setting, is excluded from the definition of λ_κ. However, we point out that, if the underlying PDE problem is strictly hyperbolic, and hence $a \equiv \mathbf{0}$, and $p_\kappa = 0$ is selected for all $\kappa \in \mathscr{T}_h$, then upon formally setting $\lambda_\kappa = 0$ for all $\kappa \in \mathscr{T}_h$, the streamline-diffusion DGFEM norm reduces to the advection-reaction DGFEM norm $|||\cdot|||_{\mathrm{ar}}$ defined in (5.10); in this setting, the proceeding analysis holds in a trivial manner.

Recalling the definition of $h_\kappa^\perp$, together with an upper bound on the constant $C_{\mathrm{INV}}(p,\kappa,F)$ defined in Lemma 11, the inverse inequality (3.13) can be written as: for each $v \in \mathscr{P}_p(\kappa)$ and $F \subset \partial\kappa$, we have

$$\begin{aligned}\|v\|_{L^2(F)}^2 &\le C_{\mathrm{INV}}(p,\kappa,F)\frac{p^2|F|}{|\kappa|}\|v\|_{L^2(\kappa)}^2 \\ &\le C_{\mathrm{inv},4}\frac{|\kappa|}{\sup_{\kappa_\flat^F\subset\kappa}|\kappa_\flat^F|}\frac{p^2|F|}{|\kappa|}\|v\|_{L^2(\kappa)}^2 \le C_{\mathrm{inv},4}\frac{p^2}{h_\kappa^\perp}d\|v\|_{L^2(\kappa)}^2. \end{aligned} \tag{5.23}$$

Further, from the definition of $\sigma|_F$ given in (5.13), in conjunction with the definition of $h_\kappa^\perp$, cf. (5.21), we deduce the following bound

$$\tilde{\sigma}_\kappa \ge \sigma|_F, \quad F \subset \partial\kappa \quad \forall \kappa \in \mathscr{T}_h. \tag{5.24}$$

Assumption 41 *For the reminder of this chapter we assume that the advection field* $\mathbf{b}$ *satisfies the following condition:*

$$\mathbf{b}\cdot\nabla_h\xi \in V^{\mathbf{p}}(\mathscr{T}_h) \quad \forall \xi \in V^{\mathbf{p}}(\mathscr{T}_h). \tag{5.25}$$

We note that Assumption 41 is a standard condition employed within the literature for the mathematical treatment of the advection operator, cf. [124], for example. We refer to Remark 44 regarding the generalization of the proceeding analysis to general advection fields.

With this notation, we now prove an inf-sup condition for the bilinear form $B(\cdot,\cdot)$ with respect to the streamline-diffusion DGFEM norm (5.18).

Theorem 42 *Let* $\mathscr{T}_h = \{\kappa\}$ *be a subdivision of* $\Omega \subset \mathbb{R}^d$, $d = 2, 3$, *consisting of general polytopic elements satisfying Assumptions 13 and 25. Then, assuming that* $\mathbf{b}$ *satisfies Assumption 41, there exists a positive constant* Λ_s, *independent of the*

mesh size h and the polynomial degree p, such that:

$$\inf_{v\in V^{\mathbf{p}}(\mathscr{T}_h)\setminus\{0\}} \sup_{\mu\in V^{\mathbf{p}}(\mathscr{T}_h)\setminus\{0\}} \frac{B(v,\mu)}{|||v|||_{\mathrm{s}}|||\mu|||_{\mathrm{s}}} \geq \Lambda_s, \tag{5.26}$$

where the discontinuity-penalization function σ is given by (5.13)*.*

Proof For every $v \in V^{\mathbf{p}}(\mathscr{T}_h)$, we select $\mu := v + \alpha v_s$, with $v_s|_\kappa := \lambda_\kappa \mathbf{b}\cdot\nabla v$ for all $\kappa \in \mathscr{T}_h$, where α is a positive real number which will be selected below, cf. (5.40). From Assumption 41, we note that $\mu \in V^{\mathbf{p}}(\mathscr{T}_h)$; thereby, the statement of the theorem immediately follows upon proving the two bounds:

$$|||\mu|||_{\mathrm{s}} \leq C^*|||v|||_{\mathrm{s}}, \tag{5.27}$$

and

$$B(v,\mu) \geq C_*|||v|||_{\mathrm{s}}^2, \tag{5.28}$$

with $\Lambda_s = C_*/C^*$, where C^* and C_* are positive constants, independent of h and p.

To prove (5.27), we first bound each term arising in $|||v_s|||_{\mathrm{ar}}$; to this end, employing Lemma 14, together with (5.19), (5.6), and inequality (5.22), gives

$$\begin{aligned}
\|c_0 v_s\|_{L^2(\Omega)}^2 &\leq \|c_0\|_{L^\infty(\Omega)}^2 \sum_{\kappa\in\mathscr{T}_h} \lambda_\kappa^2 \|\mathbf{b}\|_{L^\infty(\kappa)}^2 \|\nabla v\|_{L^2(\kappa)}^2 \\
&\leq \|c_0\|_{L^\infty(\Omega)}^2 C_{\mathrm{inv},5} \sum_{\kappa\in\mathscr{T}_h} \lambda_\kappa^2 \frac{p_\kappa^4 \|\mathbf{b}\|_{L^\infty(\kappa)}^2}{h_\kappa^2} \|v\|_{L^2(\kappa)}^2 \\
&\leq \|c_0\|_{L^\infty(\Omega)}^2 \frac{C_{\mathrm{inv},5}}{\gamma_0} \|c_0 v\|_{L^2(\Omega)}^2 \leq C_1 |||v|||_{\mathrm{s}}^2.
\end{aligned} \tag{5.29}$$

Exploiting (5.23), gives

$$\begin{aligned}
&\sum_{\kappa\in\mathscr{T}_h} \left(1/2 \|v_s^+\|_{\partial_-\kappa\cap(\partial\Omega_{\mathrm{D}}\cup\partial_-\Omega)}^2 + 1/2 \|v_s^+ - v_s^-\|_{\partial_-\kappa\setminus\partial\Omega}^2 + 1/2 \|v_s^+\|_{\partial_+\kappa\cap\partial\Omega}^2 \right) \\
&\leq \sum_{\kappa\in\mathscr{T}_h} \|\mathbf{b}\|_{L^\infty(\kappa)} \lambda_\kappa^2 \sum_{F\subset\partial\kappa} \|\mathbf{b}\cdot\nabla v\|_{L^2(F)}^2 \\
&\leq C_F C_{\mathrm{inv},4} d \sum_{\kappa\in\mathscr{T}_h} \|\mathbf{b}\|_{L^\infty(\kappa)} \frac{p_\kappa^2}{h_\kappa^\perp} \lambda_\kappa^2 \|\mathbf{b}\cdot\nabla v\|_{L^2(\kappa)}^2 \leq C_2 |||v|||_{\mathrm{s}}^2.
\end{aligned} \tag{5.30}$$

Similarly, employing Assumption 41, together with Lemma 14, the streamline-diffusion term in (5.18) can be bounded as follows:

$$\begin{aligned}\sum_{\kappa\in\mathscr{T}_h}\lambda_\kappa\|\mathbf{b}\cdot\nabla v_s\|^2_{L^2(\kappa)} &\le \sum_{\kappa\in\mathscr{T}_h}\lambda_\kappa\|\mathbf{b}\|^2_{L^\infty(\kappa)}\Big(\lambda_\kappa^2\|\nabla(\mathbf{b}\cdot\nabla v)\|^2_{L^2(\kappa)}\Big)\\ &\le \sum_{\kappa\in\mathscr{T}_h}C_{\mathrm{inv},5}\lambda_\kappa^2\frac{p_\kappa^4\|\mathbf{b}\|^2_{L^\infty(\kappa)}}{h_\kappa^2}\Big(\lambda_\kappa\|\mathbf{b}\cdot\nabla v\|^2_{L^2(\kappa)}\Big)\\ &\le \sum_{\kappa\in\mathscr{T}_h}C_{\mathrm{inv},5}\Big(\lambda_\kappa\|\mathbf{b}\cdot\nabla v\|^2_{L^2(\kappa)}\Big)\le C_3|||v|||^2_{\mathrm{s}}. \qquad (5.31)\end{aligned}$$

We now consider bounding $|||v_s|||_{\mathrm{d}}$; to this end, we make use of the upper bound for λ_κ arising via the second term inside the minimum in (5.19). Employing Lemma 14, the definition of $\tilde{\sigma}_\kappa$ in (5.20), and (5.22), gives

$$\begin{aligned}\sum_{\kappa\in\mathscr{T}_h}\|\sqrt{a}\nabla v_s\|^2_{L^2(\kappa)} &\le \sum_{\kappa\in\mathscr{T}_h}\bar{a}_\kappa\lambda_\kappa^2\|\nabla(\mathbf{b}\cdot\nabla v)\|^2_{L^2(\kappa)}\\ &\le \sum_{\kappa\in\mathscr{T}_h}C_{\mathrm{inv},5}\lambda_\kappa\frac{\bar{a}_\kappa p_\kappa^4}{h_\kappa^2}\Big(\lambda_\kappa\|\mathbf{b}\cdot\nabla v\|^2_{L^2(\kappa)}\Big)\\ &\le \sum_{\kappa\in\mathscr{T}_h}C_{\mathrm{inv},5}\frac{\bar{a}_\kappa p_\kappa^2}{\tilde{\sigma}_\kappa h_\kappa}\Big(\lambda_\kappa\|\mathbf{b}\cdot\nabla v\|^2_{L^2(\kappa)}\Big)\\ &\le \frac{C_{\mathrm{inv},5}}{C_\sigma C_{\mathrm{inv},4}d}\sum_{\kappa\in\mathscr{T}_h}\lambda_\kappa\|\mathbf{b}\cdot\nabla v\|^2_{L^2(\kappa)}\le C_4|||v|||^2_{\mathrm{s}}. \qquad (5.32)\end{aligned}$$

Finally, employing (5.23) and (5.24), we get

$$\begin{aligned}\int_{\mathscr{F}_h^{\mathscr{I}}\cup\mathscr{F}_h^D}\sigma|[\![v_s]\!]|^2\,\mathrm{d}s &\le 2\sum_{\kappa\in\mathscr{T}_h}\lambda_\kappa^2\sum_{F\subset\partial\kappa:F\in\mathscr{F}_h^{\mathscr{I}}\cup\mathscr{F}_h^D}\sigma|_F\|\mathbf{b}\cdot\nabla v\|^2_{L^2(F)}\\ &\le 2\,C_F\,C_{\mathrm{inv},4}\,d\sum_{\kappa\in\mathscr{T}_h}\lambda_\kappa\frac{\tilde{\sigma}_\kappa p_\kappa^2}{h_\kappa^\perp}\Big(\lambda_\kappa\|\mathbf{b}\cdot\nabla v\|^2_{L^2(\kappa)}\Big)\\ &\le C_5\sum_{\kappa\in\mathscr{T}_h}\Big(\lambda_\kappa\|\mathbf{b}\cdot\nabla v\|^2_{L^2(\kappa)}\Big)\le C_5|||v|||^2_{\mathrm{s}}. \qquad (5.33)\end{aligned}$$

Combining the above bounds, we deduce that

$$|||v_s|||_{\mathrm{s}}\le\hat{C}|||v|||_{\mathrm{s}}, \qquad (5.34)$$

for $\hat{C} = \sqrt{C_1 + C_2 + C_3 + C_4 + C_5}$. Exploiting the triangle inequality, therefore, yields

$$|||\mu|||_{\mathrm{s}} \leq |||\nu|||_{\mathrm{s}} + \alpha |||\nu_s|||_{\mathrm{s}} \leq (1 + \alpha \hat{C}) |||\nu|||_{\mathrm{s}} \equiv C^*(\alpha) |||\nu|||_{\mathrm{s}}, \tag{5.35}$$

which gives (5.27), as required.

To prove (5.28), we begin by observing that $B(\nu, \mu) = B(\nu, \nu) + \alpha B(\nu, \nu_s)$. We first consider the second term, i.e., $B(\nu, \nu_s)$; thereby, we have that

$$B_{\mathrm{ar}}(\nu, \nu_s) = \sum_{\kappa \in \mathscr{T}_h} \Big(\lambda_\kappa \|\mathbf{b} \cdot \nabla \nu\|^2_{L^2(\kappa)} + \int_\kappa (c + \nabla \cdot \mathbf{b}) \nu (\lambda_\kappa \mathbf{b} \cdot \nabla \nu) \, \mathrm{d}\mathbf{x} \tag{5.36}$$

$$- \int_{\partial_- \kappa \setminus \partial\Omega} (\mathbf{b} \cdot \mathbf{n}) \lfloor \nu \rfloor (\lambda_\kappa \mathbf{b} \cdot \nabla \nu)^+ \, \mathrm{d}s - \int_{\partial_- \kappa \cap (\partial\Omega_{\mathrm{D}} \cup \partial_- \Omega)} (\mathbf{b} \cdot \mathbf{n}) \nu^+ (\lambda_\kappa \mathbf{b} \cdot \nabla \nu)^+ \, \mathrm{d}s \Big).$$

Using Lemma 14 and (5.6), the second term in (5.36) may be bounded as follows:

$$\begin{aligned} &\int_\kappa (c + \nabla \cdot \mathbf{b}) \nu (\lambda_\kappa \mathbf{b} \cdot \nabla \nu) \, \mathrm{d}\mathbf{x} \\ &\qquad \leq \|(c + \nabla \cdot \mathbf{b})\|_{L^\infty(\kappa)} \|\nu\|_{L^2(\kappa)} \Big(\sqrt{C_{\mathrm{inv},5}} \, \lambda_\kappa \frac{p_\kappa^2 \|\mathbf{b}\|_{L^\infty(\kappa)}}{h_\kappa} \|\nu\|_{L^2(\kappa)} \Big) \\ &\qquad \leq \sqrt{C_{\mathrm{inv},5}} \|(c + \nabla \cdot \mathbf{b})\|_{L^\infty(\kappa)} \gamma_0^{-1} \|c_0 \nu\|^2_{L^2(\kappa)}. \end{aligned} \tag{5.37}$$

To estimate the boundary terms present in (5.36), we again exploit (5.23) along with standard arguments, to deduce

$$\begin{aligned} &\sum_{\kappa \in \mathscr{T}_h} \Big(\int_{\partial_- \kappa \setminus \partial\Omega} (\mathbf{b} \cdot \mathbf{n}) \lfloor \nu \rfloor (\lambda_\kappa \mathbf{b} \cdot \nabla \nu)^+ \, \mathrm{d}s + \int_{\partial_- \kappa \cap (\partial\Omega_{\mathrm{D}} \cup \partial_- \Omega)} (\mathbf{b} \cdot \mathbf{n}) \nu^+ (\lambda_\kappa \mathbf{b} \cdot \nabla \nu)^+ \, \mathrm{d}s \Big) \\ &\qquad \leq C_F^2 C_{\mathrm{inv},4} d \sum_{\kappa \in \mathscr{T}_h} \Big(\|\nu^+ - \nu^-\|^2_{\partial_- \kappa \setminus \partial\Omega} + \|\nu^+\|^2_{\partial_- \kappa \cap (\partial\Omega_{\mathrm{D}} \cup \partial_- \Omega)} \Big) \\ &\qquad\quad + \sum_{\kappa \in \mathscr{T}_h} \frac{\lambda_\kappa}{4} \|\mathbf{b} \cdot \nabla \nu\|^2_{L^2(\kappa)}. \end{aligned}$$

Using (5.12), together with the last two bounds, we arrive at

$$\begin{aligned} B_{\mathrm{ar}}(\nu, \mu) \geq \big(1 - \alpha \sqrt{C_{\mathrm{inv},5}} \|(c + \nabla \cdot \mathbf{b})\|_{L^\infty(\Omega)} \gamma_0^{-1}\big) \|c_0 \nu\|^2_{L^2(\Omega)} \\ + \Big(\frac{1}{2} - \alpha C_F^2 C_{\mathrm{inv},4} d \Big) \\ \times \sum_{\kappa \in \mathscr{T}_h} \Big(\|\nu^+ - \nu^-\|^2_{\partial_- \kappa \setminus \partial\Omega} + \|\nu^+\|^2_{\partial_- \kappa \cap (\partial\Omega_{\mathrm{D}} \cup \partial_- \Omega)} + \|\nu^+\|^2_{\partial_+ \kappa \cap \partial\Omega} \Big) \\ + \alpha \sum_{\kappa \in \mathscr{T}_h} \frac{3\lambda_\kappa}{4} \|\mathbf{b} \cdot \nabla \nu\|^2_{L^2(\kappa)}. \end{aligned} \tag{5.38}$$

Next, we consider $\hat{B}_{\mathrm{d}}(v, v_s)$; to this end, exploiting the continuity of $\hat{B}_{\mathrm{d}}(\cdot,\cdot)$, cf. (5.15), together with (5.32) and (5.33), gives

$$\hat{B}_{\mathrm{d}}(v, v_s) \leq C_{\mathrm{cont}}|||v|||_{\mathrm{d}}|||v_s|||_{\mathrm{d}} \leq (C_{\mathrm{cont}})^2(C_4 + C_5)|||v|||_{\mathrm{d}}^2 + \sum_{\kappa\in\mathscr{T}_h} \frac{\lambda_\kappa}{4}\|\mathbf{b}\cdot\nabla v\|_{L^2(\kappa)}^2.$$

The last bound, together with the coercivity of $\hat{B}_d(\cdot,\cdot)$, cf. (5.14), leads to

$$\hat{B}_{\mathrm{d}}(v, \mu) \geq \big(C_{\mathrm{coer}} - \alpha(C_{\mathrm{cont}})^2(C_4 + C_5)\big)|||v|||_{\mathrm{d}}^2 - \alpha \sum_{\kappa\in\mathscr{T}_h} \frac{\lambda_\kappa}{4}\|\mathbf{b}\cdot\nabla v\|_{L^2(\kappa)}^2. \tag{5.39}$$

Adding (5.38) and (5.39) and observing that the coefficients in front of the norms of the resulting estimate are all positive for sufficient small α, namely if

$$\alpha < \min\left\{ \frac{\gamma_0}{C_{\mathrm{inv},5}^{1/2}\|(c + \nabla\cdot\mathbf{b})\|_{L^\infty(\Omega)}}, \frac{1}{2C_F^2 C_{\mathrm{inv},4} d}, \frac{C_{\mathrm{coer}}}{(C_{\mathrm{cont}})^2(C_4 + C_5)} \right\}, \tag{5.40}$$

we immediately deduce the required result.

Remark 43 Theorem 42 extends the respective result for DGFEMs on meshes consisting standard element shapes, see, for example, [20, 47, 53, 127], to general polytopic ones. Moreover, it also improves upon these works in the sense that here the inf-sup constant Λ_s is also independent of the polynomial degree p.

Remark 44 The above inf-sup condition has been derived assuming that Assumption 41 holds, hence limiting the validity of the present analysis to problems with piecewise linear advection fields $\mathbf{b}$. However, an analogous inf-sup condition may be established for general $\mathbf{b}$, by utilizing the modified test function $v_s|_\kappa = \lambda_\kappa \boldsymbol{\Pi}_{L^2}(\mathbf{b}\cdot\nabla v)$, $\kappa \in \mathscr{T}_h$, $v \in V^{\mathbf{p}}(\mathscr{T}_h)$, with respect to the streamline-diffusion DGFEM norm $|||v|||_{\tilde{\mathrm{s}}} := \big(|||v|||_{\mathrm{DG}}^2 + \sum_{\kappa\in\mathscr{T}_h} \lambda_\kappa \|\boldsymbol{\Pi}_{L^2}(\mathbf{b}\cdot\nabla v)\|_{L^2(\kappa)}^2\big)^{1/2}$. However, this approach leads to suboptimal a priori error bounds with respect to the polynomial degree p, cf. Remark 49 below.

5.2.2 A Priori Error Analysis

We are now ready to develop the a priori error analysis of the DGFEM (5.8) based on exploiting an abstract error bound in the spirit of Strang's second lemma, to deal with the inconsistent nature of $\hat{B}_{\mathrm{d}}(\cdot,\cdot)$ and, consequently, of $B(\cdot,\cdot)$, cf. Lemma 28. To this end, we have the following result.

Lemma 45 *Let $u \in H^1(\Omega)$ be the analytical solution of (5.1)–(5.3), and $u_h \in V^{\mathbf{p}}(\mathscr{T}_h)$ the DGFEM approximation satisfying (5.8). Under the hypotheses of*

Theorem 42, the following bound holds

$$|||u-u_h|||_{\mathrm{s}} \le |||u-\tilde{\Pi}_{\boldsymbol{p}}u|||_{\mathrm{s}} + \frac{1}{\Lambda_s}\sup_{\omega_h\in V^{\mathbf{p}}(\mathscr{T}_h)\setminus\{0\}}\frac{|B(\tilde{\Pi}_{\boldsymbol{p}}u-u,\omega_h)|}{|||\omega_h|||_{\mathrm{s}}}$$
$$+\frac{1}{\Lambda_s}\sup_{\omega_h\in V^{\mathbf{p}}(\mathscr{T}_h)\setminus\{0\}}\frac{|B(u,\omega_h)-\hat{\ell}(\omega_h)|}{|||\omega_h|||_{\mathrm{s}}}, \tag{5.41}$$

where $\tilde{\Pi}_{\boldsymbol{p}}|_\kappa := \tilde{\Pi}_{p_\kappa}$ *for all* $\kappa\in\mathscr{T}_h$, *and* $\tilde{\Pi}_{p_\kappa}$ *is the operator defined in Lemma 23.*

Proof The result follows in a standard fashion by replacing the coercivity hypothesis in the proof of Strang's second lemma with the inf-sup stability bounds (5.27) and (5.28).

We now state and prove the following *hp*-version a priori error bound.

Theorem 46 *Let* $\mathscr{T}_h=\{\kappa\}$ *be a subdivision of* $\Omega\subset\mathbb{R}^d$, $d=2,3$, *satisfying the hypotheses of Theorem 42 and let* $\mathscr{T}_h^\sharp=\{\mathscr{K}\}$ *be an associated covering of* $\mathscr{T}_h$ *consisting of shape-regular d-simplices, cf. Definition 17. Let* $u_h\in V^{\mathbf{p}}(\mathscr{T}_h)$, *with* $p_\kappa\ge 1$ *for all* $\kappa\in\mathscr{T}_h$, *be the corresponding DGFEM solution defined by (5.8), where the discontinuity-penalization function* σ *is given in (5.13). If the analytical solution* $u\in H^1(\Omega)$ *to (5.1)–(5.3) satisfies* $u|_\kappa\in H^{l_\kappa}(\kappa)$, $(\sqrt{a}\nabla u)|_\kappa\in[H^{l_\kappa-1}(\kappa)]^d$, $l_\kappa>1+d/2$, *for each* $\kappa\in\mathscr{T}_h$, *such that* $\mathfrak{E}u|_{\mathscr{K}}\in H^{l_\kappa}(\mathscr{K})$, *where* $\mathscr{K}\in\mathscr{T}_h^\sharp$ *with* $\kappa\subset\mathscr{K}$, *then*

$$|||u-u_h|||_{\mathrm{s}}^2 \le C\sum_{\kappa\in\mathscr{T}_h}\frac{h_\kappa^{2s_\kappa}}{p_\kappa^{2l_\kappa}}\Big(\mathscr{G}_\kappa(F,C_m,p_\kappa,\lambda_\kappa)\|\mathfrak{E}u\|^2_{H^{l_\kappa}(\mathscr{K})}$$
$$+\mathscr{D}_\kappa(F,C_{\mathrm{INV}},C_m,p_\kappa)\|\mathfrak{E}(\sqrt{a}\nabla u)\|^2_{H^{l_\kappa-1}(\mathscr{K})}\Big), \tag{5.42}$$

where

$$\mathscr{G}_\kappa(F,C_m,p_\kappa,\lambda_\kappa) := \|c_0\|^2_{L^\infty(\kappa)}+\xi_\kappa^2+\lambda_\kappa^{-1}+\lambda_\kappa\beta_\kappa^2p_\kappa^2h_\kappa^{-2}+\bar{a}_\kappa p_\kappa^2h_\kappa^{-2} \tag{5.43}$$
$$+\beta_\kappa p_\kappa h_\kappa^{-d}\sum_{F\subset\partial\kappa}C_m(p_\kappa,\kappa,F)|F|+p_\kappa h_\kappa^{-d}\sum_{F\subset\partial\kappa:F\in\mathscr{F}_h^{\mathscr{I}}\cup\mathscr{F}_h^D}C_m(p_\kappa,\kappa,F)\sigma|F|,$$

and

$$\mathscr{D}_\kappa(F,C_{\mathrm{INV}},C_m,p_\kappa) := \Big(p_\kappa^3h_\kappa^{-d-2}\sum_{F\subset\partial\kappa:F\in\mathscr{F}_h^{\mathscr{I}}\cup\mathscr{F}_h^D}C_m(p_\kappa,\kappa,F)A_F\sigma^{-1}|F|$$
$$+p_\kappa^4|\kappa|^{-1}h_\kappa^{-2}\sum_{F\subset\partial\kappa:F\in\mathscr{F}_h^{\mathscr{I}}\cup\mathscr{F}_h^D}C_{\mathrm{INV}}(p_\kappa,\kappa,F)A_F\sigma^{-1}|F|\Big), \tag{5.44}$$

with $s_\kappa = \min\{p_\kappa + 1, l_\kappa\}$, $\zeta_\kappa := \|c/c_0\|_{L^\infty(\kappa)}$, c_0 *is as in* (5.6), $\beta_\kappa := \|\mathbf{b}\|_{L^\infty(\kappa)}$, *and* C *is a positive constant, which depends on the shape-regularity of* $\mathscr{T}_h^\sharp$, *but is independent of the discretization parameters.*

Proof Starting from the error bound stated in Lemma 45, we proceed by bounding each term separately. To this end, employing the approximation bounds stated in Lemma 23, together with Assumption 25, we deduce that

$$\begin{aligned}|||u - \tilde{\Pi}_{\boldsymbol{p}} u|||_{\mathrm{s}}^2 \leq C \sum_{\kappa\in\mathscr{T}_h} \frac{h_\kappa^{2s_\kappa}}{p_\kappa^{2l_\kappa}} \Big(&\|c_0\|_{L^\infty(\kappa)}^2 + \lambda_\kappa \|\mathbf{b}\|_{L^\infty(\kappa)}^2 \frac{h_\kappa^{-2}}{p_\kappa^{-2}} + \bar{a}_\kappa \frac{h_\kappa^{-2}}{p_\kappa^{-2}} \\ &+ \|\mathbf{b}\|_{L^\infty(\kappa)} \frac{h_\kappa^{-d}}{p_\kappa^{-1}} \sum_{F\subset\partial\kappa} C_m(p_\kappa,\kappa,F)|F| \\ &+ \frac{h_\kappa^{-d}}{p_\kappa^{-1}} \sum_{F\subset\partial\kappa: F\in\mathscr{F}_h^{\mathscr{I}}\cup\mathscr{F}_h^D} C_m(p_\kappa,\kappa,F)\sigma|F| \Big) \|\mathfrak{E}u\|_{H^{l_\kappa}(\mathscr{K})}^2. \end{aligned} \tag{5.45}$$

Setting $\eta = u - \tilde{\Pi}_{\boldsymbol{p}} u$, we embark on bounding the second term on the right-hand side of (5.41). Exploiting elementwise integration by parts, the advection-reaction bilinear form $B_{\mathrm{ar}}(\cdot,\cdot)$ may be written in the following form

$$\begin{aligned} B_{\mathrm{ar}}(\eta,\omega_h) = \sum_{\kappa\in\mathscr{T}_h} \Big(&\int_\kappa c\omega_h\eta \,\mathrm{d}\mathbf{x} - \int_\kappa (\mathbf{b}\cdot\nabla\omega_h)\eta \,\mathrm{d}\mathbf{x} \\ &+ \int_{\partial_-\kappa\setminus\partial\Omega} (\mathbf{b}\cdot\mathbf{n})\lfloor\omega_h\rfloor\eta^- \,\mathrm{d}s + \int_{\partial_+\kappa\cap\partial\Omega} (\mathbf{b}\cdot\mathbf{n})\omega_h^+\eta^+ \,\mathrm{d}s \Big). \end{aligned}$$

Applying the Cauchy-Schwarz inequality, we deduce that

$$\begin{aligned} |B_{\mathrm{ar}}(\eta,\omega_h)| \leq \Big(\sum_{\kappa\in\mathscr{T}_h} \big((\zeta_\kappa^2 + \lambda_\kappa^{-1})\|\eta\|_{L^2(\kappa)}^2 + 2\|\eta^-\|_{\partial_-\kappa\setminus\partial\Omega}^2 + 2\|\eta^+\|_{\partial_+\kappa\cap\partial\Omega}^2\big)\Big)^{1/2} \\ \times \Big(|||\omega_h|||_{\mathrm{ar}}^2 + \sum_{\kappa\in\mathscr{T}_h} \lambda_\kappa \|\mathbf{b}\cdot\nabla\omega_h\|_{L^2(\kappa)}^2 \Big)^{1/2}. \end{aligned}$$

Combining the above estimate with the continuity of $\hat{B}_{\mathrm{d}}(\cdot,\cdot)$, we arrive at the following bound:

$$\begin{aligned} |B(\eta,\omega_h)| &= |B_{\mathrm{ar}}(\eta,\omega_h) + \tilde{B}_{\mathrm{d}}(\eta,\omega_h)| \\ &\leq \Big(\sum_{\kappa\in\mathscr{T}_h} \Big((\zeta_\kappa^2 + \lambda_\kappa^{-1})\|\eta\|_{L^2(\kappa)}^2 + 2\|\eta^-\|_{\partial_-\kappa\setminus\partial\Omega}^2 + 2\|\eta^+\|_{\partial_+\kappa\cap\partial\Omega}^2 \\ &\quad + (C_{\mathrm{cont}})^2 \|\sqrt{\bar{a}}\nabla\eta\|_{L^2(\kappa)}^2 \Big) + (C_{\mathrm{cont}})^2 \int_{\mathscr{F}_h^{\mathscr{I}}\cup\mathscr{F}_h^D} \sigma|[\![\eta]\!]|^2 \,\mathrm{d}s \Big)^{1/2} |||\omega_h|||_{\mathrm{s}}. \end{aligned}$$

Hence, by applying the approximation results stated in Lemma 23, we deduce that

$$\begin{aligned}
&\sup_{\omega_h\in V^{\mathbf{p}}(\mathscr{T}_h)\setminus\{0\}}\frac{|\tilde{B}(\tilde{\Pi}_{\boldsymbol{p}}u-u,\omega_h)|}{|||\omega_h|||_{\mathrm{s}}}\\
&\le C\Bigg(\sum_{\kappa\in\mathscr{T}_h}\frac{h_\kappa^{2s_\kappa}}{p_\kappa^{2l_\kappa}}\Big(\zeta_\kappa^2+\lambda_\kappa^{-1}+\bar{a}_\kappa\frac{h_\kappa^{-2}}{p_\kappa^{-2}}+\|\mathbf{b}\|_{L^\infty(\kappa)}\frac{h_\kappa^{-d}}{p_\kappa^{-1}}\sum_{F\subset\partial\kappa}C_m(p_\kappa,\kappa,F)|F|\\
&\qquad+\frac{h_\kappa^{-d}}{p_\kappa^{-1}}\sum_{F\subset\partial\kappa:F\in\mathscr{F}_h^{\mathscr{I}}\cup\mathscr{F}_h^{D}}C_m(p_\kappa,\kappa,F)\sigma|F|\Big)\|\mathfrak{E}u\|^2_{H^{l_\kappa}(\mathscr{K})}\Bigg)^{1/2}.
\end{aligned}\tag{5.46}$$

To conclude the proof, we now bound the third term on the right-hand side of (5.41), which represents the residual due to the inconsistency of $\hat{B}_{\mathrm{d}}(\cdot,\cdot)$. We begin by observing that

$$B(u,\omega_h)-\hat{\ell}(\omega_h)=\int_{\mathscr{F}_h^{\mathscr{I}}\cup\mathscr{F}_h^{D}}\{\!\{\sqrt{a}(\sqrt{a}\nabla u-\boldsymbol{\Pi}_{L^2}(\sqrt{a}\nabla u))\}\!\}\cdot[\![\omega_h]\!]\,\mathrm{d}s.$$

Proceeding as in the proof of Lemma 37, we have that, for $F\subset\partial\kappa^+\cap\partial\kappa^-$, the following bound holds

$$\begin{aligned}
&\int_F\{\!\{\sqrt{a}(\sqrt{a}\nabla u-\boldsymbol{\Pi}_{L^2}(\sqrt{a}\nabla u))\}\!\}\cdot[\![\omega_h]\!]\,\mathrm{d}s\\
&=\frac{1}{2}\sum_{\kappa\in\{\kappa^+,\kappa^-\}}\int_F(\sqrt{a}\nabla u-\boldsymbol{\Pi}_{L^2}(\sqrt{a}\nabla u))|_\kappa\cdot\sqrt{a}|_\kappa[\![\omega_h]\!]\,\mathrm{d}s\\
&\le\sum_{\kappa\in\{\kappa^+,\kappa^-\}}\|\sqrt{A_F/\sigma}\big(\sqrt{a}\nabla u-\boldsymbol{\Pi}_{L^2}(\sqrt{a}\nabla u)\big)\|^2_{L^2(F\subset\partial\kappa)}+\|\sqrt{\sigma}[\![\omega_h]\!]\|^2_{L^2(F)}.
\end{aligned}\tag{5.47}$$

To bound the first term on the right-hand side of (5.47), we proceed as follows

$$\begin{aligned}
&\|\sqrt{A_F/\sigma}\big(\sqrt{a}\nabla u-\boldsymbol{\Pi}_{L^2}(\sqrt{a}\nabla u)\big)\|^2_{L^2(F\subset\partial\kappa)}\\
&\qquad\le 2\|\sqrt{A_F/\sigma}\big(\sqrt{a}\nabla u-\tilde{\boldsymbol{\Pi}}_{\boldsymbol{p}}(\sqrt{a}\nabla u)\big)\|^2_{L^2(F\subset\partial\kappa)}\\
&\qquad\quad+2\|\sqrt{A_F/\sigma}\boldsymbol{\Pi}_{L^2}\big(\sqrt{a}\nabla u-\tilde{\boldsymbol{\Pi}}_{\boldsymbol{p}}(\sqrt{a}\nabla u)\big)\|^2_{L^2(F\subset\partial\kappa)}\\
&\qquad\equiv \mathrm{I}_{F,\kappa}+\mathrm{II}_{F,\kappa}.
\end{aligned}$$

Employing the approximation estimate (3.27), yields

$$\mathrm{I}_{F,\kappa}\le C\frac{h_\kappa^{2(s_\kappa-1)}}{p_\kappa^{2(l_\kappa-1)}}\frac{h_\kappa^{-d}}{p_\kappa^{-1}}C_m(p_\kappa,\kappa,F)\frac{A_F}{\sigma|_F}|F|\|\mathfrak{E}(\sqrt{a}\nabla u)\|^2_{H^{l_\kappa-1}(\mathscr{K})}.$$

Similarly, exploiting the inverse inequality (3.13), the L^2-stability of $\boldsymbol{\Pi}_{L^2}$, and the approximation bound (3.26), gives

$$\mathrm{II}_{F,\kappa} \leq C\frac{h_\kappa^{2(s_\kappa-1)}}{p_\kappa^{2(l_\kappa-1)}}\frac{|\kappa|^{-1}}{p_\kappa^{-2}}C_{\mathrm{INV}}(p_\kappa,\kappa,F)\frac{A_F}{\sigma}|F|\|\mathfrak{E}(\sqrt{a}\nabla u)\|^2_{H^{l_\kappa-1}(\mathscr{K})}.$$

Combining the above estimates, we deduce the following bound for the residual term:

$$\begin{aligned}\Bigg(\sup_{\omega_h\in V^{\mathbf{p}}(\mathscr{T}_h)\setminus\{0\}}&\frac{|B(u,\omega_h)-\hat{\ell}(u,\omega_h)|}{|||\omega_h|||_{\mathrm{s}}}\Bigg)^2\\ &\leq C\sum_{\kappa\in\mathscr{T}_h}\frac{h_\kappa^{2(s_\kappa-1)}}{p_\kappa^{2(l_\kappa-1)}}\\ &\quad\times\sum_{F\subset\partial\kappa:F\in\mathscr{F}_h^{\mathscr{I}}\cup\mathscr{F}_h^D}\left(C_m(p_\kappa,\kappa,F)\frac{h_\kappa^{-d}}{p_\kappa^{-1}}+C_{\mathrm{INV}}(p_\kappa,\kappa,F)\frac{|\kappa|^{-1}}{p_\kappa^{-2}}\right)\frac{A_F}{\sigma}|F|\\ &\quad\times\|\mathfrak{E}(\sqrt{a}\nabla u)\|^2_{H^{l_\kappa-1}(\mathscr{K})}.\end{aligned}\tag{5.48}$$

The statement of the theorem now follows by inserting the derived bounds into inequality (5.41).

Remark 47 We note that the above *hp*-version a priori bound for the DGFEM (5.8) holds without the need to impose any assumption concerning the relative size of the faces F, $F\subset\partial\kappa$, of a given polytopic element $\kappa\in\mathscr{T}_h$. If $\mathbf{b}\equiv\mathbf{0}$ and $c\equiv 0$ on Ω, then the streamline-diffusion DGFEM norm $|||\cdot|||_{\mathrm{s}}$ degenerates to the (diffusion) DGFEM norm defined in (4.11) and the inf-sup condition is equivalent to the coercivity of the bilinear form $\hat{B}_{\mathrm{d}}(\cdot,\cdot)$. Moreover, in this setting, for uniform $p_\kappa=p\geq 1$, $h=\max_{\kappa\in\mathscr{T}_h}h_\kappa$, $s_\kappa=s$, $s=\min\{p+1,l\}$, $l>1+d/2$, under the assumption that the diameter of the faces of each element $\kappa\in\mathscr{T}_h$ is of comparable size to the diameter of the corresponding element, i.e., $\mathrm{diam}(F)\sim h_\kappa$, $h_\kappa^{\perp}\sim h_\kappa$, $F\subset\partial\kappa$, $\kappa\in\mathscr{T}_h$, so that $|F|\sim h_\kappa^{(d-1)}$, the a priori error bound of Theorem 46 reduces to

$$|||u-u_h|||_{\mathrm{d}}\leq C\frac{h^{s-1}}{p^{l-3/2}}\|u\|_{H^l(\Omega)},$$

cf. Sect. 4.2.2.

Remark 48 In the hyperbolic case, i.e., when $a\equiv\mathbf{0}$, and hence $\bar{a}_\kappa=\tilde{\sigma}_\kappa=A_F=0$, the 'inconsistency' term $\mathscr{D}_\kappa(F,C_{\mathrm{INV}},C_m,p_\kappa)$ vanishes. Thereby, the streamline-diffusion DGFEM norm $|||\cdot|||_{\mathrm{s}}$ is stronger than the advection-reaction DGFEM norm $|||\cdot|||_{\mathrm{ar}}$; note that, here $\lambda_\kappa=\mathscr{O}(h_\kappa/p_\kappa^2)$ by (5.19). In this case, for uniform orders $p_\kappa=p\geq 1$, $h=\max_{\kappa\in\mathscr{T}_h}h_\kappa$, $s_\kappa=s$, $s=\min\{p+1,l\}$, $l>1+d/2$, under the

assumption that the diameter of the faces of each element $\kappa \in \mathscr{T}_h$ is of comparable size to the diameter of the corresponding element, i.e., $\mathrm{diam}(F) \sim h_\kappa$, $h_\kappa^\perp \sim h_\kappa$, $F \subset \partial\kappa$, $\kappa \in \mathscr{T}_h$, so that $|F| \sim h_\kappa^{(d-1)}$ the a priori error bound of Theorem 46 yields

$$|||u - u_h|||_{\mathrm{ar}} \leq |||u - u_h|||_{\mathrm{s}} \leq C\frac{h^{s-\frac{1}{2}}}{p^{l-1}}\|u\|_{H^l(\Omega)}.$$

Hence, the above *hp*-bound is optimal in h and suboptimal in p by $p^{1/2}$. In this case, our bound generalizes the error estimate derived in [124] to general polytopic meshes under the same assumption $\mathbf{b} \cdot \nabla_h \xi \in V^{\mathbf{p}}(\mathscr{T}_h)$, $\xi \in V^{\mathbf{p}}(\mathscr{T}_h)$, with a slight loss of p-convergence.

Remark 49 As noted in Remark 44, the case of general advection fields $\mathbf{b}$ can be treated, based on proving an inf-sup condition with respect to a slightly different norm. In this setting, the present analysis can easily be adapted to utilize such an inf-sup condition, together with the exploitation of the L^2-projector $\boldsymbol{\Pi}_{L^2}$ onto the finite element space $V^{\mathbf{p}}(\mathscr{T}_h)$. However, this yields an error bound in the $|||\cdot|||_{\mathrm{ar}}$-norm which is optimal in h but suboptimal in p by $p^{3/2}$ for the purely hyperbolic problem. Of course, if we modify the DGFEM by including the streamline-diffusion stabilization term as in [123], then an *hp*-optimal bound can be derived without the assumption that $\mathbf{b} \cdot \nabla_h \xi \in V^{\mathbf{p}}(\mathscr{T}_h)$, $\xi \in V^{\mathbf{p}}(\mathscr{T}_h)$.

We conclude this section by briefly discussing the theoretical challenges faced when the mesh does not satisfy Assumption 25, in the sense that the number of faces the elements possess may not be uniformly bounded under mesh refinement. For instance, in the spirit of Sect. 4.3, we could instead assume the validity of Assumption 30. Within the proof of the above inf-sup condition, cf. Theorem 42, we utilize the inverse estimate (3.19) which bounds the H^1-(semi)norm of a polynomial by its L^2-norm over a polytopic element κ, $\kappa \in \mathscr{T}_h$. As noted in the proof of Lemma 14, the constant in (3.19) does not directly depend on the number of faces per element, but rather on the cardinality of each elemental covering m_κ, which must therefore be assumed to be uniformly bounded. Consequently, in the absence of Assumption 25, an a priori error analysis for the DGFEM (5.8) would require the polytopic elements to *simultaneously* satisfy both the p-coverability condition uniformly, in the sense that m_κ remains bounded under mesh refinement, *and* Assumption 30; these two conditions are essentially in competition with one another for many (useful) element shapes. In conclusion, an a priori error bound for the DGFEM (5.8) in the same setting as Sect. 4.3 remains an interesting mathematical challenge.

5.3 Space-Time DGFEMs for Time-Dependent PDEs

Equipped with the error analysis of DGFEMs for PDEs with nonnegative characteristic form, we now focus on the important subclass of parabolic problems which are abundant in applications modelling diffusion processes. In particular, for

$d = 2, 3, 4$, let $a : \mathbb{R}^d \to \mathbb{R}^{d\times d}$ and $\mathbf{b} : \mathbb{R}^d \to \mathbb{R}^d$, be given by

$$a = \begin{pmatrix} 0 & \mathbf{0} \\ \mathbf{0} & \mathbf{a} \end{pmatrix}, \qquad \mathbf{b} = \begin{pmatrix} 1 \\ \mathbf{0} \end{pmatrix},$$

and $c = 0$ with $\mathbf{a} : \mathbb{R}^d \to \mathbb{R}^{(d-1)\times(d-1)}$ a positive definite tensor. Substituting this selection into (2.1) gives rise to the classical diffusion equation of mathematical physics with the first variable signifying the time direction:

$$\partial_t u - \nabla \cdot (\mathbf{a}\nabla u) = f \quad \text{in } \Omega := J \times D, \tag{5.49}$$

with Ω now the space-time cylinder $\Omega := J \times D$, $J \subset \mathbb{R}_+$ a time-interval and $D \subset \mathbb{R}^{d-1}$ the spatial domain; here, and throughout the rest of this section, the symbols ∇ and $\nabla\cdot$ signify the gradient and divergence operators with respect to the spatial variables only.

Therefore, the DGFEM (5.8) presented above is directly applicable to linear parabolic problems also. At first sight, however, (5.8) appears to require simultaneous solution over the entire space-time computational domain Ω. This is at odds with standard numerical methods for parabolic problems which typically involve time-stepping procedures, whereby the numerical solution is computed sequentially for each subsequent time-step, rather than in a monolithic fashion, where the solution is evaluated for all times simultaneously; clearly, the latter would typically be a computationally prohibitive task.

Fortunately, judicious mesh design with respect to the time direction allows for the natural decoupling of the resulting method on each time-step—this concept was discussed in Remark 4 concerning the locally solvability of DGFEMs for hyperbolic problems. Indeed, upon subdividing the space-time domain Ω into prismatic elements, with prism-bases perpendicular to the time vector $\mathbf{b}$, we have that $\mathbf{b}$ is parallel to each unit normal vector $\mathbf{n}_F$ to each prism-base face F; we refer to Fig. 5.1b for an illustration. Thus, we must necessarily have $\mathbf{n}_F = (\pm 1, 0, \ldots, 0)^\top \in \mathbb{R}^d$ and, therefore, $A_F = \{\!\{\mathbf{n}_F^\top a \mathbf{n}_F\}\!\} = 0$ on each prism-base face F, i.e., the diffusive numerical fluxes and the discontinuity penalization terms vanish on each such F, thereby, the global (space-time) linear system arising from (2.7) is block-diagonal on each space-time slab, cf. Fig. 5.1b illustrating one such space-time slab. The DGFEM then takes the form (5.54) below.

For this section only, we shall introduce some additional notation. For brevity, we denote the $L^2(\omega)$-inner product by $(\cdot,\cdot)_\omega$ for $\omega \subset \mathbb{R}^d$. We recall the standard Bochner spaces of functions which map a (time) interval I to a Banach (function) space X. In particular, $L^2(I;X)$ and $H^s(I;X)$, $s \geq 0$, are the corresponding Lebesgue and Sobolev spaces, while $C(\bar{I};X)$ denotes the space of continuous functions. Moreover, let D be a bounded open polyhedral domain in $\mathbb{R}^{d-1}$, $d = 2, 3, 4$, and let $J := (0, T)$ be a time interval with $T > 0$. We consider the linear parabolic

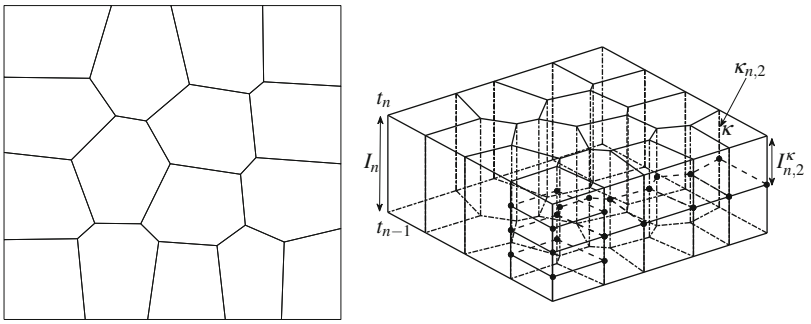

(a) (b)

Fig. 5.1 (**a**) Polygonal spatial mesh over the spatial domain $D = (0,1)^2$; (**b**) Space-time elements over $I_n \times D$ under the local time partition $\mathscr{U}_n(\mathscr{T}_h)$

problem:

$$\partial_t u - \nabla \cdot (\mathbf{a} \nabla u) \;=\; f \quad \text{in } J \times D, \tag{5.50}$$

$$u|_{t=0} = u_0 \quad \text{on } D, \quad \text{and} \quad u = g_{\mathrm{D}} \quad \text{on } J \times \partial D, \tag{5.51}$$

for $f \in L^2(J; L^2(D))$ and $\mathbf{a} \in L^\infty(J \times D)^{(d-1)\times(d-1)}$, symmetric with

$$\boldsymbol{\xi}^\top \mathbf{a}(t, \mathbf{x}) \boldsymbol{\xi} \geq \theta |\boldsymbol{\xi}|^2 > 0 \quad \forall \boldsymbol{\xi} \in \mathbb{R}^d, \quad \text{a.e.} \quad (t, x) \in J \times D, \tag{5.52}$$

for some constant $\theta > 0$, whereby $\mathbf{a}$ is allowed to depend on time t. For $u_0 \in L^2(D)$ and $g_{\mathrm{D}} = 0$ the problem (5.50), (5.51) is well-posed and there exists a unique solution $u \in L^2(J; H^1_0(D))$ with $u \in C(\bar{J}; L^2(D))$ and $\partial_t u \in L^2(J; H^{-1}(D))$.

Let $\mathscr{U}$ be a partition of the time interval J into N_t time steps $\{I_n\}_{n=1}^{N_t}$, $I_n = (t_{n-1}, t_n)$, with respective set of nodes $\{t_n\}_{n=0}^{N_t}$ defined so that $0 := t_0 < t_1 < \cdots < t_{N_t} := T$. We set $\tau_n := t_n - t_{n-1}$, the length of I_n. Deviating from the notation of the rest of this volume, we shall denote *spatial* polytopic elements by $\kappa \in \mathscr{T}_h$, where $\mathscr{T}_h$ represents the (polytopic) subdivision of the spatial domain D; see Fig. 5.1a for an illustration. Furthermore, we write $\mathscr{F}_h = \mathscr{F}_h^{\mathscr{I}} \cup \mathscr{F}_h^{\mathscr{B}}$ to denote the set of open $(d-2)$-dimensional simplicial element faces associated with the computational mesh $\mathscr{T}_h$, where $\mathscr{F}_h^{\mathscr{I}}$ denotes the set of interior element faces $F \in \mathscr{F}_h$ that are contained in D, and $\mathscr{F}_h^{\mathscr{B}} \equiv \mathscr{F}_h^D$ is the set of boundary element faces.

The space-time mesh $\mathscr{U} \times \mathscr{T}_h$ is allowed to include locally smaller time-steps as follows. Over each time interval I_n, $n = 1, \ldots, N_t$, we may consider the local time partition $\mathscr{U}_n(\mathscr{T}_h)$ that, for each space element $\kappa \in \mathscr{T}_h$, yields a subdivision of the time interval I_n into N_n^κ local time steps $I_{n,j}^\kappa = (t_{n,j-1}, t_{n,j})$, $j = 1, \ldots, N_n^\kappa$, with respect to the local time nodes $\{t_{n,j}\}_{j=0}^{N_n^\kappa}$, defined so that $t_{n-1} := t_{n,0} < t_{n,1} < \cdots < t_{n,N_n^\kappa} := t_n$. Further, we set $\tau_{n,j} := t_{n,j} - t_{n,j-1}$ to be the length of $I_{n,j}^\kappa$.

For every time interval $I_n \in \mathscr{U}$ and every space element $\kappa \in \mathscr{T}_h$, with local time partition $\mathscr{U}_n(\mathscr{T}_h)$, we define the d-dimensional space-time *prismatic* element $\kappa_{n,j} := I^{\kappa}_{n,j} \times \kappa$; see Fig. 5.1b. Let $p_{\kappa_{n,j}}$ denote the (positive) *polynomial degree* of the space-time element $\kappa_{n,j}$, and collect $p_{\kappa_{n,j}}$ in the vector $\mathbf{p} := (p_{\kappa_{n,j}} : \kappa_{n,j} \in \mathscr{U}_n(\mathscr{T}_h) \times \mathscr{T}_h)$. We define the *space-time finite element space* with respect to the time interval I_n, subdivision $\mathscr{T}_h$, local time partition $\mathscr{U}_n(\mathscr{T}_h)$, and polynomial degree $\mathbf{p}$ by

$$V^{\mathbf{p}}(I_n; \mathscr{T}_h; \mathscr{U}_n(\mathscr{T}_h)) := \{u \in L^2(I_n \times D) : u|_{\kappa_{n,j}} \in \mathscr{P}_{p_{\kappa_{n,j}}}(\kappa_{n,j}), \kappa_{n,j} \in \mathscr{U}_n(\mathscr{T}_h) \times \mathscr{T}_h\},$$

where $\mathscr{P}_{p_{\kappa_{n,j}}}(\kappa_{n,j})$ denotes the space of polynomials of *total degree* $p_{\kappa_{n,j}}$ on $\kappa_{n,j}$. The space-time finite element space $V^{\mathbf{p}}(\mathscr{U}; \mathscr{T}_h)$ with respect to $\mathscr{U}$, $\mathscr{T}_h$, $\mathbf{p}$, and, implicitly, $\mathscr{U}_n(\mathscr{T}_h)$, is defined as $V^{\mathbf{p}}(\mathscr{U}; \mathscr{T}_h) = \bigoplus_{n=1}^{N_t} V^{\mathbf{p}}(I_n; \mathscr{T}_h; \mathscr{U}_n(\mathscr{T}_h))$. As is standard in this context of local time-stepping, the resulting DGFEM is implicit with respect to all the local time-steps within the same time-interval I_n.

Note that the local elemental polynomial spaces employed in the definition of $V^{\mathbf{p}}(\mathscr{U}; \mathscr{T}_h)$ are defined in the *physical coordinate system*, without the need to map from a given reference/canonical frame. This setting is crucial to retain full approximation of the finite element space, independently of the element shape.

Remark 50 A crucial novelty of the space-time DGFEM presented below is that the space $V^{\mathbf{p}}(\mathscr{U}; \mathscr{T}_h)$ employs fewer degrees of freedom per space-time element in comparison to tensor-product polynomial bases of the same order in space and time. This is in contrast with standard methods for parabolic problems based on discontinuous Galerkin time-stepping which are typically constructed via tensorizing the time polynomial basis with the basis employed on each spatial element, cf. [166].

Given a space-time element $\kappa_{n,j} \in \mathscr{U}_n(\mathscr{T}_h) \times \mathscr{T}_h$, we write $h_{\kappa_{n,j}}$ to denote its diameter, i.e., $h_{\kappa_{n,j}} := \mathrm{diam}(\kappa_{n,j})$. Furthermore, we denote by $\tilde{F}$ a generic $(d-1)$-dimensional face of $\kappa_{n,j} \in \mathscr{U}_n(\mathscr{T}_h) \times \mathscr{T}_h$, which should be distinguished from the $(d-2)$-dimensional face F of the spatial element $\kappa \in \mathscr{T}_h$. For any space-time element $\kappa_{n,j} \in \mathscr{U}_n(\mathscr{T}_h) \times \mathscr{T}_h$, we define $\partial\kappa_{n,j}$ to be the union of all $(d-1)$-dimensional open faces $\tilde{F}$ of $\kappa_{n,j}$. For convenience, we further subdivide $\tilde{F}$ into two disjoint subsets

$$\tilde{F}^{\parallel} := \tilde{F} \subset I^{\kappa}_{n,j} \times \partial\kappa, \quad \text{and} \quad \tilde{F}^{\perp} := \tilde{F} \subset \partial I^{\kappa}_{n,j} \times \kappa, \tag{5.53}$$

i.e., parallel and perpendicular to the time direction boundaries, respectively. Hence, for each $\kappa_{n,j}$, there exists exactly two $(d-1)$-dimensional faces $\tilde{F}^{\perp}$ and the number of $(d-1)$-dimensional faces $\tilde{F}^{\parallel}$ is equal to the number of $(d-2)$-dimensional spatial faces F of the spatial element κ which forms $\kappa_{n,j}$. Upon defining

$$u_n^+ := \lim_{s \to 0^+} u(t_n + s, \cdot),\ 0 \le n \le N_t - 1, \quad u_n^- := \lim_{s \to 0^+} u(t_n - s, c\dot{)},\ 1 \le n \le N_t,$$

the *time-jump* across t_n, $n = 1, \ldots, N_t - 1$, is given by $\lfloor u \rfloor_n := u_n^+ - u_n^-$. Similarly, the *time-jump* across the interior time nodes $t_{n,j}, j = 1, \ldots, N_n^{\kappa} - 1, n = 1, \ldots, N_t$ is given by $\lfloor u \rfloor_{n,j} := u_{n,j}^+ - u_{n,j}^-$.

Remark 51 The above *time-jump* across time nodes is precisely the *upwind-jump*, due to the fact that the 'hyperbolicity' of parabolic problems is along the time direction only.

With this notation, the DGFEM for (5.50), (5.51) is given by: find $u_h \in V^{\mathbf{p}}(\mathscr{U};\mathscr{T}_h)$ such that

$$B(u_h, v_h) = \ell(v_h) \quad \text{for all } v_h \in V^{\mathbf{p}}(\mathscr{U};\mathscr{T}_h), \tag{5.54}$$

where $B : V^{\mathbf{p}}(\mathscr{U};\mathscr{T}_h) \times V^{\mathbf{p}}(\mathscr{U};\mathscr{T}_h) \to \mathbb{R}$ is defined as

$$\begin{aligned} B(w,v) := &\sum_{n=1}^{N_t} \int_{I_n} \big((\partial_t w, v)_D + B_{\mathrm{d}}(w,v)\big)\,\mathrm{d}t + \sum_{n=2}^{N_t} (\lfloor w \rfloor_{n-1}, v_{n-1}^+)_D + (w_0^+, v_0^+)_D \\ &+ \sum_{\kappa\in\mathscr{T}_h} \sum_{n=1}^{N_t} \sum_{j=2}^{N_n^\kappa} (\lfloor w \rfloor_{nj-1}, v_{nj-1}^+)_\kappa, \end{aligned} \tag{5.55}$$

with the spatial bilinear form $B_{\mathrm{d}}(\cdot,\cdot)$ given by

$$B_{\mathrm{d}}(w,v) := \sum_{\kappa\in\mathscr{T}_h} \int_\kappa \mathbf{a}\nabla w\cdot\nabla v\,\mathrm{d}\mathbf{x} - \int_{\mathscr{F}_h} \Big(\{\!\{\mathbf{a}\nabla w\}\!\}\cdot[\![v]\!] + \{\!\{\mathbf{a}\nabla v\}\!\}\cdot[\![w]\!] - \sigma[\![w]\!]\cdot[\![v]\!] \Big)\,\mathrm{d}s,$$

and the linear functional $\ell : V^{\mathbf{p}}(\mathscr{U};\mathscr{T}_h) \to \mathbb{R}$ defined by

$$\ell(v) := \sum_{n=1}^{N_t} \int_{I_n} \Big((f,v)_D - \int_{\mathscr{F}_h^D} g_{\mathrm{D}} \big((\mathbf{a}\nabla_h v)\cdot\mathbf{n} - \sigma v \big)\,\mathrm{d}s \Big)\,\mathrm{d}t + (u_0, v_0^+)_D;$$

the nonnegative function $\sigma : J \times \mathscr{F}_h \to \mathbb{R}$ appearing in $B_{\mathrm{d}}(\cdot,\cdot)$ and $\ell(\cdot)$ above is defined in an analogous fashion to the discontinuity-penalization function given in (5.13). As before, when $B_{\mathrm{d}}(\cdot,\cdot)$ contains arguments which do not belong to the finite element space $V^{\mathbf{p}}(\mathscr{U};\mathscr{T}_h)$, we assume it is replaced by its inconsistent extension $\tilde{B}_{\mathrm{d}}(\cdot,\cdot)$, cf. Sect. 5.1. Here, and for the remaining of this section, we have made a slight abuse of notation in that $B_{\mathrm{d}}(\cdot,\cdot)$ and σ now refer to the *spatial* $(d-1)$-dimensional mesh only and not the d-dimensional space-time grid.

As discussed above, the use of prismatic meshes is essential in that it allows the numerical solution to be computed for each time-step by the time-marching algorithm: for each time interval $I_n \in \mathscr{U}$, $n = 2,\dots,N_t$, the solution $U_n = u_h|_{I_n} \in V^{\mathbf{p}}(I_n;\mathscr{T}_h;\mathscr{U}_n(\mathscr{T}_h))$ is given by:

$$\begin{aligned} &\int_{I_n} \big((\partial_t U_n, V_n)_D + B_{\mathrm{d}}(U_n,V_n)\big)\,\mathrm{d}t + (U_{n-1}^+, V_{n-1}^+)_D + \sum_{\kappa\in\mathscr{T}_h} \sum_{j=2}^{N_n^\kappa} (\lfloor u \rfloor_{nj-1}, v_{nj-1}^+)_\kappa \\ &= \int_{I_n} \Big((f,V_n)_D - \int_{\mathscr{F}_h^D} g_{\mathrm{D}} \big((\mathbf{a}\nabla_h V_n)\cdot\mathbf{n} - \sigma V_n \big)\,\mathrm{d}s \Big)\,\mathrm{d}t + (U_{n-1}^-, V_{n-1}^+)_D \end{aligned} \tag{5.56}$$

for all $V_n \in V^{\mathbf{p}}(I_n; \mathscr{T}_h; \mathscr{U}_n(\mathscr{T}_h))$, with U_{n-1}^- serving as the initial datum at time step I_n; for $n = 1$, we set $U_0^- = u_0$.

To present the key ideas without excessive notational burden, in the following we shall not include the local time-stepping capability of the method. In this setting, the last term in (5.55) and the last term on the left-hand side of (5.56) vanish. The general case including local time partitions does not pose any additional mathematical difficulties.

Corresponding to (5.18), the streamline-diffusion DGFEM norm in the present setting is given by

$$|||v|||_{\mathrm{s}}^2 := |||v|||^2 + \sum_{\kappa_n \in \mathscr{U} \times \mathscr{T}_h} \lambda_{\kappa_n} \|\partial_t v\|_{\kappa_n}^2, \tag{5.57}$$

where

$$|||v||| := \Big(\int_J |||v|||_{\mathrm{d}}^2 \,\mathrm{d}t + \frac{1}{2}\|v_0^+\|_{L^2(D)}^2 + \sum_{n=1}^{N_t-1} \frac{1}{2}\|\lfloor v \rfloor_n\|_{L^2(D)}^2 + \frac{1}{2}\|v_{N_t}^-\|_{L^2(D)}^2 \Big)^{1/2}, \tag{5.58}$$

and

$$|||v|||_{\mathrm{d}} := \Big(\sum_{\kappa \in \mathscr{T}_h} \|\sqrt{\mathbf{a}}\nabla v\|_{L^2(\kappa)}^2 + \int_{\mathscr{F}_h} \sigma [\![v]\!]^2 \,\mathrm{d}s \Big)^{1/2},$$

with $\lambda_{\kappa_n} := \tau_n / \hat{p}_{\kappa_n}^2$ and

$$\hat{p}_{\kappa_n} := \max_{\tilde{F}^{\parallel} \subset \partial\kappa_n} \Big\{ \max_{\substack{\tilde{\kappa}_n \in \{\kappa_n, \kappa_n'\} \\ \tilde{F}^{\parallel} \subset \partial\kappa_n \cap \partial\kappa_n'}} \{p_{\tilde{\kappa}_n}\} \Big\} \quad \forall \kappa_n \in \mathscr{U} \times \mathscr{T}_h,$$

for $p_{\kappa_n}, \hat{p}_{\kappa_n} \geq 1$.

Theorem 52 *Given that Assumption 30 is satisfied, there exists a constant $\Lambda_s > 0$, independent of the temporal and spatial mesh sizes τ_n and h_κ, respectively, the polynomial degree p_{κ_n}, and the number of faces per element, such that:*

$$\inf_{v \in V^{\mathbf{p}}(\mathscr{U}; \mathscr{T}_h) \setminus \{0\}} \sup_{\mu \in V^{\mathbf{p}}(\mathscr{U}; \mathscr{T}_h) \setminus \{0\}} \frac{\tilde{B}(v, \mu)}{|||v|||_{\mathrm{s}} |||\mu|||_{\mathrm{s}}} \geq \Lambda_s. \tag{5.59}$$

Proof The proof is completely analogous to the one of Theorem 42.

Remark 53 The combination of the use of prismatic elements, allowing for decoupling integrals over κ_n between space and time subdomains, κ and I_n, respectively, together with the fact that the first-order derivative term in the PDE is orthogonal

to the diffusion directions, allows for a careful analysis which avoids the shape-regularity assumption stated in Assumption 13. Therefore, the time-step τ_n can be chosen independently of the local spatial mesh size $h_\kappa = \mathrm{diam}(\kappa)$. We refer to [56] for details.

The above result shows that space-time DGFEMs based on the reduced *total-degree-p* space-time basis is well posed. It extends the stability proof in the previous section to space-time elements with arbitrarily large aspect ratio between the time-step τ_n and local mesh-size h_κ for parabolic problems. Moreover, the above inf-sup condition holds *without any assumption on the number of faces per spatial mesh element*. Therefore, the scheme is stable for extremely general, possibly anisotropic, space-time meshes.

The inf-sup condition will be instrumental in the proof of the proceeding a priori error bounds presented below, as the total-degree-p space-time basis does not allow for classical space-time tensor-product arguments [166] to be employed. In order to exploit the hp-approximation results from Sects. 3.3 and 4.3, we (only now) require a shape-regularity assumption for the space-time elements. The extension of these hp-approximation results for $d = 4$, although not done explicitly within the literature, does not pose any particular challenges, so we may assume their validity in this case also.

Assumption 54 *We assume the existence of a constant $c_{reg} > 0$ such that*

$$c_{reg}^{-1} \leq h_\kappa / \tau_n \leq c_{reg},$$

uniformly for all $\kappa_n \in \mathscr{U} \times \mathscr{T}_h$, i.e., the space-time elements are also shape-regular.

Following Definition 17, we assume the existence of certain spatial mesh coverings. For each spatial element κ, $\kappa \in \mathscr{T}_h$, there exists a $\mathscr{K} \in \mathscr{T}_h^\sharp$, such that $\kappa \subset \mathscr{K}$. Moreover, we denote $\mathscr{K}_n := I_n \times \mathscr{K}$ as the covering for the space-time element $\kappa_n \in \mathscr{U} \times \mathscr{T}_h$; see Fig. 5.2 for an illustration.

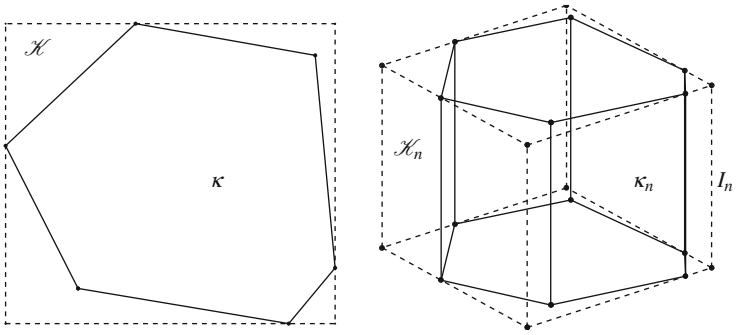

Fig. 5.2 (**a**) Polygonal spatial element κ and covering $\mathscr{K}$; (**b**) Space-time element $\kappa_n = I_n \times \kappa$ and covering $\mathscr{K}_n := I_n \times \mathscr{K}$

We first give an a priori error bound for the space-time DGFEM (5.54) in the $|||\cdot|||_{\mathrm{s}}$-norm; the derivation of this error bound is completely analogous to that of Theorem 46 and is, therefore, omitted for brevity.

Theorem 55 *Given that Assumptions 18, 30, and 54 hold, let $u_h \in V^{\mathbf{p}}(\mathscr{U};\mathscr{T}_h)$ be the space-time DGFEM approximation to the analytical solution $u \in L^2(J;H^1(D)) \cap H^1(J;H^{-1}(D))$, with the discontinuity-penalization function given by (4.26), and suppose that $u|_{\kappa_n} \in H^{l_{\kappa_n}}(\kappa_n)$, $l_{\kappa_n} \geq 1$, for each $\kappa_n \in \mathscr{U} \times \mathscr{T}_h$, such that $\mathfrak{E}u|_{\mathscr{K}_n} \in H^{l_{\kappa_n}}(\mathscr{K}_n)$. Then, the following error bound holds:*

$$|||u-u_h|||_{\mathrm{s}}^2 \leq C \sum_{\kappa_n \in \mathscr{U}\times\mathscr{T}_h} \frac{h_{\kappa_n}^{2s_{\kappa_n}}}{p_{\kappa_n}^{2l_{\kappa_n}}} \big(\mathscr{G}_{\kappa_n}(h_{\kappa_n},p_{\kappa_n}) + \mathscr{D}_{\kappa_n}(h_{\kappa_n},p_{\kappa_n})\big) \|\mathfrak{E}u\|_{H^{l_{\kappa_n}}(\mathscr{K}_n)}^2, \tag{5.60}$$

where

$$\mathscr{G}_{\kappa_n}(h_{\kappa_n},p_{\kappa_n}) := \lambda_{\kappa_n}^{-1} + \lambda_{\kappa_n} p_{\kappa_n}^2 h_{\kappa_n}^{-2} + p_{\kappa_n} h_{\kappa_n}^{-1} + \bar{\mathbf{a}}_{\kappa_n} p_{\kappa_n}^2 h_{\kappa_n}^{-2} + p_{\kappa_n} h_{\kappa_n}^{-1} \max_{\tilde{F}^{\shortparallel}\subset\partial\kappa_n} \sigma|_{\tilde{F}^{\shortparallel}},$$

and

$$\mathscr{D}_{\kappa_n}(h_{\kappa_n},p_{\kappa_n}) := \bar{\mathbf{a}}_{\kappa_n}^2 \big(p_{\kappa_n}^3 h_{\kappa_n}^{-3} \max_{\tilde{F}^{\shortparallel}\subset\partial\kappa_n} \sigma|_{\tilde{F}^{\shortparallel}}^{-1} + p_{\kappa_n}^4 h_{\kappa_n}^{-3} \max_{\tilde{F}^{\shortparallel}\subset\partial\kappa_n} \sigma|_{\tilde{F}^{\shortparallel}}^{-1} \big), \tag{5.61}$$

with $s_\kappa = \min\{p_\kappa+1, l_\kappa\}$ and $p_\kappa \geq 1$; here, the positive constant C is independent of the discretization parameters and the number of faces per element.

The above a priori bound holds *without* any assumptions regarding either the size of the spatial faces F, $F \subset \partial\kappa$, relative to the size of the underlying element κ, $\kappa \in \mathscr{T}_h$, or the number of faces a given spatial polytopic element κ, $\kappa \in \mathscr{T}_h$, possesses; i.e., elements with arbitrarily small faces and/or an arbitrarily large number of faces are permitted, as long as they satisfy Assumption 30.

Corollary 56 *Under the hypotheses of Theorem 55, set $p_{\kappa_n} = p \geq 1$ for all $\kappa_n \in \mathscr{U}_n(\mathscr{T}_h) \times \mathscr{T}_h$), $s_{\kappa_n} = s$, and $s = \min\{p+1, l\}$, $l \geq 1$. Assume also that the spatial mesh $\mathscr{T}_h$ is quasiuniform. Then, we have the bound*

$$\|u-u_h\|_{L^2(J;H^1(D,\mathscr{T}_h))} \leq C \frac{h^{s-1}}{p^{l-3/2}} \|u\|_{H^l(J\times D)},$$

where C is a positive constant, independent of the discretization parameters.

On the basis of Corollary 56, we observe that the above bound is, therefore, h-optimal and p-suboptimal by $p^{1/2}$. Next, we derive an error bound with respect to the $L^2(J;L^2(D))$-norm using a duality argument. To this end, the backward adjoint

problem of (5.50), (5.51) is defined by

$$-\partial_t z - \nabla\cdot(\mathbf{a}\nabla z) \;=\; \phi \quad \text{in } J\times D, \tag{5.62}$$

$$z|_{t=T} = g \quad \text{on } D, \quad \text{and} \quad z = 0 \quad \text{on } J\times\partial D. \tag{5.63}$$

Assuming that $g\in H_0^1(D)$ and $\phi\in L^2(J;L^2(D))$, then we have

$$z\in L^2(J;H^2(D))\cap L^\infty(J;H_0^1(D)), \quad \partial_t z\in L^2(J;L^2(D)). \tag{5.64}$$

We assume that D and $\mathbf{a}$ are such that the parabolic regularity estimate holds

$$\|z\|_{L^\infty(J;H_0^1(D))} + \|z\|_{L^2(J;H^2(D))} + \|z\|_{H^1(J;L^2(D))} \le C_{\mathfrak{R}}(\|\phi\|_{L^2(J;L^2(D))} + \|g\|_{H_0^1(D)}), \tag{5.65}$$

where $C_{\mathfrak{R}}$ is a positive constant, which depends only on D, T, and $\mathbf{a}$, cf. [92, p. 360] for smooth domains; the parabolic regularity result can be extended to convex domains by employing results in [105, Chapter 3].

Assumption 57 *For any two $(d-1)$-dimensional spatial elements κ, $\kappa'\in\mathscr{T}_h$ sharing the same $(d-2)$-facet, we have:*

$$\max(h_\kappa, h_{\kappa'}) \le c_h \min(h_\kappa, h_{\kappa'}), \quad \max(p_{\kappa_n}, p_{\kappa_n'}) \le c_p \min(p_{\kappa_n}, p_{\kappa_n'}), \tag{5.66}$$

for $n=1,\ldots,N_t$, where c_h and c_p are positive constants, which are independent of discretization parameters.

Theorem 58 *Consider the setting of Theorem 55, and assume that the parabolic regularity estimate (5.65) holds along with Assumption 57. Then, the following bound holds*

$$\|u-u_h\|^2_{L^2(J;L^2(D))} \le C \max_{\kappa_n\in\mathscr{U}\times\mathscr{T}_h} h_{\kappa_n} \sum_{\kappa_n\in\mathscr{U}\times\mathscr{T}_h} \frac{h_{\kappa_n}^{2s_{\kappa_n}}}{p_{\kappa_n}^{2l_{\kappa_n}}} \big(\mathscr{G}_{\kappa_n}(h_{\kappa_n},p_{\kappa_n}) + \mathscr{D}_{\kappa_n}(h_{\kappa_n},p_{\kappa_n})\big)\|\mathfrak{E}u\|^2_{H^{l_{\kappa_n}}(\mathscr{K}_n)},$$

where the C is a positive constant, which is independent of the discretization parameters and the number of faces per element.

Proof We set $g=0$ and $\phi = u-u_h$ in (5.62), (5.63). Then,

$$\|u-u_h\|^2_{L^2(J;L^2(D))} = \sum_{n=1}^{N_t}\int_{I_n} -(\partial_t z, u-u_h)_D + B_{\mathrm{d}}(z,u-u_h)\,\mathrm{d}t - \sum_{n=1}^{N_t-1}(\lfloor z\rfloor_n, (u-u_h)_n^-)_D + (z_{N_t}^-, (u-u_h)_{N_t}^-)_D = B(u-u_h,z), \tag{5.67}$$

with z the solution to (5.62), (5.63), cf. [166]. Now, upon considering $B(\cdot,\cdot)$, whose extension to $\mathscr{V}$ is understood to be attained by replacing $B_{\mathrm{d}}(\cdot,\cdot)$ by its inconsistent version $\tilde{B}_{\mathrm{d}}(\cdot,\cdot)$, defined in (4.8), we have

$$\|u-u_h\|^2_{L^2(J;L^2(D))} = B(u-u_h,z) - R(z,u-u_h),$$

with $R(v,\omega) := \int_J \int_{\mathscr{F}_h} \{\!\{\mathbf{a}(\nabla v - \boldsymbol{\Pi}_{L^2}(\nabla v))\}\!\} \cdot [\![\omega]\!]\,\mathrm{d}s\,\mathrm{d}t$. Further, for any $z_h \in V^{\mathbf{p}}(\mathscr{U};\mathscr{T}_h)$, we have

$$B(u-u_h,z_h) = B(u-u_h,z_h) - B(u-u_h,z_h) = R(u,z_h),$$

and also $R(u,z_h) = -R(u,z-z_h)$ since $R(u,z) = 0$. The above identities imply that

$$\|u-u_h\|^2_{L^2(J;L^2(D))} = B(u-u_h,z-z_h) - R(z,u-u_h) - R(u,z-z_h). \tag{5.68}$$

For brevity, we set $e := u-u_h$ and $\eta := z-z_h$. For the first term on the right-hand side of (5.68), using (4.14), we have

$$\begin{aligned} B(e,\eta) \le & \sum_{\kappa_n\in\mathscr{U}\times\mathscr{T}_h} \|\lambda_{\kappa_n}^{1/2}\partial_t e\|_{L^2(\kappa_n)}\|\lambda_{\kappa_n}^{-1/2}\eta\|_{L^2(\kappa_n)} + C_{\mathrm{cont}}\sum_{n=1}^{N_t}\int_{I_n} |||e|||_{\mathrm{d}}|||\eta|||_{\mathrm{d}}\,\mathrm{d}t \\ & + \sum_{n=1}^{N_t-1} \|\lfloor e\rfloor_n\|_{L^2(D)}\|\eta_n^+\|_{L^2(D)} + \|e_0^+\|_{L^2(D)}\|\eta_0^+\|_{L^2(D)} \\ \le & \Big(\sum_{\kappa_n\in\mathscr{U}\times\mathscr{T}_h} \lambda_{\kappa_n}^{-1}\|\eta\|^2_{L^2(\kappa_n)} + (C_{\mathrm{cont}})^2\sum_{n=1}^{N_t}\int_{I_n}|||\eta|||^2_{\mathrm{d}}\,\mathrm{d}t + 2\sum_{n=0}^{N_t-1}\|\eta_n^+\|^2_{L^2(D)}\Big)^{\frac{1}{2}} \\ & \times |||e|||_{\mathrm{s}}. \end{aligned} \tag{5.69}$$

Let $z_h \in V^{\mathbf{p}}(\mathscr{U};\mathscr{T}_h)$ be defined on each element $\kappa_n \in \mathscr{U}\times\mathscr{T}_h$ by

$$z_h|_{\kappa_n} := \begin{cases} \pi_{\bar{p}}^t \tilde{\Pi}_{\bar{p}} z\ , \text{for } p_{\kappa_n} \text{ even;} \\ \pi_{\bar{p}}^t \tilde{\Pi}_{\bar{p}+1} z\ , \text{for } p_{\kappa_n} \text{ odd,} \end{cases}$$

for $\bar{p} := \lfloor \frac{p_{\kappa_n}}{2} \rfloor$, with π_q^t denoting the L^2-orthogonal projection onto polynomials of degree q with respect to the time variable, and $\tilde{\Pi}_q$ is the projector defined in Lemma 23 over $(d-1)$-dimensional spatial domains. Note that this choice ensures that $z_h \in V^{\mathbf{p}}(\mathscr{U};\mathscr{T}_h)$.

We shall now estimate the terms involving η on the right-hand side of (5.69). Recalling standard *hp*-approximation bounds (see, e.g., [124]), we have for $r \in$

$\{\bar{p}, \bar{p}+1\}$,

$$\begin{aligned}
&\sum_{\kappa_n \in \mathscr{U}\times\mathscr{T}_h} \lambda_{\kappa_n}^{-1} \|\eta\|^2_{L^2(\kappa_n)} \\
&\quad \le 2 \sum_{\kappa_n \in \mathscr{U}\times\mathscr{T}_h} \lambda_{\kappa_n}^{-1} \Big(\|z - \pi_{\bar{p}}^t z\|^2_{L^2(\kappa_n)} + \|\pi_{\bar{p}}^t z - \pi_{\bar{p}}^t \tilde{\Pi}_r z\|^2_{L^2(\kappa_n)} \Big) \\
&\quad \le C \sum_{\kappa_n \in \mathscr{U}\times\mathscr{T}_h} \lambda_{\kappa_n}^{-1} \Big(\frac{\tau_n^2}{p_{\kappa_n}^2} \|\partial_t z\|^2_{\kappa_n} + \frac{h_\kappa^4}{p_{\kappa_n}^4} \|\mathfrak{E} z\|^2_{L^2(I_n;H^2(\mathscr{K}))} \Big) \\
&\quad \le C \max_{\kappa_n \in \mathscr{U}\times\mathscr{T}_h} h_{\kappa_n} \Big(\|z\|^2_{H^1(J;L^2(D))} + \max_{\kappa_n \in \mathscr{U}\times\mathscr{T}_h} \frac{h_{\kappa_n}^2}{p_{\kappa_n}^2} \|z\|^2_{L^2(J;H^2(D))} \Big); \qquad (5.70)
\end{aligned}$$

here, we have employed the triangle inequality, the stability of L^2-projection operator, Assumptions 54 and 57, and Theorem 21. Next, employing the one-dimensional version of the classical inverse estimate (3.1) in the time variable, and proceeding as before, gives

$$\begin{aligned}
\sum_{n=0}^{N_t-1} \|\eta_n^+\|^2_{L^2(D)} &\le 2 \sum_{n=0}^{N_t-1} \sum_{\kappa \in \mathscr{T}_h} \Big(\|(z - \pi_{\bar{p}}^t z)_n^+\|^2_{L^2(\kappa)} + \|(\pi_{\bar{p}}^t z - \pi_{\bar{p}}^t \tilde{\Pi}_r z)_n^+\|^2_{L^2(\kappa)} \Big) \\
&\le C \sum_{\kappa_n \in \mathscr{U}\times\mathscr{T}_h} \Big(\frac{\tau_n}{p_{\kappa_n}} \|\partial_t z\|^2_{L^2(\kappa_n)} + \frac{p_{\kappa_n}^2}{\tau_n} \|\pi_{\bar{p}}^t (z - \tilde{\Pi}_r z)\|^2_{L^2(\kappa_n)} \Big) \\
&\le C \sum_{\kappa_n \in \mathscr{U}\times\mathscr{T}_h} \Big(\frac{\tau_n}{p_{\kappa_n}} \|\partial_t z\|^2_{L^2(\kappa_n)} + \frac{h_\kappa^4}{\tau_n p_{\kappa_n}^2} \|\mathfrak{E} z\|^2_{L^2(J;H^2(\mathscr{K}))} \Big) \\
&\le C \max_{\kappa_n \in \mathscr{U}\times\mathscr{T}_h} \frac{h_{\kappa_n}}{p_{\kappa_n}} \Big(\|z\|^2_{H^1(J;L^2(D))} + \max_{\kappa_n \in \mathscr{U}\times\mathscr{T}_h} \frac{h_{\kappa_n}^2}{p_{\kappa_n}} \|z\|^2_{L^2(J;H^2(D))} \Big). \qquad (5.71)
\end{aligned}$$

Furthermore, we have that

$$\begin{aligned}
&\sum_{n=1}^{N_t} \int_{I_n} \sum_{\kappa \in \mathscr{T}_h} \|\nabla \eta\|^2_{L^2(\kappa)} \, \mathrm{d}t \\
&\quad \le 2 \sum_{\kappa_n \in \mathscr{U}\times\mathscr{T}_h} \Big(\|\nabla(z - \pi_{\bar{p}}^t z)\|^2_{L^2(\kappa_n)} + \|\nabla(\pi_{\bar{p}}^t z - \pi_{\bar{p}}^t \tilde{\Pi}_r z)\|^2_{L^2(\kappa_n)} \Big) \\
&\quad \le C \sum_{\kappa_n \in \mathscr{U}\times\mathscr{T}_h} \Big(\tau_n \|\nabla z\|^2_{L^\infty(I_n;L^2(\kappa))} + \frac{h_\kappa^2}{p_{\kappa_n}^2} \|\mathfrak{E} z\|^2_{L^2(I_n;H^2(\mathscr{K}))} \Big) \\
&\quad \le C \max_{\kappa_n \in \mathscr{U}\times\mathscr{T}_h} h_{\kappa_n} \Big(\|z\|^2_{L^\infty(J;H_0^1(D))} + \max_{\kappa_n \in \mathscr{U}\times\mathscr{T}_h} \frac{h_{\kappa_n}}{p_{\kappa_n}^2} \|z\|^2_{L^2(J;H^2(D))} \Big). \qquad (5.72)
\end{aligned}$$

Also, since $[\![z]\!] = 0 = [\![\pi_{\underline{p}}^t z]\!]$, we have $[\![z - \pi_{\underline{p}}^t \tilde{\Pi}_r z]\!] = \pi_{\underline{p}}^t [\![z - \tilde{\Pi}_r z]\!]$; hence, by Assumption 57, we deduce that

$$\begin{aligned}\sum_{n=1}^{N_t} \int_{I_n} \int_{\mathscr{F}_h} \sigma |[\![\eta]\!]|^2 \,\mathrm{d}s\,\mathrm{d}t &= \sum_{\tilde{F}^{\shortparallel} \subset J \times \mathscr{F}_h} \sigma \|[\![z - \tilde{\Pi}_r z]\!]\|^2_{L^2(\tilde{F}^{\shortparallel})} \\ &\le C \sum_{\kappa_n \in \mathscr{U} \times \mathscr{T}_h} \Big(\max_{\tilde{F}^{\shortparallel} \subset \partial \kappa_n} \sigma \Big) \frac{h_{\kappa_n}^3}{p_{\kappa_n}^3} \|\mathfrak{E} z\|^2_{L^2(J;H^2(\mathscr{K}))} \\ &\le C \max_{\kappa_n \in \mathscr{U} \times \mathscr{T}_h} \frac{h_{\kappa_n}^2}{p_{\kappa_n}} \|z\|^2_{L^2(J;H^2(D))}. \end{aligned} \tag{5.73}$$

Inserting (5.70)–(5.73) into (5.69), and employing (5.65), we get

$$B(e, \eta) \le C C_{\mathfrak{R}} \max_{\kappa_n \in \mathscr{U} \times \mathscr{T}_h} h_{\kappa_n}^{1/2} |||e|||_{\mathrm{s}} \|e\|_{L^2(J;L^2(D))}. \tag{5.74}$$

Moving on to the second term on the right-hand side of (5.68), we have

$$\begin{aligned} R(z, e) &= \sum_{n=1}^{N_t} \int_{I_n} \int_{\mathscr{F}_h} \{\!\{ \mathbf{a}(\nabla z - \boldsymbol{\Pi}_{L^2}(\nabla z)) \}\!\} \cdot [\![e]\!] \,\mathrm{d}s\,\mathrm{d}t \\ &\le \Big(\sum_{n=1}^{N_t} \int_{I_n} \int_{\mathscr{F}_h} \sigma^{-1} |\{\!\{ \mathbf{a}(\nabla z - \boldsymbol{\Pi}_{L^2}(\nabla z)) \}\!\}|^2 \,\mathrm{d}s\,\mathrm{d}t \Big)^{1/2} |||e|||_{\mathrm{s}}. \end{aligned}$$

To bound $R(z, e)$ further, it is sufficient to bound the terms

$$\mathrm{I} := \sum_{n=1}^{N_t} \int_{I_n} \int_{\mathscr{F}_h} 2\sigma^{-1} |\{\!\{ \mathbf{a}(\nabla z - \boldsymbol{\pi}_{\underline{p}}^t \tilde{\boldsymbol{\Pi}}_r(\nabla z)) \}\!\}|^2 \,\mathrm{d}s\,\mathrm{d}t,$$

$$\mathrm{II} := \sum_{n=1}^{N_t} \int_{I_n} \int_{\mathscr{F}_h} 2\sigma^{-1} |\{\!\{ \mathbf{a}\boldsymbol{\Pi}_{L^2}(\boldsymbol{\pi}_{\underline{p}}^t \tilde{\boldsymbol{\Pi}}_r(\nabla z) - \nabla z) \}\!\}|^2 \,\mathrm{d}s\,\mathrm{d}t.$$

Using Lemma 33 and working as before gives

$$\mathrm{I} \le C \max_{\kappa_n \in \mathscr{U} \times \mathscr{T}_h} \frac{h_{\kappa_n}^{3/2}}{p_{\kappa_n}^2} \Big(\|z\|^2_{L^\infty(J;H_0^1(D))} + \|z\|^2_{L^2(J;H^2(D))} \Big). \tag{5.75}$$

Employing Lemma 32, the stability of $\boldsymbol{\Pi}_{L^2}$, and proceeding as above, leads to

$$\mathrm{II} \le C \max_{\kappa_n \in \mathscr{U} \times \mathscr{T}_h} h_{\kappa_n} \Big(\|z\|^2_{L^\infty(J;H_0^1(D))} + \|z\|^2_{L^2(J;H^2(D))} \Big). \tag{5.76}$$

Therefore, (5.75) and (5.76), together with (5.65) give

$$R(z,e) \le CC_{\mathfrak{R}} \max_{\kappa_n \in \mathscr{U}\times\mathscr{T}_h} h_{\kappa_n}^{1/2} |||e|||_{\mathrm{s}} \|e\|_{L^2(J;L^2(D))}. \tag{5.77}$$

Next, we bound the last term on the right-hand side of (5.68), which is given by

$$R(u,\eta) = \sum_{n=1}^{N_t} \int_{I_n} \int_{\mathscr{F}_h} \{\!\{\mathbf{a}(\nabla_h u - \boldsymbol{\Pi}_{L^2}(\nabla_h u))\}\!\} \cdot [\![\eta]\!] \,\mathrm{d}s\,\mathrm{d}t.$$

Exploiting the Cauchy-Schwarz inequality together with (5.73), gives

$$\begin{aligned} &R(u,\eta) \\ &\le \Big(\sum_{n=1}^{N_t} \int_{I_n} \int_{\mathscr{F}_h} \sigma^{-1} |\{\!\{\mathbf{a}(\nabla_h u - \boldsymbol{\Pi}_{L^2}(\nabla_h u))\}\!\}|^2 \,\mathrm{d}s\,\mathrm{d}t \Big)^{\frac{1}{2}} \Big(\sum_{n=1}^{N_t} \int_{I_n} \int_{\mathscr{F}_h} \sigma [\![\eta]\!]^2 \,\mathrm{d}s\,\mathrm{d}t \Big)^{\frac{1}{2}} \\ &\le CC_{\mathfrak{R}} \max_{\kappa_n \in \mathscr{U}\times\mathscr{T}_h} \frac{h_{\kappa_n}}{p_{\kappa_n}^{1/2}} \|e\|_{L^2(J;L^2(D))} \Big(\sum_{\kappa_n \in \mathscr{U}\times\mathscr{T}_h} \frac{h_{\kappa_n}^{2s_{\kappa_n}}}{p_{\kappa_n}^{2l_{\kappa_n}}} \mathscr{D}_{\kappa_n}(h_{\kappa_n}, p_{\kappa_n}) \|\mathfrak{E}u\|^2_{H^{l_{\kappa_n}}(\mathscr{K}_n)} \Big)^{1/2}. \end{aligned} \tag{5.78}$$

Combining (5.74), (5.77) and (5.78) with (5.68), we deduce the statement of the theorem.

We note that the $L^2(J;L^2(D))$-norm error bound stated in Theorem 58 is suboptimal with respect to the mesh size h by half an order of h, and is suboptimal in p by $p^{3/2}$. If, however, we instead employ a tensor-product space-time polynomial basis within the DGFEM, the above argument will result in an $L^2(J;L^2(D))$-norm error bound which is h-optimal and p-suboptimal by one order of p. Numerical experiments presented in [56] confirm the suboptimality in h predicted by Theorem 58, but at the same time highlight its competitiveness compared with the standard (optimal) space-time DGFEM, employing tensor-product polynomial bases, as the order p increases. Indeed, the reduced number of elemental basis functions admitted by $V^{\mathbf{p}}(\mathscr{U};\mathscr{T}_h)$ are able to counteract the mild loss of optimality as p increases, cf. Sect. 6.4.2; see, also, the recent work [84] for a p-approximation result in this direction.

Chapter 6
Implementation Aspects

In this chapter we briefly outline some of the implementation aspects of DGFEMs posed on general computational meshes consisting of polytopic elements. To this end, we focus on three key topics: mesh generation, construction of the elemental polynomial basis, and efficient numerical integration over polytopic elements. Finally, we end this chapter by presenting some numerical examples to highlight the sharpness of the a priori error bounds derived in Chap. 5 for both a steady advection-diffusion-reaction problem and a (degenerate) evolution problem.

6.1 Mesh Generation

General meshes consisting of polytopic elements can be constructed in a number of different ways; in particular, a Voronoi tessellation of the underlying geometry may be generated, cf. [88, 165], for example. Alternatively, a flexible approach for meshing complicated geometries, is to exploit some form of agglomeration algorithm, whereby the underlying polytopic elements are formed by taking the union of a set of elements from a given geometry-conforming fine mesh $\mathscr{T}_h^{\text{fine}}$. We point out that $\mathscr{T}_h^{\text{fine}}$ is typically constructed by employing standard shaped elements, i.e., simplices or tensor-product elements; in this setting, the resulting underlying FEM is often referred to as a *composite* FEM, cf. [8, 12, 106, 107], or an *agglomerated* FEM, cf. [32, 34]. The construction of agglomerated meshes may be undertaken using two key approaches: firstly, in the series of articles [8, 12, 106, 107] a hierarchy of overlapping (so-called) reference and logical meshes, consisting of standard-shaped elements, are constructed based on successive adaptive refinement of elements which intersect the boundary $\partial\Omega$ of the computational domain Ω. Once a sufficiently fine logical mesh has been constructed, possibly by moving nodes onto $\partial\Omega$, a sequence of coarse geometry-conforming physical meshes, consisting

A. Cangiani et al., *hp-Version Discontinuous Galerkin Methods on Polygonal and Polyhedral Meshes*, SpringerBriefs in Mathematics,
DOI 10.1007/978-3-319-67673-9_6

of general polytopic elements, may be constructed via agglomerating elements which share the same parent within the underlying refinement tree. Secondly, the fine mesh $\mathscr{T}_h^{\text{fine}}$ may be constructed using a standard mesh generator, for example, Triangle [157] or Tetgen [158], and then subsequently agglomerated into polytopes using graph partitioning algorithms; for this purpose, in the numerical investigations presented in this volume, we employ METIS [130], though we stress that many other such packages also exist.

6.2 Construction of Basis Functions on Polytopes

In the case when the computational mesh $\mathscr{T}_h$ consists of standard element shapes, the construction of the underlying finite element space $V^{\mathbf{p}}(\mathscr{T}_h)$ is typically undertaken by mapping each element κ in $\mathscr{T}_h$ to a given reference or canonical element, denoted by κ_{R}. Thereby, on κ_{R} local spaces of polynomials may be constructed in a simple manner, subject to the enforcement of any inter-element continuity constraints, for example, in the case when C^0-conforming elements are employed; for further details, we refer to, for example, [78, 129, 160], and the references cited therein. While this approach is used quite universally within most FEM software packages, a disadvantage is that the calculation of high-order derivatives of the computed numerical solution is rather cumbersome when non-affine element mappings are employed. Moreover, in this setting, the order of approximation of the underlying FEM may be adversely affected by mesh distortion, unless a sufficiently rich local space is employed, cf. [17, 19].

The flexibility of the DGFEM allows for the elemental basis to be constructed within the physical frame, without the need to map to a given reference/canonical element, cf. [33], for example; indeed, this is an essential feature of DGFEMs which allows them to admit general polytopic elements in a simple fashion. In [33] basis functions are constructed on general meshes consisting of agglomerated elements, based on employing a Gram-Schmidt orthogonalization process applied to a given set of polynomial functions defined on each κ, $\kappa \in \mathscr{T}_h$. An alternative approach proposed in [54] is based on first defining polynomial spaces over a suitably chosen bounding box of each element κ, $\kappa \in \mathscr{T}_h$; then the element basis is simply constructed by restricting this space to κ. More precisely, given an element $\kappa \in \mathscr{T}_h$, we write B_κ to denote its corresponding bounding box; selecting, for example, B_κ to be the Cartesian bounding box, i.e., the sides of B_κ are aligned with the Cartesian axes, then B_κ can be easily constructed, such that $\bar{\kappa} \subseteq \bar{B}_\kappa$, cf. Figure 6.1 for the case of a polygonal element κ in $\mathbb{R}^2$. On this Cartesian bounding box B_κ we may define a standard polynomial space $\mathscr{P}_{p_\kappa}(B_\kappa)$ spanned by a set of basis functions $\{\phi_{i,\kappa}\}$, $i = 1, \ldots, \dim(\mathscr{P}_{p_\kappa}(B_\kappa))$; note that tensor-product polynomial spaces $\mathscr{Q}_{p_\kappa}(B_\kappa)$ may also be employed, though in the absence of non-affine element mappings, the approximation order of both spaces will be identical.

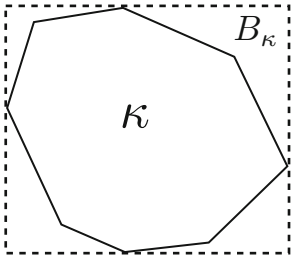

Fig. 6.1 Bounding box B_κ of an element $\kappa \in \mathscr{T}_h$

Writing $B_\kappa := \mathscr{I}_1 \times \mathscr{I}_2 \times \cdots \times \mathscr{I}_d$, where $\mathscr{I}_j := (x_1^j, x_2^j), j = 1, \ldots, d$, and selecting $\kappa_{\mathrm{R}} := (-1, 1)^d$ to be the reference hypercube, the bounding box B_κ may be affinely mapped to κ_{R}, via the mapping

$$\mathbf{x} = J_\kappa \hat{\mathbf{x}} + \mathbf{c}, \tag{6.1}$$

where $J_\kappa := \mathrm{diag}(h_1, \ldots, h_d)$, $\mathbf{c} := (m_1, \ldots, m_d)^\top$, and $\hat{\mathbf{x}}$ is a general point in κ_{R}. Furthermore, $h_j, j = 1, \ldots, d$, is half of the length of the jth-side of B_κ, respectively, i.e., $h_j := (x_2^j - x_1^j)/2, j = 1, \ldots, d$, and $m_j := (x_1^j + x_2^j)/2, j = 1, \ldots, d$, is the midpoint of $\mathscr{I}_j$.

For convenience, on κ_{R} we employ tensor-product Legendre polynomials; to this end, writing $\{\hat{L}_i(\hat{x})\}_{i=0}^{\infty}$ to denote the family of $L^2(-1, 1)$-orthogonal Legendre polynomials, cf. [156], for example, the space of polynomials $\mathscr{P}_{p_\kappa}(\kappa_{\mathrm{R}})$ of total degree p_k over κ_{R} is given by

$$\mathscr{P}_{p_\kappa}(\kappa_{\mathrm{R}}) := \mathrm{span}\{\hat{\phi}_{i,\kappa}\}_{i=1}^{\dim(\mathscr{P}_{p_\kappa}(\kappa_{\mathrm{R}}))},$$

where

$$\hat{\phi}_{i,\kappa}(\hat{\mathbf{x}}) = \hat{L}_{i_1}(\hat{x}_1)\hat{L}_{i_2}(\hat{x}_2)\cdots\hat{L}_{i_d}(\hat{x}_d), \quad i_1 + i_2 + \ldots + i_d \leq p_\kappa, \;\; i_k \geq 0, \; k = 1, \ldots, d,$$

and $\hat{\mathbf{x}} = (\hat{x}_1, \hat{x}_2, \ldots, \hat{x}_d)$. Writing $L_i(x) = \hat{L}_i((x - m_j)/h_j)$, under the transformation (6.1), the space of polynomials $\mathscr{P}_{p_\kappa}(B_\kappa)$ of total degree p_k over B_κ is given by

$$\mathscr{P}_{p_\kappa}(B_\kappa) = \mathrm{span}\{\phi_{i,\kappa}\}_{i=1}^{\dim(\mathscr{P}_{p_\kappa}(B_\kappa))},$$

where

$$\phi_{i,\kappa}(\mathbf{x}) = L_{i_1}(x_1)L_{i_2}(x_2)\cdots L_{i_d}(x_d), \quad i_1 + i_2 + \ldots + i_d \leq p_\kappa, \;\; i_k \geq 0, \; k = 1, \ldots, d,$$

and $\mathbf{x} = (x_1, x_2, \ldots, x_d)$. Thereby, the polynomial basis over the general polytopic element κ may be defined by simply restricting the support of $\{\phi_{i,\kappa}\}$, $i =$

$1, \ldots, \dim(\mathscr{P}_{p_\kappa}(B_\kappa))$ to κ; i.e., the polynomial basis defined over κ is given by $\{\phi_{i,\kappa}|_\kappa\}$, $i = 1, \ldots, \dim(\mathscr{P}_{p_\kappa}(B_\kappa))$.

Remark 59 We stress that the choice of B_κ is arbitrary; indeed, alternative bounding boxes, other than the Cartesian aligned one presented above, may be employed, provided that the construction of the underlying polynomial basis may be undertaken in a simple fashion. For example, for anisotropic polytopic elements, it may be more desirable to select a 'rotated' bounded box which is aligned with the principle axes of the element.

6.3 Quadrature Rules

The design of efficient and accurate quadrature rules for general polytopes is a challenging task; while several approaches have been proposed within the literature, cf. below, this still remains an open and active area of research. Below we review three prominent approaches which have been proposed; for further details, we refer to [14].

6.3.1 Sub-Tessellation

The simplest, and perhaps most natural approach is to simply construct a sub-tessellation of each polytopic element into standard element shapes, upon which standard quadrature rules may be employed, cf. [54, 55, 125], for example. More precisely, given $\kappa \in \mathscr{T}_h$, we first construct a non-overlapping sub-tessellation $\kappa_\mathscr{S} := \{\tau_\kappa\}$ consisting of standard element shapes; here, a general hybrid sub-tessellation consisting of quadrilateral and triangular elements in $\mathbb{R}^2$, or tetrahedral, hexahedral, prismatic, and pyramidal elements in $\mathbb{R}^3$, may be constructed. On agglomerated meshes, the sub-tessellation will already be available; however, for reasons of efficiency, one may still wish to construct an alternative sub-tessellation which comprises of a minimal number of elements. As an example, if we consider computing the DGFEM mass matrix, restricted to κ, $\kappa \in \mathscr{T}_h$, then we have that

$$\int_\kappa wv \,\mathrm{d}\mathbf{x} = \sum_{\tau_\kappa \in \kappa_\mathscr{S}} \int_{\tau_\kappa} wv \,\mathrm{d}\mathbf{x} \approx \sum_{\tau_\kappa \in \kappa_\mathscr{S}} \sum_{i=1}^{q_{\tau_\kappa}} w(F_\kappa(\boldsymbol{\xi}_i)) v(F_\kappa(\boldsymbol{\xi}_i)) \det(J_{F_\kappa}(\boldsymbol{\xi}_i)) w_i,$$

where $F_\kappa : \kappa_\mathrm{R} \to \tau_\kappa$ is the mapping from the reference element κ_R to τ_κ, with Jacobi matrix J_{F_κ}, and $(\boldsymbol{\xi}_i, w_i)_{i=1}^{q_{\tau_\kappa}}$ denotes the quadrature rule defined on κ_R. Quadrature rules on standard element shapes which form the sub-tessellation may be constructed based on employing tensor-product Gauss quadratures on the reference square or cube in $\mathbb{R}^2$ or $\mathbb{R}^3$, respectively; for non-tensor-product elements, such as simplices, for example, the resulting quadrature may be computed based on

employing the Duffy transformation, whereby the reference tensor-product element is mapped to the reference simplex, cf. [86, 129, 171]. For alternative quadratures on non-tensor-product elements, we refer to, for example, [78, 87, 160], and the references cited therein.

An alternative approach based on employing Stokes' theorem in $\mathbb{R}^2$ over polygons has been studied in [161]. While this idea does not directly require a sub-tessellation of the underlying element domain κ, $\kappa \in \mathscr{T}_h$, a judicious choice of parameters within the resulting formula, which ensures that all of the quadrature points lie within κ, essentially leads to a compound quadrature scheme defined on an appropriate sub-tessellation of κ.

We point out that while quadrature schemes based on employing a sub-tessellation of each polytopic element are straightforward to implement, they tend to be computationally expensive, in the sense that, depending on the cardinality of the sub-tessellation, the number of required function evaluations may be very large. This is particularly the case when the sub-tessellation employed is simply the background fine mesh $\mathscr{T}_h^{\text{fine}}$ used to construct a coarse agglomerated grid. Thereby, it is desirable to attempt to minimise the resulting number of points; one such approach is outlined in the next section.

6.3.2 Moment Quadratures

Quadrature rules such as those based on sub-tessellation outlined above can be optimized based on employing a node elimination scheme, together with the least squares Newton method, cf. [175]; for related work, we refer to [141]. In this way, (near)-minimal quadrature schemes can be constructed. To illustrate this approach, following [175], let $\kappa \in \mathscr{T}_h$ be a polytopic element. Given a user-defined set of functions $\mathscr{V}_\kappa = \{\phi_1, \phi_2, \ldots, \phi_n\}$, $n \geq 1$, defined over κ, and a quadrature rule $(\mathbf{x}_j, w_j)_{j=1}^{q_\kappa}$ on κ, $q_\kappa \geq n$, which is *assumed* to integrate all functions in $\mathscr{V}_\kappa$ exactly, we arrive at the following system of equations:

$$A\mathbf{w} = \mathbf{I}, \tag{6.2}$$

where A is an $n \times q_\kappa$ matrix with entries $A_{ij} := \phi_i(\mathbf{x}_j)$, $i = 1, \ldots, n$, $j = 1, \ldots, q_\kappa$, $\mathbf{w} := (w_1, \ldots, w_{q_\kappa})^\top$ is the vector of quadrature weights, and $\mathbf{I}$ is a vector of dimension n, with entries $\mathbf{I}_i := \int_\kappa \phi_i \, \mathrm{d}\mathbf{x}$, $i = 1, \ldots, n$. We note that as in [175] a weight function ω may also be included within the integral; for simplicity, here we set $\omega \equiv 1$.

The initial quadrature rule $(\mathbf{x}_i, w_i)_{i=1}^{q_\kappa}$ may be selected in a number of different ways; for example, the sub-tessellation approach outlined above may be exploited. The essential idea to optimise the initial quadrature is to continuously eliminate points until the solution of (6.2) can no longer be determined. More precisely, for each quadrature point and weight, the corresponding *significance index* s_j,

$j = 1, \ldots, q_\kappa$, is computed; in [175] the following two expressions are proposed:

$$s_j := w_j \sum_{i=1}^{n} \phi_i^2(\mathbf{x}_j), \quad \text{or} \quad s_j := \sum_{i=1}^{n} \phi_i^2(\mathbf{x}_j),$$

$j = 1, \ldots, q_\kappa$. Then, the quadrature point and weight $(\mathbf{x}_k, w_k)$, for some k, $1 \leq k \leq q_\kappa$, which has the smallest significance factor is removed from the quadrature rule, i.e., $s_k := \min_{j=1}^{q_\kappa} s_j$. The least-squares version of Newton's method is then applied to (6.2) to compute a new quadrature $(\mathbf{x}_j, w_j)_{j=1}^{q_\kappa - 1}$ with $(q_\kappa - 1)$ points and weights. This process is continuously repeated until the Newton algorithm fails to converge; at the end of this process, an *optimized* quadrature rule which can precisely integrate all of the functions present in the space $\mathscr{V}_\kappa$ will be computed. An alternative approach proposed in [140] is to simply fix a set of quadrature points, which may even be randomly located points, and solve (6.2) to determine the corresponding weights.

While this approach is very appealing from a computational point of view, this process must first be applied to all elements κ in the computational mesh $\mathscr{T}_h$, and the resulting quadrature scheme stored elementwise, before assembly of the underlying matrix system can be undertaken. We also stress that while the quadrature constructed using the above algorithm is exact for the set of functions in $\mathscr{V}_\kappa$, their accuracy in terms of integrating general functions is unclear; moreover, for general polytopes, the resulting quadrature weights may be negative, cf. [140].

6.3.3 Integration of Homogeneous Functions

Lasserre's method for integrating homogeneous functions over convex polytopes was first introduced in [134]; this technique was subsequently extended to general non-convex polytopes in the recent article [63]. The essential idea here is to exploit Stokes' theorem, together with Euler's homogeneous function theorem. More precisely, given a polytopic element $\kappa \in \mathscr{T}_h$, and a sufficiently regular function f, defined over κ, we wish to evaluate

$$\int_\kappa f \, \mathrm{d}\mathbf{x}.$$

Assuming that f is a positively homogeneous function of degree q, i.e.,

$$f(\lambda \mathbf{x}) = \lambda^q f(\mathbf{x}),$$

for $\lambda > 0$, then assuming f is continuously differentiable, Euler's homogeneous function theorem states that

$$q f(\mathbf{x}) = \mathbf{x} \cdot \nabla f(\mathbf{x}). \tag{6.3}$$

Moreover, given any vector-valued function $\mathbf{g}$, again assumed to be sufficiently smooth, Stokes' theorem states that

$$\int_\kappa (\nabla \cdot \mathbf{g}) f \, \mathrm{d}\mathbf{x} = \int_{\partial\kappa} (\mathbf{g} \cdot \mathbf{n}_\kappa) f \, \mathrm{d}s - \int_\kappa \mathbf{g} \cdot \nabla f \, \mathrm{d}\mathbf{x}, \tag{6.4}$$

where $\mathbf{n}_\kappa$ denotes the unit outward normal vector to the boundary $\partial\kappa$ of κ. Thereby, selecting $\mathbf{g} = \mathbf{x}$ in (6.4) and employing (6.3), we deduce that

$$\int_\kappa f \, \mathrm{d}\mathbf{x} = \frac{1}{d+q} \int_{\partial\kappa} (\mathbf{x} \cdot \mathbf{n}_\kappa) f \, \mathrm{d}s; \tag{6.5}$$

i.e., the integral over κ is reduced to an integration over the boundary $\partial\kappa$. Writing $\partial\kappa = \bigcup_{i=1}^{n_F} F_i$, where F_i, $i = 1, \ldots, n_F$, denote the planar $(d-1)$-dimensional facets which form the boundary of κ, Eq. (6.5) may be rewritten in the following equivalent form

$$\int_\kappa f \, \mathrm{d}\mathbf{x} = \frac{1}{d+q} \sum_{i=1}^{n_F} \int_{F_i} (\mathbf{x} \cdot \mathbf{n}_{F_i}) f \, \mathrm{d}s, \tag{6.6}$$

where $\mathbf{n}_{F_i}$ denotes the restriction of the unit outward normal vector $\mathbf{n}_\kappa$ to the facet F_i, $i = 1, \ldots, n_F$.

We note that this process can be repeated in order to yield a formula which involves integration on lower dimensional facets. For example, given F_i, for some (fixed) i, $1 \le i \le n_F$, we write

$$\partial F_i = \{F_{ij} = F_i \cap F_j : F_i \cap F_j \neq \emptyset, \ i \neq j\}$$

to denote the set of $(d-2)$-dimensional facets of κ, i.e., F_{ij} is an edge of a polyhedron in $\mathbb{R}^3$ which lies on the boundary of the face F_i. Furthermore, we define $\mathbf{n}_{F_{ij}}$ to be the unit normal vector to F_{ij} which lies in the plane F_i. Given an arbitrary point $\mathbf{x}_i \in F_i$ and a $(d-1)$-dimensional orthonormal basis $\{\mathbf{e}_j^i\}_{j=1}^{d-1}$ on the facet F_i, i.e., any $\mathbf{x} \in F_i$ may be written in the form

$$\mathbf{x} = \mathbf{x}_i + \sum_{k=1}^{d-1} \alpha_k \mathbf{e}_k^i,$$

for some scalars α_k, $k = 1, \ldots, d-1$. Then, upon application of (6.4) to a given facet F_i, $1 \le i \le n_F$, with $\mathbf{g} = \mathbf{x} - \mathbf{x}_i$, we deduce that

$$\int_{F_i} f \, \mathrm{d}s = \frac{1}{d+q-1} \left(\sum_{F_{ij} \subset \partial F_i} \int_{F_{ij}} ((\mathbf{x} - \mathbf{x}_j) \cdot \mathbf{n}_{F_{ij}}) f \, \mathrm{d}s + \int_{F_i} (\mathbf{x}_i \cdot \nabla f) \, \mathrm{d}s \right), \tag{6.7}$$

cf. [63, 134]. In $\mathbb{R}^2$, we note that the first term on the right-hand side of (6.7) simply involves evaluations of the integrand at the points which form the underlying face (edge) F_i, $1 \leq i \leq n_F$. Thereby, for the integration of polynomial functions, repeated application of (6.7) yields an (exact) integration rule which only requires evaluation of f and its partial derivatives at the vertices of κ, $\kappa \in \mathscr{T}_h$. In $\mathbb{R}^3$, proceeding as above, we first rewrite the integral over F_{ij} to be an integral over its $(d-2)$-dimensional facets (points), and an integral involving the derivative of f over F_{ij}; thereby, again for polynomial functions, recursive application of this formula then only requires the evaluation of f and its partial derivatives at the vertices of κ in order to precisely evaluate the integral of f over κ, $\kappa \in \mathscr{T}_h$. For further details and implementation of this approach in the context of DGFEMs, we refer to [14]. To give an example of the potential performance improvement of employing this approach in comparison to the use of quadrature schemes defined on a sub-tessellation of each polytopic element κ in the mesh $\mathscr{T}_h$, in Fig. 6.2 we compare the time taken to assemble the local element stiffness matrix for the Poisson equation in two-dimensions, cf. the DGFEM bilinear form given in Sect. 4.1, cf. also Sect. 2.3. Here, the polygonal meshes are constructed using PolyMesher [165], cf. above. For clarity, in Fig. 6.2a we plot the time taken to assemble the element stiffness matrix via exact integration of homogeneous functions on a series of uniform polygonal meshes for polynomial degrees p between 1 and 6. Figure 6.2b then presents a comparison of these results with the corresponding timings based on employing quadrature on a sub-tessellation. Here, the sub-tessellation is constructed by inserting one internal point within each element κ, $\kappa \in \mathscr{T}_h$, located at the element centroid, and connecting this point to each pair of nodes defining the faces of κ; thereby, the number of elements within the sub-tessellation is equal to the number of faces that each element $\kappa \in \mathscr{T}_h$ possesses.

As a final remark, we note that this approach may also be extended to integrate functions which may be represented as the sum of homogeneous functions; in particular, the integral may be computed without explicit knowledge of the individual terms which form this sum. However, this leads to the introduction of evaluation points within the interior of κ, $\kappa \in \mathscr{T}_h$, and even points which may lie outside κ; in the simplest case, for example, for star-shaped polytopes, this can be viewed as undertaking a subdivision, relative to a point lying in the ball for which κ is star-shaped, cf. [63], for further details.

6.4 Numerical Experiments

In this section we present two computational examples to numerically to highlight the practical performance of the DGFEMs studied in Chap. 5 on general polytopic meshes; see also [54–56] for further numerical experiments.

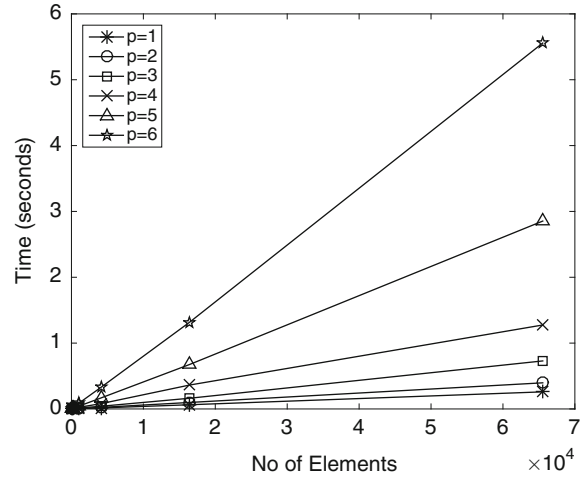

(a)

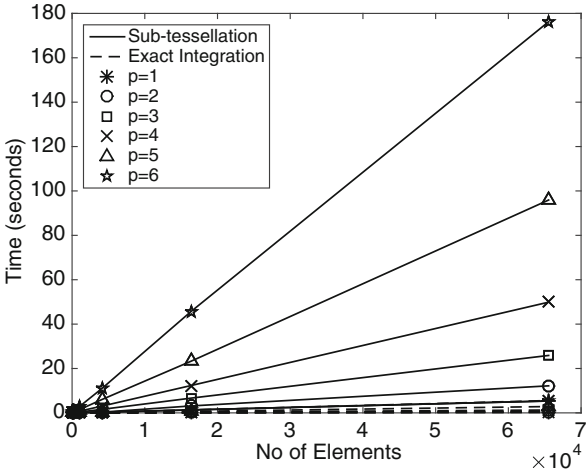

(b)

Fig. 6.2 Time required to assemble the element stiffness matrix for the Poisson equation in two-dimensions: (**a**) Exploiting exact integration of homogeneous functions; (**b**) Comparison between quadrature employed on a sub-tessellation and exact integration

6.4.1 Example 1: Advection-Diffusion-Reaction Problem

We consider the discretization of the advection-diffusion-reaction problem: find u such that

$$-\nabla \cdot (a\nabla u) + \nabla \cdot (\mathbf{b}u) + cu = f \quad \text{in } (0,1)^2, \tag{6.8}$$

where $a = \delta I_2$, $\delta = \epsilon\, \mathrm{e}^{-20r}$, $r^2 = x^2 + y^2$, $\epsilon > 0$, $\mathbf{b} = (2 - y^2, 2 - x)^\top$, and $c = (1+x)(1+y)^2$; f is then selected so that the analytical solution to (6.8), subject to appropriate inhomogeneous boundary conditions, is given by

$$u(x, y) = 1 + \sin(\pi(1 + x)(1 + y)^2/8),$$

cf. [123].

We study the asymptotic behaviour of the DGFEM (5.8) on a sequence of successively finer square and polygonal meshes for different values of the polynomial degree p in both the diffusion-dominated and advection-dominated regimes. In each case we consider two types of polygonal meshes: grids generated using PolyMesher [165], cf. Fig. 6.3a, as well as grids stemming from the agglomeration of a given (fixed) fine mesh $\mathscr{T}_h^{\text{fine}}$. In the latter case, we employ a fine mesh consisting of 262,144 elements; the corresponding coarse agglomerated mesh $\mathscr{T}_h$ is then constructed by exploiting the graph partitioning package METIS [130]. We note that for METIS to partition the fine mesh $\mathscr{T}_h^{\text{fine}}$, the logical structure of $\mathscr{T}_h^{\text{fine}}$ is first stored in the form of a graph, where each node represents an element domain of $\mathscr{T}_h^{\text{fine}}$, and each link between two nodes represents a face shared by the two elements represented by the graph nodes. The resulting partition of $\mathscr{T}_h^{\text{fine}}$ constructed by METIS is produced with the objective of minimizing the number of neighbours among each of the resulting partitions, or more precisely, the resulting polygonal elements. In Fig. 6.3b we show the resulting polygonal mesh generated by METIS with 256 elements.

We first study the diffusion-dominated case; to this end, we set $\epsilon = 1$. In Fig. 6.4 we investigate the convergence of the DGFEM on sequences of finer square and polygonal meshes with polynomial degrees p between 1 and 4. In each case we

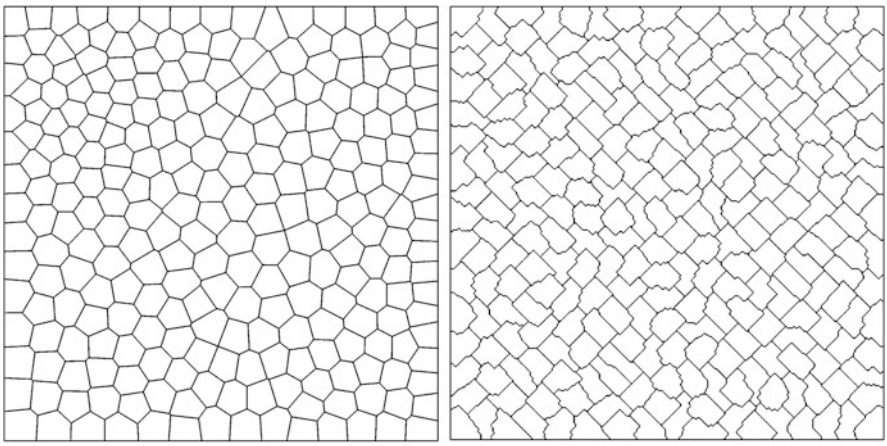

Fig. 6.3 Example 1. Polygonal meshes consisting of 256 elements generated based on employing: (**a**) Voronoi tessellation generated by PolyMesher [165]; (**b**) Agglomeration using METIS [130]

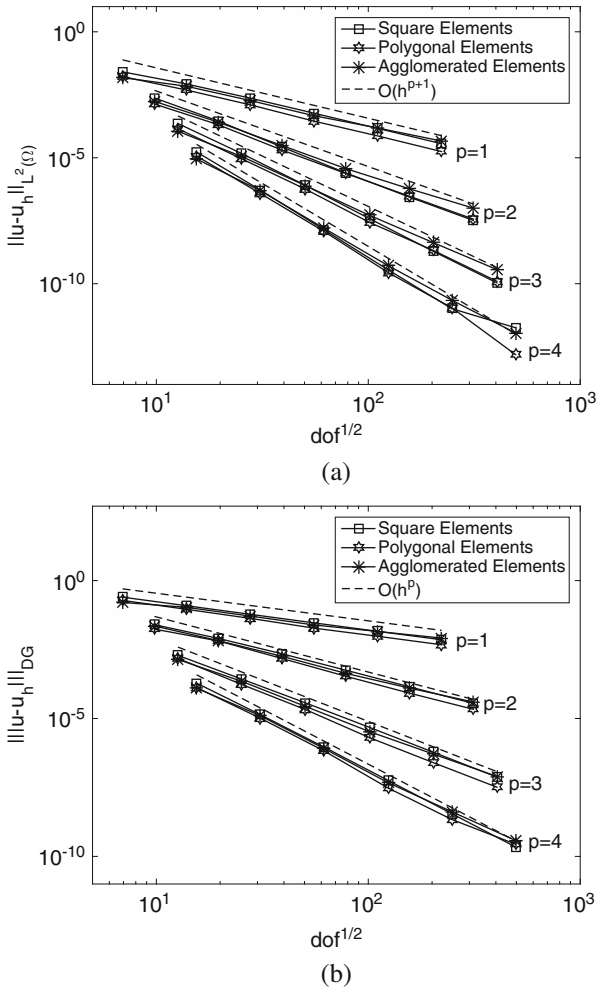

Fig. 6.4 Example 1. Convergence of the DGFEM with h-refinement for $\epsilon = 1$: (**a**) $\|u - u_h\|_{L^2(\Omega)}$; (**b**) $|||u - u_h|||_{\mathrm{DG}}$

plot the error, measured in terms of both the $L^2(\Omega)$ and DGFEM norm, against the square root of the number of degrees of freedom in the underlying finite element space $V^{\mathbf{p}}(\mathscr{T}_h)$. Here, we clearly observe that $\|u-u_h\|_{L^2(\Omega)}$ and $|||u - u_h|||_{\mathrm{DG}}$ converge to zero at the optimal rates $\mathscr{O}(h^{p+1})$ and $\mathscr{O}(h^p)$, respectively, as the mesh size h tends to zero for each fixed p. The latter set of numerical results confirm the optimality of Theorem 46 in the diffusion-dominated setting, cf. Remark 47. Moreover, from Fig. 6.4 we observe that the accuracy of the DGFEM is very similar on all three sets of meshes employed here, given the same number of degrees of freedom, though in general we observe a slight improvement in $|||u - u_h|||_{\mathrm{DG}}$ when the polygonal elements generated by Polymesher are employed, in comparison to the

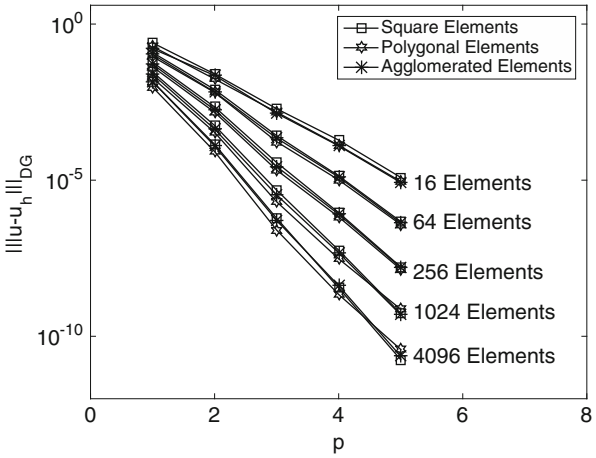

Fig. 6.5 Example 1. Convergence of the DGFEM with p-refinement for $\epsilon = 1$

corresponding quantity computed based on exploiting either square or agglomerated meshes. In Fig. 6.5 we investigate the convergence behaviour of the DGFEM under p-refinement, for a given fixed mesh. For each mesh, we plot $|||u - u_h|||_{\mathrm{DG}}$ against the polynomial degree p on a linear-log scale; in each case we clearly observe exponential convergence of the DGFEM.

Secondly, we consider the convergence of the DGFEM in the advection-dominated regime, whereby, we now set $\epsilon = 10^{-6}$. In Fig. 6.6 we plot $\|u - u_h\|_{L^2(\Omega)}$ and $|||u - u_h|||_{\mathrm{DG}}$ against the square root of the number of degrees of freedom in the underlying finite element space $V^{\mathbf{p}}(\mathscr{T}_h)$ on a sequence of uniform square and polygonal meshes for fixed p. In this case, we observe that while the $L^2(\Omega)$ norm of the error converges to zero at the optimal rate $\mathscr{O}(h^{p+1})$, the DGFEM norm behaves like $\mathscr{O}(h^{p+1/2})$, as h tends to zero, for each fixed p; in the latter case, this is indeed the optimal rate predicted by Theorem 46, cf. Remark 48. As above, we again observe a slight improvement in the computed error when the Voronoi meshes generated by PolyMesher are employed, as opposed to square or agglomerated meshes. Figure 6.7 plots $|||u - u_h|||_{\mathrm{DG}}$ against the polynomial degree p for a given set of fixed uniform meshes; as above, we observe exponential convergence of the DGFEM under p-refinement.

For further numerical experiments, and in particular, for comparisons between both standard (conforming) Galerkin FEMs and DGFEMs employing local tensor-product polynomial bases ($\mathscr{Q}_p$-basis), we refer to the articles [54, 55].

6.4.2 *Example 2: Degenerate Evolution Equation*

Computational experiments for the space-time DGFEM (5.54), cf., also, (5.56), have been presented in the recent article [56] for the case when $\mathbf{a}$ is positive definite,

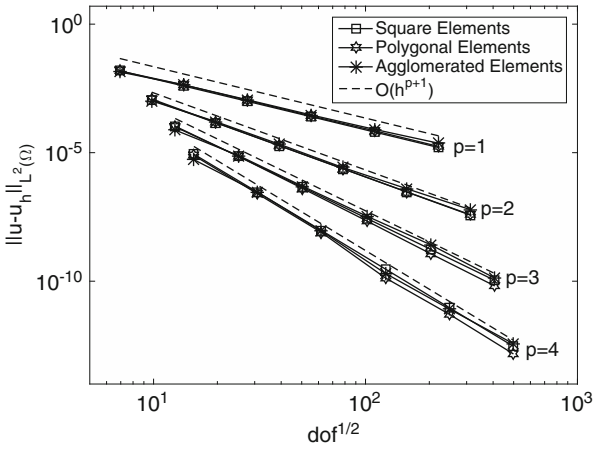

(a)

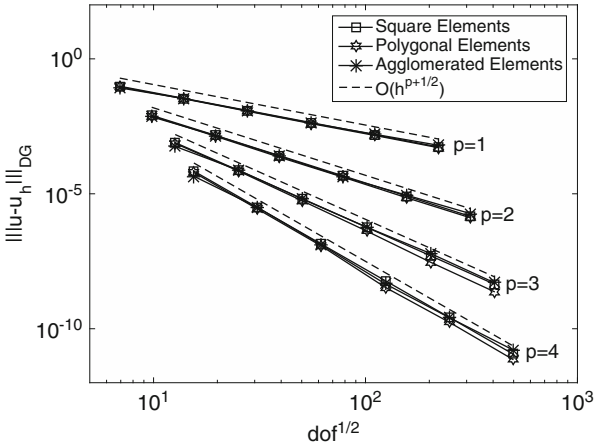

(b)

Fig. 6.6 Example 1. Convergence of the DGFEM with h-refinement for $\epsilon = 10^{-6}$: (**a**) $\|u - u_h\|_{L^2(\Omega)}$; (**b**) $|||u - u_h|||_{\mathrm{DG}}$

i.e., when (5.52) holds. Thereby, to test the necessity of this hypothesis in terms of generalizing the a priori error bounds derived in Sect. 5.3 to degenerate parabolic PDEs, we consider the following example: find $u = u(t, x, y)$ such that

$$\partial_t u - x^2 \partial^2_{xx} u - x \partial_y u = f \quad \text{in } \Omega := J \times D, \tag{6.9}$$

where $J = (0, 1)$ and $D = (0, 1)^2$. We note that (6.9) can be written in the general form (2.1), cf., also, (5.1); indeed, setting $\mathbf{x} := (t, x, y)^\top$ and $\nabla := (\partial_t, \partial_x, \partial_y)^\top$, we select $a_{22} = x^2$, $a_{ij} = 0$ for $i, j = 1, 2, 3$, $i, j \neq 2$, $\mathbf{b} = (1, 2x, -x)^\top$, and $c = -2$. Furthermore, we stress that the PDE (6.9) is not hypoelliptic on the plane $\{x = 0\}$

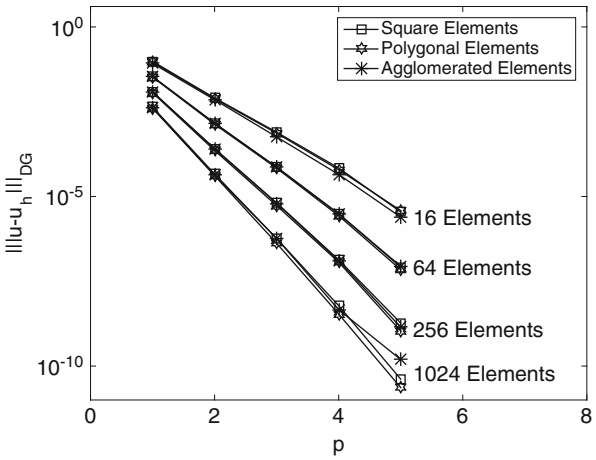

Fig. 6.7 Example 1. Convergence of the DGFEM with p-refinement for $\epsilon = 10^{-6}$

which is contained in $J \times \partial D$ and may, therefore, lead to singularities in the analytical solution u in the vicinity of the boundary, depending on the choice of the boundary conditions imposed and/or the selection of f.

In this section, the forcing function f is selected so that, upon supplementing (6.9) with appropriate inhomogeneous Dirichlet boundary conditions and initial condition, the analytical solution is given by

$$u(t,x,y) = \mathrm{e}^{-5((x-1/2)^2+(y-1/2)^2)}\ \sin(x-t+2y).$$

In Fig. 6.8 we investigate the convergence of the space-time DGFEM on sequences of finer (space-time) hexahedral (rectangular in space) and prismatic (polygonal prism base in space) meshes, for polynomial degrees p between 1 and 4. In each case we plot the error measured in terms of both the $L^2((0,1);L^2(D))$ and $L^2((0,1);H^1(D,\mathscr{T}_h))$ norms with respect to the third root of the number of degrees of freedom in the underlying space-time finite element space $V^{\mathbf{p}}(\mathscr{U};\mathscr{T}_h)$. Here, we employ spatial meshes consisting of 16, 64, 256, 1024, and 4096 elements, with 8, 16, 32, 64, and 128 time-steps, respectively. Firstly, from Fig. 6.8b we observe that $\|u-u_h\|_{L^2((0,1);H^1(D,\mathscr{T}_h))}$ converges to zero at the optimal rate $\mathscr{O}(h^p)$ as the space-time mesh size h tends to zero for each fixed p; this is in accordance with the rate predicted by Corollary 56, though we stress that in this generalized setting, the conditions of Theorem 55 (and, therefore, of Corollary 56) are not fulfilled. Secondly, from Fig. 6.8a we observe some deterioration in the rate of convergence of the space-time DGFEM with respect to the $L^2((0,1);L^2(D))$ norm, cf. the discussion at the end of Sect. 5.3; indeed these numerics seem to indicate a loss of (roughly) between half and one order in h, as the mesh is refined for each fixed p.

Finally, we investigate the computational efficiency of employing the space-time DGFEM (5.54) with different space-time elemental polynomial bases on

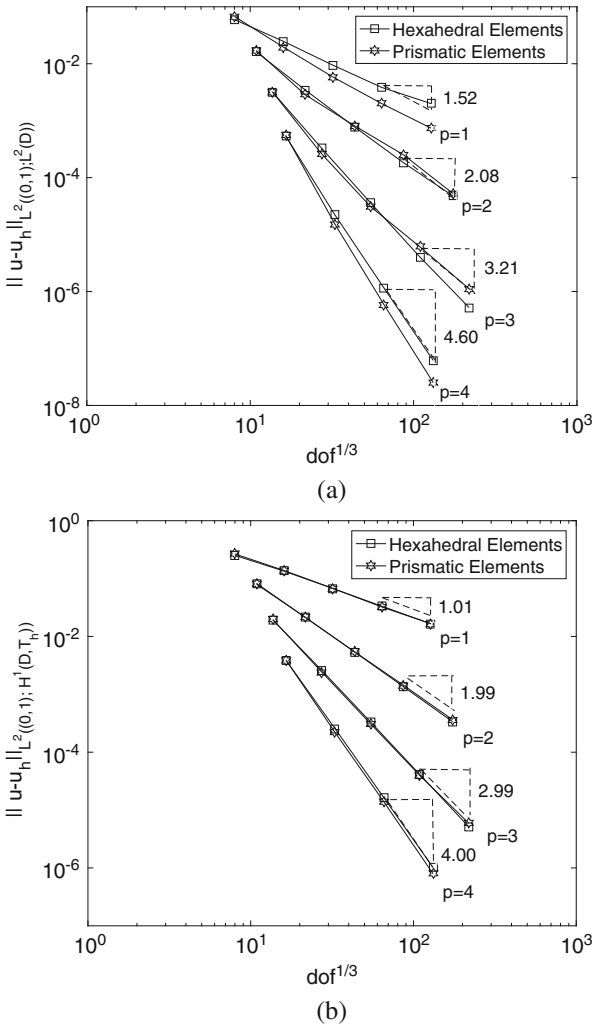

Fig. 6.8 Example 2. Convergence of the space-time DGFEM with h-refinement on cubic (square elements in space) and prismatic (polygonal elements in space) meshes: (**a**) $\|u - u_h\|_{L^2((0,1);L^2(D))}$; (**b**) $\|u - u_h\|_{L^2((0,1);H^1(D,\mathscr{T}_h))}$

both hexahedral and prismatic meshes. In particular, writing $\kappa_n := I_n \times \kappa$ to denote a given space-time element, where $\kappa \in \mathscr{T}_h$ is a spatial element and I_n, $n = 1, \ldots, N_t$, is a given time interval, we consider the following three choices for the (elementwise) polynomial space, denoted by $\mathscr{R}_p(\kappa_n)$: (1) $\mathscr{R}_p(\kappa_n) := \mathscr{P}_p(\kappa_n)$, i.e., polynomials of total degree p are employed on each element, cf. Sect. 5.3; (2) $\mathscr{R}_p(\kappa_n) := \mathscr{P}_p(I_n) \times \mathscr{P}_p(\kappa)$, i.e., polynomials of total degree p are employed in time and space, and these are tensorized to form a space-time basis defined on κ_n; (3) $\mathscr{R}_p(\kappa_n) := \mathscr{P}_p(I_n) \times \mathscr{Q}_p(\kappa)$, i.e., polynomials of total degree p are employed

in time, while tensor-product polynomials of degree p in each coordinate direction are exploited in space; these spaces are then tensorized to form a space-time basis defined on κ_n. These schemes will be denoted, respectively, by DG(P), DG(QP), and DG(Q).

In Fig. 6.9 we investigate the convergence behaviour of these three schemes under p-refinement for fixed h; for brevity, we only consider space-time prismatic meshes for the first scheme, i.e., for DG(P). Here, we have employed 64 spatial

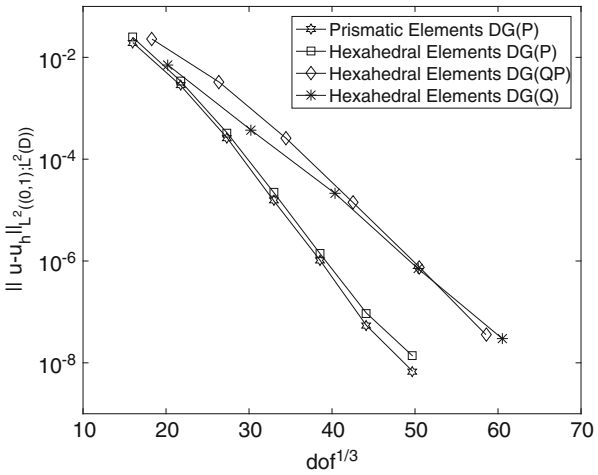

(a)

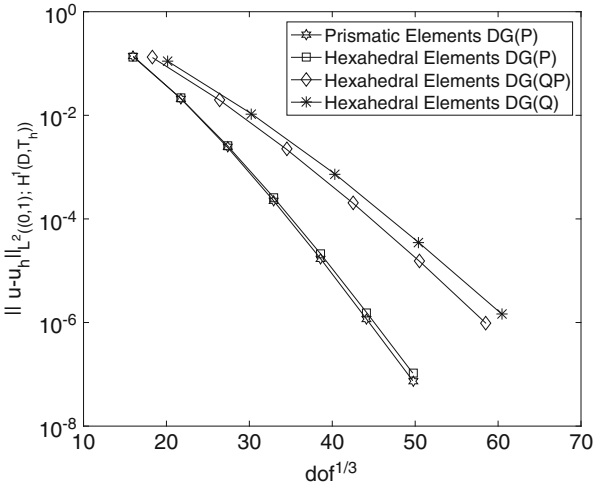

(b)

Fig. 6.9 Example 2. Comparison of the space-time DGFEMs: DG(P), DG(QP), and DG(Q) under p-refinement with 64 spatial elements and 16 time-steps: (**a**) $\|u - u_h\|_{L^2((0,1);L^2(D))}$; (**b**) $\|u - u_h\|_{L^2((0,1);H^1(D,\mathscr{T}_h))}$

elements and 16 time-steps. Firstly, we observe exponential convergence for all three choices of the elemental polynomial bases, in the sense that, on the linear-log scale, the convergence plots become straight lines as p is increased. Moreover, we observe that, under p-refinement, DG(P) is more efficient than both DG(QP) and DG(Q), in the sense that the error, computed in terms of both the $L^2((0,1);L^2(D))$ and $L^2((0,1);H^1(D,\mathscr{T}_h))$ norms is smaller, for a given number of degrees of freedom, when the former scheme is employed.

Chapter 7
Adaptive Mesh Refinement

We now turn our attention to the automatic adaptive mesh refinement of polytopic meshes generated on the basis of agglomeration of a given background geometry-conforming fine mesh $\mathcal{T}_h^{\text{fine}}$; see, for example, [103, 104] where overlapping agglomerated meshes have been employed, and [76] where mesh partitioning techniques are exploited. For the purposes of this chapter, we adopt the latter strategy, whereby METIS, cf. [130], is employed for both the generation of the coarse geometry-conforming mesh $\mathcal{T}_h$, as well as the subsequent subdivision of agglomerated elements marked for refinement, cf. below. The underlying adaptive refinement algorithm is constructed by exploiting, so-called, goal-oriented dual-weighted-residual (DWR) a posteriori error estimation techniques. Here, the aim of the computation is to accurately approximate the value of a given target or output functional of the solution. Relevant examples include point values, local averages, and flux integrals of the solution, force coefficients of a body immersed in a fluid, and so on. The general DWR approach is based on a duality argument analogous to that employed for the derivation of a priori error bounds for FEMs. This idea was originally pioneered by Johnson and his collaborators, cf. [89] and the references cited therein; subsequent work, based on introducing an alternative minimalistic approach, was developed by Rannacher and his collaborators, cf. [29, 36] and the references cited therein. For a recent review of the application of DWR error estimation to nonlinear hyperbolic conservation laws, we refer to [119].

The outline of this chapter is as follows. In Sect. 7.1 we briefly review the DWR error estimation approach for the FEM approximation of general linear PDEs; for further details, and in particular the application of these ideas to DGFEMs applied to both linear and nonlinear PDE problems, we refer to [112, 115, 116, 119] and the references cited therein. Section 7.2 discusses the implementation of the DWR error estimator, together with the design of the underlying adaptive mesh refinement algorithm, by employing general agglomerated polytopic meshes. Finally, in Sect. 7.3 we present a series of numerical experiments to highlight the practical performance of the proposed refinement strategy for PDE problems posed

A. Cangiani et al., *hp-Version Discontinuous Galerkin Methods on Polygonal and Polyhedral Meshes*, SpringerBriefs in Mathematics,
DOI 10.1007/978-3-319-67673-9_7

on complicated geometries; here, we will consider a wider range of application areas than those that have been studied in this volume, including incompressible fluid flow and linear elasticity.

7.1 DWR A Posteriori Error Estimation

We present a brief overview of the DWR error estimation technique within an abstract setting. To this end, given that $\mathscr{X}$ and $\mathscr{Y}$ are two Hilbert spaces, $\mathscr{B}(\cdot,\cdot)$ is a bounded bilinear functional defined on $\mathscr{X} \times \mathscr{Y}$, and $\ell(\cdot)$ is a bounded linear functional defined on $\mathscr{Y}$, we suppose that u is the unique solution to the variational problem: find $u \in \mathscr{X}$ such that

$$\mathscr{B}(u, v) = \ell(v) \quad \forall v \in \mathscr{Y}. \tag{7.1}$$

Here, (7.1) can be thought of as the weak formulation of a linear PDE on $\mathscr{X}$. In order to construct the Galerkin (and, indeed, the DGFEM) discretization of (7.1) we write $\{\mathscr{X}_{h,p}\}$ and $\{\mathscr{Y}_{h,p}\}$, to denote a sequence of finite-dimensional linear subspaces of $\mathscr{X}$ and $\mathscr{Y}$, respectively, parameterized by h and p. In the FEM setting, $\mathscr{X}_{h,p}$ and $\mathscr{Y}_{h,p}$ consist of piecewise polynomial functions of degree p defined over a computational mesh $\mathscr{T}_h$, of granularity h. Hence, the Galerkin approximation u_h of u then satisfies: find $u_h \in \mathscr{X}_{h,p}$ such that

$$\mathscr{B}_h(u_h, v_h) = \ell_h(v_h) \quad \forall v_h \in \mathscr{Y}_{h,p}, \tag{7.2}$$

where $\mathscr{B}_h(\cdot,\cdot) : \mathscr{X} \times \mathscr{Y} \to \mathbb{R}$ and $\ell_h(\cdot) : \mathscr{Y} \to \mathbb{R}$ are a suitably chosen bilinear form and linear functional, respectively, which define an appropriate discretization scheme.

Throughout this section we assume that the discretization (7.2) is consistent in the sense that the analytical solution $u \in \mathscr{X}$ to (7.1) satisfies the following identity:

$$\mathscr{B}_h(u, v) = \ell_h(v) \qquad \forall v \in \mathscr{Y}. \tag{7.3}$$

In our context of DGFEMs, given sufficient regularity of the analytical solution, we can make use of consistent versions of DGFEM bilinear forms to satisfy this assumption.

On the basis of (7.3), we note that the following Galerkin orthogonality property holds:

$$\mathscr{B}_h(u, v_h) - \mathscr{B}_h(u_h, v_h) = \mathscr{B}_h(u - u_h, v_h) = 0 \qquad \forall v_h \in \mathscr{Y}_{h,p}. \tag{7.4}$$

Throughout this chapter we assume that the key quantity of practical interest is the numerical approximation of a given linear target functional, denoted by $J(\cdot)$, of the analytical solution. To derive an error representation formula for $J(\cdot)$, we first introduce $J_h(\cdot)$ to denote a discrete consistent reformulation of $J(\cdot)$ in the sense that, given the analytical solution $u \in \mathscr{X}$ to (7.1), we have that

$$J_h(u) \equiv J(u), \tag{7.5}$$

cf. [119]. The introduction of $J_h(\cdot)$ is often critical to ensure that optimal rates of convergence for the numerical approximation $J_h(u_h)$ to $J(u)$ are computed in practice; this is closely related to the adjoint consistency of the resulting adjoint/dual problem, cf. below. For a detailed discussion of this topic, we refer to [18, 112, 113, 116, 136, 145], for example.

The starting point for the DWR a posteriori error analysis is to introduce the following adjoint/dual problem: find $z \in \mathscr{Y}$, such that

$$\mathscr{B}_h(w, z) = J_h(w) \quad \forall w \in \mathscr{X}; \tag{7.6}$$

henceforth, we simply use the terminology dual problem rather than adjoint/dual problem. Employing (7.5) and the linearity of $J_h(\cdot)$, together with (7.6), (7.4), and (7.1), we deduce that

$$\begin{aligned} J(u) - J_h(u_h) &= J_h(u) - J_h(u_h) = J_h(u - u_h) \\ &= \mathscr{B}_h(u - u_h, z) = \mathscr{B}_h(u - u_h, z - z_h) \\ &= \ell_h(z - z_h) - \mathscr{B}_h(u_h, z - z_h) \quad \forall z_h \in \mathscr{Y}_{h,p}\,. \end{aligned} \tag{7.7}$$

On the basis of the general error representation formula (7.7), a posteriori bounds on the true error in the computed target functional $J(\cdot)$ may be derived. To this end, we first decompose the right-hand side of (7.7) as a summation of local error indicators η_κ over the elements κ in the computational mesh $\mathscr{T}_h$; more precisely, we write (7.7) in the form

$$J(u) - J_h(u_h) = \ell_h(z - z_h) - \mathscr{B}_h(u_h, z - z_h) \equiv \sum_{\kappa \in \mathscr{T}_h} \eta_\kappa. \tag{7.8}$$

The simplest, and most practical approach, in terms of ensuring the construction of optimal computational meshes which are specifically designed for the efficient control of the error in the computed target functional $J(\cdot)$, is to simply apply the triangle inequality; thereby, we deduce the following so-called weighted a posteriori error bound.

Lemma 60 *Let u and u_h denote the solutions of (7.1) and (7.2), respectively, and suppose that the dual problem (7.6) is well-posed. Then, the following a posteriori error bound holds:*

$$|J(u) - J_h(u_h)| \leq \sum_{\kappa \in \mathscr{T}_h} |\eta_\kappa|$$

for all $z_h \in \mathscr{Y}_{h,p}$.

Strictly speaking, the estimate presented in Lemma 60 is only an a posteriori bound upon complete knowledge of the analytical dual solution $z \in \mathscr{Y}$, which is, of course, not available in practice. Nevertheless, we shall use this customary abuse of terminology for the rest of this chapter. We stress that the weighting terms, involving the difference between the dual solution z and its projection/interpolant z_h onto the finite element space $\mathscr{Y}_{h,p}$, present within the error representation formula (7.8), and the resulting a posteriori bound stated in Lemma 60, provide invaluable information concerning the global transport of the error. Thereby, we refrain from eliminating z in the definition of η_κ, $\kappa \in \mathscr{T}_h$; indeed, z will be numerically approximated as part of the proposed adaptive mesh refinement algorithm in the next section.

7.2 Implementation Aspects and Adaptive Mesh Refinement

We now discuss the implementation of the DWR a posteriori error bound derived in Lemma 60 within an automatic adaptive refinement algorithm based on employing DGFEMs on polytopic meshes.

7.2.1 Numerical Approximation of the Dual Problem

We stress that the error representation formula derived in (7.8), depends on the dual solution z defined by (7.6) and, hence, must be numerically approximated as part of the error estimation process. Writing $z_{\hat{h},\hat{p}}$ to denote a numerical approximation to z, we first note that $z_{\hat{h},\hat{p}}$ cannot be computed using the same finite element (test) space employed for the primal problem, otherwise the resulting error representation formula will be identically zero. Following [119], there are essentially three approaches that may be employed for computing the numerical approximation $z_{\hat{h},\hat{p}}$ of z: firstly, we may keep the degree p of the approximating polynomial used to compute u_h fixed, and evaluate $z_{\hat{h},\hat{p}}$ on a sequence of alternative (dual) finite element meshes which, in general, differ from the primal meshes. Secondly, we may keep the underlying mesh $\mathscr{T}_h$ fixed and evaluate $z_{\hat{h},\hat{p}}$ using higher-order piecewise polynomials than those employed for the numerical approximation of the primal problem. Thirdly, we may compute the approximate dual problem using the same finite element space employed for the numerical approximation of the primal problem, and subsequently exploit patchwise recovery/reconstruction techniques to improve the accuracy of $z_{\hat{h},\hat{p}}$, cf. [29, 36].

In our own work, we tend to favour the second approach since it generally leads to highly efficient error estimation, without excessive computational overhead. For example, for nonlinear PDE problems, we note that if the mesh refinement parameters are chosen so that the number of degrees of freedom employed in the dual finite element space is roughly the same as the number of degrees of freedom in the new primal finite element space after an adaptive refinement has been undertaken, then the cost of computing the dual solution will be roughly equivalent to the cost of a single Newton step in the computation of u_h on the newly designed adaptive mesh.

7.2.2 *Adaptive Algorithm*

For the purposes of this chapter we assume that the computational mesh $\mathscr{T}_h$, consisting of general polytopic elements, is constructed by agglomerating an underlying fine mesh $\mathscr{T}_h^{\text{fine}}$ using graph partitioning techniques; to this end, we exploit the METIS package, cf. [130]. On the basis of this coarse mesh $\mathscr{T}_h$, together with the DWR a posteriori error analysis presented in the previous section, here we consider the design of a mesh adaptation algorithm which automatically refines the agglomerates which form $\mathscr{T}_h$ based on repartitioning elements which possess a large error contribution. To this end, recalling the local error indicators $\eta_\kappa \equiv \eta_\kappa(u_h, z-z_h)$, $\kappa \in \mathscr{T}_h$, cf. (7.8), we introduce the (computable) approximate error representation formula:

$$J(u) - J_h(u_h) \approx \sum_{\kappa \in \mathscr{T}_h} \hat{\eta}_\kappa,$$

where $\hat{\eta}_\kappa := \eta_\kappa(u_h, z_{\hat{h},\hat{p}} - z_h)$, $\kappa \in \mathscr{T}_h$, with $z_{\hat{h},\hat{p}}$ denoting the numerical approximation of the dual problem (7.6).

On the basis of the size of the modulus of the (approximate) local error indicators $|\hat{\eta}_\kappa|$, $\kappa \in \mathscr{T}_h$, the elements in the mesh $\mathscr{T}_h$ may be flagged for refinement. Typical element marking strategies include equidistribution, fixed fraction, Dörfler marking, optimized mesh criterion, and so on, cf. [122], for example. Once an element $\kappa \in \mathscr{T}_h$ has been marked for refinement, then assuming that κ is formed from the union of a set of elements belonging to $\mathscr{T}_h^{\text{fine}} \equiv \mathscr{T}_h^{\text{fine},(l)}$, $l = 0$, i.e., $\kappa = \cup_{\kappa' \in \mathscr{S}_\kappa^{(l)}} \kappa'$, where $\mathscr{S}_\kappa^{(l)} \subset \mathscr{T}_h$ denotes the set of fine elements which form κ, then METIS may be applied to the corresponding graph representation of $\mathscr{S}_\kappa^{(l)}$ to yield a local partition of κ consisting of ι_κ agglomerated elements; given the number of elements generated using isotropic refinement of standard shaped elements, we select $\iota_\kappa = 2^d$. However, when the local granularity of the polytopic mesh $\mathscr{T}_h$ is comparable to that of the fine mesh $\mathscr{T}_h^{\text{fine}}$, then adaptive refinement of $\mathscr{T}_h^{\text{fine}}$ must first be undertaken. More precisely, when $\iota_\kappa > \text{card}(\mathscr{S}_\kappa^{(l)})$ for any element $\kappa \in \mathscr{T}_h$ which has been marked for refinement, then the elements $\kappa' \in \mathscr{S}_\kappa^{(l)}$, $\kappa \in \mathscr{T}_h$, are first

refined using standard adaptive isotropic mesh refinement to yield a new fine mesh $\mathscr{T}_h^{\text{fine},(l+1)}$. Once $\mathscr{T}_h^{\text{fine},(l+1)}$ has been constructed, then new local partitions $\mathscr{S}_\kappa^{(l+1)}$ of each element $\kappa \in \mathscr{T}_h$ may be computed and, for those marked for refinement, subsequently subdivided using graph partitioning techniques. The iteration counter l is then updated, and the above procedure repeated, until sufficient accuracy in the computed target functional of interest has been attained. As noted in [76], in the case when $\mathscr{T}_h^{\text{fine}}$ is sufficiently fine, in the sense that it does not require adaptive mesh refinement to be undertaken, then refinement of $\mathscr{T}_h$ can be carried out in a straightforward manner by only exploiting graph partitioning algorithms, without the need to implement complicated tree data structures, which are typically employed within refinement procedures for standard element types.

7.3 Numerical Experiments

In this section, we present a series of computational examples to illustrate the practical performance of the adaptive mesh refinement algorithm outlined in the previous section. Throughout this section, the elements are marked for refinement using the fixed fraction strategy with refinement parameter `REF`.

7.3.1 Example 1: Interstitial Flow Modelling

We begin by considering an example related to interstitial drug transport to cancer cells; see, for example, [149]. To this end, we consider the two-dimensional advection–diffusion problem: find u such that

$$-\nabla\cdot(a\nabla u)+\nabla\cdot(\mathbf{b}u)=0 \quad \text{in } \Omega, \tag{7.9}$$

where the computational domain Ω consists of the rectangular box $(0,2)\times(0,1)$ which has had a series of uniformly spaced circular holes of radius $1/10$ removed, cf. Fig. 7.1; the circular holes represent tumour cells. Here, $a=\epsilon(x,y)I_2$, where

$$\epsilon=\frac{\delta}{2}(1-\tanh((r-1/4)(r+1/4)/\gamma)),$$

I_2 is the identity matrix, $r^2=(x-1)^2+(y-1/2)^2$ and $\delta\geq 0$ and $\gamma>0$ are constants, cf. [112]; as in [112], we set $\delta=10^{-2}$ and $\gamma=5\times 10^{-2}$. We point out that for $\delta>0$ and $0<\gamma\ll 1$, the diffusion parameter ϵ is approximately equal to δ in the circular region given by $r<1/4$, where the underlying PDE is uniformly elliptic. For $r>1/4$, ϵ rapidly decays to zero within a layer of width $\mathscr{O}(\delta)$. Indeed, for $r>0.336$ we have $\epsilon<10^{-15}$; thereby, from the computational point of view ϵ is zero to within rounding error. Hence, in this region the PDE essentially undergoes a change of type becoming, in effect, hyperbolic.

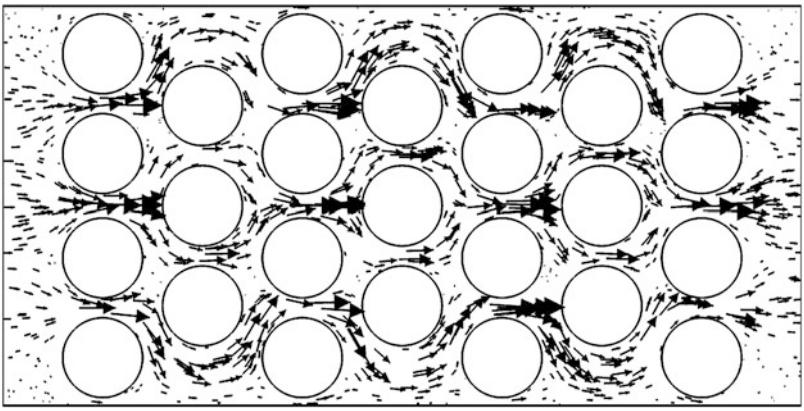

Fig. 7.1 Example 1. Computational geometry Ω and flow field $\mathbf{b}$

The flow field $\mathbf{b}$ is computed by numerically approximating the incompressible Navier–Stokes equations on a fine background mesh $\mathscr{T}_h^{\text{fine}}$ consisting of 188,850 triangular elements, using the standard (conforming) Galerkin FEM with piecewise quadratic polynomials for the discretization of the velocity and piecewise linear polynomials for the pressure. Here, a Poiseuille flow profile (of height $1/4$) is specified on the inlet boundary located at $x = 0$, a homogeneous Neumann condition is imposed on the outlet boundary at $x = 2$, and solid wall boundary conditions are defined on the remaining boundaries, i.e., on the top and bottom boundaries, given by $y = 1$ and $y = 0$, respectively, as well as on the boundary of the circular holes. The computed velocity field with corresponding Reynolds number equal to 10 is depicted in Fig. 7.1. Finally, we supplement (7.9) with the Dirichlet boundary condition $u = \mathrm{e}^{-30(y-1/2)^2}$ along $x = 0$, together with compatible Dirichlet boundary conditions along $y = 0$ and $y = 1$; homogeneous Dirichlet boundary conditions are imposed on the boundary of the circular holes, while a homogeneous Neumann condition is imposed along $x = 2$.

For the purposes of this example, we select the functional of interest to be the value of the solution u evaluated at the point $(1.75, 0.25)$, i.e.,

$$J(u) = u(1.75, 0.25);$$

on the basis of a fine mesh calculation we compute the approximate value of the functional $J(u) \approx 0.07477539204$. The underlying fine mesh $\mathscr{T}_h^{\text{fine}}$ is chosen to be the same mesh upon which the velocity field $\mathbf{b}$ has been computed; this is then agglomerated using METIS to generate a coarse polygonal mesh $\mathscr{T}_h$ comprising of only 128 elements, cf. Fig. 7.2. In Fig. 7.3a we show the convergence history of the proposed agglomeration-based adaptive refinement strategy using a polynomial order of degree $p = 1$, with $\texttt{REF} = 25\%$. Additionally, in Fig. 7.3b we plot the effectivity index $\theta = \sum_{\kappa \in \mathscr{T}_h} \hat{\eta}_\kappa / (J(u) - J(u_h))$. As noted in [104], here we observe that, even on very coarse finite element meshes, the quality of the

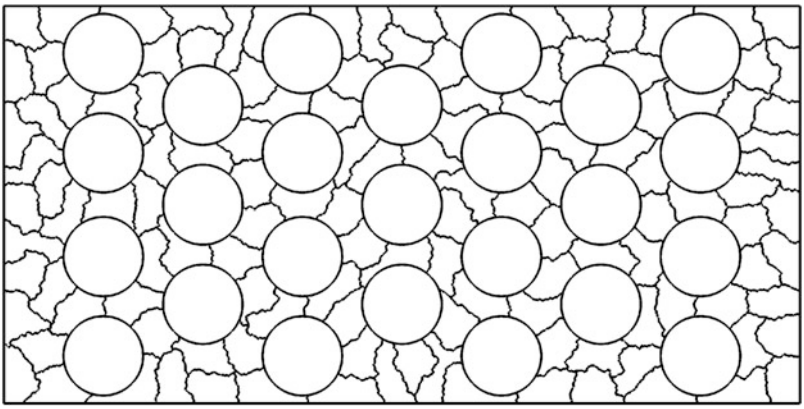

Fig. 7.2 Example 1. Initial agglomerated mesh consisting of 128 elements

computed error representation formula is relatively good, in the sense that the effectivity indices are not too far away from unity. In particular, accuracy which is sufficient for practical/engineering calculations can be attained with a relatively small number of degrees of freedom. Finally, in Fig. 7.4 we show the agglomerated polytopic meshes generated after 2, 4, and 6 adaptive refinements. The design of the underlying meshes is closely related to the structure of the dual solution; indeed, from Fig. 7.5, we observe that in the region of the domain where the underlying PDE is essentially hyperbolic, the dual solution consists of a single 'spike' solution originating from the point of interest which is transported upstream along the single characteristic passing through the point of interest $(1.75, 0.25)$. In the vicinity of the circular region where the PDE essentially undergoes a change of type from hyperbolic to elliptic, the spike in the dual solution is diffused. Thereby, the domain of dependence of the point of interest consists of the single characteristic passing through $(1.75, 0.25)$, the circular region where the underlying PDE is essentially of elliptic type, together with the part of the computational domain enclosed by the intersection of the inflow boundary along $x = 0$ and the two extreme characteristics emanating from the circular elliptic region, cf. [112]. Indeed, given this information, we see that the computational mesh is refined within these regions of the domain, with more refinement being undertaken to resolve the spike present in the dual solution. However, away from this domain of dependence, we observe that the computational mesh is kept extremely coarse, and indeed by employing such general polytopic elements, additional refinement of the mesh to resolve the boundary of the circular holes is not required.

7.3.2 Example 2: Incompressible Fluid Flow

We now consider the flow of an incompressible fluid, governed by Stokes equations, through a region in $\Omega \subset \mathbb{R}^3$ which contains a number of spherical holes. To this

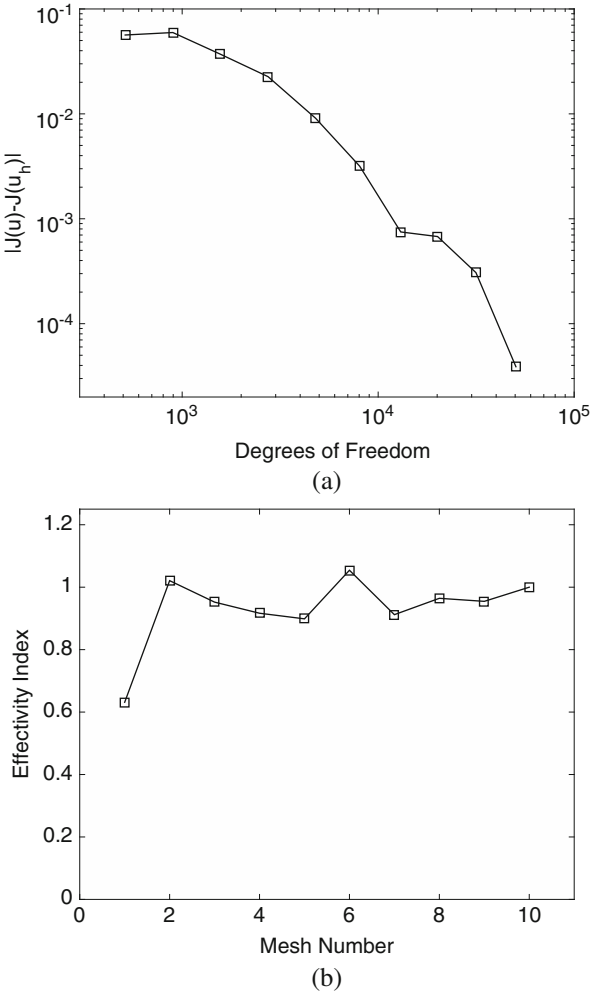

Fig. 7.3 Example 1. Convergence of the adaptive mesh refinement algorithm: (**a**) absolute error in the functional of interest; (**b**) effectivity index of the DWR error estimator

end, we approximate the velocity $\mathbf{u}$ and pressure p which satisfy

$$-\Delta\mathbf{u} + \nabla p = \mathbf{0}, \quad \text{in } \Omega, \tag{7.10}$$

$$\nabla \cdot \mathbf{u} = 0, \quad \text{in } \Omega. \tag{7.11}$$

The computational domain Ω is shown in Fig. 7.6; here, the geometry is given in terms of a series of voxels, cf. [12], and is enclosed within the cube $\Omega_{\text{cube}} := (0, 0.1875)^3$. We decompose the boundary $\partial\Omega$ into the two disjoint subsets $\partial\Omega_{\text{D}}$ and $\partial\Omega_{\text{N}}$ whose union is $\partial\Omega$, i.e., $\partial\Omega = \partial\Omega_{\text{D}} \cup \partial\Omega_{\text{N}}$. Moreover, we define $\partial\Omega_{\text{N}}$ to consist of the two sides of Ω_{cube} given by $x = 0$ and $x = 0.1875$, which form part

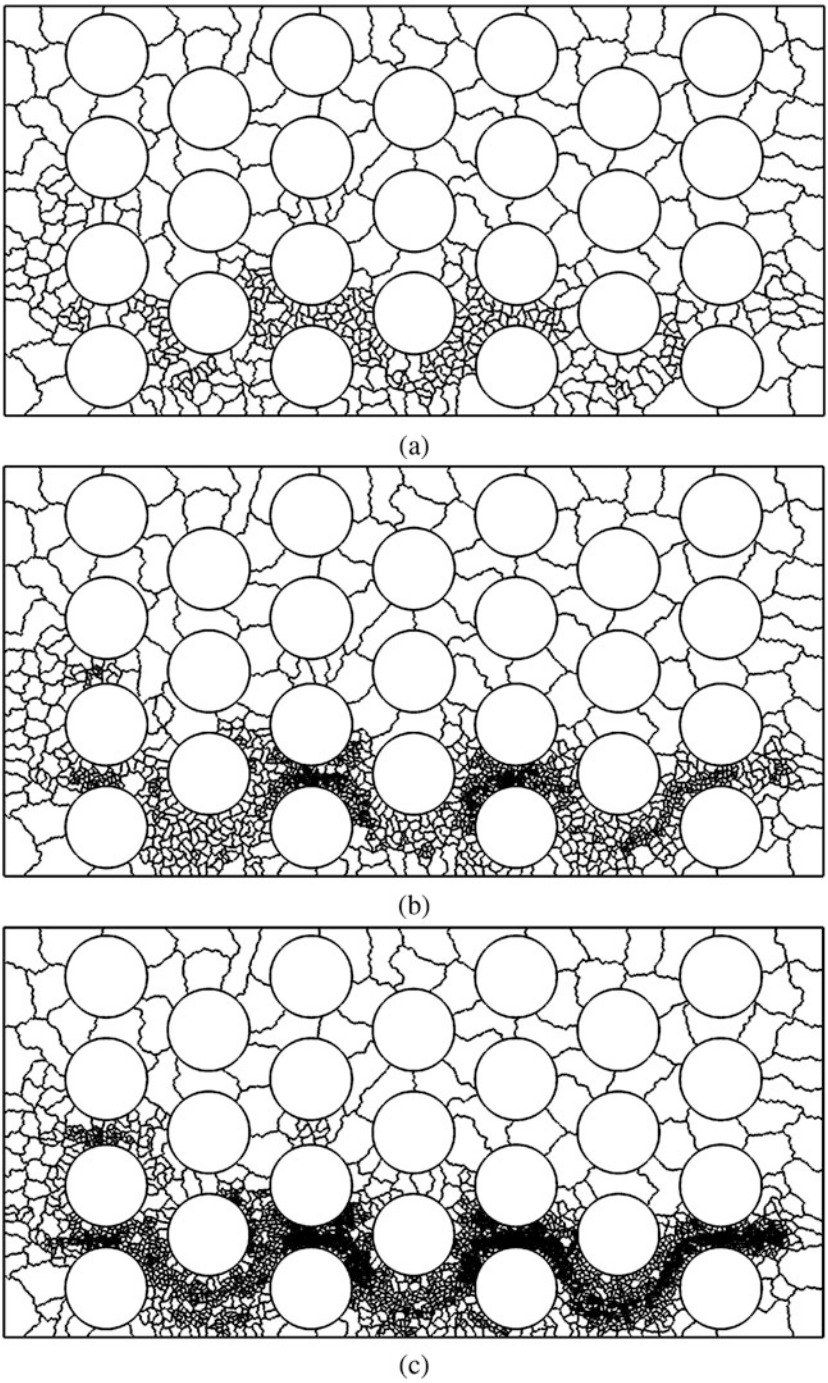

Fig. 7.4 Example 1. Agglomerated mesh after: (**a**) 2 refinements, with 392 elements; (**b**) 4 refinements, with 1199 elements; (**c**) 6 refinements, with 3260 elements

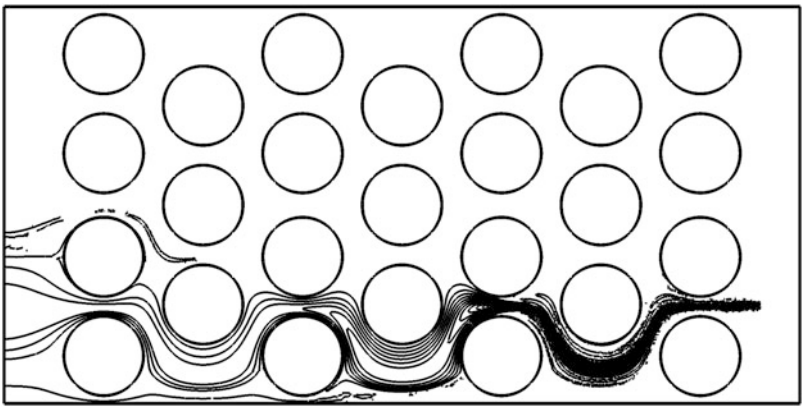

Fig. 7.5 Example 1. Dual solution

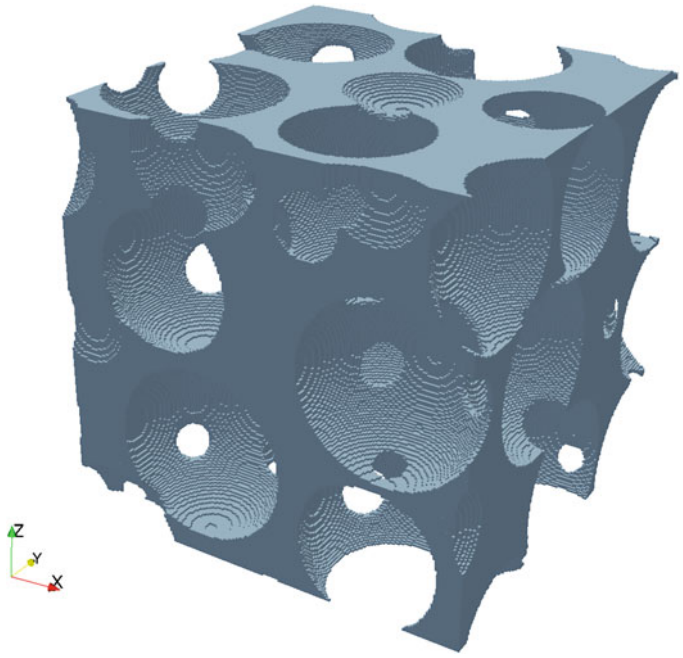

Fig. 7.6 Example 2. Computational geometry

of the boundary of Ω; thereby, $\partial\Omega_{\mathrm{D}} = \partial\Omega \backslash \partial\Omega_{\mathrm{N}}$. With this notation, we impose the following boundary conditions

$$\mathbf{u} = \mathbf{0} \quad \text{on } \partial\Omega_{\mathrm{D}}, \qquad \frac{\partial \mathbf{u}}{\partial \mathbf{n}} - p\mathbf{n} = \mathbf{g}_{\mathrm{N}} \quad \text{on } \partial\Omega_{\mathrm{N}}, \tag{7.12}$$

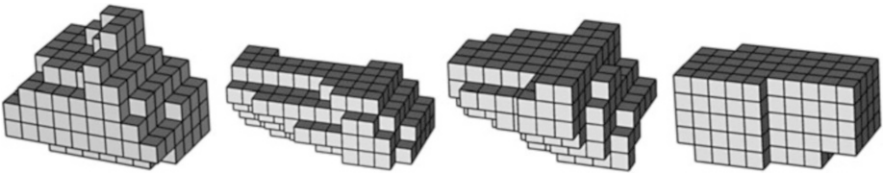

Fig. 7.7 Example 2. First 4 elements in the agglomerated coarse mesh $\mathscr{T}_h$

where $\mathbf{g}_{\mathrm{N}} = (1,0,0)^{\top}$ when $x = 0$ and $\mathbf{g}_{\mathrm{N}} = \mathbf{0}$ when $x = 0.1875$. For the discretization of the incompressible flow problem given by (7.10)–(7.12) we employ an interior penalty mixed DGFEM for the velocity and pressure; see [111, 155, 168].

Here we select the functional of interest to be the integral average of the x-component of the velocity vector; i.e., writing $\mathbf{u} = (u_1, u_2, u_3)^{\top}$, we have that

$$J(\mathbf{u}, p) = \frac{1}{|\Omega|} \int_{\Omega} u_1 \, \mathrm{d}\mathbf{x}.$$

On the basis of a fine mesh calculation, we compute the approximate value of the functional $J(\mathbf{u}, p) \approx 1.7944 \times 10^{-4}$. In this example, the underlying fine mesh $\mathscr{T}_h^{\mathrm{fine}}$ consists of the hexahedral voxels which define the computational geometry Ω; here, $\mathscr{T}_h^{\mathrm{fine}}$ consists of 2,869,962 elements. Starting from $\mathscr{T}_h^{\mathrm{fine}}$, we construct an initial coarse mesh consisting of only 200 agglomerated elements. In Fig. 7.7 we show the first 4 elements in the initial coarse mesh $\mathscr{T}_h$. In Fig. 7.8 we demonstrate the performance of the proposed agglomeration-based adaptive strategy employing discontinuous piecewise linear polynomials for the approximation of the velocity, and piecewise constant elements for pressure; furthermore, we set $\mathtt{REF} = 10\%$ and plot the relative error in the computed target functional of interest against the number of degrees of freedom in the underlying finite element space. As noted in the previous example, we observe that, even on very coarse finite element meshes, the quality of the computed error representation formula is relatively good, in the sense that the effectivity indices θ are not too far away from unity; indeed, for this particular example, we observe that θ lies approximately in the range $(1/2, 1)$.

7.3.3 *Example 3: Modelling Trabecular Bone*

In this final example, we consider the linear elastic analysis of a section of trabecular bone; for further details, we refer to [76, 170]. More precisely, given $\Omega \subset \mathbb{R}^3$, we wish to determine the displacement $\mathbf{u} = (u_1, u_2, u_3)^{\top}$ such that

$$-\nabla \cdot \boldsymbol{\sigma}(\mathbf{u}) = \mathbf{f} \ \text{ in } \Omega, \tag{7.13}$$

where $\boldsymbol{\sigma}$ is the stress tensor for a homogeneous isotropic material, i.e., $\boldsymbol{\sigma}(\mathbf{u}) = 2\mu\boldsymbol{\varepsilon}(\mathbf{u}) + \lambda\nabla \cdot \mathbf{u}\, I_3$, I_3 is the identity matrix, $\boldsymbol{\varepsilon}(\mathbf{u}) = 1/2(\nabla\mathbf{u} + \nabla\mathbf{u}^{\top})$, and μ and λ are the Lamé coefficients, which satisfy the relation $0 < \min\{\mu, \mu + \lambda\}$. In order to supplement (7.13) with appropriate boundary conditions, we first divide $\partial\Omega$ into

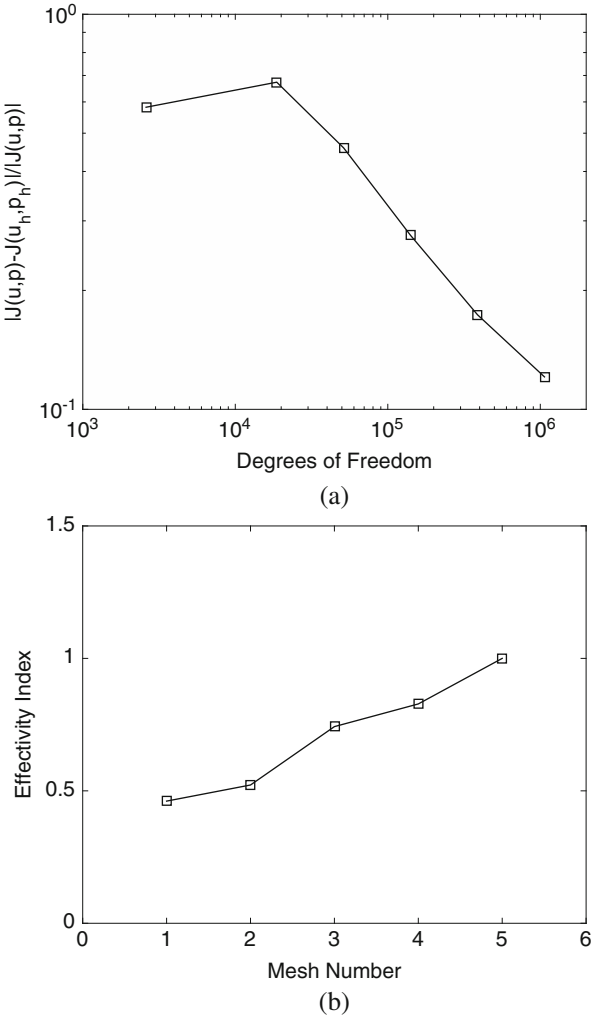

Fig. 7.8 Example 2. Convergence of the adaptive mesh refinement algorithm: (**a**) relative error in the functional of interest; (**b**) effectivity index of the DWR error estimator

the disjoint subsets $\partial\Omega_{\mathrm{D}}$, $\partial\Omega_{\mathrm{ND}}$, and $\partial\Omega_{\mathrm{N}}$ whose union is $\partial\Omega$, with $\partial\Omega_{\mathrm{D}}$ or $\partial\Omega_{\mathrm{ND}}$ nonempty and relatively open in $\partial\Omega$. With this notation, we set

$$\begin{aligned} \mathbf{u} &= \mathbf{g}_{\mathrm{D}} \quad \text{on } \partial\Omega_{\mathrm{D}}, \qquad \boldsymbol{\sigma}(\mathbf{u})\mathbf{n} = \mathbf{g}_{\mathrm{N}} \quad \text{on } \partial\Omega_{\mathrm{N}}, \\ \mathbf{u}\cdot\mathbf{n} &= g_{\mathrm{ND}} \quad \text{on } \partial\Omega_{\mathrm{ND}}, \quad \boldsymbol{\sigma}(\mathbf{u})\mathbf{n}\cdot\mathbf{t} = 0 \quad \text{on } \partial\Omega_{\mathrm{ND}}, \end{aligned} \tag{7.14}$$

where $\mathbf{n}$ and $\mathbf{t}$ denote the unit outward normal vector and unit tangential vector(s) on the boundary $\partial\Omega$. The DGFEM discretization of (7.13), (7.14) is given in [76]; cf., also, [45, 111, 174].

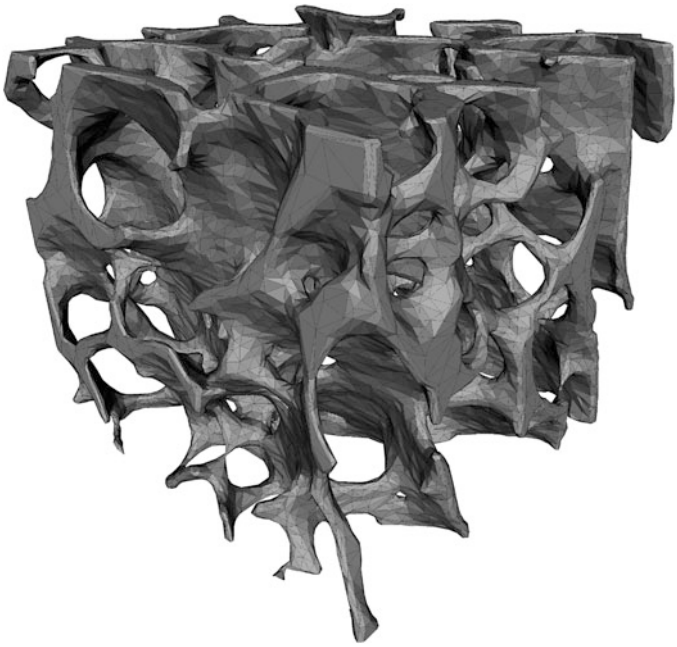

Fig. 7.9 Example 3. Section of trabecular bone, cf. [146]

We select Ω to be the portion of trabecular bone depicted in Fig. 7.9, cf. [146], which is contained within the three-dimensional cuboid $\Omega_{\text{cube}} := \Pi_{i=1}^{3}(x_i^{\min}, x_i^{\max})$. Writing $\partial\Omega_{\text{cube}}$ to denote the boundary of Ω_{cube}, i.e., the planar sides of the cuboid, we define $\partial\Omega_{\text{ND}} = \partial\Omega \cap \partial\Omega_{\text{cube}}$ and $\partial\Omega_{\text{N}} = \partial\Omega \setminus \partial\Omega_{\text{ND}}$; hence, $\partial\Omega_{\text{D}} = \emptyset$. With this notation, we set $g_{\text{ND}} = \bar{u} = 0.02L_3$, $L_3 = x_3^{\max} - x_3^{\min}$, on the top section of $\partial\Omega_{\text{ND}}$, i.e., where $x_3 = x_3^{\max}$, and $g_{\text{ND}} = 0$ on all other portions of $\partial\Omega_{\text{ND}}$; this corresponds to a 2% tensile straining. Furthermore, we set $\mathbf{g}_{\text{N}} = \mathbf{0}$ on $\partial\Omega_{\text{N}}$. With this notation, we select the target functional of interest $J(\cdot)$ to be the (scaled) effective Young's modulus of the section of trabecular bone defined by Ω. More precisely, writing E to denote the Young's modulus and ν the Poisson ratio, $J(\cdot)$ is given by

$$J(\mathbf{u}) = \frac{1}{E}\frac{L_d}{\bar{u}|\Omega_{\text{cube}}|}\int_{\Omega} \sigma_{33}(\mathbf{u})\,\mathrm{d}\mathbf{x},$$

cf. [76, 170]. Setting the Young's modulus $E = 10GPa$ and the Poisson ratio $\nu = 0.3$, the approximate (computed) value of the (scaled) effective Young's modulus is given by $J(\mathbf{u}) \approx 0.1205$. The initial fine mesh $\mathscr{T}_h^{\text{fine}}$ consists of 1,179,569 tetrahedral elements, which is then agglomerated to generate a coarse polytopic mesh $\mathscr{T}_h$ comprising of only 8000 elements; in Fig. 7.10 we show the first 4 elements of $\mathscr{T}_h$.

In Fig. 7.11 we plot the error in the computed target functional against the number of degrees of freedom in the underlying finite element space as the proposed

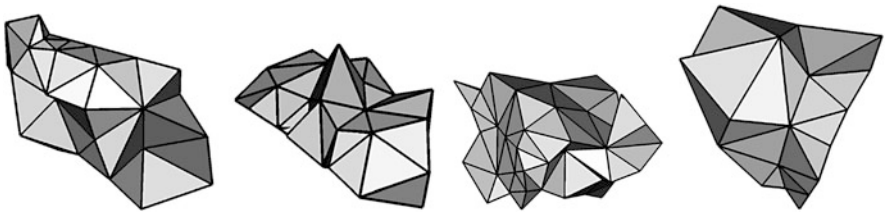

Fig. 7.10 Example 3. First 4 elements in the agglomerated coarse mesh $\mathscr{T}_h$

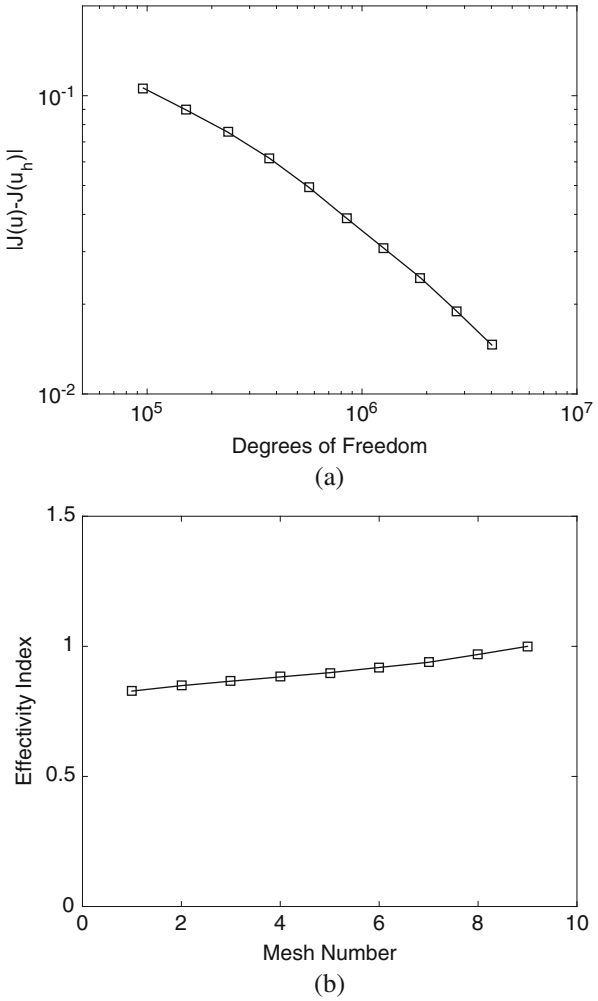

Fig. 7.11 Example 3. Convergence of the adaptive mesh refinement algorithm: (**a**) absolute error in the functional of interest; (**b**) effectivity index of the DWR error estimator

adaptive refinement strategy proceeds with $p = 1$; as before, we set $\texttt{REF} = 10\%$. As in the previous numerical experiments, we notice that the effectivity indices θ are relatively good, given the coarse nature of the finite element meshes employed. Indeed, as the mesh is refined, we observe that θ improves and approaches unity. Again, here we observe that a sufficiently accurate (in terms of engineering accuracy) approximation to the target functional of interest may be computed with a very small number of degrees of freedom.

Chapter 8
Summary and Outlook

In this volume we have presented an overview of recent developments concerning the mathematical analysis and practical application of DGFEMs on general meshes consisting of polytopic elements with a variable number of faces per element. The use of such general computational meshes in conjunction with DGFEMs has a number of key advantages; most notably: the number of degrees of freedom within the underlying finite element space is *independent* of the complexity of the geometry. Thereby, coarse approximations, which may possess sufficient accuracy for engineering applications, may be computed in an efficient manner. Moreover, adaptivity may subsequently be employed to improve solution accuracy by adding resolution in regions of the computational domain which directly affect output quantities of interest. The flexibility of DGFEMs means that the underlying discretization scheme naturally admits high-order polynomial degrees. While not directly discussed within this volume, the exploitation of general polytopic meshes, and in particular, meshes employing agglomerated elements, are essential for the design of efficient multi-level solvers; for recent work in this direction, we refer to [9, 13, 15], for example.

We have systematically studied interior penalty DGFEMs for the numerical approximation of general second-order PDEs with nonnegative characteristic form, which includes a wide class of problems, including PDEs of mixed elliptic-parabolic-hyperbolic type. The underlying mathematical tools have been carefully developed in the sense that they are not only explicit in terms of the underlying (variable) polynomial degree, but are also robust with respect to the shape of the elements. In particular, in the latter setting, the resulting bounds are sharp with respect to $(d-k)$-dimensional facet degeneration, $k = 1, 2, \ldots, d-1$. While our analysis has focused on interior penalty DGFEMs, we stress that the work presented here naturally generalizes to other DGFEMs, such as the local discontinuous Galerkin method of Cockburn and Shu [70], or any other discontinuous Galerkin formulation whose analysis relies on the technical tools developed in Chaps. 3 and 4.

A. Cangiani et al., *hp-Version Discontinuous Galerkin Methods on Polygonal and Polyhedral Meshes*, SpringerBriefs in Mathematics,
DOI 10.1007/978-3-319-67673-9_8

Despite their recent development, key aspects of which have been presented in this volume, DGFEMs on general polytopic meshes remain an extremely exciting area for current and future research. Indeed, the exceptional flexibility offered by DGFEMs in the design of compatible discretizations through the judicious selection of numerical fluxes (for example, ones with various conservation and/or stability properties) in conjunction with virtually arbitrary element shapes offer unprecedented capabilities in the design of the next generation of numerical methods for large scale PDE-based simulations. For instance, the application of these techniques to more general PDE problems posed on complicated (fixed or time-varying) geometries is of great importance; such problems naturally arise in many areas of engineering interest, including applications related to flows in porous media, healthcare applications, such as cancer modelling, and composite materials. In this way, such approaches can be exploited for the efficient computation of multiscale problems.

Furthermore, these techniques are proving to be invaluable for the numerical approximation of interface problems of various types. Indeed, DGFEMs have long been considered a promising numerical framework for such problems; see, for example, [48, 109]. The mesh flexibility afforded by meshes consisting of polytopic elements, with an arbitrary number of faces per element, or, in the 'Riemann-sum'-limit, elements with general curved faces, has only been partially exploited in multi-compartment PDE problems, closed by non-linear interface conditions, modelling various physical, biological, or engineering processes, such as mass transfer through semi-permeable membranes and transmission problems, cf. [35, 58, 137, 153]. This is an area of tremendous potential for DGFEMs on polytopic meshes, especially in the context of multiscale or moving interfaces.

Further work on both the mathematical analysis and the implementation of fast solution methods is required, as well as improvements in the efficient assembly of DGFEM matrices on general polytopic meshes, especially in the context of multiscale and/or nonlinear problems. Nevertheless, the speed of development of this class of methods, together with the strong interest in numerical methods on polytopic meshes at large, shows the value in engaging further in this exciting research direction.

Acknowledgements The authors would like to express their sincere gratitude to Paola Antonietti, Donald Brown, Joe Collis, Stefano Giani, Giorgio Pennesi, Younis Sabawi, and Oliver Sutton, for helpful discussions on the subject of this volume.

References

1. R.A. Adams, J.J.F. Fournier, *Sobolev Spaces*. Pure and Applied Mathematics (Amsterdam), vol. 140, 2nd edn. (Elsevier/Academic, Amsterdam, 2003)
2. B. Ahmad, A. Alsaedi, F. Brezzi, L.D. Marini, A. Russo, Equivalent projectors for virtual element methods. Comput. Math. Appl. **66**(3), 376–391 (2013)
3. P.F. Antonietti, B. Ayuso, Schwarz domain decomposition preconditioners for discontinuous Galerkin approximations of elliptic problems: non-overlapping case. ESAIM Math. Model. Numer. Anal. **41**(1), 21–54 (2007)
4. P.F. Antonietti, B. Ayuso, Multiplicative Schwarz methods for discontinuous Galerkin approximations of elliptic problems. ESAIM Math. Model. Numer. Anal. **42**(3), 443–469 (2008)
5. P.F. Antonietti, B. Ayuso, Two-level Schwarz preconditioners for super penalty discontinuous Galerkin methods. Commun. Comput. Phys. **5**(2–4), 398–412 (2009)
6. P.F. Antonietti, P. Houston, A class of domain decomposition preconditioners for *hp*-discontinuous Galerkin finite element methods. J. Sci. Comput. **46**(1), 124–149 (2011)
7. P.F. Antonietti, P. Houston, Preconditioning high-order discontinuous Galerkin discretizations of elliptic problems, in *Domain Decomposition Methods in Science and Engineering XX*, ed. by R. Bank, M. Holst, O. Widlund, J. Xu. Lecture Notes in Computational Science and Engineering, vol. 91 (Springer, Berlin, 2013)
8. P.F. Antonietti, S. Giani, P. Houston, *hp*-Version composite discontinuous Galerkin methods for elliptic problems on complicated domains. SIAM J. Sci. Comput. **35**(3), A1417–A1439 (2013)
9. P.F. Antonietti, S. Giani, P. Houston, Domain decomposition preconditioners for discontinuous Galerkin methods for elliptic problems on complicated domains. J. Sci. Comput. **60**(1), 203–227 (2014)
10. P.F. Antonietti, M. Sarti, M. Verani, Multigrid algorithms for *hp*-discontinuous Galerkin discretizations of elliptic problems. SIAM J. Numer. Anal. **53**(1), 598–618 (2015)
11. P.F. Antonietti, P. Houston, I. Smears, A note on optimal spectral bounds for nonoverlapping domain decomposition preconditioners for *hp*-version discontinuous Galerkin methods. Int. J. Numer. Anal. Model. **13**(4), 513–524 (2016)
12. P.F. Antonietti, A. Cangiani, J. Collis, Z. Dong, E.H. Georgoulis, S. Giani, P. Houston, Review of discontinuous Galerkin finite element methods for partial differential equations on complicated domains, in *Building Bridges: Connections and Challenges in Modern Approaches to Numerical Partial Differential Equations*, ed. by G.R. Barrenechea, F. Brezzi, A. Cangiani, E.H. Georgoulis (Springer International Publishing, Cham, 2016), pp. 281–310

A. Cangiani et al., *hp-Version Discontinuous Galerkin Methods on Polygonal and Polyhedral Meshes*, SpringerBriefs in Mathematics,
DOI 10.1007/978-3-319-67673-9

13. P.F. Antonietti, M. Sarti, M. Verani, Multigrid algorithms for high order discontinuous Galerkin methods. Lect. Notes Comput. Sci. Eng. **104**, 3–13 (2016)
14. P.F. Antonietti, P. Houston, G. Pennesi, Fast evaluation of DGFEMs on polytopic meshes (2017, in preparation)
15. P.F. Antonietti, P. Houston, X. Hu, M. Sarti, M. Verani, Multigrid algorithms for *hp*-version interior penalty discontinuous Galerkin methods on polygonal and polyhedral meshes, in *CALCOLO* (2017). https://doi.org/10.1007/s10092-017-0223-6
16. D.N. Arnold, An interior penalty finite element method with discontinuous elements. SIAM J. Numer. Anal. **19**(4), 742–760 (1982)
17. D.N. Arnold, D. Boffi, R.S. Falk, L. Gastaldi, Finite element approximation on quadrilateral meshes. Commun. Numer. Meth. Eng. **17**(11), 805–812 (2001)
18. D.N. Arnold, F. Brezzi, B. Cockburn, L.D. Marini, Unified analysis of discontinuous Galerkin methods for elliptic problems. SIAM J. Numer. Anal. **39**, 1749–1779 (2001)
19. D.N. Arnold, D. Boffi, R.S. Falk, Approximation by quadrilateral finite elements. Math. Comput. **71**(239), 909–922 (2002)
20. B. Ayuso, L.D. Marini, Discontinuous Galerkin methods for advection-diffusion-reaction problems. SIAM J. Numer. Anal. **47**(2), 1391–1420 (2009)
21. E. Baas, J.H. Kuiper, A numerical model of heterogeneous surface strains in polymer scaffolds. J. Biomech. **41**, 1374–1378 (2008)
22. E. Baas, J.H. Kuiper, Y. Yang, M.A. Wood, A.J. El Haj, In vitro bone growth responds to local mechanical strain in three-dimensional polymer scaffolds. J. Biomech. **43**, 733–739 (2010)
23. I. Babuška, The finite element method with penalty. Math. Comput. **27**(122), 221–228 (1973)
24. I. Babuška, J.E. Osborn, Generalized finite element methods: their performance and their relation to mixed methods. SIAM J. Numer. Anal. **20**(3), 510–536 (1983)
25. I. Babuška, M. Suri, The *h-p* version of the finite element method with quasi-uniform meshes. RAIRO Modél. Math. Anal. Numér. **21**(2), 199–238 (1987)
26. I. Babuška, M. Suri, The optimal convergence rate of the *p*-version of the finite element method. SIAM J. Numer. Anal. **24**(4), 750–776 (1987)
27. G.A. Baker, Finite element methods for elliptic equations using nonconforming elements. Math. Comput. **31**(137), 45–59 (1977)
28. G.A. Baker, W.N. Jureidini, O.A. Karakashian, Piecewise solenoidal vector fields and the Stokes problem. SIAM J. Numer. Anal. **27**(6), 1466–1485 (1990)
29. W. Bangerth, R. Rannacher, *Adaptive Finite Element Methods for Differential Equations* (Birkhäuser Verlag, Basel, 2003)
30. G.R. Barrenechea, F. Brezzi, A. Cangiani, E.H. Georgoulis (eds.), *Building Bridges: Connections and Challenges in Modern Approaches to Numerical Partial Differential Equations*. Lecture Notes in Computational Science and Engineering, vol. 114 (Springer International Publishing, Cham, 2016)
31. R.F. Bass, *Diffusion and Elliptic Operators* (Springer, New York, 1997)
32. F. Bassi, L. Botti, A. Colombo, S. Rebay, Agglomeration based discontinuous Galerkin discretization of the Euler and Navier-Stokes equations. Comput. Fluids **61**, 77–85 (2012)
33. F. Bassi, L. Botti, A. Colombo, D.A. Di Pietro, P. Tesini, On the flexibility of agglomeration based physical space discontinuous Galerkin discretizations. J. Comput. Phys. **231**(1), 45–65 (2012)
34. F. Bassi, L. Botti, A. Colombo, Agglomeration-based physical frame dG discretizations: an attempt to be mesh free. Math. Models Methods Appl. Sci. **24**(8), 1495–1539 (2014)
35. P. Bastian, C. Engwer, An unfitted finite element method using discontinuous Galerkin. Int. J. Numer. Methods Eng. **79**(12), 1557–1576 (2009)
36. R. Becker, R. Rannacher, An optimal control approach to a-posteriori error estimation in finite element methods, in *Acta Numerica*, ed. by A. Iserles (Cambridge University Press, Cambridge, 2001), pp. 1–102
37. L. Beirão da Veiga, F. Brezzi, A. Cangiani, G. Manzini, L.D. Marini, A. Russo, Basic principles of virtual element methods. Math. Models Methods Appl. Sci. **23**(1), 199–214 (2013)

38. L. Beirão da Veiga, K. Lipnikov, G. Manzini, *The Mimetic Finite Difference Method for Elliptic Problems*. MS&A. Modeling, Simulation and Applications, vol. 11 (Springer, Cham, 2014)
39. L. Beirão da Veiga, F. Brezzi, L.D. Marini, A. Russo, Serendipity nodal VEM spaces. Comput. Fluids **141**, 2–12 (2016)
40. C. Bernardi, M. Dauge, Y. Maday, Polynomials in the Sobolev world. HAL report (2007). hal-00153795
41. K.S. Bey, T. Oden, *hp*-Version discontinuous Galerkin methods for hyperbolic conservation laws. Comput. Methods Appl. Mech. Eng. **133**, 259–286 (1996)
42. S.C. Brenner, L.R. Scott, *The Mathematical Theory of Finite Element Methods*. Texts in Applied Mathematics, vol. 15, 3rd edn. (Springer, New York, 2008)
43. F. Brezzi, A. Russo, Choosing bubbles for advection-diffusion problems. Math. Models Methods Appl. Sci. **4**, 571–587 (1994)
44. F. Brezzi, P. Houston, D. Marini, E. Süli, Modeling subgrid viscosity for advection-diffusion problems. Comput. Methods Appl. Mech. Eng. **190**(13), 1601–1610 (2000)
45. L.J. Bridgeman, T.P. Wihler, Stability and a posteriori error analysis of discontinuous Galerkin methods for linearized elasticity. Comput. Methods Appl. Mech. Eng. **200**(13), 1543–1557 (2011)
46. A.N. Brooks, T.J.R. Hughes, Streamline upwind/Petrov-Galerkin formulations for convection dominated flows with particular emphasis on the incompressible Navier-Stokes equations. Comput. Methods Appl. Mech. Eng. **32**(1), 199–259 (1982)
47. A. Buffa, T.J.R. Hughes, G. Sangalli, Analysis of a multiscale discontinuous Galerkin method for convection-diffusion problems. SIAM J. Numer. Anal. **44**(4), 1420–1440 (2006)
48. E. Burman, P. Hansbo, An interior-penalty-stabilized Lagrange multiplier method for the finite-element solution of elliptic interface problems. IMA J. Numer. Anal. **30**, 870–885 (2010)
49. E. Burman, P. Hansbo, Fictitious domain finite element methods using cut elements: I. A stabilized Lagrange multiplier method. Comput. Methods Appl. Mech. Eng. **199**, 2680–2686 (2010)
50. E. Burman, P. Hansbo, Fictitious domain finite element methods using cut elements: II. A stabilized Nitsche method. Appl. Numer. Math. **62**, 328–341 (2012)
51. A. Cangiani, The residual-free bubble method for problems with multiple scales, Ph.D. thesis, University of Oxford, 2004
52. A. Cangiani, E.H. Georgoulis, M. Jensen, Discontinuous Galerkin methods for mass transfer through semipermeable membranes. SIAM J. Numer. Anal. **51**(5), 2911–2934 (2013)
53. A. Cangiani, J. Chapman, E.H. Georgoulis, M. Jensen, On the stability of continuous-discontinuous Galerkin methods for advection-diffusion-reaction problems. J. Sci. Comput. **57**(2), 313–330 (2013)
54. A. Cangiani, E.H. Georgoulis, P. Houston, hp-Version discontinuous Galerkin methods on polygonal and polyhedral meshes. Math. Models Methods Appl. Sci. **24**(10), 2009–2041 (2014)
55. A. Cangiani, Z. Dong, E.H. Georgoulis, P. Houston, *hp*-Version discontinuous Galerkin methods for advection–diffusion–reaction problems on polytopic meshes. ESAIM Math. Model. Numer. Anal. **50**(3), 699–725 (2016)
56. A. Cangiani, Z. Dong, E.H. Georgoulis, *hp*-Version space-time discontinuous Galerkin methods for parabolic problems on prismatic meshes. SIAM J. Sci. Comput. **39**(4), A1251–A1279 (2017)
57. A. Cangiani, E.H. Georgoulis, T. Pryer, O.J. Sutton, A posteriori error estimates for the virtual element method. Numer. Math. **137**(4), 857–893 (2017)
58. A. Cangiani, E.H. Georgoulis, Y. Sabawi, Adaptive discontinuous Galerkin methods for elliptic interface problems. Math. Comp. (2017, online). https://doi.org/10.1090/mcom/3322

59. A. Cangiani, G. Manzini, O.J. Sutton, Conforming and nonconforming virtual element methods for elliptic problems. IMA J. Numer. Anal. **37**(3), 1317–1354 (2017)
60. C. Canuto, A. Quarteroni, Approximation results for orthogonal polynomials in Sobolev spaces. Math. Comp. **38**(157), 67–86 (1982)
61. C. Carstensen, S.A. Funken, Constants in Clément-interpolation error and residual based a posteriori error estimates in finite element methods. East-West J. Numer. Math. **8**(3), 153–175 (2000)
62. A. Chernov, Optimal convergence estimates for the trace of the polynomial L^2-projection operator on a simplex. Math. Comput. **81**(278), 765–787 (2012)
63. E.B. Chin, J.B. Lasserre, N. Sukumar, Numerical integration of homogeneous functions on convex and nonconvex polygons and polyhedra. Comput. Mech. **56**(6), 967–981 (2015)
64. P.G. Ciarlet, *The Finite Element Method for Elliptic Problems*. Studies in Mathematics and Its Applications (North-Holland, Amsterdam, 1978)
65. B. Cockburn, An introduction to the discontinuous Galerkin method for convection-dominated problems, in *Advanced Numerical Approximation of Nonlinear Hyperbolic Equations (Cetraro, 1997)* (Springer, Berlin, 1998), pp. 151–268
66. B. Cockburn, Discontinuous Galerkin methods for convection-dominated problems, in *High-Order Methods for Computational Physics* (Springer, Berlin, 1999), pp. 69–224
67. B. Cockburn, Static condensation, hybridization, and the devising of the HDG methods, in *Building Bridges: Connections and Challenges in Modern Approaches to Numerical Partial Differential Equations*, ed. by G.R. Barrenechea, F. Brezzi, A. Cangiani, E.H. Georgoulis (Springer International Publishing, Cham, 2016), pp. 129–177
68. B. Cockburn, C.-W. Shu, TVB Runge-Kutta local projection discontinuous Galerkin finite element method for conservation laws. II. General framework. Math. Comput. **52**(186), 411–435 (1989)
69. B. Cockburn, C.-W. Shu, The Runge-Kutta discontinuous Galerkin method for conservation laws. V. Multidimensional systems. J. Comput. Phys. **141**(2), 199–224 (1998)
70. B. Cockburn, C.-W. Shu, The local discontinuous Galerkin method for time-dependent convection-diffusion systems. SIAM J. Numer. Anal. **35**(6), 2440–2463 (1998)
71. B. Cockburn, S.Y. Lin, C.-W. Shu, TVB Runge-Kutta local projection discontinuous Galerkin finite element method for conservation laws. III. One-dimensional systems. J. Comput. Phys. **84**(1), 90–113 (1989)
72. B. Cockburn, S. Hou, C.-W. Shu, The Runge-Kutta local projection discontinuous Galerkin finite element method for conservation laws. IV. The multidimensional case. Math. Comput. **54**(190), 545–581 (1990)
73. B. Cockburn, G.E. Karniadakis, C.-W. Shu (eds.), *Discontinuous Galerkin Methods* (Springer, Berlin, 2000). Theory, computation and applications, Papers from the 1st International Symposium held in Newport, RI, May 24–26, 1999
74. B. Cockburn, J. Gopalakrishnan, R. Lazarov, Unified hybridization of discontinuous Galerkin, mixed, and continuous Galerkin methods for second order elliptic problems. SIAM J. Numer. Anal. **47**(2), 1319–1365 (2009)
75. B. Cockburn, D.A. Di Pietro, A. Ern, Bridging the hybrid high-order and hybridizable discontinuous Galerkin methods. ESAIM Math. Model. Numer. Anal. **50**(3), 635–650 (2016)
76. J. Collis, P. Houston, Adaptive discontinuous Galerkin methods on polytopic meshes, in *Advances in Discretization Methods: Discontinuities, Virtual Elements, Fictitious Domain Methods*, ed. by G. Ventura, E. Benvenuti (Springer International Publishing, Cham, 2016), pp. 187–206
77. C. Dawson, S. Sun, M.F. Wheeler, Compatible algorithms for coupled flow and transport. Comput. Methods Appl. Mech. Eng. **193**(23–26), 2565–2580 (2004)
78. L. Demkowicz, in *Computing with hp-Adaptive Finite Elements: One and Two Dimensional Elliptic and Maxwell Problems*. Chapman & Hall/CRC Applied Mathematics and Nonlinear Science Series, vol. 1 (Chapman & Hall/CRC, Boca Raton, FL, 2007)
79. D.A. Di Pietro, A. Ern, *Mathematical Aspects of Discontinuous Galerkin Methods*. Mathématiques & Applications (Berlin) [Mathematics & Applications], vol. 69 (Springer, Heidelberg, 2012)

80. D.A. Di Pietro, A. Ern, A hybrid high-order locking-free method for linear elasticity on general meshes. Comput. Methods Appl. Mech. Eng. **283**, 1–21 (2015)
81. D.A. Di Pietro, A. Ern, Hybrid high-order methods for variable-diffusion problems on general meshes. C. R. Math. Acad. Sci. Paris **353**(1), 31–34 (2015)
82. D.A. Di Pietro, A. Ern, J.-L. Guermond, Discontinuous Galerkin methods for anisotropic semidefinite diffusion with advection. SIAM J. Numer. Anal. **46**(2), 805–831 (2008)
83. D.A. Di Pietro, A. Ern, S. Lemaire, An arbitrary-order and compact-stencil discretization of diffusion on general meshes based on local reconstruction operators. Comput. Methods Appl. Math. **14**(4), 461–472 (2014)
84. Z. Dong, On the exponent of exponential convergence of *hp*-finite element spaces (2017, submitted for publication). arXiv:1704.08046
85. J. Douglas, T. Dupont, Interior penalty procedures for elliptic and parabolic Galerkin methods, in *Computing Methods in Applied Sciences: Second International Symposium December 15–19, 1975*, ed. by R. Glowinski, J.L. Lions (Springer, Berlin, Heidelberg, 1976), pp. 207–216
86. M.G. Duffy, Quadrature over a pyramid or cube of integrands with a singularity at a vertex. SIAM J. Numer. Anal. **19**(6), 1260–1262 (1982)
87. D.A. Dunavant, High-degree efficient symmetric Gaussian quadrature rules for the triangle. Int. J. Numer. Methods Eng. **21**, 1129–1148 (1985)
88. M.S. Ebeida, S.A. Mitchell, Uniform random Voronoi meshes, in *Proceedings of the 20th International Meshing Roundtable*, ed. by W.R. Quadros (Springer, Berlin/Heidelberg, 2012), pp. 273–290
89. K. Eriksson, D. Estep, P. Hansbo, C. Johnson, Introduction to adaptive methods for differential equations, in *Acta Numerica*, ed. by A. Iserles (Cambridge University Press, Cambridge, 1995), pp. 105–158
90. A. Ern, J.-L. Guermond, *Theory and Practice of Finite Elements*. Applied Mathematical Sciences (Springer, New York, 2004)
91. A. Ern, A.F. Stephansen, P. Zunino, A discontinuous Galerkin method with weighted averages for advection-diffusion equations with locally small and anisotropic diffusivity. IMA J. Numer. Anal. **29**(2), 235–256 (2009)
92. L.C. Evans, *Partial Differential Equations*. Graduate Studies in Mathematics, vol. 19, 2nd edn. (American Mathematical Society, Providence, RI, 2010)
93. R.S. Falk, G.R. Richter, Local error estimates for a finite element method for hyperbolic and convection-diffusion equations. SIAM J. Numer. Anal. **29**(3), 730–754 (1992)
94. X. Feng, O.A. Karakashian, Two-level additive Schwarz methods for a discontinuous Galerkin approximation of second order elliptic problems. SIAM J. Numer. Anal. **39**(4), 1343–1365 (2001)
95. G. Fichera, Sulle equazioni differenziali lineari ellittico-paraboliche del secondo ordine. Atti Accad. Naz. Lincei. Mem. Cl. Sci. Fis. Mat. Nat. Sez. I. (8) **5**, 1–30 (1956)
96. G. Fichera, On a unified theory of boundary value problems for elliptic-parabolic equations of second order, in *Boundary Problems in Differential Equations* (University of Wisconsin Press, Madison, 1960), pp. 97–120
97. B. Fischer, A. Ramage, D.J. Silvester, A.J. Wathen, On parameter choice and iterative convergence for stabilised discretisations of advection-diffusion problems. Comput. Methods Appl. Mech. Eng. **179**(1), 179–195 (1999)
98. T.-P. Fries, T. Belytschko, The extended/generalized finite element method: an overview of the method and its applications. Int. J. Numer. Methods Eng. **84**(3), 253–304 (2010)
99. E.H. Georgoulis, Inverse-type estimates on *hp*-finite element spaces and applications. Math. Comput. **77**(261), 201–219 (2008)
100. E.H. Georgoulis, A. Lasis, A note on the design of *hp*-version interior penalty discontinuous Galerkin finite element methods for degenerate problems. IMA J. Numer. Anal. **26**(2), 381–390 (2006)

101. E.H. Georgoulis, E.J.C. Hall, J.M. Melenk, On the suboptimality of the *p*-version interior penalty discontinuous Galerkin method. J. Sci. Comput. **42**(1), 54–67 (2010)
102. S. Giani, P. Houston, Domain decomposition preconditioners for discontinuous Galerkin discretizations of compressible fluid flows. Numer. Math. Theory Methods Appl. **7**(2), 123–148 (2014)
103. S. Giani, P. Houston, *hp*-Adaptive composite discontinuous Galerkin methods for elliptic problems on complicated domains. Numer. Methods Partial Differ. Equ. **30**(4), 1342–1367 (2014)
104. S. Giani, P. Houston, Goal-oriented adaptive composite discontinuous Galerkin methods for incompressible flows. J. Comput. Appl. Math. **270**, 32–42 (2014)
105. P. Grisvard, *Elliptic Problems in Nonsmooth Domains*. Monographs and Studies in Mathematics, vol. 24 (Pitman (Advanced Publishing Program), Boston, MA, 1985)
106. W. Hackbusch, S.A. Sauter, Composite finite elements for problems containing small geometric details. Part II: implementation and numerical results. Comput. Vis. Sci. **1**, 15–25 (1997)
107. W. Hackbusch, S.A. Sauter, Composite finite elements for the approximation of PDEs on domains with complicated micro-structures. Numer. Math. **75**, 447–472 (1997)
108. E.J.C. Hall, P. Houston, S. Murphy, *hp*–Adaptive discontinuous Galerkin methods for neutron transport criticality problems. SIAM J. Sci. Comput. **39**(5), B916–B942 (2017)
109. A. Hansbo, P. Hansbo, An unfitted finite element method, based on Nitsche's method, for elliptic interface problems. Comput. Methods Appl. Mech. Eng. **191**(47–48), 5537–5552 (2002)
110. P. Hansbo, C. Johnson, *Streamline Diffusion Finite Element Methods for Fluid Flow* (Von Karman Institute for Fluid Dynamics, Rhode St. Genése, 1995)
111. P. Hansbo, M.G. Larson, Discontinuous finite element methods for incompressible and nearly incompressible elasticity by use of Nitsche's method. Comput. Methods Appl. Mech. Eng. **191**, 1895–1908 (2002)
112. K. Harriman, P. Houston, B. Senior, E. Süli, *hp*-Version discontinuous Galerkin methods with interior penalty for partial differential equations with nonnegative characteristic form, in *Recent Advances in Scientific Computing and Partial Differential Equations*, ed. by C.-W. Shu, T. Tang, S.-Y. Cheng. Contemporary Mathematics, vol. 330 (AMS, Providence, RI, 2003), pp. 89–119
113. R. Hartmann, Adjoint consistency analysis of discontinuous Galerkin discretizations. SIAM J. Numer. Anal. **45**(6), 2671–2696 (2007)
114. R. Hartmann, Numerical analysis of higher order discontinuous Galerkin finite element methods, in *VKI LS 2008-08: CFD - ADIGMA course on very high order discretization methods, Oct. 13–17, 2008*, ed. by H. Deconinck (Von Karman Institute for Fluid Dynamics, Rhode Saint Genèse, 2008)
115. R. Hartmann, P. Houston, Adaptive discontinuous Galerkin finite element methods for nonlinear hyperbolic conservation laws. SIAM J. Sci. Comput. **24**, 979–1004 (2002)
116. R. Hartmann, P. Houston, Error estimation and adaptive mesh refinement for aerodynamic flows, in *VKI LS 2010-01: 36th CFD/ADIGMA Course on hp-Adaptive and hp-Multigrid Methods, Oct. 26–30, 2009*, ed. by H. Deconinck (Von Karman Institute for Fluid Dynamics, Sint-Genesius-Rode, 2010)
117. J.S. Hesthaven, T. Warburton, *Nodal Discontinuous Galerkin Methods*. Texts in Applied Mathematics, vol. 54 (Springer, New York, 2008). Algorithms, analysis, and applications
118. L. Hörmander, Hypoelliptic second order differential equations. Acta Math. **119**, 147–171 (1967)
119. P. Houston, Adjoint error estimation and adaptivity for hyperbolic problems, in *Handbook of Numerical Analysis: Handbook of Numerical Methods for Hyperbolic Problems. Applied and Modern*, vol. 18, ed. by R. Abgrall, C.-W. Shu (Elsevier, Amsterdam, 2017), pp. 233–261
120. P. Houston, N. Sime, Numerical modelling of MPA-CVD reactors with the discontinuous Galerkin finite element method. J. Phys. D Appl. Phys. **50**(29), 295202 (2017)

121. P. Houston, E. Süli, Stabilised *hp*–finite element approximation of partial differential equations with nonnegative characteristic form. Computing **66**(2), 99–119 (2001)
122. P. Houston, E. Süli, Adaptive finite element approximation of hyperbolic problems, in *Error Estimation and Adaptive Discretization Methods in Computational Fluid Dynamics*, ed. by T. Barth, H. Deconinck. Lecture Notes in Computational Science and Engineering, vol. 25 (Springer, Berlin/Heidelberg, 2002), pp. 269–344
123. P. Houston, C. Schwab, E. Süli, Stabilized *hp*-finite element methods for first-order hyperbolic problems. SIAM J. Numer. Anal. **37**(5), 1618–1643 (2000)
124. P. Houston, C. Schwab, E. Süli, Discontinuous *hp*-finite element methods for advection-diffusion-reaction problems. SIAM J. Numer. Anal. **39**(6), 2133–2163 (2002)
125. A. Johansson, M.G. Larson, A high order discontinuous Galerkin Nitsche method for elliptic problems with fictitious boundary. Numer. Math. **123**(4), 607–628 (2013)
126. C. Johnson, *Numerical Solution of Partial Differential Equations by the Finite Element Method* (Cambridge University Press, Cambridge, 1987)
127. C. Johnson, J. Pitkäranta, An analysis of the discontinuous Galerkin method for a scalar hyperbolic equation. Math. Comput. **46**(173), 1–26 (1986)
128. C. Johnson, U. Nävert, J. Pitkäranta, Finite element methods for linear hyperbolic problems. Comput. Methods Appl. Mech. Eng. **45**(1–3), 285–312 (1984)
129. G.E. Karniadakis, S. Sherwin, *Spectral/hp Finite Element Methods in CFD* (Oxford University Press, Oxford, 1999)
130. G. Karypis, V. Kumar, A fast and highly quality multilevel scheme for partitioning irregular graphs. SIAM J. Sci. Comput. **20**(1), 359–392 (1999)
131. M.V. Keldyš, On certain cases of degeneration of equations of elliptic type on the boundary of a domain. Dokl. Akad. Nauk SSSR (N.S.) **77**, 181–183 (1951)
132. D. Kröner, *Numerical Schemes for Conservation Laws* (Wiley-Teubner, Chichester, 1997)
133. M.G. Larson, F. Bengzon, *The Finite Element Method: Theory, Implementation, and Applications* (Springer, Heidelberg, 2013)
134. J.B. Lasserre, Integration on a convex polytope. Proc. Am. Math. Soc. **126**(8), 2433–2441 (1998)
135. P. Lesaint, P.-A. Raviart, On a finite element method for solving the neutron transport equation, in *Mathematical Aspects of Finite Elements in Partial Differential Equations*. Proceedings of Symposia, Mathematics Research Center, University of Wisconsin, Madison, WI, 1974, vol. 33 (Mathematics Research Center, University of Wisconsin-Madison, Academic, New York, 1974), pp. 89–123
136. J. Lu, An a posteriori error control framework for adaptive precision optimization using discontinuous Galerkin finite element method, PhD thesis, M.I.T., 2005
137. A. Massing, Analysis and implementation of finite element methods on overlapping and fictitious domains, Ph.D. thesis, University of Oslo, 2012
138. J.M. Melenk, T. Wurzer, On the stability of the boundary trace of the polynomial L_2-projection on triangles and tetrahedra. Comput. Math. Appl. **67**(4), 944–965 (2014)
139. P. Monk, E. Süli, The adaptive computation of far-field patterns by a posteriori error estimation of linear functionals. SIAM J. Numer. Anal. **36**(1), 251–274 (1998)
140. S.E. Mousavi, N. Sukumar, Numerical integration of polynomials and discontinuous functions on irregular convex polygons and polyhedrons. Comput. Mech. **47**(5), 535–554 (2011)
141. S.E. Mousavi, H. Xiao, N. Sukumar, Generalized Gaussian quadrature rules on arbitrary polygons. Int. J. Numer. Methods Eng. **82**(1), 99–113 (2010)
142. R. Muñoz-Sola, Polynomial liftings on a tetrahedron and applications to the *h-p* version of the finite element method in three dimensions. SIAM J. Numer. Anal. **34**(1), 282–314 (1997)
143. J. Nitsche, Über ein Variationsprinzip zur Lösung von Dirichlet Problemen bei Verwendung von Teilräumen, die keinen Randbedingungen unterworfen sind. Abh. Math. Sem. Uni. Hamburg **36**, 9–15 (1971)
144. O.A. Oleinik, E.V. Radkevič, *Second Order Equations with Nonnegative Characteristic Form* (American Mathematical Society, Providence, 1973)

145. T.A. Oliver, D.L. Darmofal, Analysis of dual-consistency for discontinuous Galerkin discretizations of source terms. SIAM J. Numer. Anal. **47**(5), 3507–3525 (2009)
146. E. Perilli, F. Baruffaldi, Proposal for shared collections of X-ray microCT datasets of bone specimens, in *ICCB03, 24–26 September 2003, Zaragoza* (I3A, Zaragoza, 2003), pp. 235–236
147. I. Perugia, D. Schötzau, An *hp*-analysis of the local discontinuous Galerkin method for diffusion problems. J. Sci. Comput. **17**(1–4), 561–571 (2002)
148. W.H. Reed, T.R. Hill, Triangular mesh methods for the neutron transport equation. Technical Report LA-UR-73-479 Los Alamos Scientific Laboratory (1973)
149. K.A. Rejniak, V. Estrella, T. Chen, A.S. Cohen, M.C. Lloyd, D.L. Morse, The role of tumor tissue architecture in treatment penetration and efficacy: an integrative study. Front. Oncol. **3**, 1–13 (2013)
150. M. Renardy, R.C. Rogers, *An Introduction to Partial Differential Equations*. Texts in Applied Mathematics, vol. 13 (Springer, New York, 1993)
151. B. Rivière, *Discontinuous Galerkin Methods for Solving Elliptic and Parabolic Equations*. Frontiers in Applied Mathematics (Society for Industrial and Applied Mathematics, Philadelphia, PA, 2008). Theory and implementation
152. B. Rivière, M.F. Wheeler, V. Girault, Improved energy estimates for interior penalty, constrained and discontinuous Galerkin methods for elliptic problems. I. Comput. Geosci. **3**(3–4), 337–360 (2000, 1999)
153. Y. Sabawi, Adaptive discontinuous Galerkin methods for interface problems, PhD thesis, University of Leicester, 2017
154. S.A. Sauter, R. Warnke, Extension operators and approximation on domains containing small geometric details. East-West J. Numer. Math. **7**(1), 61–77 (1999)
155. D. Schötzau, C. Schwab, A. Toselli, Mixed *hp*-DGFEM for incompressible flows. SIAM J. Numer. Anal. **40**, 2171–2194 (2003)
156. C. Schwab, *p- and hp-Finite element methods: Theory and Applications in Solid and Fluid Mechanics* (Oxford University Press, Oxford, 1998)
157. J.R. Shewchuk, Triangle: Engineering a 2D quality mesh generator and Delaunay triangulator, in *Applied Computational Geometry: Towards Geometric Engineering*, ed. by M.C. Lin, D. Manocha. Lecture Notes in Computer Science, vol. 1148 (Springer, Berlin/Heidelberg, 1996), pp. 203–222. From the First ACM Workshop on Applied Computational Geometry
158. H. Si, TetGen, a Delaunay-based quality tetrahedral mesh generator. ACM Trans. Math. Softw. **41**(2), 11:1–11:36 (2015)
159. N. Sime, Numerical modelling of chemical vapour deposition reactors, Ph.D. thesis, University of Nottingham, 2016
160. P. Solin, K. Segeth, I. Dolezel, in *Higher-Order Finite Element Methods*. Studies in Advanced Mathematics (Chapman & Hall/CRC, Boca Raton, London, 2004)
161. A. Sommariva, M. Vianello, Product Gauss cubature over polygons based on Green's integration formula. BIT Numer. Math. **47**(2), 441–453 (2007)
162. E.M. Stein, *Singular Integrals and Differentiability Properties of Functions* (Princeton University Press, Princeton, NJ, 1970)
163. G. Strang, G.J. Fix, *An Analysis of the Finite Element Method*. Prentice-Hall Series in Automatic Computation. (Prentice-Hall, Englewood Cliffs, NJ, 1973)
164. N. Sukumar, A. Tabarraei, Conforming polygonal finite elements. Int. J. Numer. Methods Eng. **61**(12), 2045–2066 (2004)
165. C. Talischi, G.H. Paulino, A. Pereira, I.F.M. Menezes, Polymesher: a general-purpose mesh generator for polygonal elements written in Matlab. Struct. Multidiscip. Optim. **45**, 309–328 (2012)
166. V. Thomée, *Galerkin Finite Element Methods for Parabolic Problems*. Lecture Notes in Mathematics, vol. 1054 (Springer, Berlin, 1984)
167. E.F. Toro, *Riemann Solvers and Numerical Methods for Fluid Dynamics* (Springer, Berlin, 1997)
168. A. Toselli, *hp*-Discontinuous Galerkin approximations for the Stokes problem. Math. Models Methods Appl. Sci. **12**, 1565–1616 (2002)

169. R. Verfürth, On the constants in some inverse inequalities for finite element functions. Technical Report 257, University of Bochum (1999)
170. C.V. Verhoosel, G.J. van Zwieten, B. van Rietbergen, R. de Borst, Image-based goal-oriented adaptive isogeometric analysis with application to the micro-mechanical modeling of trabecular bone. Comput. Methods Appl. Mech. Eng. **284**, 138–164 (2015)
171. T. Warburton, Spectral/*hp*-methods on polymorphic multi-domains: algorithms and applications, PhD thesis, Brown University, 1999
172. T. Warburton, J.S. Hesthaven, On the constants in *hp*-finite element trace inverse inequalities. Comput. Methods Appl. Mech. Eng. **192**(25), 2765–2773 (2003)
173. M.F. Wheeler, An elliptic collocation-finite element method with interior penalties. SIAM J. Numer. Anal. **15**(1), 152–161 (1978)
174. T.P. Wihler, Locking-free adaptive discontinuous Galerkin FEM for linear elasticity problems. Math. Comput. **75**(255), 1087–1102 (2006)
175. H. Xiao, Z. Gimbutas, A numerical algorithm for the construction of efficient quadrature rules in two and higher dimensions. Comput. Math. Appl. **59**(2), 663–676 (2010)